Dissertation zur Erlangung des Doktorgrades
der Fakultät für Chemie und Pharmazie
der Ludwig-Maximilians-Universität München

Single-round rhabdovirus replicons and an augmented RBD: A safe and effective combination for a SARS-CoV-2 vaccine

Alexandru Adrian Dorman, geb. Hennrich
aus
Temeschburg, Rumänien
2021

Erklärung

Diese Dissertation wurde im Sinne von § 7 der Promotionsordnung vom 28. November 2011 von Herrn Prof. Dr. Karl-Klaus Conzelmann betreut und von Herrn Prof. Dr. Klaus Förstemann von der Fakultät für Chemie und Pharmazie vertreten.

Eidesstattliche Versicherung

Diese Dissertation wurde eigenständig und ohne unerlaubte Hilfe erarbeitet.

München, den 20.12.2021

Alexandru Adrian Dorman

Dissertation eingereicht am	20.12.2021
1. Gutachter:	Prof. Dr. Klaus Förstemann
2. Gutachter:	Prof. Dr. Karl-Klaus Conzelmann
Mündliche Prüfung am	07.02.2022

„He was too simple to wonder when he had attained humility. But he knew he had attained it and he knew it was not disgraceful and it carried no loss of true pride.“

— Ernest Hemingway, The Old Man and the Sea

This thesis has been prepared in the laboratory of Prof. Dr. Karl-Klaus Conzelmann at the Max von Pettenkofer-Institute and Gene Center of the Ludwig-Maximilians-University Munich

Danksagung

Lieber Leser, bevor es ans Eingemachte geht möchte ich mich bei allen bedanken die mich auf diesem langen, schrecklich-schönen Weg begleitet haben. Dazu gehört zuallererst Prof. Dr. Klaus Förstemann, der es mir ermöglicht hat diese Arbeit an der Fakultät für Chemie und Pharmazie anzufertigen. Insbesondere geht mein Dank an Prof. Dr. Karl-Klaus Conzelmann für viele Jahre unerschrockene, unerschütterliche Unterstützung und die Möglichkeit diese Arbeit (sowie das ein oder andere Nebenprojekt) in seinem Labor durchzuführen, Ideen zu verwirklichen (oder zu verwerfen), kreativ zu werden und ein tiefgründiges Interesse an Viren zu hegen und zu pflegen.

Dankbar bin ich auch allen Wegbegleitern und Mitarbeitern, die den Laboralltag weniger zu Arbeit und mehr zu einem Hobby, zumindest ein Stück weit, gemacht haben. In Reihenfolge des Entschwindens: Nadin, Kerstin, Konstantin, Daniel, Marco, Alex, Yassine, Max, Dominik und Verena. Und neben allen Verschwindern natürlich auch dem konstanten Inventar, Doro, und allen anderen guten Geistern des Genzentrums, die gleich einer geölten Maschine unauffällig und effizient dafür sorgen dass der Laden läuft.

Ohne die Unterstützung meiner Eltern wäre nichts von alledem möglich gewesen. Das ist zwar eh klar, aber manchmal sollte es doch auch ausgesprochen werden. Deswegen: Vielen Dank, Mama, vielen Dank, Papa, für euren Glauben an mich, das Vertrauen und die Unterstützung. Ihr seid die Besten!

Zu guter Letzt möchte ich mich bei der wichtigsten Person in meinem Leben bedanken, ohne die vielleicht fast alles möglich, aber ungleich weniger schön und lebenswert gewesen wäre. Danke für alles, meine Klara.

Dem weißen Phantom der Feodor-Lynen-Straße sein hiermit auch gedankt (herzlichst), und allen die ab und an ihren Augen nicht getraut haben.

Contents

Zusammenfassung

Die anhaltende SARS-CoV-2-Pandemie kann nur durch konzertierte, weltweite Impfaktionen eingedämmt werden. Impfstoffe gegen pandemische Erreger stellen eine freiwillige, vorbeugende Prävention am Gesunden dar und erfordern Anwendung bei dem Großteil der Bevölkerung, um eine effektive Herdenimmunität herbeizuführen zu können. Daher müssen Impfstoffe höchstmögliche Sicherheitsstandards erfüllen und gleichzeitig eine effektive, spezifische Immunreaktion und einen verlässlichen Schutz gegen den jeweiligen Erreger auslösen. Um diese funktionell gegensätzlichen Ziele zu erreichen, haben wir eine Impfstoffplattform entwickelt und getestet, die auf sich nicht ausbreitenden, sog. „single-round“ Rhabdovirus-Vektoren basiert, welche ein hoch immunogenes Antigenkonstrukt exprimieren. Dieses besteht aus der zelloberflächenverankerten Rezeptorbindungsdomäne (RBD) des SARS-CoV-2 Spike (S) Proteins, die sowohl auf der Zellmembran transduzierter Zellen als auch in Rhabdovirus-Virionen und nicht-infektiösen Pseudovirus-Partikel eingebaut und präsentiert wird. Die RBD-Sequenz wurde vom ursprünglichen SARS-CoV-2-Wuhan-Stamm abgeleitet und genetisch mit dem extrazellulären Stamm, der Transmembran- und Intrazellulärdomäne des Tollwutvirus-Glykoproteins (G) fusioniert. Dieses sogenannte „Minispike“ wurde im Detail charakterisiert, wobei effiziente Expression, posttranslationale Modifikation und Insertion in Zellmembranen und Viruspartikel gezeigt werden konnten. Die korrekte Faltung in eine biologisch relevante Konformation wurde durch die spezifische Erkennung des Konstrukts durch COVID-19-Patientenseren und SARS-CoV 2 S-bindende monoklonale Antikörper sowohl in Lebendzell-Mikroskopie als auch auf fixierten Zellen bestätigt. Eine Reihe nicht ausbreitungsfähiger, „single-round“ rekombinanter Viren, bei denen das Gen für das virale Glykoprotein gegen eine bis drei Kopien des Minispike-Gens ausgetauscht war, wurden im Hinblick auf Expressionslevel des Minispike-Proteins und Attenuierung charakterisiert. Anschließend wurden BALB/c-Mäuse mit einem Konstrukt immunisiert, welches auf dem G-deletierten Vektorvirus VSV basiert und eine Kopie des Minispike-Gens (VSVΔG minispike eGFP) aufweist. Immunseren von diesen Mäusen wurden auf ihre Fähigkeit getestet, eine SARS-CoV 2 S-vermittelte Infektion zu neutralisieren, wobei sowohl S-pseudotypsierte Pseudoviren als auch authentisches SARS-CoV-2 zum Einsatz kamen. Eine erhebliche Neutralisationsaktivität, vergleichbar mit denen schwerkranker COVID-19 Patienten, wurde bereits nach der Grundimpfung induziert und durch eine Auffrischimpfung weiter erhöht. Diese Minispike-Immunseren wurden weiter auf ihre Neutralisationskapazität gegen besorgniserregende vorherrschende SARS-CoV-2-Varianten (einschließlich Alpha, Beta, Gamma und Delta) getestet und zeigten eine bemerkenswerte Resistenz gegen Immunevasion. Die Delta-Variante wies dabei mit einer 8- bis 12-fachen Reduktion der Neutralisationstiter den höchsten Immun-Escape auf. Im Gegensatz dazu wurde die Beta-Variante, für die sowohl bei Genesenen als auch bei Geimpften der

ausgeprägteste Immun-Escape-Phänotyp beschrieben wurde, hocheffektiv (mit einer Reduktion um 50%) neutralisiert. Diese Ergebnisse sprechen für die Induktion einer breiten und robusten neutralisierenden Antikörperantwort nach VSVΔG Minispike-Immunisierung, die auf mehrere, unabhängige Epitope der S RBD abzielt. Diese Ergebnisse wurden in SARS-CoV-2 Challenge Experimenten in K18-hACE-Mäusen bestätigt. Sowohl bei Challenge mit dem ursprünglichen SARS-CoV 2 als auch mit der Delta-Variante reichte eine einzelne Impfung mit VSVΔG minispike eGFP aus, um alle Mäuse vollständig vor sämtlichen klinischen Anzeichen einer SARS-CoV 2-induzierten Erkrankung zu schützen. Besonders hervorzuheben ist dabei, dass die Mäuse gegen die Delta-Variante ebenso gut geschützt waren, wie gegen das parentale Virus, obwohl die Neutralisationstiter gegen diese Variante die höchste Reduktion aufwiesen. Dies unterstreicht die Robustheit eines durch eine einzelne Impfung mit VSVΔG Minispike eGFP hervorgerufene Schutzwirkung.

Summary

The ongoing SARS-CoV-2 pandemic can only be curbed by a concerted, global vaccination effort. Vaccines are used in healthy populations and represent a voluntary, preventative intervention while requiring application in most of the populace to induce herd immunity. Therefore, vaccines must meet the highest possible safety standards and at the same time induce a beneficial immune reaction and protection against the pathogen in question. To address these functionally opposite goals, we designed, created, and tested a vaccine platform based on non-spreading, single-round rhabdovirus vectors expressing a highly immunogenic antigen construct consisting of a cell surface-anchored SARS-CoV-2 receptor binding domain (RBD) that, in addition to being presented on the cell surface of transduced cells, is incorporated into budding rhabdovirus virions and non-infectious pseudovirus particles. The RBD sequence was derived from the ancestral SARS-CoV-2 Wuhan strain and genetically fused to the RABV G stem, transmembrane domain, and intracellular tail. This so termed "minispike" was characterized in detail, revealing efficient expression, post-translational modification, and insertion into cell membrane and viral particles. Correct folding and adoption of a biologically relevant conformation was demonstrated by specific recognition of the construct by COVID-19 patient sera and SARS-CoV-2 S binding mAbs on both live and fixed cells. A series of G-deleted, single-round vectors containing one to three copies of the minispike cistron was cloned, rescued and characterized in regard to minispike expression levels and viral titers. We then chose VSVΔG-minispike-eGFP (monovalent, non-spreading) to immunize BALB/c mice. Sera from these mice was tested for the capacity to neutralize SARS-CoV-2 S-mediated infection in authentic and surrogate virus neutralization assays. Considerable neutralization titers comparable to convalescents from severe COVID-19 were induced already after prime vaccination and further improved by boost vaccination. The minispike immune sera were further tested for their neutralization capacity against prevalent SARS-CoV-2 variants of concern (including alpha, beta, gamma and delta), displaying a remarkable resistance to escape. The delta variant showed the most severe reduction in neutralizing titers (8- to 12-fold). In contrast, the beta variant, which is described to have the most pronounced immune escape phenotype for both convalescents and vaccinees, was readily neutralized with only a two-fold reduction in neutralizing titers. These findings indicate the induction of a diverse and robust neutralizing antibody response targeting multiple distinct epitopes on the S RBD by minispike immunization. Finally, live virus challenge experiments in susceptible K18-hACE mice with ancestral SARS-CoV-2 as well as the delta variant revealed that a single vaccination with VSVΔG-minispike-eGFP is sufficient to completely protect the mice from all clinical signs of SARS-CoV-2 induced disease. Remarkably, even though we saw the highest decline in neutralizing titers against delta, mice were still equally well protected against this variant.

Introduction

Vesicular Stomatitis virus

Vesicular stomatitis virus (VSV) is a nonsegmented, negative stranded RNA virus and the prototypic member of the genus Vesiculovirus, family *Rhabdoviridae*, order *Mononegavirales* [1]. VSV disease was first described in army horses during the U.S. civil war [2]. VSV is transmitted by hematophagous insects like mosquitos, sand- and blackflies [3] and naturally infects livestock, causing lesions in mouth and udders clinically similar to the more severe and consequential foot and mouth disease caused by the aphthovirus foot-and-mouth disease virus. VSV outbreaks thereby instigate significant alarm and cause considerable economic losses in affected farms [4, 5]. The most important member of the Vesiculoviridae is VSV Indiana strain (VSIV) which, for the sake of brevity, will be from now on synonymously used for VSV. Other relevant vesiculoviruses for which infections in humans have been reported include Chandipura virus (CHPV), Cocal virus (COCV), Isfahan virus (ISFV), Piry virus (PIRYV), Vesicular stomatitis Alagoas virus (VSAV) and Vesicular stomatitis New Jersey virus (VSNJV). Natural infections with these viruses typically cause light, influenza-like symptoms.

VSV Genomic structure

The RNA genome of VSV is approximately 11 kilobases (kb) long. It comprises an untranslated, uncapped 3´-Leader sequence that serves as promoter for sequential transcription of five monocistronic genes: The nucleoprotein N, phosphoprotein P, matrix protein M, glycoprotein G and the RNA-dependent RNA polymerase (RdRP) or large protein L, arranged from 3´to 5´in the conserved order N-P-M-G-L. During the replication step, the Leader fulfils the role of promoter for replication of the antigenome. At the 5´-terminus a Trailer sequence serves as promoter for replication of the full-length genome.

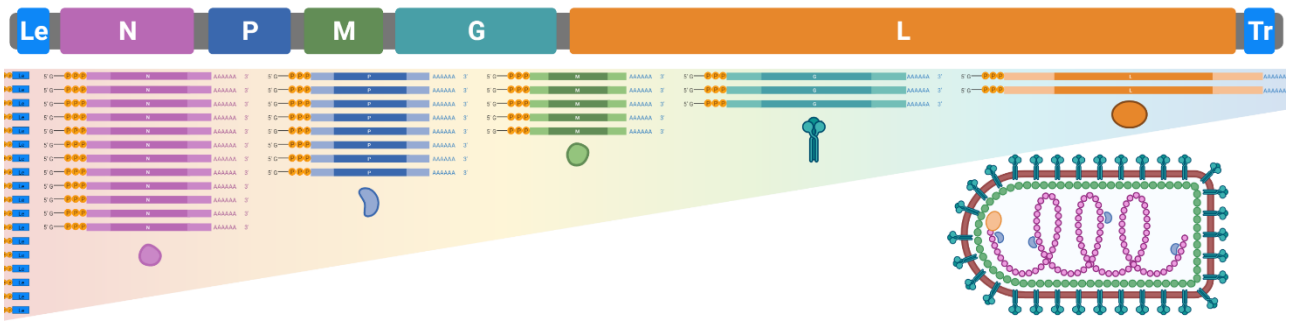

Figure 1: VSV genome organization and schematic virion structure. The negative-sense RNA genome is oriented 3´-5´ and flanked by a Leader (Le) and Trailer (Tr) sequence at the termini. The Le sequence is the promoter for the sequential transcription of the 5 genes. According to the STOP-START mechanism of transcription, the polymerase complex (consisting

of L and P) engages the genome exclusively at the Le sequence and starts transcribing the first gene (N). After transcription and polyadenylation, the polymerase complex encounters a transcription stop signal followed by a short intergenic region and the transcription start signal of the next gene (P). The probability of re-initiation is around 70 %, leading to a transcription gradient from N to L. When sufficient N levels are reached, the polymerase switches from transcription to replication mode, ignoring the intergenomic STOP START signals and producing full-length antigenomes, which are co-transcriptionally encapsidated in N. The antigenome-RNPs in turn serve as template for Tr-driven replication of the genome.

The virion is bullet-shaped, with a single condensed RNP inside a layer of M, which in concert with the G proteins decorating the lipid bilayer effectuates budding of the nascent virions from the plasma membrane.

Nucleoprotein N

The viral genomic and antigenomic RNA is co-transcriptionally encapsidated by N, forming the so-called ribonucleoprotein complex (RNP). Each N subunit accommodates 9 RNA nucleotides [6]. Only encapsidated RNA is recognized by the RdRP and can serve as template for transcription of the monocistronic genes. Throughout transcription of subgenomic RNAs, the RdRP engages the ribonucleoprotein complex exclusively at the 3´ terminus and transcribes the mRNAs according to a Stop-Start model in an obligatory sequential manner whereby the transcription of a downstream gene relies on the successful termination of the upstream gene. At each gene junction, the polymerase has a chance of approximately 30 % to release the template and terminate the transcription event, initiating anew at the Le sequence. Correspondingly, transcription of the respective genes is attenuated at each gene junction, resulting in fewer transcripts for downstream genes and a transcription gradient N > P > M > G > L [7].

Phosphoprotein P

The phosphoprotein P fulfils multiple roles: it is an essential cofactor of the RdRP, plays an important role for L stability [8], binds to and chaperones nascent N protein and thereby aids in specific encapsidation of the newly synthesized viral RNA [9, 10].

Matrixprotein M

The matrix protein M has two major functions: on the one hand, it is the driving force behind virus particle assembly and budding, mainly by attaching the RNP to the host cell plasma membrane [11-13] and initiating the budding process [14-16]. On the other hand, M is the main interferon antagonist in vesiculoviruses and, together with G, responsible for most of the cytotoxicity [17-19]. Interferon antagonism is enacted in a nonspecific manner at the transcriptional and translational level by a general shutdown of host cell mRNA transcription, export of host mRNAs into the cytoplasm and translation. VSV variants that lack host translation shutdown and interferon antagonism due to one or more mutations introduced into the M gene such as M(M51R), MΔ51, or Mq have been described [17, 18, 20].

Glycoprotein G

The surface glycoprotein G is the sole factor for cell attachment and entry [21]. It is categorized as class III fusion protein and one of the founding members of this class [22, 23]. G mainly utilizes the ubiquitously expressed low-density lipoprotein receptor (LDL-R) family as entry port and therefore shows an extremely broad and pantropic infectivity [24]. This has led to the widespread use of VSV G for transcomplementation of lentiviral vectors. Furthermore, overexpression in itself is sufficient for the "budding" of fusogenic vesicles from transfected cells [25] and has been used for virus-free delivery of diverse payloads, for example Cas9-sgRNA protein complexes, into target cells [26].

Large protein L

The RdRP or Large protein is the main component of the viral replicase machinery, the other part being the P protein, and is responsible for transcription and replication of the viral genome. The L protein is multifunctional; it synthesizes, caps, methylates and polyadenylates the nascent mRNA transcripts which are then, in part mediated by the M-induced shutdown of host translation, in part by sheer abundance and favorable spatiotemporal conditions, preferentially translated by the host cell ribosomes [27-30]. Importantly, like almost all *Riboviria* polymerases, the VSV RdRP has no proof-reading capacity and, consequently, a low fidelity compared to proof-reading polymerases found in higher organisms, resulting in a high mutational load. On the one hand, this limits the maximal viable genome size; on the other hand, it allows the virus to quickly adapt to evolutionary pressure.

Formation of virions

Genome replication is dependent on adequate N-levels [31] and differs from transcription on multiple points. Both genome and anti-genome are tightly encapsidated in N. Full-length, encapsidated genomes associate with P and L, forming the nucleocapsid complex, which is then further condensed by M into a coiled, helical assembly, giving rise to the characteristic bullet-shaped structure. The condensed nucleocapsid is actively transported to areas of the host cell membrane enriched in G [32] where the progeny virions acquire a G-trimer-decorated lipid bilayer envelope by budding. The resulting particle is rod- or bullet-shaped and approximately 185 nm x 75 nm in size [33].

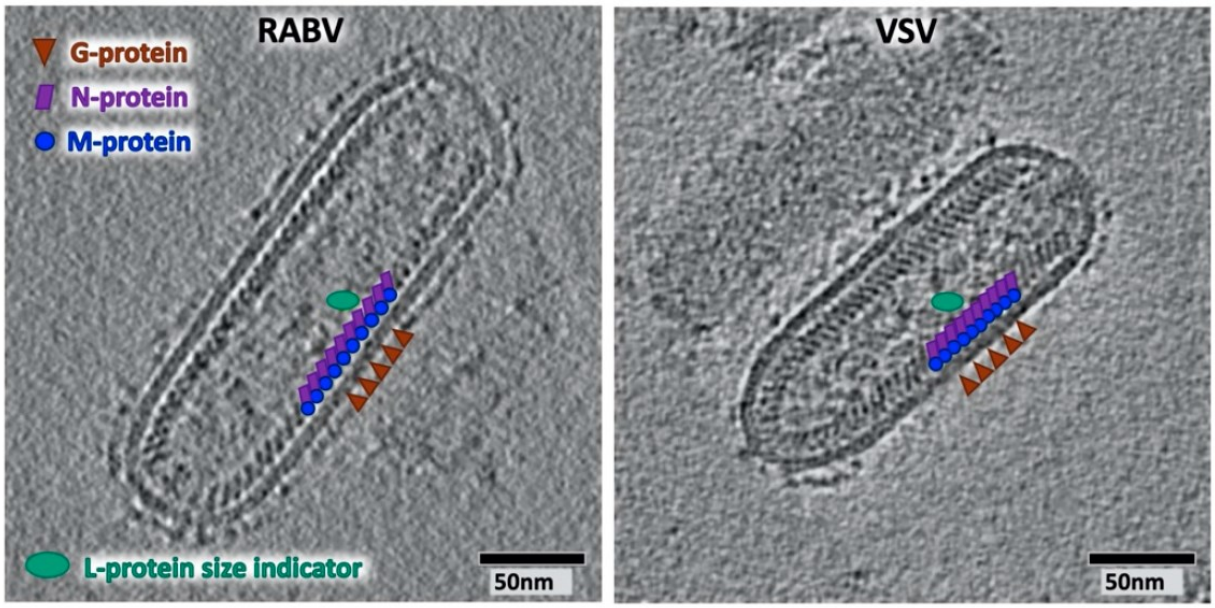

Figure 2: Cryo-EM pictures of rhabdovirus particles (left: rabies virus, right: VSV). The individual proteins are marked by brown triangles (G), violet squares (N), blue circles (M) or turquoise ovals (L). Picture adapted from [34]

VSV life cycle

The viral life cycle starts with the binding of a VSV virion to its cellular receptor LDL-R and the subsequent uptake by clathrin-mediated endocytosis [35, 36]. The acidic pH in the endosomes triggers structural rearrangements in the VSV glycoprotein, activating the fusion machinery and culminating in fusion of viral and endosomal membrane, whereby the RNP sheds the M layer and is liberated into the cytoplasm [37]. During the next step, primary transcription takes place, i.e., transcription exclusively by the machinery that was packaged in the virus particle. The polymerase complex starts transcribing the subgenomic, individual mRNAs from the viral genes, which after translation nucleate additional replication complexes. In the course of infection, N protein levels accumulate and L switches from transcription mode to replication mode, ignoring STOP-RESTART signals in the gene junctions and synthesizing full-length antigenomes and genomes, which are co-transcriptionally encapsidated in N.

Viral RNA synthesis takes place, somewhat shielded from host pattern recognition receptors, in specialized, phase-separated liquid compartments, with expression of N, P and L being sufficient to drive the generation of these characteristic “liquid factories” [38], which correspond to the infamous Negri bodies of rabies virus infected neurons. The viral N, P and L proteins are targeted post-translationally to these factories, where they form new RNPs. These are then transported to viral assembly sites by diverse mechanisms [39] where they are subsequently condensed and coated by M [40]. Budding happens at G-enriched domains in the cell plasma membrane, releasing infectious particles by fission and thus completing the viral live cycle. One infected cell yields 50-8000 progeny

virions [41, 42], which, on the one hand, is very interesting in respect to the sheer variability and on the other hand, explains the rapid spread of VSV in cell culture.

G-deleted virions and transcomplementation

As the G protein is the sole attachment and entry factor for VSV but M is sufficient to drive virion assembly and budding, removal of the G gene from the virus genome by reverse genetics leads to spreading-deficient, non-infectious constructs that are still able to bud "bald" particles, albeit at an approximately ten-fold lower efficiency, expressing no viral glycoprotein on their surface and therefore unable to attach to and infect further cells [43]. These so-called ΔG rhabdoviruses can be transcomplemented or pseudotyped; this means that a functional glycoprotein is offered *in trans*, for example by transient plasmid transfection or by cell lines stably expressing the glycoprotein of choice. While VSV readily incorporates a wide array of different glycoproteins into its membrane, other rhabdoviruses like rabies virus are more stringent in their requirements. Previous work has demonstrated that the rabies virus G-protein derived transmembrane domain and especially the C-terminal, intracellular "tail" is required for interaction with M and subsequent incorporation into budding virions. The thus generated viruses are decorated with G or equivalent, transcomplemented compensatory surface proteins. The G protein acquired during production in packaging cells is sufficient to mediate entry into and infection of the first round of susceptible cells the virions encounter. However, as the virus genome does not contain genetic information to produce these proteins *de novo* and the target cells do not express compatible glycoproteins, no further infectious particles are generated and, consequently, no sequential rounds of infection take place. Under biosafety considerations, ΔG rhabdoviruses are therefore extremely safe. The term "non-replicating viral vector" often used is not strictly true, however, as, these constructs do replicate their genome and express their gene products at a very high level in an infected cell; however in contrast to a full-length or non-deficient virus they are not able to spread further from the original cell. Unlike other "non-replicating" viral vectors that were generated by de-adaption from human cells by serial passaging on non-target cells, i.e., chicken embryos, the rhabdovirus ΔG gene expression machinery is perfectly functional. This replicating, but non-spreading nature is perfectly suited for vaccination approaches, as the immunogen payload of choice is potently expressed and amplified. Another benefit is that they are unable to regain their ability to spread and therefore revert to a pathogenic phenotype by escape mutations, because the coding sequence for the glycoprotein is completely removed, in contrast to being simply mutated.

VSV and interferon

VSV highly sensitive to interferon. While other rhabdoviruses like RABV evolved potent immunoevasive functions and strategies that specifically interfere with multiple steps of the interferon induction and signaling pathways [44], VSV mainly relies on its fast replication and a matrix protein induced general shutdown of host mRNA translation (including interferon and other antiviral gene products) by blocking mRNA transcription and export from the nucleus [45-47]. Probably partially due to constraints in genome size, most virus proteins are highly multifunctional, which can become a two-sided sword from the virus´ point of view, as it limits the amount of adaption and optimization they can undergo to fulfil a single function. M plays indispensable roles in virus budding, which requires it to interact with multiple viral and host proteins [48], relegating interferon antagonism to an ancillary function. The methionine at position 51 (M51) is the key residue for host shut-down and interferon inhibition, and deletion or substitution thereof (ΔM51) leads to highly IFN inducing mutants that still allow for effective budding and primarily unaffected replication in interferon-defective cells [49]. Strikingly, in passaging experiments on interferon-competent cells, VSV ΔM51 was unable to regain this M function and instead developed weak compensatory interferon antagonism by its P protein [47] which again implies that multifunctional viral proteins are heavily restricted in their adaptability to any single function, and, once lost, certain functions cannot be readily reacquired. This is a compelling "safety feature", especially important pertaining to the high-titer use of replication-competent recombinant vectored vaccines in large populations, including immunocompromised individuals.

Uses of VSV

The advent of reverse genetics for nonsegmented negative stranded RNA viruses was pioneered by the seminal rescue of infectious rabies virus from cDNA [33] and the demonstration that rhabdoviruses are able to stably express foreign genes from their genome [50, 51]. These principles were rapidly applied to other *Mononegavirales,* including VSV [51-54], and since then numerous and diverse genes have been inserted into and expressed from the genome of VSV. VSV-based systems have been widely used in the field to study different aspects of not only VSV biology itself [31, 55], but, through pseudotyping [56] of VSVΔG [57] with heterologous glycoproteins also of a plethora of other pathogens. The tropism of these pseudoviruses is determined exclusively by the glycoprotein that is provided *in trans* and therefore reflects receptor usage and tropism of the parental virus. This enables studies on the functions of proteins from highly pathogenic viruses like Ebola virus, Lassa virus [58, 59], Lujo virus [60], or Hanta virus [61] and their interactions with host cells in regard to receptor usage and entry mechanisms under reduced biosafety level conditions. Usually, to allow for tracing and monitoring of

infection, the gene for VSV G is exchanged for a reporter gene i.e., fluorescent proteins, luciferases or other bioindicators.

VSV as vaccine vector

VSV fulfils many requirements of an ideal vaccine vector. Rhabdoviruses in general and VSV in particular have been proposed as vaccine platforms for both infectious diseases and cancer [62]. Owing in part to its relatively small genome size of about 12 kb, it is comparably trivial to manipulate VSV on the genetic level. By exchanging the VSV G gene for one or more exogenous surface glycoprotein or other genes of choice, one basically creates a VSV that completely relies on the foreign glycoprotein for entry but retains its other properties that make it such a well-suited vaccine vector. First, the replication in the cytoplasm without a DNA stage, which is an important safety aspect, as integration into the host genome with consequent persistence and or transformation of cells is not possible.

Second, the strong induction of innate immune responses and activation of both cellular and humoral immune pathways with the first biased towards a protective Th1 response [63].

Third, the replication and growth to high titers in almost all routinely used cell types when complemented with a functional glycoprotein (*in cis* or *in trans*), which allows for easy propagation and makes VSV-based viral vector production highly scalable. This point is of special significance as it is one of the key determinants separating interesting, hypothetically useful approaches from successful concepts translated into real-world feasibility. In the context of a VSV-based HIV vaccine, it has been suggested (somewhat optimistically) that one liter of cell culture supernatant could suffice to vaccinate one billion people [64].

Additionally, only four VSV genes remain after replacement of G, all of which are relatively well characterized and understood. Importantly, it has been speculated that, compared to other vector systems, the remaining VSV gene products compete less for the attention of the immune system, instead allowing it to “focus” on the foreign glycoprotein. In a study comparing the immunogenicity of the HIV envelope protein (env) when expressed from VSV or from a vaccinia virus based viral vector, humoral and cellular immune responses to HIV env appeared 6-10 fold higher when expressed from VSV [64], which might be a reflection of the fact that vaccina virus encodes about 200 proteins of its own, all of which might be immunogenic to some degree.

Together with the very low pathogenicity for humans and a low seroprevalence in the majority of the population, these traits make VSV a very promising vaccine vector candidate. An additional boon is the already mentioned ability to switch envelopes which allows to almost completely mitigate or circumvent either pre-existing or exposure-induced vector-specific immunity as neutralizing antibody

(Ab) responses against VSV are almost entirely directed against G [65]. More in-depth assessments of VSV as a vaccine vector have been extensively reviewed elsewhere [66-68].

VSV-based vaccines were designed, generated and tested against an impressive range of viral pathogens, including, but not limited to Marburg virus (MARV)[69], Lassa virus (LASV)[70], Crimean-Congo hemorrhagic fever virus (CCHFV)[71], Nipah virus (NIV)[72], Zika virus (ZIKV)[73], SARS-1, SARS-2, and MERS coronaviruses [74-77] and, recently, influenza virus [78]. In all studies, the antiviral response has been found to be very robust, almost exclusively directed against the chosen immunogen, defined by a strong induction of both binding and neutralizing antibodies (nAb), safe and well-tolerated and, above all, effective and protective against the respective pathogen in all cases. A recent comprehensive review on this topic can be found here [68].

The trailblazer and, to date, sole VSV-based vaccine approved for human use, however, is the rVSVΔG-ZEBOV-GP Ebola vaccine or Ervebo®, a vaccine for the prevention of Ebola virus disease (EVD) that has been approved by the U.S. Food and Drug Administration (FDA) on December 19, 2019. Originally simply envisioned as a vector for expression of Ebola glycoprotein GP to investigate its pathogenicity in mice back in 2004, it soon became apparent that vaccinated mice neither developed EVD-like symptoms after rVSVΔG-ZEBOV-GP inoculation nor were they susceptible anymore to an otherwise lethal mouse-adapted EBOV strain [79]. The rest, as they say, is history. However, another decade went by until the first world felt sufficiently threatened by the 2014 Ebola epidemic in Western Africa to push for a vaccine in earnest. Twelve fast-paced clinical trials later the world had its first VSV-based vaccine for human use, which then proved to be an invaluable success.

A key aspect of every trial is the generation and evaluation of safety data; this is especially important for replication-competent viral vectors introduced to immunocompromised individuals. Ebola outbreaks most often happen in vulnerable populations with a high HIV incidence. Fortunately, rVSVΔG-ZEBOV-GP was well tolerated in immunocompromised mouse and non-human primate models, but vaccine efficacy was significantly reduced and protection upon challenge with EBOV was achieved only in two thirds of the animals [80]. Safety- and efficacy data in HIV-positive humans so far is limited; preliminary results indicate a benign safety profile with no increase in severe adverse events (SAE) compared to the placebo group but unfortunately also a reduced immune response with a decreased induction of protective antibodies [81].

Even though rVSVΔG-ZEBOV-GP was administered as a single-shot vaccine in all clinical trials as well as in emergency “real world” use during recent outbreaks, estimated efficacy was reported between 97 and 100 %, which underlines the potency of VSV as a vaccine vector even against extremely aggressive and virulent pathogens. Adding to that, the safety profile so far has also been very favorable with no

unresolved SAE even in children and women unknowingly pregnant at vaccination, leading regulatory bodies to offer vaccination to infants as well as pregnant and lactating women who are contacts of confirmed EVD cases [68].

Drug-controllable VSV: The SMASh system

Unfortunately, while VSV has many advantageous traits for the above biomedical prophylactic and therapeutic approaches, effective and specific directly acting antiviral drugs or other control measures to stop replication and spread of rVSV are not available. Especially considering administration as a vaccine in immunocompromised individuals or potentially hazardous high-dosage therapy when used as an oncolytic agent, application of replication-competent viral vectors demands increased caution. The importance of this is stressed by a recent report of a fatal case of vaccine-associated disseminated measles [82]. Even though such cases are extremely rare, each and every one of them is a tragedy that should be prevented at all costs. Therefore, a possibility to control and if necessary to stop replication of viruses used as vaccine vectors or therapeutics would be highly advantageous. Alas, RNA viruses are not amenable to conditional recombinant DNA techniques, and RNA interference or RNA CRISPR is poorly effective against rhabdoviruses like VSV due to the inaccessibility of their tightly packaged RNP genomes [83-85]. However, a viable option to control virus growth of rhabdoviruses is by targeting of essential viral proteins, a strategy already successfully employed for negative-strand RNA viruses like measles virus [86], influenza virus [87] and rabies virus (Ghanem, Eklund, Pfaffinger, personal communication) and, recently, also VSV [88]. A variety of systems for targeting proteins to the lysosomal and proteasomal pathways for degradation are available, such as PROTAC/SNIPER, FKBP12-, or Auxin-inducible degron (AID) technologies, but delivery of regulators is demanding [89, 90].

A promising possibility is the Small Molecule Assisted Shutoff (SMASh) system [86]. The SMASh system is based on a self-cleaving protein tag that consists of a drug controllable protease and a degron mediating quick proteolytic degradation, both derived from hepatitis C virus (HCV). By fusing the tag via a linker containing the protease cleavage site to a protein of interest it is possible to control the expression levels of the protein. In the absence of HCV protease inhibitors like Danoprevir® (DNV), the protease cleaves the linker and thereby excises itself and the degron from the protein of interest, is targeted to the proteasome and quickly degraded. In presence of the inhibitor, the protease activity is blocked, the tag with the degron remain fused to the protein of interest and the whole construct is targeted to the proteasome and degraded.

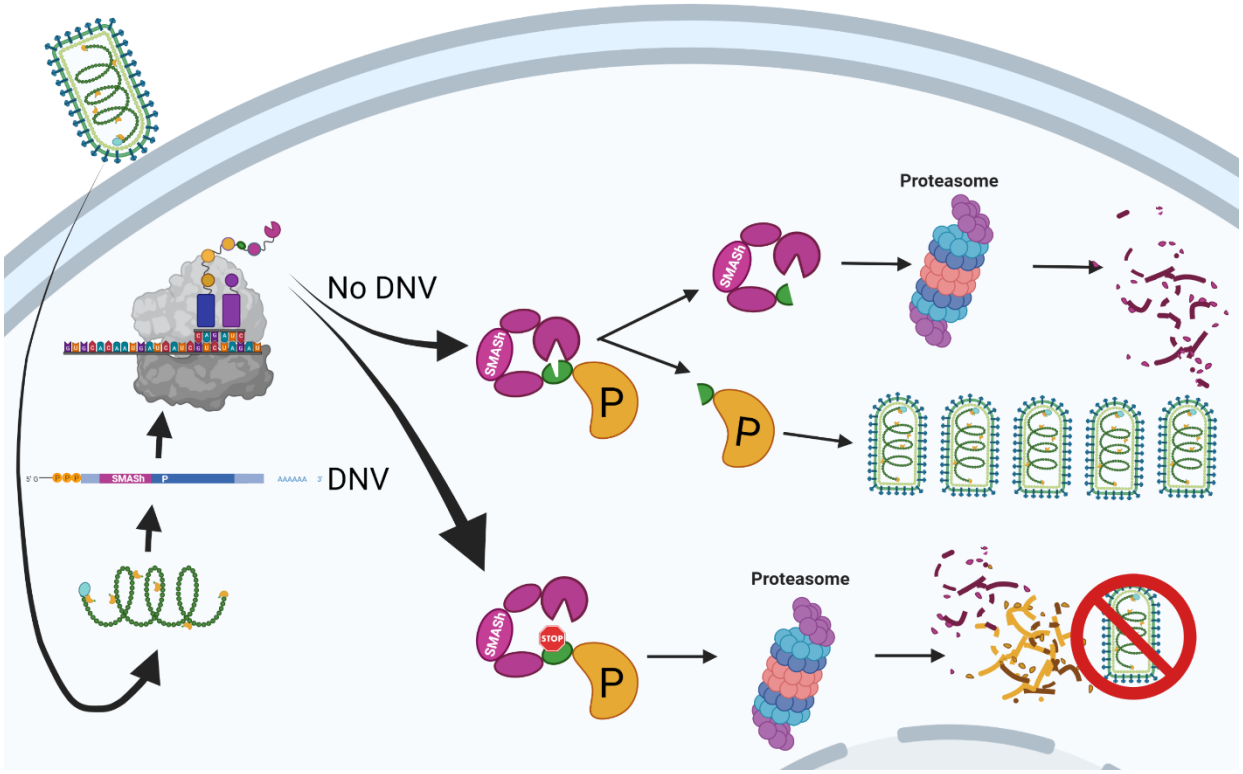

Figure 3: The SMASh system adapted to VSV. By fusing the SMASh-tag to the essential viral protein P, VSV replication becomes drug-controllable. In the absence of a HCV protease inhibitor, the protease is active and autocatalytically removes itself and the majority of the SMASh-tag, including the degron sequence, from P. P is then able to fulfill its role in the viral life cycle and the virus is replicating. When the inhibitor is present, the SMASh tag remains fused to P, rendering it nonfunctional and targeting it for proteasomal degradation. Consequently, virus replication is stopped.

To achieve control over VSV replication, the tag is genetically fused to an essential viral protein that tolerates N- or C-terminal tagging, such as P. Without inhibitor, the active protease excises the SMASh-tag from P. The tag is then degraded, and P fulfils its role in the viral life cycle, enabling the virus to replicate normally. Upon addition of the drug, the protease is inhibited, the tag remains fused to P and the entire construct is targeted to the proteasome, leading to degradation of all newly synthesized P molecules. This freezes all further virus replication, as no new RNPs can be formed due to the lack of functional P. The pre-existing RNPs remain active, but are naturally decaying, tapering virus activity until no operational RNPs remain and the virus is “dead”. As the system is protein-based, removal of the drug while P is still actively translated should restart the virus. The ability to control expression of VSV vectors by approved small molecule drugs, and to halt and cure infections *in vitro* and *in vivo* would represent an important safety feature for VSV based biomedicals. This is of utmost importance in high titer applications in highly vulnerable populations, i.e., oncolytic virotherapy and vaccination of immunocompromised persons.

Interim summary VSV

Focusing on the data generated by the ERVEBO trials, VSV has proven to be a tolerable, safe vaccine vector system. However, residual toxicity remains, as demonstrated by side effects like arthritis that led to termination of some of the trials. However, generally, the vaccine proved to be safe, importantly also in children and when used inadvertently in pregnant women, leading to the offer of vaccination to pregnant or lactating women and children under 12 months of age. Protection offered by the vaccine was shown to be almost perfect and the immune response robust and long-lasting with antibodies remaining detectable for at least two years. and vaccine satisfaction was high. Conclusively, these data illustrate the suitability of VSV as a vaccine vector. Spreading-deficient and drug-controllable engineered versions of VSV would address the remaining Achilles Heel of replicating VSV by increasing vector safety.

SARS-CoV-2

The coronavirus disease 2019 (COVID-19) pandemic, caused by a novel betacoronavirus that emerged the end of 2019, is the by far most devastating calamity afflicting humankind in the 21st century. By end of September 2021, 21 months after the first reported cases, 232.861.440 people have contracted SARS-CoV-2 and 4.747.341 individuals succumbed to COVID-19. Third time´s a harm, in this case, as the causative agent, severe acute respiratory syndrome coronavirus 2 (SARS-CoV-2), is the third highly pathogenic betacoronavirus spilling over into human population in the third millennium [91-93]. With a 79.5 % identity at the nucleotide level, SARS-CoV-2 is a close relative to the original SARS virus that was responsible for a notable, but quickly contained outbreak in 2003 [94, 95] and Middle Eastern respiratory syndrome coronavirus (MERS-CoV, 50 % identity) [96] which was first reported in 2012 but so far has been limited to under 3000 cases.

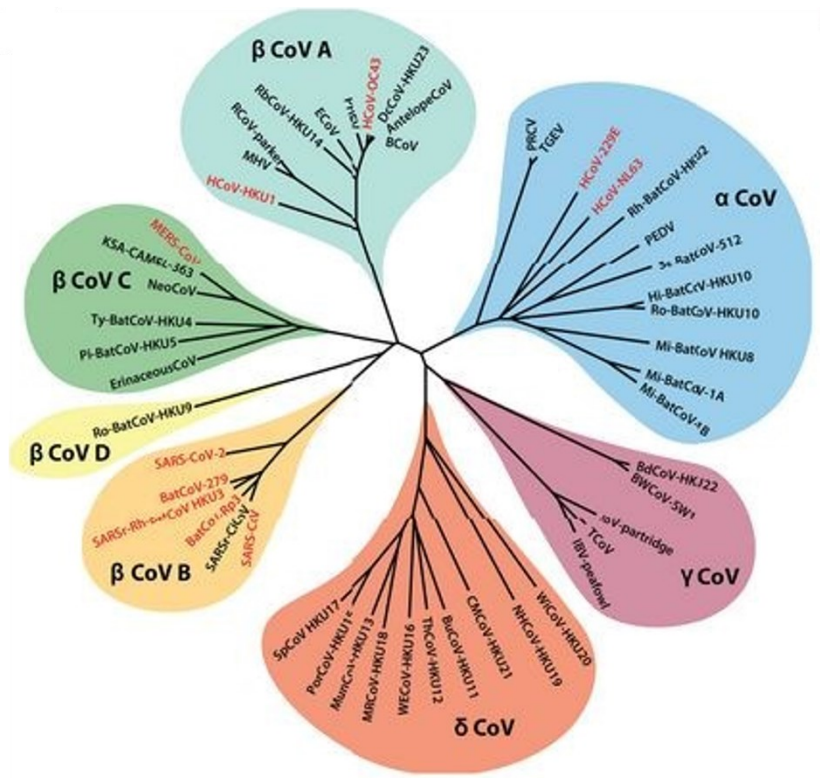

Figure 4: Phylogeny tree of 50 coronavirus sequences, adapted from [97].

Although the case fatality rate for the first two is markedly higher than for SARS-CoV-2, the latter is much more transmissible: By end of February 2020, already 83.256 cases had been reported to the World Health Organization (WHO), surpassing the case number of the entire 2002-2003 SARS-CoV-1 outbreak by tenfold. The origins of SARS-CoV-2 are still under investigation and topic of heated debate [98-101]. In December 2019, the first cases of viral pneumonia of unknown cause in Wuhan City, a

metropolis of 10 million inhabitants and the capital of China´s Hubei Province, were reported to the WHO. Some three weeks later, on January 23, 2020, a first putative genome of the novel coronavirus suspected to be responsible for these cases was uploaded to GenBank by the Wuhan State Key Laboratory of Virology (GenBank: MN988668.1). Following reports of human-to-human spread [102, 103] and the observation that non- or pre-symptomatic hosts are still infectious [104] the WHO declared COVID-19 a global pandemic on March 11, 2020.

SARS-CoV-2 is a positive-strand RNA virus and a member of the order *Nidovirales*, which are notable for having the longest RNA genomes described to date. Almost immediately it was predicted and shortly after demonstrated that SARS-CoV-2 relies primarily on the same entry receptor as SARS-CoV-1, namely angiotensin-converting-enzyme 2 (ACE2) [92, 105]; however with a markedly higher binding affinity to human ACE2 (hACE2) [106] which is consistent with the higher infectivity in humans observed for SARS-CoV-2. Building on previous work on SARS-CoV-1 and MERS, key findings could be translated to SARS-CoV-2 and provided valuable blueprints and insights for the development of COVID-19 vaccines. Perhaps most importantly for vaccination approaches, Buchholz and colleagues had shown that the SARS-CoV-1 surface spike (S) glycoprotein is the only virus protein that stimulates the production of virus neutralizing antibodies (VNAbs) [107], which are crucial for most vaccine approaches. Accordingly, S is the main target of current COVID-19 vaccines and vaccine candidates [108] and VNAbs are established in the meantime as a major correlate of protection after infection or vaccination against COVID-19 in humans and animal models [109-114]. A high-resolution structure of the SARS-CoV-2 Spike protein was soon solved and published [115] as well as confirmation that the SARS-CoV-2 Spike and especially the RBD are targeted by VNAbs in the sera of convalescent patients [116, 117].

SARS-CoV-2 Spike

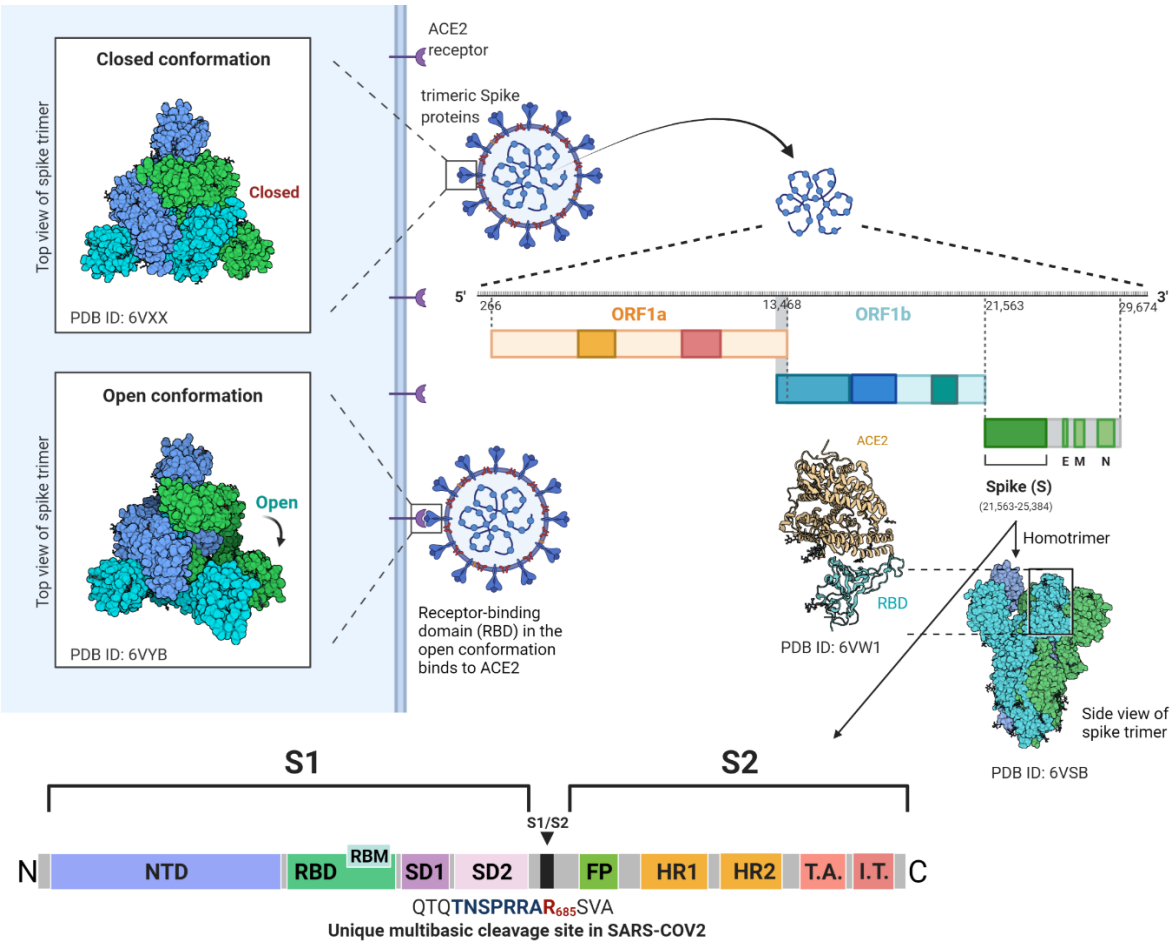

Figure 5: S is the main surface protein of SARS-CoV-2 and responsible for receptor recognition, attachment, and entry. It is a homotrimer encoded by an open reading frame (ORF) immediately downstream of ORF1a and ORF1b. The receptor binding domain (RBD) of the S is mediating binding of S to ACE2. It can be oriented in an open, "up" and closed, "down" conformation, with at least one RBD protomer in the "up" conformation necessary for receptor binding. The S is functionally comprised of the S1 domain, consisting of the NTD, RBD and two additional conserved subdomains. The S2 domain contains the fusion machinery, the trimerizing stem, transmembrane anchor, and intracellular tail. S1 and S2 are connected by a multibasic cleavage site (S1/S2). NTD: N-terminal domain; RBD: receptor binding domain; RBM: receptor binding motif; SD1, SD2: subdomain 1 & 2; FP: fusion peptide; HR1, HR2: heptad repeat domain 1 & 2; T.A.: transmembrane anchor; I.T.: intracellular tail.

The trimeric class I transmembrane protein S is the primary determinant of coronavirus tropism and transmission. The 1273 amino acid (aa), 180 kilodalton (kDa) S precursor protein consists of two main subunits, the N-terminal S1 and C-terminal S2 and is processed by cellular proteases into the mature form, in which S1 and S2 are non-covalently associated in a metastable prefusion state [118-121]. S1 contains a N-terminal domain (NTD), the receptor-binding domain (RBD, residues 331-524), and the conserved subdomains 1 and 2 (SD1 and SD2) with the notorious polybasic S1/S2 cleavage site located at the end of SD2. The RBD is mediating attachment of the virus to the main cellular receptor, ACE2 [115, 122] and is the main determinant of cell tropism. The receptor binding motif (RBM) inside the RBD are the residues that directly contact ACE2.

S2 forms the trimeric stalk and contains the fusion machinery, which is partially shielded by the S1 domains with the RBDs [123, 124]. Binding of the RBD to the receptor leads to shedding of the S1 domain, which unmasks the S2´ site and enables proteolytic cleavage by furin [125], cathepsins [126] or serine proteases like transmembrane protease serine 2 (TMPRSS2). Subsequent liberation of the fusion peptide results in profound structural rearrangements, virus-target cell membrane fusion and finally release of the viral RNA genome into the cytoplasm [127]. Molecular differences to SARS-CoV-1 S include aforementioned higher binding affinity of the RBD to the ACE2 receptor [115, 122, 128] and the presence of a multibasic (Asn-Ser-Pro-**Arg-Arg**-Ala-**Arg**$_{685}$↓-Ser-Val-Ala) insertion between S1 and S2 which forms a functional minimal recognition site for furin [106, 120], an ubiquitously expressed host cell protease. This results in vastly improved proteolytic maturation and transport of the protein in human cells [91, 118, 119]. Together, these factors likely contribute to an extended host and organ range and the high contagiousness of SARS-CoV-2 in humans [129-131]. The spike is incorporated into the virus membrane in homotrimers with the three RBDs on "top". An individual RBD has two major states, "up" or open and "down" or closed, and intermediate swing states in between. The three RBDs of a S trimer can consequently either be 3 down, 2 down 1 up, 1 down two up or three up, however for the original Wuhan spike mainly the first two conformations are observed. To engage ACE2, at least one RBD is required in the "up" conformation.

The SARS-CoV-2 Spike RBD

Due to the high similarity between SARS-CoV-1 and SARS-CoV-2 most of the insights on the former could be adapted and translated to the latter. Like SARS-CoV-1, SARS-CoV-2 utilizes ACE2 as cellular entry receptor. Recognition and binding to ACE2 is mediated by the S RBD. The RBD is in the C-terminus of the S1 domain, spanning residues 319-541 [132]. Residues 437-508 form the RBM and convey the direct interactions with ACE2.

A major finding that could be transferred to SARS-CoV-2 is that expression of the SARS-CoV-1 RBD on its own is translated into a correctly folded subunit protein that is readily recognized by antibodies against the RBD in a "natural" context, i.e. the whole spike protein, and, importantly, vaccination with RBD constructs can elicit long-lasting and highly protective antibodies able to neutralize SARS-CoV-1 efficiently [133].

An early study on recombinant SARS-CoV-2 RBD found that it retains its ability to bind hACE2, can inhibit attachment of both the SARS-CoV-1 RBD and SARS-CoV-2 RBD to ACE2 by competition and is recognized by some SARS-CoV-1 specific antibodies. Intriguingly, it was also reported that SARS-CoV-1 RBD-induced antisera could cross-neutralize SARS-CoV-2 [128], emphasizing the validity of RBD-based vaccines and hinting at a robust immune recognition, even though the identity between the two RBDs

is only 75 %. Additionally, while there have been findings that full-length S can induce detrimental antibodies that can enhance infectivity of SARS-CoV-1 *in vitro* [134], no such observations were made with RBD-based vaccines. A further benefit is the, compared to full-length S, small size while retaining most protective epitopes [135-137].

In a study comparing immunogenicity and antibody signature of different SARS-CoV-2 S subunits (S ectodomain (S1+S2), S1, RBD, S2) it was found that all immunogens except the S2 domain were able to induce neutralizing antibodies. Intriguingly, the RBD-elicited antibodies showed a five times higher affinity to native S antigens compared to the other immunogens (i.e. S ectodomain, S1 and S2) which also strongly correlated with neutralizing titers [138].

Induction of distinct antibody classes directed against S

Infection with SARS-CoV-2 or vaccination leads to the induction of a neutralizing, protective antibody response targeted against the S protein. So far, a very limited number of regions on the S (two located in the S1 subunit, one in S2) have been described as valid and vulnerable targets for neutralizing antibodies: the NTD and the RBD in the S1 domain and, recently, the fusion machinery stem helix in S2 [139-141]. The latter is the target of very weakly, but broadly acting nAbs and has not been in the focus of research as much as the other two sites of vulnerability.

RBD-binding Abs can be divided into four classes, depending on their mode of binding, competition with ACE2 and the accessibility of their epitope. Class-1 and class-2 Abs interfere with ACE2 binding, class-3 and class-4 Abs do not. The epitope of class-1 and class-2 Abs is located withing the RBM; consequently, they compete with and can block binding of ACE2. While the binding site for class-1 Abs is accessible only in the RBD-up conformation of S, the epitope of class-2 Abs is also accessible in the RBD-down state. Class-3 Abs bind the RBD outside of the RBM in all orientations, whereas class-4 Abs recognize a cryptic epitope accessible only in the RBD-up conformation [142, 143]. Class-1 to -3 Abs show a characteristic and specific reduction in binding to diverse RBD mutants whereas the class-4 epitope shows significant conservation throughout SARS-CoV-2 and its variants, SARS-CoV-1 and MERS [144, 145].

Prevalent mutations and variants

The RdRP of RNA viruses is generally very error prone, partly due to the lack of a proofreading function. Per round of replication, the misincorporation rate is at approximately 10^{-6} - 10^{-4} per base [146-148]. This has important implications: on the one hand, during replication in a host cell, the virus is present in so-called quasispecies, i.e., a multitude of virus genomes with slight variation in their mutational profile. While most mutations either have no or even a detrimental effect, a few might impart

increased fitness of the virus and adaption to external stressants. If the benefit is large enough, these variants are selected naturally, accumulating in the viral population and in time becoming the main isoforms. This allows RNA viruses to readily adapt to new environments and circumstances, for example after a spillover into a new host species, if given enough replication cycles. On the other hand, it limits their maximal genome size, because the chances for an error-free replication of the genome quickly diminish with increasing genome length, and an accumulation of deleterious mutations quickly results in a so-called "error catastrophe", abrogating viral viability [149]. Consequently, genome size of RNA viruses is usually limited to 12-15 kilobases, with the average length being well below that at 9 kb [150].

SARS-CoV-2 is different. *Coronaviridae* are part of the order *Nidoviridales*, which includes viruses with the longest RNA genomes described so far (with an impressive maximum genome size of 41kb for Planarian secretory-cell nidovirus (PSCNV)). What sets the long apart from the short is a proofreading 3´-5´ exonuclease activity termed ExoN that was first identified and described in SARS-CoV-1 [151, 152]. It has since been found in the "longest" eight out of the fourteen families that are members of the *Nidovirales* order [153] (and in *Arenaviridae*). By cleaving erroneously incorporated 3´ nucleotides during the replication process, the ExoN activity increases fidelity by ~21-fold and therefore vastly improves genome stability [154]. As a result, SARS-CoV-2 has a relatively low mutational activity; however, the sheer number of hosts invariably leads to improved adaption and escape from immune pressure.

Spike D614G

The first mutation to appear and almost completely supersede the parental Wuhan strain was a simple A-to-G point mutation at nucleotide position 23403 of the original Wuhan reference strain. This causes an aa change from aspartic acid (D) to glycine (G) at aa residue 614 in the S protein, or in short S: D614G [155]. D614 is in the SD2 of the S1 subunit, and the substitution to glycine has since been shown to increase S stability and incorporation into virus particles and importantly, also virus infectivity. G614 stabilizes the trimeric prefusion state and reduces premature spontaneous transformation into the postfusion state. While 75 % of recombinantly produced D614 spike proteins are present as postfusion S2 trimers and shedded S1 monomers and therefore not able to mediate infection, almost all G614 spikes are described to be in the trimeric prefusion conformation and able to facilitate infection [156]. Additionally, the RBDs in the S trimer can be oriented either in a "up" or "down" conformation, whereby only the "up" conformation exposes the receptor binding motif and is needed to engage ACE2. Typically, the S trimer is transferring between a 3-RBD-down or "locked" conformation and a 1-RBD-up-2-down "open" conformation. In spikes carrying the D614G mutation,

the probability for the 1-RBD-up conformation is increased [157], which augments receptor binding and therefore infectivity [158].
Conversely and fortunately, it also leads to an increased susceptibility to neutralization by RBD-binding antibodies by the same principles that make it more infectious, i.e., an enhanced predisposition for an "open" conformation with an exposed receptor-binding motif [159].

Spike 681H/R

The next most common, recurrent mutations are located around the S1/S2 cleavage site, at residue 681 [160-162]. The original proline is frequently mutated to histidine (P681H, present for example in the B.1.1.7 or alpha lineage of strains), arginine (P681R, present in the B.1.617 lineages delta and kappa) or leucine. Surprisingly, no change in phenotype could be linked to the P681H mutation found in alpha and multiple other strains to date [163], arguing for the possibility that their high prevalence is mainly due to "being on the right strain at the right time". Conversely, the substitution of P681 to arginine appears to have a more profound impact. Recent studies on the SARS-CoV-2 delta variant correlate an increase in infectivity and viral fitness to more efficient furin processing mediated by the P681R substitution [164-166]. The P681R mutation is also present on the recently emerging strain A.23.1 that is prevalent in Uganda and Rwanda [167, 168], possibly being one of the driving forces behind the regional dominance.

Spike N501Y

A further, recurrent and abundant mutation is N501Y, and it has been demonstrated to have a major impact on ACE2 binding. It is a highly recurrent mutation and evolved convergently in the main 501Y lineages of SARS-CoV-2 (501.V1/B.1.1.7/alpha; 501.V2/B.1.351/beta; 501.V3/P.1/gamma). N501 is located within the RBD and one of the residues directly interacting with ACE2. Substitutions at residue 501 have been reported as early as August 2020 [169] and mutation to Y (N501Y) has been shown to increase transmissibility [170, 171] by enhancing binding affinity to ACE2 by four-to-ten-fold [171-177]. Additionally, while mice are non-permissive for SARS-CoV-2, the N501Y mutation also increases S affinity to mouse ACE2 and therefore plays a pivotal role in adaption of SARS-CoV-2 to mice [178]. Fortunately, the mutation is not immune-evasive and does not cause a marked decline in the neutralizing titers of convalescents or vaccinees by itself [179].

Spike K417N/T

K417 is also located in the RBD, but not interacting directly with ACE2, and substitutions to T or N are present in the variants of concern beta and gamma, and, from April 2021 on, repeatedly emerged also

in sequences assigned to B.1617.2 or delta [180]. Unlike N501Y, K417N/T decreases the affinity to ACE2 and is found mostly in combination with N501Y, which has been shown to rescue binding to ACE2. K417N/T is associated with evasion from some monoclonal antibodies (mAbs). It is located within the epitope recognized by class-1 RBD targeting antibodies and forms multiple key interactions that are severely compromised by mutation to N or T [143]. Binding and neutralization efficacy of these antibodies is consequently reduced or abrogated [144]. The delta variant with K417N (termed delta+) has been shown to be significantly more resistant to neutralization by polyclonal vaccinee serum compared to kappa (B.1617.1) and delta, decreasing neutralizing titers 2-3 fold compared to the parental variants [166].

Spike E484K/Q

Residue E484 is part of an immunodominant epitope recognized by class-2 RBD nAbs and plays a key role in the neutralization efficacy of human convalescent and vaccinee sera. Substitution to K has been shown to destabilize the of the RBD tip, which in E484 acquires a “Hook-like” conformation and is integral to the binding of class-2 Abs. In K484 mutants, the “hook” region instead assumes a predominantly disordered state, abrogating recognition and binding of these Abs [181]. As the neutralizing antibody response of COVID-19 convalescents is primarily dominated by class-2 nAbs, substitution of E484 (as seen in beta and gamma) has been found to have the biggest impact on serum neutralizing activity [144, 182]. Binding of class-2 antibodies to recombinant E484K-RBD constructs is severely compromised [143, 183], explaining partial escape of neutralization by polyclonal sera [179, 184-188].

NTD mutations

All antibodies with neutralizing capacity targeting the NTD recognize the same antigenic supersite [189, 190], which comprises five exposed loops termed N1-N5 [191] corresponding to residue stretches 14 to 26, 67 to 79, 141 to 156, 177 to 186, and 246 to 260. The epitope is structurally surrounded by four N-linked glycans at N17, N74, N122 and N149. Mutations and especially deletions in that region potentially alter the conformation of the whole supersite and are occurring at a high rate [192]. Even more problematically, the deletions in the NTD found on multiple evolving strains, most importantly the VOCs alpha, beta and delta, are able to almost completely (alpha) or completely (beta, delta) abrogate neutralizing activity of all NTD-targeting nAbs characterized so far. Even a recently described NTD Ab, which retains binding to beta and delta is escaped by the deletion of residue Y144 (Δ144) present in alpha and some delta strains [166], questioning the utility of the neutralizing NTD epitope for the induction of a robust and cross-reactive antibody response [193]. In contrast, the higher number of independent epitopes in the RBD results in reduced susceptibility to mutational escape and

abolished binding is usually limited to subclasses of mAbs [194], although artificial escape RBDs have been demonstrated [195, 196].

Challenges

Due to the dynamic landscape of host-adaption and immune-evasion driven SARS-CoV-2 mutations and the large number of infected hosts, a critical and informed choice of vaccine targets is of superior importance. Suboptimal epitopes and/or constructs have the potential to have a detrimental effect with a reach far surpassing the immediate consequence for the vaccinee, especially in the age of vaccination skepticism and social media, where fake news and alternative truths can spread like a wildfire. Narrowing down the immunogen from the full-length spike down to the RBD has both advantages and dangers. On the on hand, the focus on a small stretch with a high density of neutralizing epitopes can increase both safety and efficacy, which are the hallmarks of successful vaccination. On the other hand, losing out on other protective epitopes can lead to a higher susceptibility to immune escape by mutated viruses and breakthrough infections. The breadth and robustness of the immune response to RBD immunogens in regards protection from variants remains to be examined.

To combat the pandemic, effective, protective and safe vaccines are desperately needed, and although the currently approved mRNA vaccines so far do an impressive job, availability is still an issue, especially in developing countries, where in addition to all obvious problems it can be very challenging to maintain a -80°C cold chain. On that note, VSV has been demonstrated to be quite robust in demanding physical conditions [197].

Displaying the SARS-CoV-2 RBD

Taking this all together, using the RBD as immunogen instead of full-length S, other S-based subunit vaccines or even other SARS-CoV-2 proteins would appear as a valid rationale. Unfortunately, the isolated, soluble SARS-CoV-2 RBD was described as having a poor immunogenicity as a subunit vaccine by multiple reports, with RBD-based systems either requiring multiple applications or very high doses in combination with adjuvants to elicit satisfactory neutralizing antibody titers in mice [198-201].
There is, however, the age-old conundrum of mice and men to consider, and findings in mouse models are not necessarily directly transferable to primates in general and humans in particular.
A recent study comparing different S subunit vaccines in different vaccination regimens in mice and nonhuman primates came to some interesting findings: On the one hand, their results are consistent with previous data: In mice, RBD-based prime immunization was inferior in terms of immunogenicity compared to full length S, with reduced germinal center and T follicular helper cell activity. Boost

immunization of S-primed mice worked equally well with S and RBD, with the RBD-boost having the upper hand in VNAb induction.
On the other hand, and very importantly, the difference was not seen in macaques, with RBD and S prime immunization working equally well and inducing VNAb levels generally surpassing those of convalescent COVID-19 patients [202]. Although this indicates that the RBD might be a sufficiently good immunogen on its own in primates, there is considerable room for improvement.

Successful immunization culminating in beneficial activation of the immune system and induction of protective immunity, both cellular and humoral, relies on two key principles: The provision and display of native, conformationally correct antigens of biologic relevance and doing so in a way that is as immunogenic as possible [203]. The choice of antigen(s) is the foundation for all that comes after; fortunately, it turned out that for SARS-CoV-2 it´s not as complex a task as for other pathogens (i.e., RSV or HIV-1) and even suboptimal antigens like the labile native, non-stabilized, full-length S used by some first-generation vaccines and vaccine candidates provide acceptable protection.
To minimize the induction of non-beneficial and potentially detrimental antibodies and following the rationale elucidated earlier, the RBD remains a promising target. The challenge is how to best present it in a relevant, native way optimizing the immune response and inducing robust, long-lasting protection.
To find an archetype of a highly efficient system for presenting viral antigens one needn´t look far: During eons of coexistence, in an ongoing evolutionary arms race with “survival” and “reproduction” as strong incentives, the immune system and pathogens have fought and adapted to each other, and the immune system has “trained” and evolved to recognize foreign or novel antigens presented on pathogens and infected, transduced or otherwise transformed cells. Therefore, when aiming for immunization against a pandemic, highly successful virus pathogenic for humans, it is only logical to make use of a viral vector system that is readily recognized and eliminated by said human host. VSV is one such vector system, and that the approach is feasible has been demonstrated by the success of the VSV-based vector vaccine Ervebo® providing (almost) complete protection against EVD.

Three key properties make viruses highly immunogenic [204, 205]:

(a) The surface of many viruses is highly ordered and repetitive. This is especially true for small viruses whose capsid structure relies on the oligomerization of a limited number of distinct proteins
(b) Representing ancient natural nanotechnology, their size allows for transportation to B cell follicles directly by lymph without any cellular transport and therefore intact. Consequently, they can interact with B cells in their native form. Additionally, by presenting a highly repetitive

matrix of immunogens on their surface they can crosslink B cell receptors and thereby strongly activate B cells.

(c) The ability to trigger pattern recognition receptors (PRRs) that evolved to detect them in the first place. This activates the innate immunity and the complement cascade which in turn enhances both magnitude and duration of IgG responses and leads to isotype switching.

Viruses, especially those with an RNA genome, have typically a very limited coding capacity, with genomes averaging 9 kb in size for *Riboviridae* and *Coronaviridae* as an extreme outlier clocking in at 29 kb. Accordingly, they have only a limited number of unique proteins to their disposal for their whole life cycle and therefore rely on the oligomerization of just one or two proteins for forming their envelopes and cores. This has the consequence that they possess tightly packed, quasi-crystalline surfaces made up of highly ordered, repetitive structures [203]. The number of unique building blocks and the repetitiveness of a structure necessarily correlate inversely. As such extracellular structures are virtually absent in the vertebrate body, the immune system has evolved to detect antigens organized this way as a foreign structure associated with pathogens or pathogen-associated structural pattern [204]. Additionally, arrays of evenly spaced antigens can crosslink specific B cell receptors (BCRs) on B cells, which amplifies B cell activation and can lead to a T cell independent IgM response [206]. Thus, proteins expressed in a uniform, repetitive array are more readily recognized and more immunogenic that soluble ones. The optimal "packing" density is thought to be 20-25 epitopes spaced by 5-10 nm [207], which, unsurprisingly, corresponds very well to epitopes presented on many viruses and virus-like particles (VLP) [208].

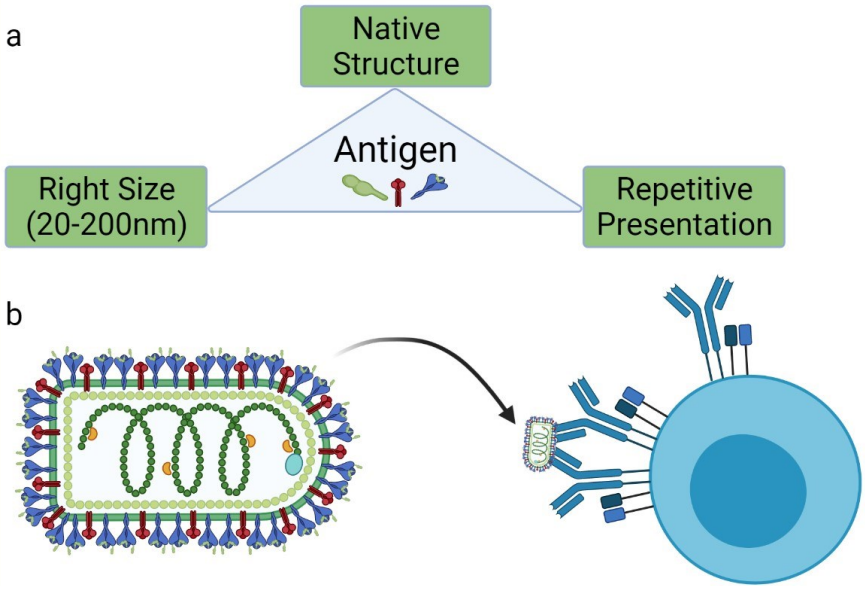

Figure 6: A: Key determinants of antigen quality and immunogenicity. Antigens presented in their native, intact structure are most relevant for an effective and potent immune response. Presentation in a repetitive manner leads to an improved immunogenicity while sizing in the 20-200 nm range allows for direct transport to B cells. B: Antigens decorating viruses and VLPs combine these properties and can further activate B cells by BCR-crosslinking [203].

The rhabdoviruses VSV and RABV also display such highly immunogenic antigen arrays, and additionally they bud even in absence of a functional glycoprotein [43, 209], effectively creating non-infectious, "VLP-like" particles. Reverse genetics approaches are an established technique, and both viruses grow readily to high titers in cell culture. Consequently, they represent auspicious backbones for an RBD-based virus vectored vaccine.

Integrating immunogens into rhabdovirus envelopes

To facilitate integration of the SARS-CoV-2 RBD protein into rhabdovirus particles, one can make use of the fact that genetic fusion of the rabies virus G cytoplasmic tail (c-tail) to the carboxy-terminus of the protein of interest is sufficient to facilitate effective incorporation into the envelope of budding virus particles [210, 211]. While the requirements for the incorporation into RABV particles is more stringent due to obligatory interactions between M and the G c-tail, i.e. the authentic RABV c-tail is necessary, VSV will happily incorporate anything with a C-terminal cytoplasmic domain, including the RABV c-tail [209]. Hence, the transmembrane anchor of RABV is compatible with the intracellular budding structure of both rhabdoviruses, and possibly lentiviruses, and therefore efficiently incorporated into virions and VLPs released to the extracellular space if present at the site of budding.

Facilitating cell surface localization of an immunogen

Proteins destined for the secretory pathway which explicitly includes proteins inserted into cellular membranes or targeted to organelles like the ER, the Golgi or endosomes initiate translocation via a signal peptide. A signal peptide is a short (15-30 aa) stretch of aa at the N-terminus of a nascent protein that is comprised of a positively charged N-terminal region, a hydrophobic central region and a neutral, polar C-terminal region. It is recognized co-translationally by the signal recognition particle (SRP), leading to the formation of an SRP-ribosome-nascent chain (SRP-RNC). This is transported to the SRP-receptor in the endoplasmic reticulum (ER) membrane where it engages a membrane-bound translocon which facilitates translocation of the polypeptide chain into the lumen of the ER. Finally, the signal peptide is cleaved off by specialized signal peptide peptidase. A construct expressing the SARS-CoV-2 RBD on the cell surface therefore needs to contain a signal peptide.
Importantly, signal peptides, while being very heterogenic, have a significant impact on protein expression and secretion and are therefore a target for optimization [212-214].

Aim of the Thesis

The current SARS-CoV-2 pandemic necessitates the vaccination of a majority of the entire human population in an unprecedented miniscule amount of time. Impressively, safe, efficient, scalable, and cost-efficient vaccines have been developed from conceptualization to approval to production of multiple billions of doses in roughly the time it would take to complete a Hohmann transfer orbit to Mars and back.

Rhabdoviruses like VSV and RABV are promising starting points for vector vaccines and were previously used with great success to combat the recent Ebola outbreak. The aim of this thesis was to design, establish and test a highly protective and safe COVID-19 vaccine based on either a spreading-deficient or replication-controllable rhabdovirus replicon system with an optimized efficacy – safety – tolerability footprint.

The resultant chimeric VSVΔG "minispike" was then characterized in regard to expression, transport and localization, correct folding and incorporation into virus particles and finally tested for efficacy and protection against SARS-CoV-2 infection and disease in a transgenic SARS-CoV-2-permissive mouse model. To measure the virus neutralization activity of sera from vaccinated animals under BSL-1 conditions, another aim was to establish a bimodal eGFP-*Gaussia* Luciferase pseudovirus assay relying on different SARS-CoV-2 Spike variants for entry.

The sera from vaccinated animals were to be further tested for neutralization efficacy and robustness to immune escape by emerging variants of concern.

Partial results of the presented work have been published in [215] and the manuscript of a follow-up study is currently in preparation.

Materials and Methods

Ethics statement

Mouse immunization studies were carried out in the animal housing facility of the Paul-Ehrlich-Institute, Langen, Hesse, Germany in compliance with the regulations of German animal protection laws and authorized by the responsible state authority (V54-19c20/15-F107/1058 and V54-19c18-F107/2006). Diagnostic use of anonymous patient sera was approved by the Ethics Committee of the Medical Faculty of the LMU.

Materials

Laboratory equipment

Equipment	Model	Supplier
Centrifuges	5418	Eppendorf
	5804 R	Eppendorf
	Varifuge 3.0R	Heraeus
	Allegra X-22R	Beckman Coulter
	Optima L-80 xp ultracentrifuge	Beckman Coulter
Microscope	Axiovert 200M	Zeiss
	Light microscope TMS	Nikon
	UV-Light microscope DMi8	Leica
Miscellaneous	T3 Thermocycler	Biometra
	Chemiluminescence developing system (Fusion FX7)	Vilber-Lourmat
	Multiplate Reader Mithras LB 940	Berthold
	Magnetic stirrer/heater	VELP Scientifica
	pH-meter	VWR International
	accu-jet® pro	Brand
	Pipettes (2/10/200/1000 µl)	Eppendorf
	Polyacrylamide gel electrophoresis system	Peqlab
	Agarose gel electrophoresis system	Peqlab

	Roller mixer SRT2	Stuart
	Semi-Dry blotting system	Peqlab
	Spectrophotometer Nanodrop ND-1000	Peqlab
	Thermocycler T3	Biometra
	Thermomixer 5436	Eppendorf
	Thermostated hot-block 5320	Eppendorf
	Horizontal Shaker Swip SM-25	Edmund Bühler GmbH
	Digital Sonifier® Cell Disruptor	Branson
	GJ Balance	Kern
	LUNA Automated Cell Counter	Logos biosystems
	Cell Strainer 40 µM Nylon strainer	Corning

Chemicals & Reagents

Chemical	Supplier
Acetic Acid, 100 %	Carl Roth
Acetone (Rotipuran 99.8 %)	Carl Roth
Agar	BD Biosciences
Acrylamide/Bisacrylamide solution ROTIPHORESE®Gel 30	Carl Roth
Agarose (Ultrapure)	Invitrogen/Thermo Fisher
Albumin Fraction V (BSA)	Carl Roth
Ammonium chloride	Merck
Ammonium persulfate (APS)	Sigma-Aldrich
Ampicillin sodium salt (Amp)	Roth
Bis(2-hydroxyethyl)amino-tris(hydroxymethyl)methane (BIS-TRIS)	Carl Roth
Bromophenol blue	Sigma-Aldrich
Clarity Western ECL substrate	Bio-Rad
Dimethyl sulfoxide (DMSO)	Carl Roth
Dimethylformamide	Merck
Disodium hydrogen phosphate	Merck

Ethanol	Merck
Ethidium bromide solution 1 %	Carl Roth
Ethylene diamine tetraacetic acid (EDTA)	Sigma-Aldrich
Fetal calf serum (FCS)	PAN-Biotech
Geneticin sulfate (G418)	Carl Roth
Glycerol	Carl Roth
4-(2-hydroxyethyl)-1-piperazineethanesulfonic acid (HEPES)	Carl Roth
Hydrochloric acid 37 %	Carl Roth
Imidazole	Merck
Isopropanol	Carl Roth
Kanamycin monosulfate	Sigma-Aldrich
Leptomycin B (LMB)	Santa Cruz Biotech.
Magnesium chloride hexahydrate	Fluka
Magnesium sulfate heptahydrate	Merck
Methanol	Carl Roth
Mifepristone	Sigma-Aldrich
Milk powder, blotting grade	Carl Roth
MOPS	Carl Roth
7-Hydroxy-8-phenylazo-1,3-naphthalenedisulfonic acid disodium salt, 1-Phenylazo-2-naphthol-6,8-disulfonic acid disodium salt (Orange G)	Sigma-Aldrich
Ortho-phosphoric acid, 85 %	Merck
Paraformaldehyde 16 %, methanol free (PFA)	Thermo Fisher
Poly-D-lysine hydrobromide	Sigma-Aldrich
Poly(ethyleneimine), branched (PEI)	Sigma-Aldrich
Potassium acetate, extra pure	Merck
Potassium chloride	Merck
Potassium dihydrogen phosphate	Merck
RNASe A	Carl Roth
Sodium bisulfite	Sigma
Sodium chloride	Carl Roth
Sodium dihydrogen phosphate	Merck

Sodium dodecyl sulfate (SDS)	Serva
Sodium hydroxide	VWR Chemicals
Tetramethylethylenediamine (TEMED)	Carl Roth
Tris-(hydroxymethyl)-amino methane (Tris)	Carl Roth
Triton X-100	Merck
Tryptone	BD
Tween-20	Carl Roth
Yeast extract	BD
β-Mercaptoethanol	Sigma-Aldrich

Plasticware & Microscopy

Item	Supplier
Cell culture dishes (6 cm ⌀, 10 cm ⌀, 15 cm ⌀)	Sarstedt
Cell culture flasks (T25, T75, T175)	Sarstedt
Cell culture plates, clear wall (6-well, 12-well, 24-well, 48-well, 96-well)	Sarstedt
Cell culture plates opaque	Thermo Fisher
Cell culture plates black wall, optical bottom	Thermo Fisher
Cryo tubes 1,8 ml	Sarstedt
Serological pipettes (2 ml, 5 ml, 10 ml, 25 ml, 50 ml)	Sarstedt
Reaction tubes (1.5 & 2.0 ml)	Sarstedt
Reaction tubes (15 & 50 ml)	Sarstedt
Glass bottom dish ⌀ 35 mm	Ibidi
Anti-Fade Fluorescence Mounting Medium	Abcam
Microscope slides	Carl Roth
Microscope cover glasses	Carl Roth
Sterile syringe filters 0.22 µm	Merck-Millipore
Thinwall polypropylene tubes for ultracentrifugation, 38,5 ml	Beckman Coulter
PCR tubes (500 µl, 200 µl)	Nippon genetics
8-well PCR Tube Strips (100 µl)	Nippon genetics

Pipette filter tips (1250 µl, 300 µl, 20 µl, 10 µl, 2 µl)	StarLab

Cell culture media

All cell culture base media were purchased from Gibco (Thermo Fisher). The following media and supplements were used:

Medium/Reagent	Catalog number (ThermoFisher)
D-MEM (high glucose, GlutaMAX™ supplement)	10566016
DMEM/F-12 (GlutaMAX™ supplement)	10565018
G-MEM (L-Glutamine, high glucose)	11710035
CD Hybridoma medium	11279023
Opti-MEM	31985070
OptiPro serum-free medium	12309019
DPBS (no calcium, no magnesium)	14190136
HEPES, 1M buffer Solution	15630049
L-Glutamine (200 mM)	25030123
Penicillin-Streptomycin (Pen/Strep)	15070063
Tryptose phosphate broth	18050039
MEM amino acids (50x)	11130036
MEM Non-Essential Amino Acids Solution (100X)	11140035
Trypsin-EDTA	25300096

Media compositions

- D-MEM 3+: 10 % FCS, 2 ml Pen/Strep
- DMEM/F-12 3+: 10 % FCS, 2 ml Pen/Strep, 10 ml MEM NEAA
- G-MEM 4+: 10 % FCS, 2 ml Pen/Strep, 19,5 ml Tryptose phosphate broth, 10 ml MEM amino acids

Bacteria culture medium

- Lysogeny (LB24) broth [216] : 10 g tryptone, 24 g yeast extract, 5 g NaCl
- LB++: LB24 broth with 10 mM $MgSO_4$ and 2.5 mM KCl

Buffers:

Buffer	Content
20x MOPS Buffer	1M Tris, 1M MOPS, 20 mM EDTA, 2 % SDS
1x MOPS Buffer	diluted 1:20 from 20x MOPS buffer; addition of 2.5 M Sodium Bisulfite stock solution (1:500) immediately before usage
Xtra-Dry blotting buffer	48 mM Tris, 20 mM HEPES, 1mM EDTA, 1.3 mM Sodium bisulfite, 1.3 mM Dimethylformamide
PBS	137 mM NaCl, 2.7 mM KCl, 1.18 mM KH2PO4, 6.4 mM N2HPO4, pH 7.4
PBS-T	PBS with additional 0.05 % Tween-20
TBS	50 mM Tris, 150 mM NaCl, pH 7.4
TBS-T	TBS with additional 0.05 % Tween-20
SDS sample lysis buffer	30 % Glycerol, 15 % β-Mercaptoethanol, 10 % SDS, 62 mM Tris/HCl pH 6.8, 0.012 % Bromophenole blue
3,5x BIS-TRIS	1.25 M Bis-Tris HCl pH 6.8
SDS Stacking gel (6 %) premix	1x BIS-TRIS, 6 % ROTIPHORESE®Gel 30
Stacking gel:	10 ml stacking gel premix, 100 µl 10 % APS, 10 µl TEMED (per medium gel)
SDS separating gel (10 %) premix	1x BIS-TRIS, 10 % ROTIPHORESE®Gel 30
Flexi I	100 mM Tris, 10 mM EDTA, 200 µg/ml RNAse A, pH 7.5
Flexi II	200 mM NaOH, 1 % SDS
Flexi III	3 M Potassium acetate in 100 % acetic acid

Kits and reagents

Kits, Reagents and Enzymes	Supplier
alamarBlue™ HS Cell Viability reagent	Invitrogen
NucleoBond Xtra Midi	Macherey-Nagel
QIAquick Gel Extraction Kit	Qiagen
QIAquick PCR purification kit	Qiagen
Dual Luciferase Reporter Assay System	Promega

Renilla Luciferase Assay System	Promega
Mammalian Transfection Kit	Agilent Technologies
Q5 High Fidelity PCR Kit	New England Biolabs (NEB)
Q5 Site Directed Mutagenesis Kit	New England Biolabs (NEB)
NEBuilder HiFi DNA Assembly Cloning Kit	New England Biolabs (NEB)
Restriction enzymes	New England Biolabs (NEB)
T4 DNA Ligase	New England Biolabs (NEB)
Recombinant Shrimp alkaline phosphatase (rSAP)	New England Biolabs (NEB)
Instant Sticky End Master Mix	New England Biolabs (NEB)
DNAse, RNAse free	Qiagen
Transcriptor Reverse Transcriptase	Roche
Lipofectamine 3000	Invitrogen/Thermo Fisher

Cell Lines

Cell line	Culture medium	Source
HEK 293T/17	DMEM3+	ATCC (ATCC® CRL-11268™)
HEK 293T PKR KO cloneA1	DMEM3+	Veit Hornung
SH-SY5Y	DMEM/F-12 3+	Sigma-Aldrich
BHK-21	G-MEM 4+	ATCC (ATCC® CCL-10™)
BHK-G43	G-MEM 4+	Georg Herrler/Gert Zimmer[217]
BSR-T7	G-MEM 4+	This lab [218]
BSR-MGon	G-MEM 4+	This lab [219]
Neuro-2a (N2a)	DMEM3+	ATTC (ATCC® CCL-131™)
N2a CVS-N2c-G	DMEM3+	This lab, unpublished
I1-Hybridoma	CD Hybridoma	ATTC (ATTC® CRL-2700™)
Epithelioma Papulosum Cyprini (EPC)	G-MEM Fish	ATCC (ATCC® CRL-2872™)
NEB® Stable Competent *E. coli*	LB24	New England Biolabs (NEB)

Primary Antibodies

Epitope	Host	Manufacturer, #
Beta actin	rabbit	Abcam, ab8227
HSPD1	rabbit	Sigma-Aldrich, HPA001523
RABV-P	rabbit	This lab, peptide serum 160-5
RABV-N/P	rabbit	anti-RABV-RNP, kindly provided by James H. Cox,
RABV-G c-tail	rabbit	This lab, HCA05/-1
VSV Virion (N, M, G)	rabbit	Anti-VSV, VSV-S32, kindly provided by James H. Cox
GFP	rabbit	Cell Signaling Technology, D5.1
mNeonGreen	mouse	Chromotek, 32F6
PARP	rabbit	Cell Signaling Technology, 46D11
PKR	rabbit	Cell Signaling Technology, D7F7
Phospho-PKR (phospho-T446)	rabbit	Abcam, ab32036
Phospho-PKR (phospho-T451)	rabbit	Abcam, ab81303
eIF2α	rabbit	Cell Signaling Technology, D7D3
Phospho-eIF2α	rabbit	Cell Signaling Technology, D9G8
DYKDDDDK-Tag (FLAG®)	rabbit	Cell Signaling Technology, D6W5B
HA-Tag	rabbit	Santa Cruz, Y-11
MAVS	rabbit	Cell Signaling Technology, 3993
SARS-CoV-1/2 S (CR3022)	human	Abcam ab273073
FITC Anti-Rabies Monoclonal Globulin (Centocor®)		Fujirebio 800-092

Secondary Antibodies

Conjugate	Target species	Manufacturer, #
Alexa Fluor® Plus 405	mouse	ThermoFisher, A48255
Alexa Fluor® Plus 405	rabbit	ThermoFisher, A48258
Alexa Fluor® Plus 488	mouse	Thermo Fisher, A32723
Alexa Fluor® Plus 488	rabbit	Thermo Fisher, A32731
Alexa Fluor® 488	human	Thermo Fisher, A11013
Alexa Fluor® Plus 555	mouse	Thermo Fisher, A32727
Alexa Fluor® Plus 555	rabbit	Thermo Fisher, A32732
Alexa Fluor® 555	human	Thermo Fisher, A-21433
Alexa Fluor® Plus 647	mouse	Thermo Fisher, A32728
Alexa Fluor® Plus 647	rabbit	Thermo Fisher, A32733
Horseradish Peroxidase (HRP)	mouse	Jackson ImmunoResearch
Horseradish Peroxidase (HRP)	rabbit	Jackson ImmunoResearch
Horseradish Peroxidase (HRP)	human	ThermoFisher, 31420

Methods

Cell culture

Cell lines were kept in respective, indicated growth media in cell culture flasks in incubators at 37°C and 5 % CO_2 unless otherwise mentioned.

Generally, growing cells were split every three to four days at ratios around 1:8 to 1:20 depending on cell type and growth rate. Adherent cells were trypsinized with Trypsin-EDTA (0,05 % trypsin, 0,02 % EDTA, Gibco/Thermo Fisher); suspension cell lines were split by directly diluting the culture in fresh media.

Cell seeding

Cell numbers for seeding were estimated according to the following table:

Cell culture vessel	volume [ml]	Cell number at confluency	Seeding density [cells]
T25	8	2.8×10^6	0.7×10^6
T75	15	8.4×10^6	2.1×10^6
T175	25	23.3×10^6	4.9×10^6
6-well plate	2	1.2×10^6	0.3×10^6
12-well plate	1	0.5×10^6	0.1×10^6
24-well plate	0,5	0.24×10^6	0.05×10^6
48-well plate	0,2	0.12×10^6	0.03×10^6
96-well plate	0,1	0.04×10^6	0.01×10^6
10cm dish	15	8.8×10^6	2.2×10^6

For transfections, cells were incubated over night after seeding to allow for proper adhesion. For infections, cells were either infected directly in suspension or 2h post seeding.

Transfection

Transfections using Lipofectamine3000 (ThermoFisher) were carried out according to the manufacturer´s protocol. Briefly, the amount of DNA and Lipofectamine (2,5 µl per µg of DNA) needed were calculated and diluted individually in OptiMEM pre-warmed to room temperature according to the manufacturer´s guidelines and mixed gently. 2 µl of P3000 enhancer per µg DNA were added to the diluted DNA, mixed gently and incubated 5min at RT. The DNA mix was then added to the

lipofectamine mix, mixed well by pipetting up and down for exactly 23 times and incubated 15min at RT. The mixture was then carefully added dropwise to the cells.

Transfection using PEI were performed accordingly, with PEI instead of lipofectamine and without the addition of the P3000 enhancer.

Polymerase Chain Reaction (PCR)

PCR can be utilized to generate and specifically amplify a desired DNA sequence. For all experiments in this thesis the Q5 PCR kit from NEB was utilized according to the manufacturer´s instructions.

Primer design

The Q5 polymerase is a thermostabilized, proof-reading PCR enzyme and can stabilize primer-template binding. Therefore, annealing temperatures for primers tend to be higher when using the Q5 polymerase, compared to regular, non-proof-reading polymerases. Accordingly, the NEB Tm calculator (http://tmcalculator.neb.com/#!/main) was utilized to compute primer annealing temperatures. Primers were designed following some basic guidelines: 20-40 nucleotides in length, GC content 40 % - 60 %, and a difference in Tm of 5°C or less between the primer pair. All primers were ordered from Eurofins Genomics as “custom DNA oligos”, purification “salt free”. PCR reactions were set up in a 500 µl PCR tube on ice according to the following scheme:

Component	Volume [µl]	final concentration
5X Q5 reaction buffer	10	1x
10 µM forward primer	2,5	0,5 µM
10 µM reverse primer	2,5	0,5 µM
10mM dNTPs	1	200 µM
template	1	1 pg-1 ng/µl
Q5 polymerase [2 U/µl]	0,5	0,02 U/µl
water, nuclease free	32,5	

The PCR preparation was mixed by pipetting and transferred to a thermocycler with a heated lid preheated to the denaturing temperature of the polymerase (98°C).

Step	Temperature [°C]	time [s]
initial denaturation	98	30
PCR amplification (25 cycles)	98	10
	50-72, depending on primer	30
	72	15-30s/kbp
Final Extension	72	300
hold	4	∞

Overlap extension PCR

Overlap extension PCR was utilized to combine two or more DNA fragments into one fused template. To combine fragment A and fragment B to fragment AB, the neighboring primers *A reverse* and *B forward* were designed to contain a complementary sequence needed for the amplification of the respective fragment as well as an overlapping part complementary to the other fragment. All primers were designed to have the same Tm (Tm1) while the overlap was designed to have a Tm 5°C higher than the Tm1. First, a PCR of Fragment A and Fragment B was performed according to standard protocol. The products were purified by gel electrophoresis. In a second PCR step, the fragments were added as templates in an equimolar proportion. For overlap extension, the Tm was raised by 5°C during the first five cycles. As this temperature is above the Tm of the outer primers, no amplification should occur; instead, the two fragments should prime each other and create a fused, full-length template. Subsequently, 25 cycles with a Tm corresponding to the Tm of the outer primers is performed and amplification of the fused template can take place.

Fragment generation	Temperature [°C]	time [s]
initial denaturation	98	30
PCR amplification (25 cycles)	98	10
annealing	Tm1: 50-72	30
Elongation	72	20-30s/kbp
Final Extension	72	300
hold	4	∞

Overlap Extension PCR	Temperature [°C]	time [s]
initial denaturation	98	30
PCR amplification (25 cycles)	98	10
annealing	Tm1+5	30
elongation	72	20-30s/kbp
PCR amplification (25 cycles)	98	10
annealing	Tm1	30
elongation	72	20-30s/kbp
Final Extension	72	300
hold	4	∞

Mutagenesis PCR

To induce desired point mutations in a DNA template the NEB Q5® site-directed mutagenesis kit was used according to the manufacturer´s instructions. Primers were designed using the NEBaseChanger website (http://nebasechanger.neb.com/). As the method relies on PCR amplification of the whole plasmid, the desired DNA sequence was cloned into a suitable vector to keep total length under seven kbp if necessary. The subsequent PCR reaction was set up on ice according to the following scheme:

Component	volume [µl]	final concentration
Q5 Hot Start High-Fidelity 2X Master Mix	12,5	1X
10 µM Forward Primer	1,25	0.5 µM
10 µM Reverse Primer	1,25	0.5 µM
Template DNA (1–25 ng/µl)	1	1-25 ng
Nuclease-free water	9	

PCR was performed according to parameters given by the NEBasechanger tool. In the following step, phosphorylation of DNA ends, *DpnI* digestion of remaining template and ligation of the newly synthesized linear plasmid took place. The reaction mix was combined based on the following table.

Component	volume [µl]	final concentration
PCR Product	1 µl	
2X KLD Reaction Buffer	5 µl	1X
10X KLD Enzyme Mix	1 µl	1X
Nuclease-free Water	3 µl	

The preparation was mixed by pipetting and incubated at room temperature for five minutes. Finally, 100 µl of chemically competent bacteria were transformed with 5 µl of the preparation.

Ligation

DNA vector and fragments with compatible ends were ligated utilizing T4 DNA Ligase (NEB). A molar ratio of insert: vector of 3:1 was used by default for sticky end ligations and 5:1 for blunt end ligations. For blunt end ligations, the vector backbone ends were dephosphorylated prior to ligation with rSAP (NEB).

Component	amount
Vector	100 ng
Insert	3-fold molar amount of vector
T4 DNA Ligase	1 µl
T4 Ligase Buffer	2 µl
Nuclease-free Water	Ad 20 µl

Ligation reactions were incubated for 2h at 23°C or overnight at 16°C and directly transformed into chemically competent *E. coli*.

Transformation

Chemically competent *E. coli* (NEB stable) were thawed on ice. 100 µl of the bacteria were transformed with 10 µL ligation mix or 1 µl of plasmid in case of retransformation. After a 20min incubation on ice the bacteria were heat shocked for 1min at 42°C and transferred back to ice for five minutes. After addition of 700 µl LB++ the bacteria were incubated for one hour at 37°C under constant shaking and plated onto agar plates prewarmed to room temperature containing the appropriate antibiotic at a concentration of 25mg/ml. The plates were inverted and incubated at 37°C o/n.

Mini Preparation

Single colonies were inoculated into 2 ml Eppendorf tubes containing 1 ml of LB medium with the appropriate antibiotic. The bacteria were incubated o/n at 37°C on a thermoshaker under constant shaking (800rpm). The next day, the bacteria were centrifuged (30sec, 14000g, RT), the supernatant was aspirated, and the pellet was resuspended in 200 µl Flexi I. For alkaline lysis, 200 µl Flexi II was added and the preparations were incubated at room temperature for five minutes. 200 µl of Flexi III

were added for neutralization, the samples were incubated for five minutes on ice and centrifuged for 15 minutes (14000g, RT). The supernatant was transferred to new 1,5 ml reaction tubes containing 400 µL 2-Propanol absolute, mixed well and centrifuged (14000g, 20min, RT). The supernatant was aspirated and an ethanol washing step was performed by adding one ml 70 % EtOH, incubating for five minutes at room temperature, centrifugation (14000g, 10min, RT) and aspiration of the supernatant. The pellet was air dried for 10 minutes and resuspended in 50 µl H_2O.

Mini Digestion

To check for correct clones, the plasmid DNA isolated in the previous step was analyzed by restriction enzyme digestion. Enzymes were chosen to generate a recognizable band pattern (visualized by the 'Simulate Agarose Gel' function of SnapGene). The reaction mix was set up according to below scheme:

Component	volume [µl]
Mini DNA	3 µl
10x CutSmart Reaction Buffer	1,5 µl
Enzyme A	0,2 µl
Enzyme B	0,2 µl
Nuclease-Free H_2O	10,1 µl

The reaction was incubated for 2 h at 37°C, mixed with 5 µl 5x loading dye and run on an agarose gel.

Agarose gel electrophoresis

A mix containing 0,7-1 % of agarose in 1x TAE buffer was heated just below boiling in a microwave and stirred for 10min at room temperature. The solution was then either directly used or stored for a later time point in an oven set to 60°C. Agarose gels were run in 1x TAE running buffer containing 0.006 % ethidium bromide under high voltage (120V, 400 mA) for an hour and visualized on a BioRad GelDoc imaging system.

Gel extraction:

Bands of the correct size were cut out of the agarose gel and the DNA was purified using the QIAquick Gel Extraction Kit (Qiagen) according to the manufacturer´s instructions.

Midi preparation

Correct clones were retransformed into bacteria and spread onto agar plates containing the respective antibiotic. A single clone was then seeded into either 50 or 100 ml of LB broth containing the appropriate antibiotic and incubated over night at 37°C under constant shaking.

Bacteria were centrifuged for 20 min at 3000 g, the supernatant discarded, and the pellet processed using a Macherey & Nagel Nucleobond Xtra Midi kit according to the manufacturer´s instructions. Briefly, the pellet was resuspended in 8 ml RES buffer, incubated with 8 ml LYS buffer for 5 min at room temperature, neutralized with 8 ml NEU buffer and loaded onto a column with a paper filter pre-equilibrated with 12 ml EQU buffer. After flow-through the filter was rinsed with 5 ml EQU and discarded. The column was washed with 8 ml WASH buffer, and the DNA finally eluted using 5 ml ELU buffer. DNA was precipitated by adding 3,5 ml 2-Propanol absolute, split into four 2 ml Eppendorf reaction tubes and pelleted in a precooled centrifuge for 60 min at 4°C and 14000g. The supernatant was carefully aspirated, and the pellet washed with 1,8 ml 70 % EtOH per tube for 10 min at room temperature. Finally, after another centrifugation step (10 min, 14000 g, room temperature) the supernatant was aspirated, and the pellet air-dried. The DNA was finally solubilized in 50-100 µl H_2O per tube, the contents of the four tubes were merged and concentration determined using a Nanodrop 1000 (Peqlab).

Sanger Sequencing

30 µl of a DNA preparation was adjusted to approximately 100 ng/µl with H_2O and sent to Sanger sequencing by GATC (part of Eurofins genomics) using the SupremeRun Tube protocol with appropriate primers. Primers were chosen to bind in ~900 nt increments in case the insert of interest was longer than ~1500 bps. Constructs smaller 1500 bps were forward- and reverse-sequenced from the respective termini. The results were processed and visualized in SnapGene (version 4.2)

Virus rescue

VSV virus rescue

VSV rescue was performed in HEK293T cells transfected with the viral cDNA plasmid directing T7 RNA polymerase-driven transcription of viral antigenome (+) RNA from a T7 promoter along with expression plasmids encoding the T7 RNA polymerase and virus helper proteins N, P, and L. Additionally, an expression plasmid encoding the respective glycoprotein (G) was included in case of single-round, G-deleted viruses (ΔG).

A T25 flask of confluent HEK293T cells was trypsinized and resuspended in 15 ml DMEM3+. 2 ml of cell suspension per well were seeded into a 6-well-plate and incubated overnight at 37°C. Helper plasmids and viral full-length cDNA plasmids were calculated for one well and then multiplied according to the used number of wells. As a general rule for non-SMASh viruses, 3-6 wells were used per rescue attempt.

Plasmid	amount [ng/well]
pCAG-N	1000
pCAG-P	500
pCAG-L	500
pCAG-G	500
pCAG-T7	1000
Full length cDNA constructs	1000

Successful rescue was determined either by the appearance of fluorescent foci in case of recombinant viruses expressing a fluorescent protein or by observation of a cytopathic effect in case of non-fluorescent VSVs. Two to three days after transfection, the supernatant was centrifuged to discard cell debris (900 g, 10 min, RT) and was added to BHK-21 or BSR-T7/5 cells for replication competent viruses or BSR-MGon or BHK-G43 cells for single round, ΔG viruses to propagate spread. The rescue was confirmed by staining with a serum recognizing VSV N, M and G proteins (VSV S32).

Rabies virus rescue

Recombinant rabies cDNA was generated as described before [220]. To rescue cDNA into infectious virus, N2a N2c-CVS-G IRES crimson cells (a N2a derived cell line stably expressing the N2c-CVS glycoprotein; A. Ghanem, unpublished) were transfected with T7-driven SAD helper plasmids (pTIT SAD-N, pTIT SAD-P, pTIT SAD-L, pTIT SAD-G), the T7-driven viral full length cDNA plasmid and an expression plasmid encoding for the T7 polymerase driven by a synthetic promoter (cytomegalovirus (CMV) enhancer fused to the chicken beta-actin promoter, CAG) (pCAG-T7). The medium was exchanged after overnight incubation and cells were screened for fluorescent foci 48-96h post transfection in case of recombinant viruses expressing fluorescent proteins. Non-fluorescent viruses were identified with FITC Anti-Rabies Monoclonal Globulin (Centocor®). The supernatant was harvested 96h post transfection, centrifuged to remove cell debris (10min, 1000g, 4°C), aliquoted and frozen at -80°C.

Virus Titration

To determine the number of infectious units in a rescue stock or viral preparation, a confluent T25 flask of BHK-21, BSR-T7, HEK293T or VeroE6 cells was aspirated and trypsinized. Cells were resuspended in 25 ml medium (DMEM3+ for VeroE6, HEK293T and GMEM4+ for BHK-21, BSR-T7/5) and seeded into 96-well plates (100 µl/well). Virus-containing culture supernatant was serially diluted 1:10 in DMEM without any supplements six to eight times. 3 h post seeding, the cells were infected with 100 µl of the virus dilutions in duplicates or triplicates. Cells were incubated either over night with VSV-based viruses or for 48 h with rabies-based viruses, washed once with PBS, fixed with 80 % acetone in PBS for 20 min at room temperature and dried for 30 min. Infected cells were detected by Centocor® in case of rabies viruses or by rabbit anti-VSV serum32 for two hours at room temperature. Cells were washed three times with PBS and directly visualized (Centocor®) or stained with AlexaFluor® 488-labeled anti-rabbit IgG (1:2000 in PBS) for one hour at room temperature, washed three times with PBS and visualized with a fluorescence microscope.

Infection experiments

Infection experiments were performed similar to titrations; cells were seeded in multiwell plates or cell culture dishes at the respective densities 3h pre infection and infected with the calculated multiplicity of infection (MOI) with freshly thawed virus stock preparations. A MOI of one hereby corresponds to theoretically equal number of cells and infectious particles (e.g., one infectious particle per cell), a MOI of 0.1 to one infectious particle per ten cells, a MOI of three to three particles per cell. A MOI of three is usually deemed sufficient to infect almost all cells.

Generation of virus stocks

Rabies virus stocks

Full length, replication competent rabies virus stocks were generated on BSR-T7/5 cells. One confluent T75 flask of BSR-T7/5 cells was split into three T75 flasks. Two hours post seeding, the cells were infected with the respective rabies virus with a MOI of 0.01-0.05. After over-night incubation at 37°C, the medium was exchanged. The cells were then incubated for three days and monitored for infection status under a fluorescence microscope if applicable. After three days, the supernatant was harvested for the first time and replaced by fresh medium. The harvested supernatant was centrifuged (1000 g, 4°C, 10 min) to discard cell debris, transferred to a new 50 ml tube, mixed well and either further purified by ultracentrifugation or directly aliquoted and stored at -80°C. The second harvest was collected 48 h after the first and treated as before. Virus stocks were then titrated as described above.

Replication-deficient, single round ΔG rabies virus stocks were produced in BSR-MGon cells expressing SAD M and G after induction with Doxycycline. The cells were split 1:3 and infected with a MOI of 0.1. The expression of M and G was induced simultaneously with infection by addition of Doxycycline to the medium. This exogenous transcomplementation with G (and M) enables the spread and amplification of genetically G (and/or M) -deficient viruses. Infection status was monitored by fluorescence microscopy and supernatant was first harvested after 96 h. After addition of fresh medium, the cells were incubated for another 48 h, and the supernatant was again harvested and processed as described above.

VSV virus stocks

Stock preparation of replication-competent VSV viruses was done on BHK-21 cells. One T75 flask was split into two T75 flasks (as the rapid replication and lytic nature of VSV does not allow for prolonged proliferation of cells and therefore necessitates a higher cell density at seeding) and infected with VSV viruses at a MOI of 0.01 two hours post seeding. The cells were incubated at 34°C overnight and monitored for infection and cytopathic effect (CPE) under a fluorescence microscope. Supernatant was harvested as described for rabies virus but due to the lytic replication of VSV cells were discarded after the first harvest. Spreading-deficient, single round ΔG VSV stocks were generated on BHK-VSVG(43) cells inducibly expressing VSV G. Cells were seeded, induced with Mifepristone (10^{-9} M) six hours pre infection and infected as above. The cells were further treated as described above.

Virus stock purification through ultracentrifugation

To further purify and concentrate virus preparations, centrifuge tubes were filled with 5 ml of a 30 % sucrose solution in TEN buffer. The virus preparation was carefully added onto the top of this sucrose cushion and the virions were pelleted by centrifugation (2 h, 24000 rpm in a Beckman-Coulter SW32 rotor, 4°C). The supernatant was carefully aspirated, the pellet resuspended in OptiMEM or PBS overnight at 4°C under constant shaking, aliquoted and stored at -80°C.

SDS-PAGE and Western Blot

Sodium-Dodecyl-sulfate Polyacrylamide gel electrophoresis (SDS-PAGE)

Proteins were separated according to their molecular weight using Bis-Tris polyacrylamide gels described by Updyke & Engelhorn (Invitrogen, US-Pat. 6162338) Basically, the SDS-PAGE is performed at a slightly acidic pH to prevent deamination and alkylation of proteins. Separating gels generally contained 10 % PAA unless otherwise stated while stacking gels contained 6 %. For further gel

composition see table below. The stacking gel was cast on top of the separating gel in a Peqlab gel chamber. Cells or purified virions were lysed in Laemmli lysis buffer and incubated at 95°C for 5 min to ensure complete denaturation. The samples were loaded onto the gel and run alongside the Precision Plus Protein Marker (BioRad). The running buffer (1x MOPS) was spiked with sodium bisulfite (5 mM final concentration) and gels were first run at 100 V for 1h to allow for migration into the stacking gel and then for three hours at 150 V. The indicated times are for medium-sized gels.

Western Blotting

To detect the proteins of interest separated by the preceding SDS PAGE, they were transferred to a PVDF membrane (Immobilon-P, Millipore) as described previously [221]. PVDF membranes were activated by a brief soak in 100 % methanol and then equilibrated in transfer buffer for 10 min. The separating gels and six sheets of blotting paper per gel were also equilibrated in transfer buffer for 10 min under gently shaking. The blotting chamber was then assembled by stacking three sheets of blotting paper, the membrane, the gel and another three sheets of blotting paper. Air bubbles were carefully squeezed out and the lid was screwed on hand tight. The blotting was performed for 45 min at 700 mA for one gel or 50 min at 1000 mA for two gels. After blotting, the blotting paper sheets and the gel were discarded, and the membrane was rinsed once in 1x TBS-T and blocked with 5 % BSA in TBS-T for one hour at room temperature under constant shaking. Primary antibodies were diluted (1:1000 unless otherwise mentioned) in 5 ml TBS-T containing 1 % BSA, transferred together with the membrane into 50 ml Falcon tubes and incubated over night at 4°C followed by another 60 min at room temperature on a rolling shaker. The membranes were washed three times for 5 min in TBS-T and incubated with horseradish-peroxidase conjugated secondary antibodies (1:20000 in TBS-T) against the respective species of the primary antibody for at least one hour at room temperature under constant, gentle shaking. After three washing steps with TBS-T the protein bands were detected by addition of Clarity Western ECL blotting substrate and visualization of the luminescence using a Fusion FX7 system (Vilber Lourmat).

Pseudovirus neutralization assay

Generation of SARS-CoV-2 VOC S expression constructs

The S protein sequence (protein id: YP_009724390.1) from the NCBI Reference Sequence NC_045512.2 of nCoV, Wuhan isolate 1, was used as template for a S expression plasmid. A *EcoRI* cleavage site followed by a Kozak sequence (*GAATTC*GCCACC) was added upstream of the start codon, a human influenza hemagglutinin (HA)-tag (aa sequence YPYDVPDYA) inserted immediately upstream of the

stop codon to allow for detection of the protein and finally a *NotI* restriction site downstream of the stop codon.

The sequence was optimized for human codon usage and synthesized (GeneArt, ThermoFisher). The construct was then cloned into a pCR3 expression plasmid using the *EcoRI* and *NotI* restriction sites, resulting in pCR3_SARS-CoV-2-S(Wuhan)-HA. This S construct was then C-terminally truncated by 19 residues by PCR to improve incorporation into VSV particles. To this end, we inserted a stop codon and a *NotI* restriction site after S residue C1254 (CSCGSCC$_{1254}$**NotI*) by PCR and inserted the resulting construct again into pCR3, giving rise to pCR3_SARS-CoV-2-S(Wuhan)ΔC19.

To further improve pseudovirus infectivity, five additional C-terminal residues were removed, resulting in SARS-CoV-2-S(Wuhan)ΔC24. This plasmid was then used to generate pCR3_SARS-CoV-2-S(Wuhan D614G)ΔC24 by site-directed mutagenesis PCR (Asp614➔Gly; GAC➔GGC) using the Q5® site directed mutagenesis kit.

VOC strain S expression plasmids were created accordingly, and all had the same C-terminal 24 aa truncation. Mutations relative to the parental Wuhan isolate 1 strain are listed in the following table, with mutations located in the RBD and therefore diverging from the minispike sequence underlined:

Alpha	H69-V70 del, Y144 del, <u>N501Y</u>, A570D, D614G, P681H, T716I, S982A, D1118H, ΔC24
Beta	D80A, D215G, L242_A243_L244 del, <u>K417N, E484K, N501Y</u>, D614G, A701V, ΔC24
Gamma	L18F, T20N, P26S, D138Y, R190S, <u>K417T, E484K, N501Y</u>, D614G, H655Y, T1027I, ΔC24
Delta	T19R, E156-F157 del, R158G, <u>L452R, T478K</u>, D614G, P681R, D950N, ΔC24
AV.1	D80G, T95I, G142D, Y144 del, <u>N439K, E484K</u>, P681H, I1130V, D1139H, ΔC24

All constructs were inserted as described into pCR3.

Generation of VSV-ΔG GaussiaLuc [SARS-CoV-2 S] stocks

To generate SARS-CoV-2 S pseudotyped VSV-ΔG stocks, 293T cells were seeded in poly-D-lysine coated 10 cm dishes, aiming for 90 % confluency after overnight incubation. The next day, 10 µg of pCR3_SARS-CoV-2-SΔC24 expression plasmid was transfected per plate with Lipofectamine3000 according to the manufacturer´s protocol. All following incubation steps were performed in a humified incubator set to 32°C, 5 % CO_2 [222].The transfected cells were incubated for 24 h, infected with VSVeGFP-ΔG-GaussiaLuc [VSV G] viruses at a MOI of 3 and incubated for two hours. Afterwards, the cells were washed twice with PBS (with a volume exceeding that of the infection inoculum to eliminate input virions sticking to the walls) and incubated with anti-VSV-G hybridoma supernatant diluted 1:5 in DMEM 3+ for one hour. Afterwards, they were washed again twice with PBS and finally 10 ml fresh

DMEM3+ containing 10 % anti-VSV-G hybridoma supernatant was added and the cells were incubated for 20-24 h at 32°C, 5 % CO_2. The supernatant was harvested, centrifuged (1000 g, 5 min, 4°C) to remove cell debris, sterile filtered through a 0.22 µm sterile syringe filter unit, aliquoted and frozen at -80°C.

Titration of VSV-ΔG GaussiaLuc [SARS-CoV-2 S] stocks

Titration of SARS-CoV-2 S pseudotyped viruses was carried out on VeroE6 cells which show a strong ACE2 expression. One confluent T25 was trypsinized, resuspended in 25 ml of DMEM3+ and 100 µl of the cell suspension were seeded per well into 96-well plates two hours prior to titration. To determine the infectious particles per ml, an aliquot of each stock was thawed and serially diluted 1:10 six times. 100 µl of undiluted stock and serial dilutions were added in duplicates to the cells. To control for residual VSV-G mediated infectivity, 1 µL, 5 µL, 10 µL and 20 µl of undiluted stock were incubated with 1 µl of either anti-VSV-G hybridoma supernatant, a highly neutralizing human BTN162b2 vaccinee serum or a human control serum with no neutralizing activity against SARS-CoV-2 for 1 h and added to the cells. Titers were determined by counting fluorescent cells after overnight incubation at 32°C.

Virus neutralization assays

Virus neutralization assays were done in VeroE6 cells in black-wall optical bottom 96-well-plates that allow for sequential fluorescent imaging and direct luciferase measurement in the same plate. A confluent T25 flask of VeroE6 cells was trypsinized and resuspended in 30 ml of DMEM3+. 100 µl of cell suspension were seeded per well and cells were incubated overnight at 37°C.

A serial 2-fold dilution of sera or antibody preparation in OptiPro serum-free medium or DMEM3+ was made, starting with a 1:50 or 1:100 dilution, calculated based on the neutralization volume. Neutralization volume describes the reaction volume in which the neutralization takes place, including immune serum + diluent (medium) + virus preparation. In this case, the neutralization volume equaled 25 µl. As multiple sera were handled simultaneously, dilutions were done in sterile 96-well PCR plates by prefilling each well except the top row with 25 µl and the top row with twice that volume plus additional 10 % (in total 55µl). A volume of serum (one serum per column) corresponding to a 1:50 or 1:100 dilution (after addition of the virus volume, so for example 1,32 µL (1:50) or 0,66 µl (1:100) for a virus volume of 5 µl per well) was then added to the top row and mixed thoroughly by pipetting with a multichannel pipette. 25 µl from the first row where then transferred into the second and mixed well. This procedure was repeated until the second to last row. On the second-to-last row (now containing twice the volume of the other rows), half of the volume was discarded. The last row was used as baseline infection control and contained no serum. A volume containing to 200-400 infectious units of

pseudovirus preparation (this corresponded to 1-5 µl of VSV-ΔG-GaussiaLuc [SARS-CoV-2 S] stocks) were added without further dilution directly to the serum dilutions and the control row, the plates were covered with sealing foil and incubated for one hour at 32°C in a humified incubator. Afterwards, the foil was removed and 20 µl of the serum/virus mix was added to the cells. Cells were then incubated for 24-36 hours at 32°C. All wells were photographed on a Leica DMi8 automated fluorescence microscope and counted using Fiji/ImageJ [223]. Afterwards, the supernatant was aspired, the cells were lysed using 25 µl passive lysis buffer per well (Promega) for 30 minutes under constant shaking. Luciferase activity was then measured in a Berthold Mithras LB 940 Multimode Microplate Reader. The data were analyzed and visualized using GraphPad Prism version 9.2 for Windows (GraphPad Software, San Diego, California USA, www.graphpad.com).

Results

Design of a SARS-CoV-2 RBD-minispike construct

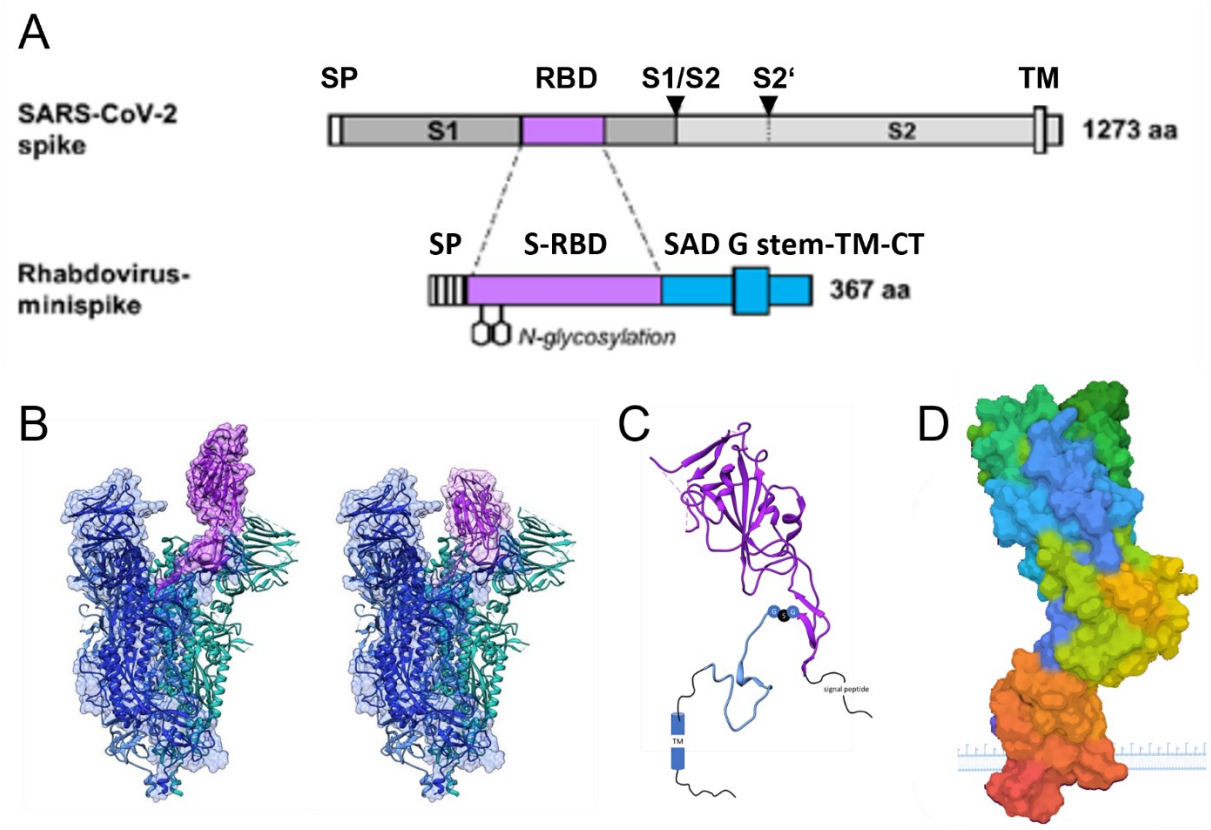

Figure 7: A: schematic representation of SARS-CoV-2 S domain organization (top) and minispike. B: Model of S in an RBD-up (left) and RBD-down (right) conformation. The RBD is colored in purple. C: Structural Modeling of the minispike construct. Residues corresponding to the S RBD are colored in purple; the SAD G derived stem, transmembrane domain and c-tail in blue. D: Structure prediction of the minispike construct with RoseTTAFold [224]; residues are colored according to the spectrum starting at the N-terminus (blue) to the C-terminus (red).

The RBD of the SARS-CoV-2 spike protein was identified by sequence homology to the SARS-CoV-1 RBD and by functional studies [106, 122, 128, 132]. Structural analyses revealed an autonomously folding, discrete globular-shaped domain, able to switch between “up” and “down” configurations in the context of the pre-fusion form of the S protein, and in which the up-conformation is needed to engage ACE2 [115, 121]. The RBM comprises residues 437-508 (NSNNL…GYQPY) and forms the direct interactions with the receptor. In the RBD-down state, it is partially inaccessible to antibodies. Based on the structure analysis we selected residues 314-541 (QTSN...KCVNF) to be included in a chimeric transmembrane minispike in which the entire RBD domain should be presented in a natural conformation. In addition, the minispike was designed to be compatible for presentation on the cell membrane as well as for its incorporation into the envelope of rhabdoviruses, including VSV and RABV, and virus-like particles (VLPs).

To ensure high-level translation into the endoplasmic reticulum as well as correct folding and posttranslational modifications to our RBD immunogen construct, we fused the highly efficient signal peptide of Immunoglobulin Heavy Variable 3-7 (IGHV3-7) to the N-terminus of the SARS-CoV-2-RBD to facilitate the incorporation into the membrane of infected cells. Efficient SP recognition and cleavage was then calculated with SignalP 5.0 (http://www.cbs.dtu.dk/services/SignalP/)[225], which predicted a highly probable (96,93 %) and efficient cleavage between aa 19 and 20. Subcellular localization prediction with DeepLoc-1.0 [226] further indicated a correct, cell membrane-bound presentation of the minispike construct.

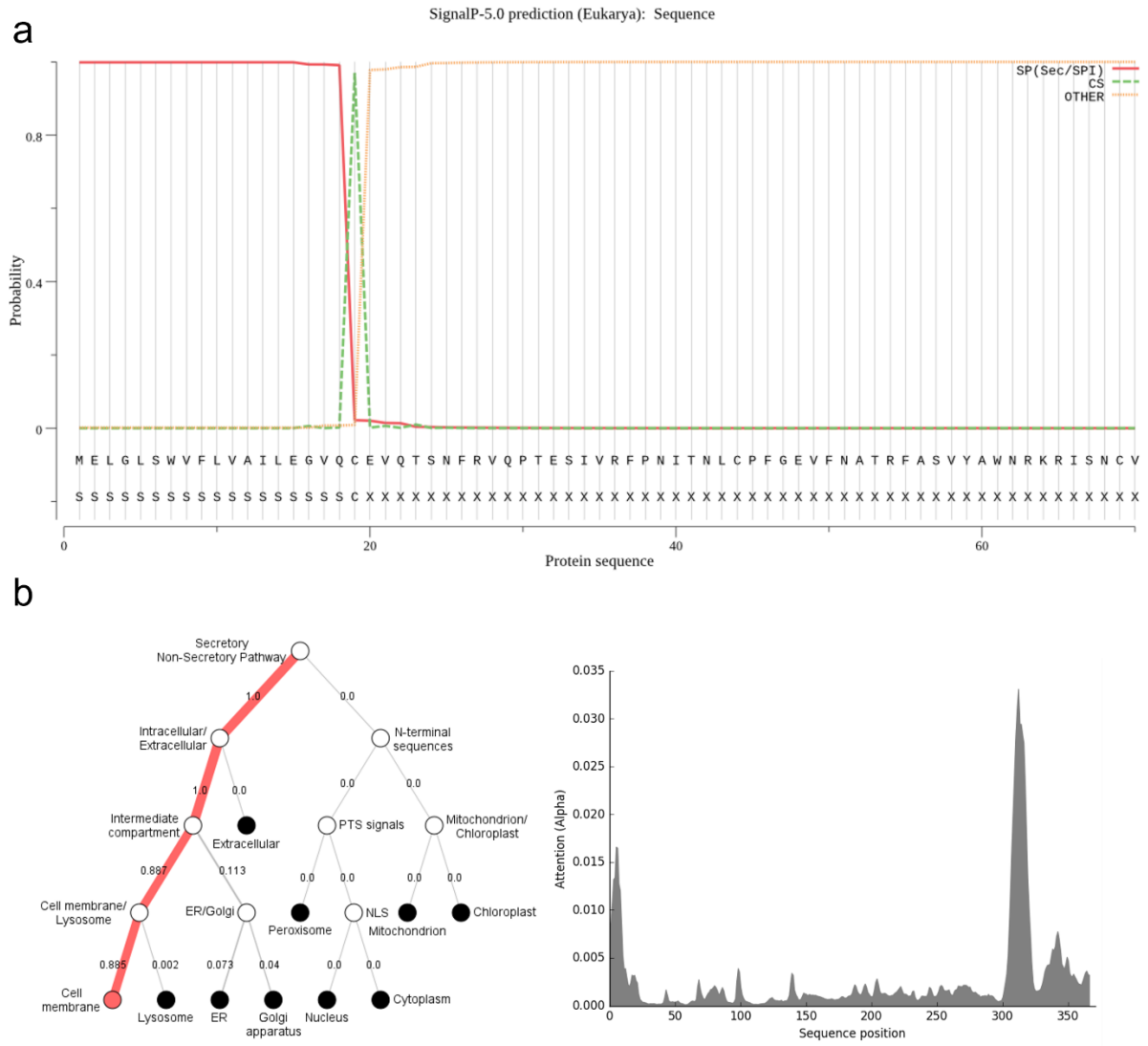

Figure 8: a.) Prediction of signal peptide recognition and cleavage of the minispike construct with SignalP-5.0 [225]. b.) Prediction of cellular localization (left) and position importance in regard to localization (right) with DeepLoc-1.0 [226]

The carboxy-terminus of the RBD sequence was connected to a transmembrane stem-anchor derived from the glycoprotein (G) of the RABV strain SAD via a short, flexible synthetic linker (Gly-Ser-Gly). The stem-anchor comprises the membrane proximal part of the G ectodomain (stem), the trans-membrane domain, and the cytoplasmic sequence of SAD G (VIPLV…GETRL*) [227]. The entire construct contains

367 aa, including the signal sequence, and two N-glycosylation sites in the RBD moiety ($\underline{N}_{331}\underline{IT}$NLCPFGEVF$\underline{N}_{343}\underline{AT}$). Importantly, N_{343} is a critical residue forming a highly conserved epitope targeted by potent pan-sarbecovirus neutralizing mAbs [228]. The SAD G stem was selected because it should allow incorporation into the envelopes of not only RABV, but also of non-RABV rhabdoviruses, such as VSV, which has less stringent sequence requirements for membrane protein incorporation [209, 229]. In the case of VSV, the heterologous RABV-derived stem-anchor was predicted not to critically compete with VSV G incorporation needed during production of infectious single cycle VSV replicon viruses. The DNA encoding the minispike construct was synthesized *de novo* by GeneArt and contained the VSV G 5´-UTR downstream of the *MluI* restriction site, a Kozak sequence (GCCACC) immediately upstream of the coding sequence (CDS) and the VSV G 3´-UTR followed by the *XhoI* restriction site. The minispike CDS including the Kozak sequence was PCR amplified with a forward primer introducing a *EcoRI* restriction site immediately upstream of the Kozak sequence and a reverse primer introducing a *NotI* restriction site downstream of the Stop-Codon, digested with *EcoRI* and *NotI* and ligated into a pCR3 vector backbone also digested with *EcoRI* and *NotI* resulting in pCR3-minispike.

Generation of minispike variants corresponding to emerging VOCs

To create minispike variants corresponding to emerging variants and especially VOCs, the minispike residues matching to S residues K417, L452, T478, E484, and N501 (corresponding minispike residues: K125, L160, T186, E192, and N209) were mutated by sequential mutagenesis PCR to their respective targets, e.g., for a minispike variant based on the S from beta that should comprise K417N, E484K and N501Y the codons encoding residues K125, E192 and N209 were mutated to encode N, K and Y, respectively. The variants generated in this manner included alpha (N209Y), beta (K125N, E192K, N209Y), gamma (K125T, E192K, N209Y), epsilon or Cal.20.C (L160R), delta (L160R, T186K), and kappa (L160R, E192Q).

The minispike construct is expressed and post-translationally modified

Expression of the minispike construct in HEK293T cells after transfection with plasmid-encoded minispike (pCR3-minispike) was at first analyzed by Western blot with an anti-SAD G C-tail peptide serum (HCA-5) recognizing the RABV-derived intracellular part of the anchor sequence. Minispike proteins were of the predicted molecular weight range. As two putative N-glycosylation sites are present in the RBD part of the minispike ($\underline{N}_{39}\underline{IT}$NLCPFGEVF$\underline{N}_{51}\underline{AT}$), we conducted deglycosylation experiments with PNGase F (which removes all types of N-linked glycans) and Endo-H (which removes all sugars up to high mannose glycans, but not more complex processed sugars). As control, we also processed the parental SAD G, which has four predicted N-glycosylation sites. Treatment with both

enzymes led to a decrease of the apparent size on Western blot. While the untreated minispike protein is detected at the predicted size of 40 kDa, PNGase F treatment led to a single band at approximately 30 kDa, arguing for complete cleavage of all glycans. EndoH treatment generated two bands, one at 40 kDa corresponding to fully glycosylated minispike, the other at the size of the PNGase F band. Similarly, RABV G revealed the presence of EndoH-resistant proteins. This confirmed the presence of (EndoH-resistant) complex sugar chains and indicated correct processing and transport of the minispike protein through the Golgi apparatus.

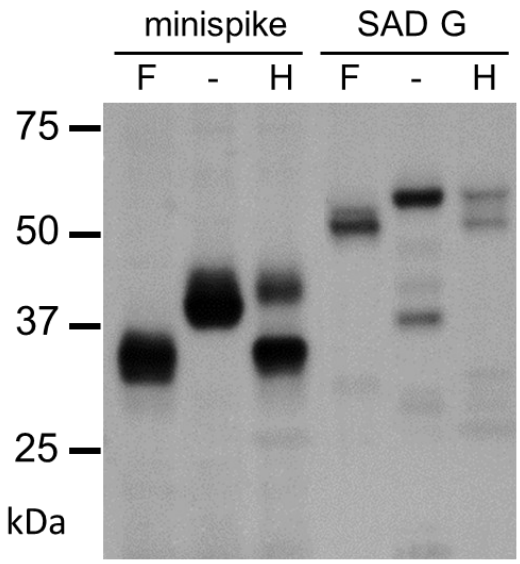

Figure 9: Deglycosylation experiments on the minispike construct and SAD G reveal complex glycosylation and successful transport through the Golgi apparatus. Nontreated (-) minispike and SAD G show bands corresponding to the calculated size. Treatment with PNGase F (F) leads to complete deglycosylation and reduction in apparent size. Treatment with EndoH (H), which cleaves only high mannose, leads to size decrease in only part of the proteins, arguing for the presence of highly processed sugars and thus productive processing in the Golgi apparatus for both minispike and SAD G.

Minispike protein is transported to the cell surface and recognized by patient sera

Expression of the minispike protein at the cell surface was further demonstrated by microscopic imaging. Positive staining of pCR3-minispike transfected unfixed live cells with serum from convalescent COVID-19 patients and an anti-human IgG secondary antibody, but not from sera with SARS-CoV-2 naïve healthy donors indicated that the minispike construct is transported to the cell surface and recognized by COVID-19 specific IgG antibodies, arguing that the minispike acquires a conformation corresponding to the natural S RBD. Positive staining with the RBD mAb CR3022, which in the context of the S protein binds to an epitope of the RBD only accessible in the up conformation [112, 230] indicates that the minispike RBD construct acquires a conformation that displays epitopes exclusively exposed in the vulnerable “up” configuration of the natural SARS-CoV-2 RBD. After surface staining, cells were fixed with 4 % PFA and counter-stained with HCA5 recognizing the SAD G derived c-tail of the minispike construct to confirm the origin of the positive staining. Indeed, both stainings

overlapped, indicating that positive staining with COVID-19 patient sera and CR3022 depends on minispike expression.

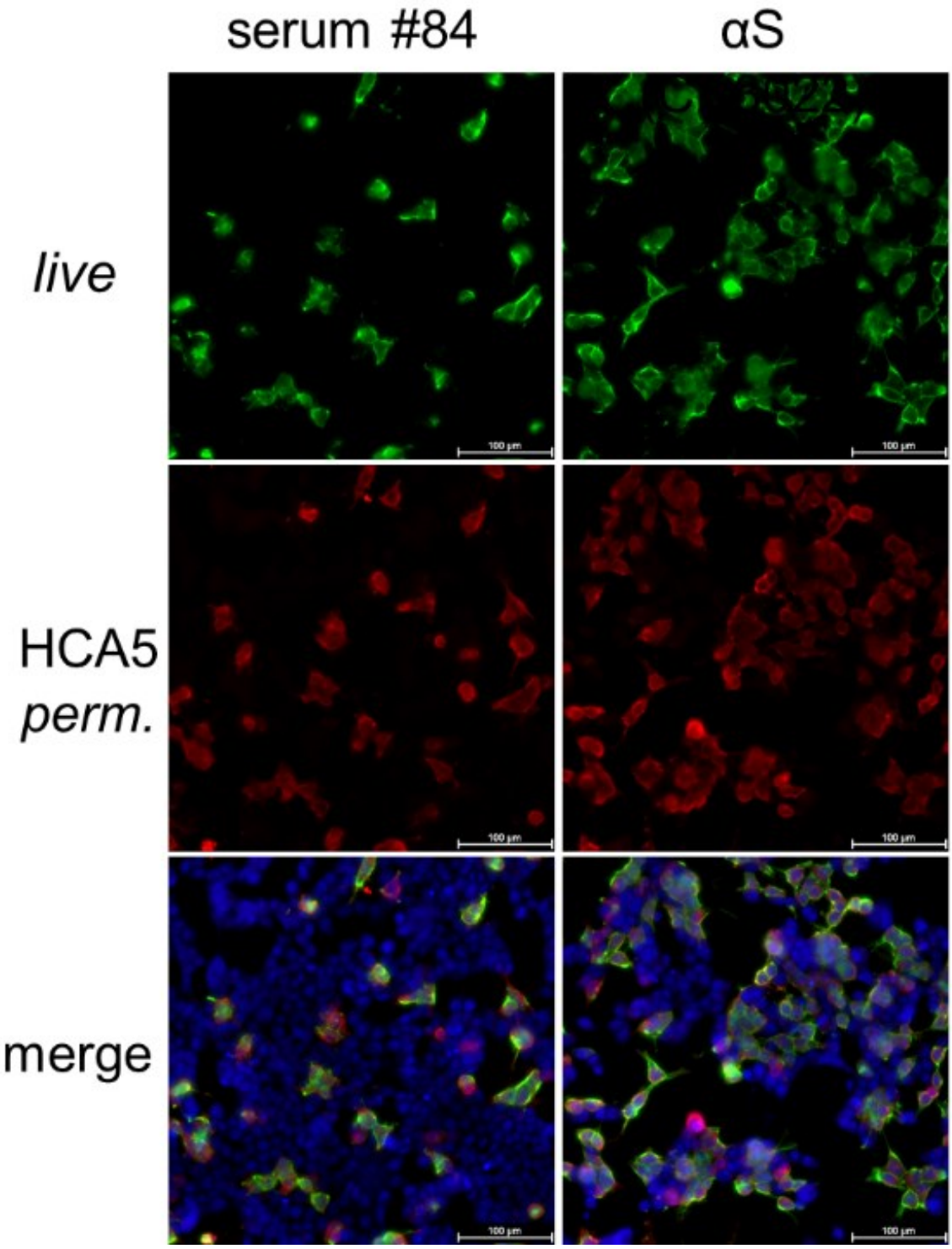

Figure 10: Live cell surface staining of minispike-expressing HEK293T cells with COVID-19 patient sera (serum#84, green) and RBD mAb CR3022 (αS, green) reveals specific recognition of minispike-positive cells as determined by HCA5-straining (red). Cell nuclei were stained with DAPI and are depicted in blue. 200x magnification.

Construction of minispike-expressing rhabdoviruses

A molecular clone of the Indiana strain of VSV (VSIV) [52] comprising an additional transcription unit encoding for eGFP between the G and L gene (VSV eGFP) was used as a basis for generation of a series of G gene deleted VSV replicons (VSVΔG) encoding the minispike. The constructs included eGFP reporter viruses and viruses expressing single or multiple copies of the minispike gene inserted either upstream of the L gene, or at the 3' proximal gene position, which in rhabdoviruses is transcribed most abundantly [231, 232]. The minispike construct and VSV-eGFP were digested with *MluI* and *XhoI* and ligated, resulting in the exchange of the G gene for the minispike gene (genome organization 3´-Le-N-P-M-Minispike-eGFP-L-Tr-5´; VSVΔG-minispike-eGFP). VSVΔG-minispike-eGFP variants expressing minispike constructs with point mutations corresponding to the S proteins from VOCs, e.g., B.1.351 or beta (VSVΔG-minispike(B.1.351)-eGFP) were generated equivalently.

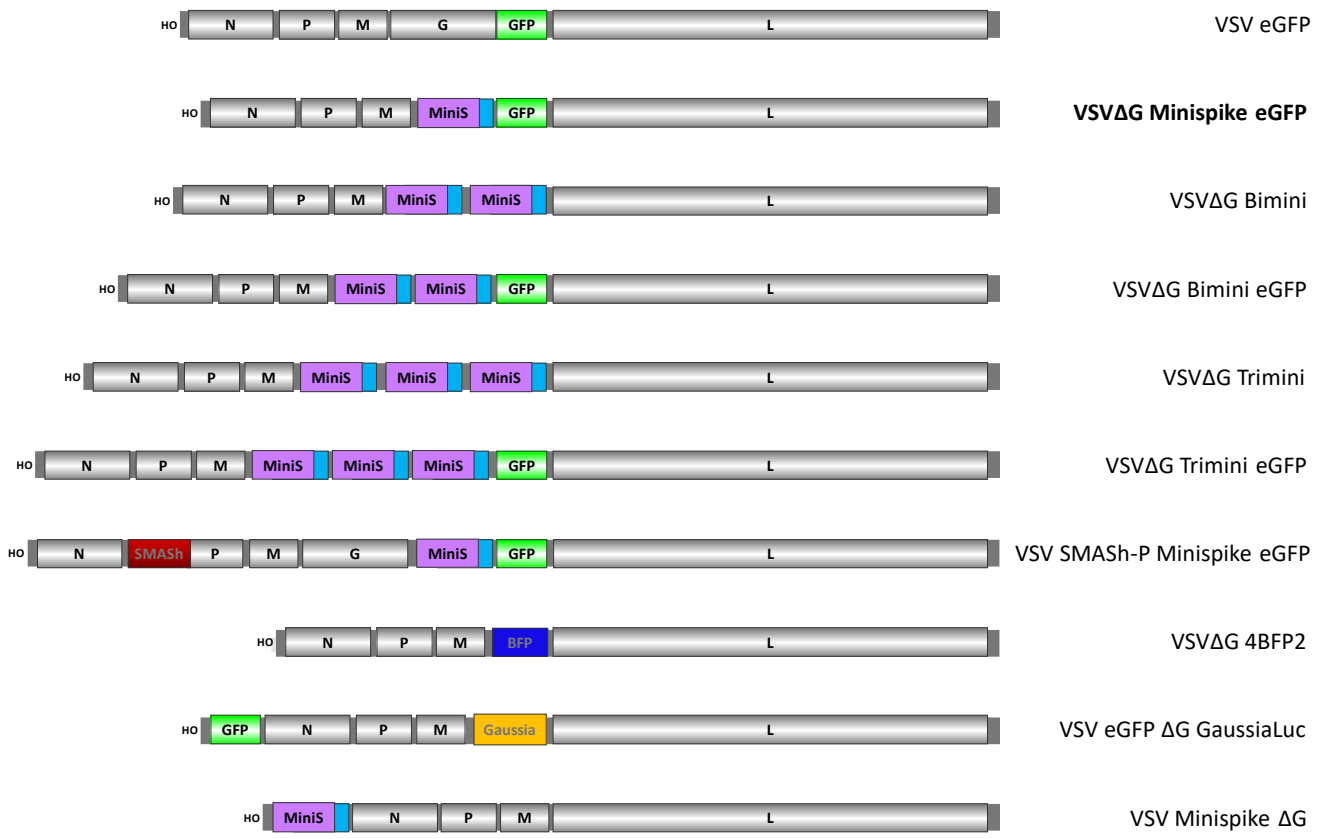

Figure 11: VSV constructs used in this thesis. VSVΔG-minispike-eGFP was created by exchanging the VSV G CDS of VSV-eGFP with the minispike CDS. VSVΔG-bimini was obtained by exchange of the eGFP CDS of VSVΔG-minispike-eGFP by another minispike CDS. VSVΔG-bimini-eGFP was generated by substituting the eGFP cassette of VSVΔG-minispike-eGFP by a tandem minispike-eGFP cassette.

Construction of multivalent minispike-expressing rhabdoviruses

Viruses encoding for multiple copies of the minispike were generated by PCR amplification of a fragment comprised of the two adjacent transcription units minispike and eGFP with primers introducing a *SalI*-site at the 5´-end of the minispike gene and a *NotI*-site at the 3´-end of the eGFP gene (*SalI*-minispike-eGFP-*NotI*). Restriction with *SalI* creates compatible DNA overhangs to *XhoI*, allowing to replace the eGFP transcription unit (which is flanked by *XhoI* and *NotI* restriction sites) in VSV-ΔG-minispike-eGFP with the tandem cassette minispike eGFP, resulting in VSV-ΔG-minispike-minispike-eGFP, which we named VSV-ΔG-bimini-eGFP. Importantly, this strategy introduces an "intact" eGFP transcription unit flanked by unique *XhoI* and *NotI* restriction sites, which allows for repetition of the entire procedure. We followed this strategy to create a virus with three minispike cistrons (VSV-ΔG-trimini-eGFP), but in theory this can be continued until the maximal length tolerated by the RNA polymerase and therefore genome stability is reached.

By amplifying and inserting only the minispike transcription unit with primers introducing flanking *SalI* and *NotI* restriction sites we generated VSV-ΔG-bimini and VSV-ΔG-trimini, i.e., constructs lacking the eGFP gene. Due to the introduction of repetitive cistrons with identical nucleotide sequence, Sanger sequencing is only possible from the flanking regions and only up to the length of a typical sequencing run, i.e., roughly 1000 bases. To ensure the correct size of the inserted DNA, analytic digestions with the restriction enzymes flanking the inserts, *MluI* and *NotI*, were performed. The resulting band pattern shows, as expected, an identical backbone band of 12723 bps and an insert band of 1892 bp (minispike eGFP), 2272 bp (bimini), 3048 bp (bimini eGFP), 3428 bp (trimini) or 4204 bp (trimini-eGFP) for the respective constructs. Two different clones of each construct were analyzed.

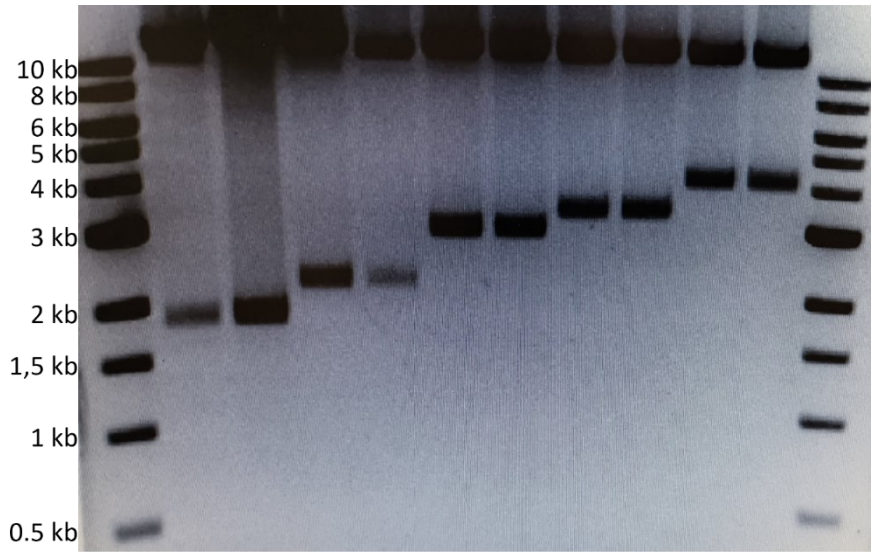

Figure 12: VSV Δ minispike constructs; analytic digest with MluI *and* NotI *restriction enzymes, flanking the region 3´ of M and 5´ of L (antigenomic orientation). Loading scheme: Marker-minispike eGFP(1892bp)-bimini(2272bp)-bimini eGFP (3048 bp)-trimini(3428 bp)-trimini-eGFP(4204 bp); duplicate constructs were loaded)*

Generation of stoppable VSV-SMASh-P-eGFP and VSV-SMASh-P-minispike-eGFP viruses

As residual toxicity of replicating, spreading-competent VSV cannot be excluded and might indeed pose a significant problem [233], it is invaluable to implement control mechanisms. The SMASh tag as originally described [86] comprises a highly active HCV NS3/4A protease construct, which recognizes the minimal consensus cleavage sequence (D/ExxxxC/TS) fused to the N- or C- terminus of the protease [234-236]. In addition to autocatalytic cleavage in *cis*, off-target cleavage can affect both viral proteins and/or cell proteins needed for efficient virus amplification, thus restricting or abrogating virus growth. Indeed, theoretical NS3/4A recognition sequences are present in VSV N, G and L proteins (not shown). We therefore examined first if SMASh expression would interfere with VSV infection. Transient expression experiments in VSV-infected cells, however, did not indicate obvious interference of NS3/4A protease activity with VSV-encoded GFP expression (not shown). We then proceeded to construct two recombinant VSV constructs with SMASh-tagged P proteins. While VSV-eGFP and VSV-eGFP-minispike viruses grew with comparable kinetics to similar titers, both VSV SMASh-P eGFP versions showed a growth attenuation and reached approximately one log lower titers. This was also reflected by reduced GFP expression in infected cells.

Drug-controllable VSV infection

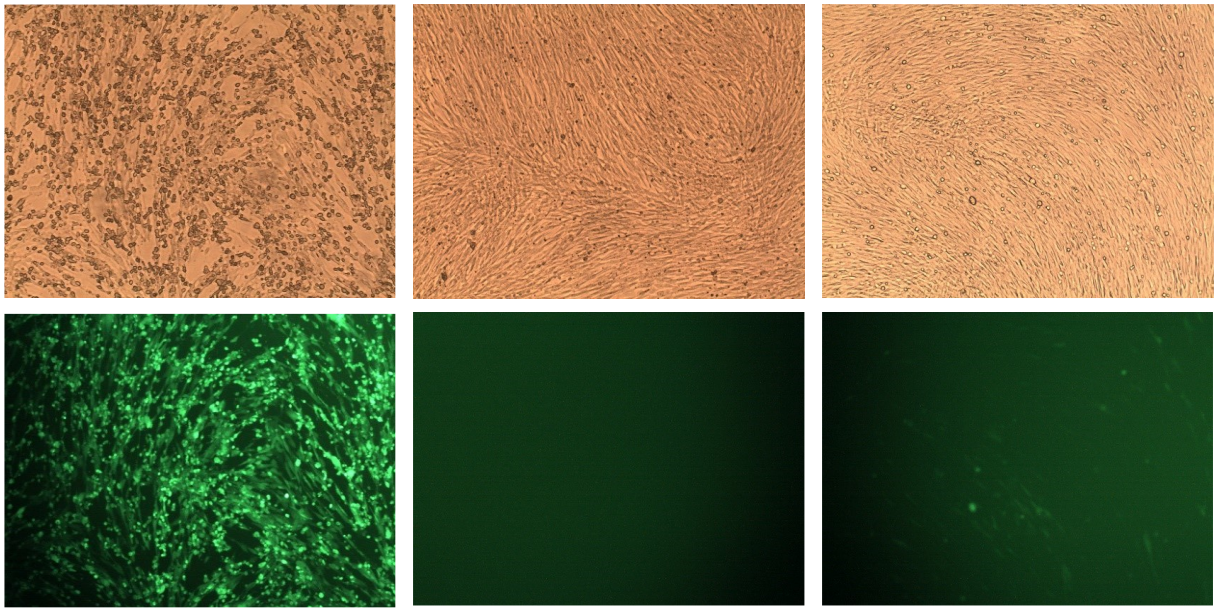

no DNV DNV at infection DNV 4h post infection

Figure 13: VSV SMASh-P eGFP virus infection can be inhibited and stopped by previrs. First column: BHK-21 cells were infected with VSV SMASh-P eGFP at a MOI of 0.1 and visualized 24h post infection. Infection spread to the whole cell culture and the cells exhibit a cytopathic phenotype. Middle column: BHK-21 cells were infected with VSV SMASh-P eGFP and treated at infection with 3 µM DNV. No visible eGFP expression is detectable and cells form a healthy monolayer after 24h. Third column: BHK-21 cells were infected with VSV SMASh-P eGFP and treated with 3 µM DNV 4 h post infection. Infection was established in roughly 10 % of cells as demonstrated by eGFP expression but did not advance further. Cells formed a healthy monolayer without visible cytopathic effect 24h post infection.

To investigate whether VSV SMASh-P eGFP infection can be controlled by HCV protease inhibitors (previrs), BHK-21 cells were infected with replication-competent VSV SMASh-P eGFP at a MOI of 0.1 and treated with 3 µM Danoprevir (DNV) or DMSO as a control at infection or at 4 h post infection. The infection status was monitored by virus-encoded eGFP expression 24 h post infection. In the absence of DNV (left column), virus replication and spread were not hampered and after 24 h, the whole well was infected. At this time point, the cells started to show the VSV-characteristic cytopathic phenotype correlating with a strong eGFP expression. Addition of DNV at infection completely prevented visible eGFP expression (middle column). While some primary transcription should take place, expression of eGFP did not reach levels high enough to be distinguishable from background. The cells formed a healthy, confluent monolayer. When added 4 h post infection, viral infection was established but DNV prohibited further expansion (right column). The first line of infected cells exhibited a low, but clearly noticeable eGFP signal. Further virus spread was abrogated, and the cells did not develop a cytopathic phenotype.

Curing of infected cell cultures from replication- and spreading-competent VSV

As prevention of NS3/4A-dependent virus replication by previrs has been demonstrated with other negative-strand RNA viruses [86, 87], it was not entirely surprising that the results with VSV are similar. However, the question remained open whether previrs can halt ongoing infections and whether curing of cell cultures from viruses is possible, which was not shown previously. To address this issue, we infected HEK293T and BHK-21 cell cultures at low MOIs, incubated for two hours to allow for attachment and entry and washed, trypsinized and reseeded the cells into new plates to remove all input virus. The infection was then allowed to proceed until approximately 20 % of the cell culture was infected. We then added 3 µM DNV to stop virus expansion, which was monitored by eGFP fluorescence and titration of viruses released into the supernatant. The medium was replaced every day. As treatment with previrs in this system is virostatic and not virucidal and only newly synthesized proteins are rendered non-functional or degraded, we washed out DNV after increasing incubation times, to determine whether non-proliferative (or inutilely active) RNPs are able to resume viral replication in the absence of the drug. The timeframe during which removal of the drug leads to a resurgence of infection is largely a function of RNP stability in the cellular environment. As no functional P is synthesized de novo while the inhibitor is present, the pre-existing P levels are declining according to the half-life (t=1/2) of the protein. The critical point in time is when no infectious virions remain in the supernatant, P protein levels in infected cells have deteriorated to an extent that no functional RNP complexes can be formed or maintained, and no functional P mRNA transcripts are present. Removal of the drug before that point would arguably lead to a recommencement of infection, whereas after that time point removal of the drug would not have any effect on the virus and the cell or cell culture would be cured. Titers of control cell cultures infected but not treated with DNV reached 10^7 IU/ml one day post infection. Infection rapidly progressed and cytopathic effects became visible. This resulted in steadily diminishing supernatant titers that reached non-detectable levels after 13 days. In the presence of DNV, the titers reached 10^4 IU/ml after one day of treatment and already after two days no infectious particles were detectable in the supernatant, implying a discontinuation of progeny virus production. DNV removal after nine days post treatment resulted in an immediate restart of virus replication as demonstrated by rapidly resurging supernatant titers and spread of the infection to the whole cell culture accompanied by eventual cell lysis. This implies the presence of either functional RNP complexes (or P transcripts and sufficient N and L protein as well as genome RNA to assemble new RNP complexes) as late as nine days post replication stop.

In contrast, continuous treatment with the drug for 16 days prior to removal of DNV resulted in “curing” of the cell culture, as no recommencement of the viral infection was observed after that time point. Taken together, these results suggest that intracellular VSV RNPs can persist for at least nine days, but

not as long as 16 days. Strikingly, this also implies that a typically lytic acute VSV infection can be tolerated in infected cells for a prolonged period when it is suspended by the SMASh system.

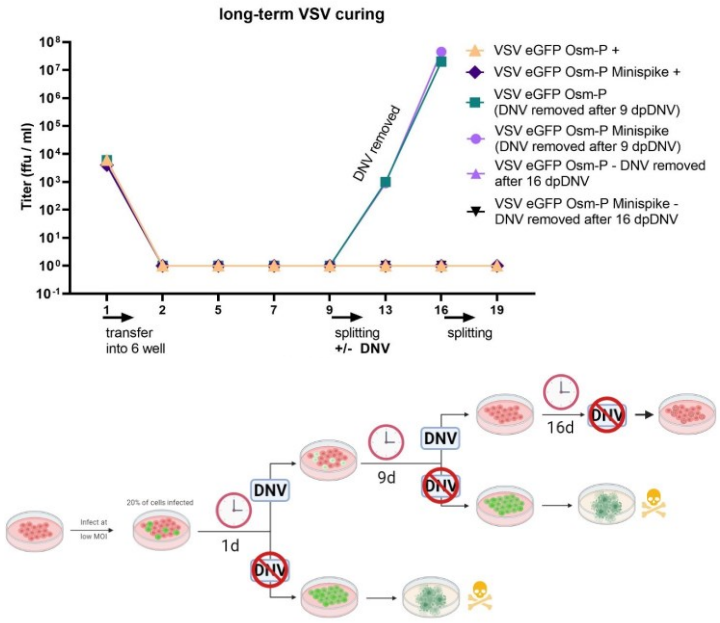

Figure 14: Curing of infected cell cultures from spreading-competent VSV: cells were infected with VSV eGFP SMASh-P and VSV eGFP SMASh-P minispike at low MOI and virus infection was allowed to proceed until 20 % of the cell culture was eGFP-positive. Addition of the NS3/4A inhibitor Danoprevir (DNV) led to arrest of the infection and decreasing supernatant titers, whereas without DNV the infection spread to all cells and led to eventual lysis of the cell culture. Medium was exchanged each day and supernatant titers were determined. Removal of DNV after nine days led to recommencement of infection for both viruses. After 16 days of continuous DNV treatment, no resurgence of infection was observed, and the cell culture was deemed cured.

Rescue and characterization of minispike-expressing single round rhabdoviruses

Rescue of minispike-expressing rhabdoviruses from cDNA

Recombinant G gene-deficient viruses were rescued in HEK293T cells and propagated in 293T cells transfected with VSV G plasmids or in a cell line with inducible VSV G expression (BHK-G43) [217]. All VSVΔG viruses were rescued efficiently and yielded comparable titers in the range of 5x 10^7 to 4x 10^8 IU/ml after 20-24 h of infection. G gene-deficient RABV cDNA and replicons were generated based on SADΔG-eGFP and grown as described before [229, 237-239].

Characterization of minispike VLPs and mosaic viruses

As the minispike stem-anchor is derived from the G protein of the RABV SAD strain, we first studied incorporation into virions of the autologous SADΔG-minispike-mNeonGreen and SADΔG-bimini-mNeonGreen. To this end, the SADΔG replicons were grown for three days in HEK293T cells transfected previously with G or without G. Supernatant virions were concentrated by ultracentrifugation through a sucrose cushion and equivalent volumes were processed for Western

blot analysis with a RABV P serum, and HCA05 serum to detect virus-associated minispikes and SAD G. Minispike protein was effectively incorporated into particles both in the absence and in presence of the parental SAD G. However, in the presence of SAD G, less minispike was observed in RABV particles, suggesting competition of the homologous SAD G and the minispike carrying a homologous G stem/anchor sequence for incorporation.

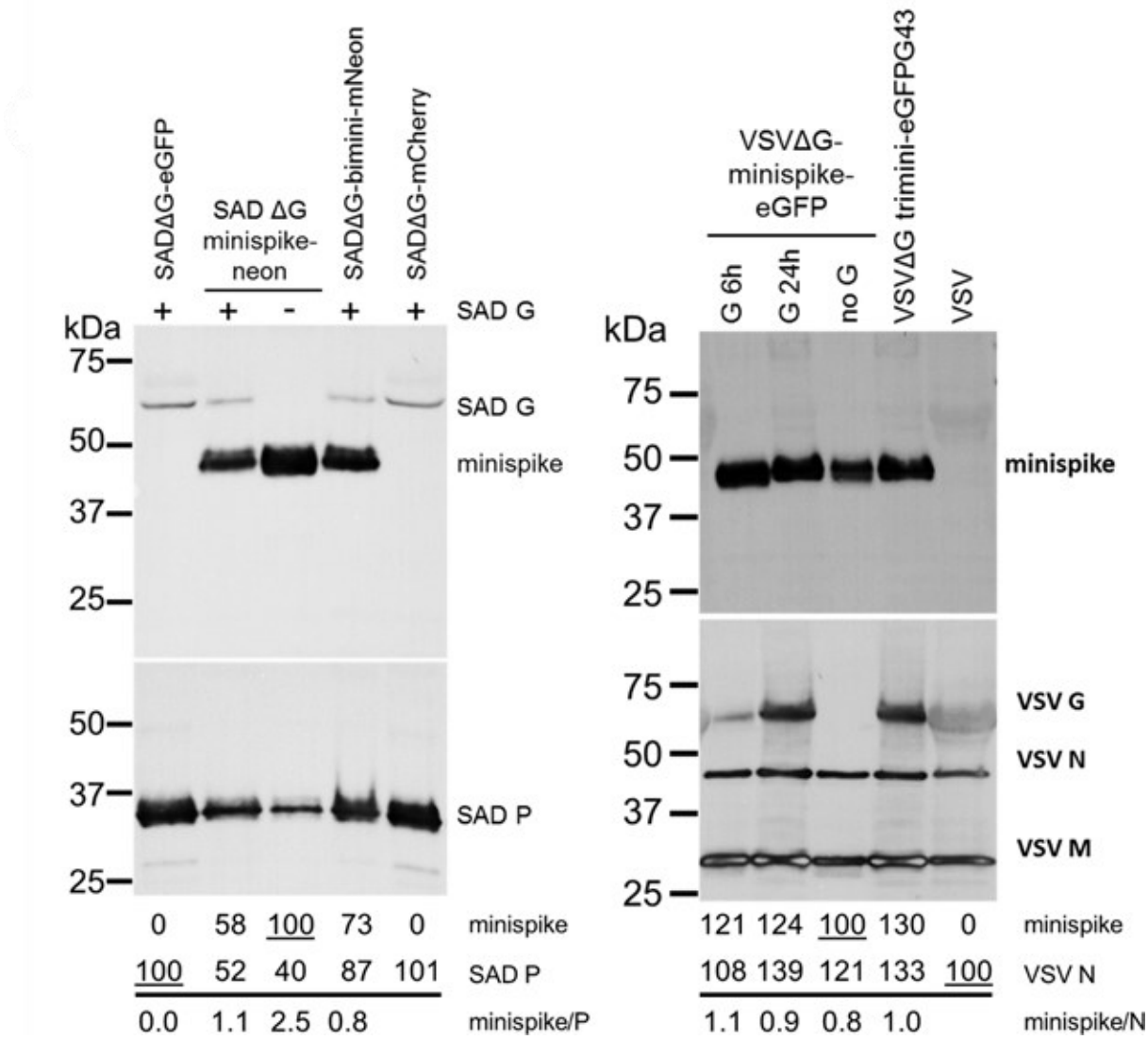

Figure 15: Incorporation of minispike into the membranes of rhabdovirus ΔG minispike virions. Left upper blot: Western blot of control virus preparations (SADΔG-eGFP, SADΔG-mCherry) and minispike-expressing viruses (SADΔG-minispike-mNeon, SADΔG-bimini-mNeon) transcomplemented with SAD G (lane 1, 2, 4, 5) or not transcomplemented (lane 3). Minispike and SAD G were detected with HCA05 recognizing the SAD G c-tail also present in minispike. Left lower blot: Samples from above, probed with an antibody recognizing the structural protein SAD P. Right upper blot: Western blot of control virus preparations (VSV) and minispike expressing viruses (VSVΔG-minispike-eGFP, VSVΔG-trimini-eGFP) complemented with VSV G (lane 1, 2, 4) or not complemented (lane 3, 5. Lane 5 is full-length, G-expressing VSV). Detected with HCA05. Lower blot: samples as above, detected with S32 serum recognizing VSV M, N and G.

To examine incorporation of the “heterologous” minispike into the envelope of VSV particles, VSVΔG-minispike-eGFP stocks were produced in cells transfected with VSV G expression plasmids. For preparation of one stock, VSV G was expressed only 6 hours before infection with VSVΔG-minispike-eGFP, in another preparation VSV G was allowed to accumulate to high levels for 24 hours before infection. Western blot analysis of 1 million infectious units of each with anti-VSV serum revealed effective incorporation of the minispike along with VSV G. Marked competition of VSV G and minispike for incorporation was not observed.

Rhabdovirus G proteins are incorporated into viral envelopes as G trimers which is driven by interaction of the ectodomains and of the C-tails with the internal M-coated viral RNP [240-242], and their incorporation supports virus budding [43, 209]. Hypothetically, the presence of minispike protein in VSV envelopes could be due to its co-incorporation with VSV G molecules as hetero-trimeric complexes. To determine whether minispike alone supports budding of VSV VLPs, VSVΔG-minispike-eGFP stocks were produced in non-complementing cells and processed as above. Despite the absence of VSV G the minispike was incorporated efficiently into viral particles, revealing autonomous incorporation and release of non-infectious minispike VSV VLPs from infected, non-complementing cells. Notably, comparable amounts of minispikes were observed in VSV particles irrespective of the presence or absence of G.

Characterization of multivalent VSVΔG minispike viruses

The small size of the minispike gene allows for addition of multiple copies into the VSV-ΔG backbone without exceeding VSV coding capacity. We generated VSVΔG viruses encoding multiple minispike genes, sequentially in genome positions 4-6 (bimini, trimini), anticipating an increased expression of the minispike protein. However, the transcription of downstream genes in VSV is attenuated at each gene junction, and as the L gene is the terminal gene in all constructs, transcription and replication might be affected by each additional transcription unit.

As the original VSV-ΔG-minispike-eGFP expresses the minispike gene at position 4 and rhabdoviruses show a transcription gradient with the gene at position 1 (usually the nucleo- or N-protein) being the most abundantly transcribed and the gene at the last position (5, Large- or L-protein) the least abundant, we cloned and rescued VSV ΔG constructs in which the minispike is expressed from position 1. Furthermore, while providing several experimental benefits, the expression of a fluorescent protein is not beneficial for vaccination purposes. Therefore, for some of the second generation of constructs, we omitted the eGFP gene. The genome organization therefore is 3´-Minispike-N-P-M-L-5´ or 3´-Minispike-N-P-M-eGFP-L. The constructs were rescued, stocks were generated, and further characterization is ongoing.

Supernatant titers of multivalent minispike viruses

To determine if attenuation by an increased number of transcription units is reflected by viral supernatant titers we performed parallel infections on G-complementing BHK-VSVG43 cells and titrated the progeny viruses. Despite the addition of up to three kb of coding sequence and two additional gene junctions to the VSV-ΔG-minispike-eGFP genome, supernatant titers of all tested constructs were within one log range. There is however a trend towards lower titers with increasing number of genes, with the highest titers observed with VSV-ΔG-minispike-eGFP (4,3x 10^8 IU/ml) and the lowest with VSV-ΔG-trimini-eGFP (5x 10^7 IU/ml).

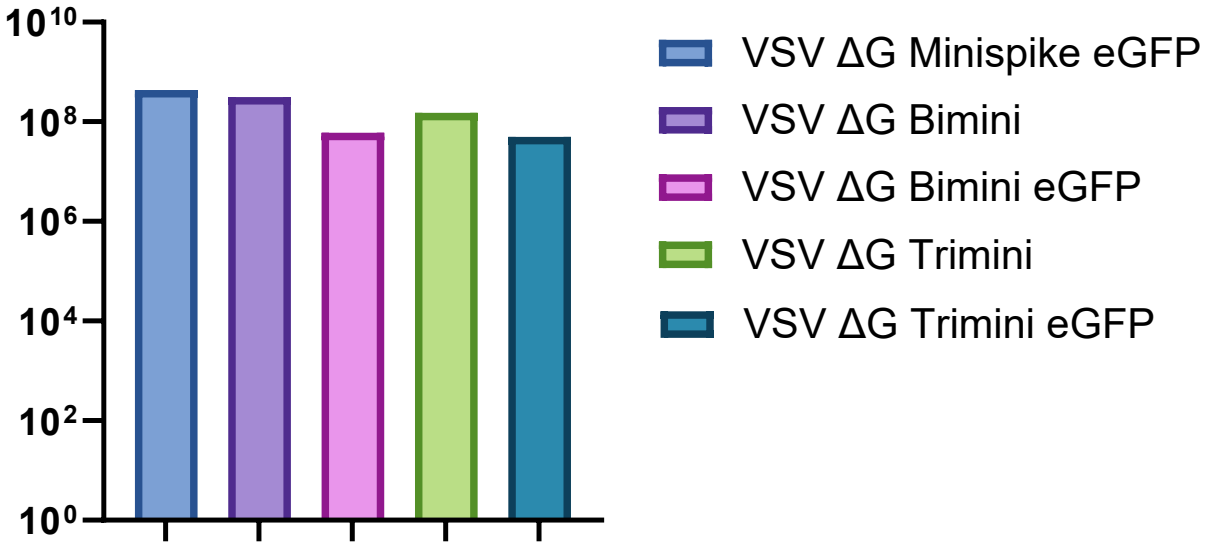

Figure 16: Supernatant titers of VSVΔG minispike constructs with increasing numbers of cistrons (VSVΔG minispike eGFP: 6 cistrons, VSVΔG bimini: 6 cistrons, VSVΔG bimini eGFP: 7 cistrons, VSVΔG trimini: 7 cistrons, VSVΔG trimini eGFP: 8 cistrons). BHK-VSVG43 cells were infected with indicated viruses at a MOI of 0.01 and VSV G expression was induced at infection. The cells were then incubated for 24h. Supernatants were titrated on BHK-21 cells and titers were determined by counting of minispike-positive cells.

Minispike expression levels of polyvalent constructs

As the viral titers were not reduced more than a log even after addition of two extra genes to the original VSVΔG-minispike-eGFP construct, we studied minispike expression levels in cells infected with the different constructs. To rule out variation in titers and ensure comparable infection levels, we used VSV G complementing cells, resulting in eventual complete infection of the cell cultures. In theory, more gene copies should equal more transcripts and more protein, however gene copy number did not obviously correlate with a higher minispike-specific signal in western blot, instead expression levels appeared relatively uniform with the highest signal for VSVΔG-bimini (five gene junctions upstream of L) and a considerable decline for VSVΔG-trimini-eGFP (seven gene junctions upstream of L). Generally, for viruses with the same number of gene junctions, two copies of the minispike gene appear to result

in higher minispike protein expression compared to one minispike gene and eGFP (VSVΔG-bimini vs. VSVΔG-minispike-eGFP and VSVΔG-trimini vs. VSVΔG-bimini-eGFP). Adding further cistrons and gene junctions lead to an apparent decrease in detected protein, although this was not quantified. As no construct showed a markedly improved minispike expression as determined by Western blot, the single copy VSVΔG-minispike-eGFP was chosen for further analyses.

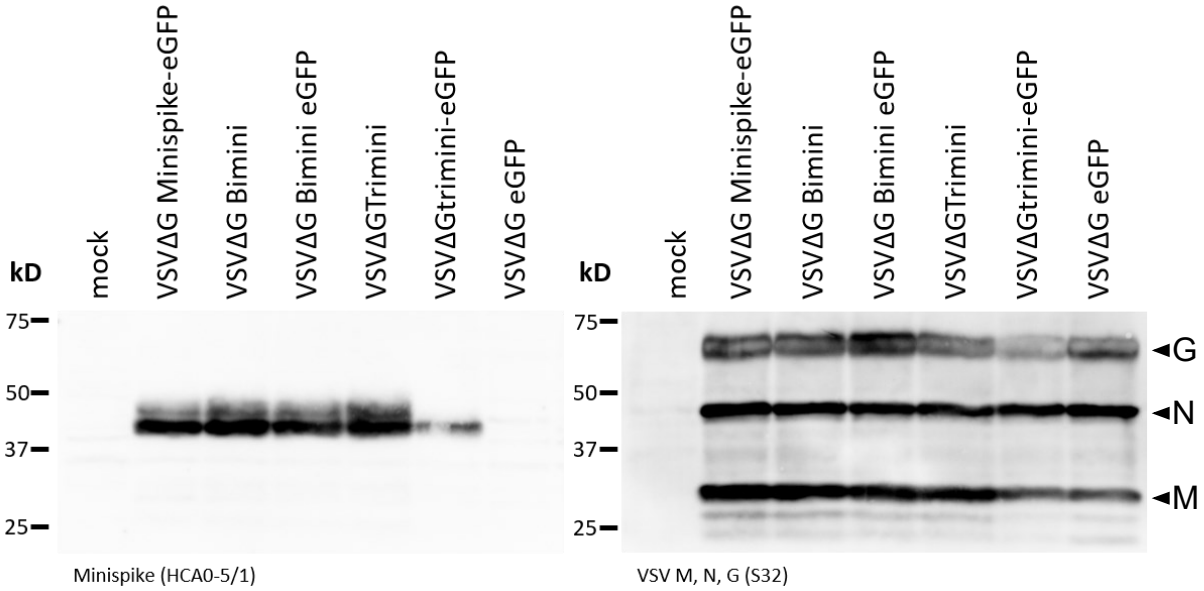

Figure 17: expression levels of polyvalent VSV-ΔG minispike constructs. BHK-VSVG43 cells were mock-infected (lane 1) or infected with VSV-ΔG-minispike-eGFP (lane 2), VSV-ΔG bimini (lane3), VSV-ΔG bimini eGFP (lane4), VSV-ΔG trimini (lane 5), VSV-ΔG trimini eGFP (lane 6) or VSV-ΔG eGFP (lane 7) at a MOI of 1. VSV G expression was induced at infection in infected cells. Cells were harvested 24h p.i. and minispike or viral proteins M, N and G were detected by Western blot. Left: detection with HCA05/1 recognizing the minispike c-tail. Right: detection with S32, recognizing VSV M, N and G.

Cryo-EM studies of viral envelopes

The composition of viral envelopes was studied in more detail by cryo-electron tomography by a collaborating scientist. In the absence of a rhabdovirus G protein, VSV as well as RABV minispike VLPs contained a homogenous surface glycoprotein layer, reflecting autonomous incorporation of the minispike as suggested by the above Western blot experiments. As the size of the globular RBD has been reported to be about 60 x 35 Å [115, 121], the surface-anchored minispike construct should consequently protrude between 6 and 11 nm from the membrane. The prefusion form of rhabdovirus G protein is protruding about 8.5 nm from the virus membrane, whilst the post-fusion form is protruding about 13 nm [243]. Measuring out RABV virions expressing only G or minispike, or the combination of both, revealed differences in length of the surface protrusions. G-covered particles had surface proteins with an average length of 8.15 nm (n = 99, STD 1.07 nm) whilst in minispike VLPs this length was reduced to 7.70 nm (n = 77, STD 1.35). In the presence of both G and minispike, surface

protein protrusions had an average length of 8.45 nm (n = 111, STD 1.47 nm). A direct morphological separation between G and minispike was not possible, and no higher order arrangement of the surface glycoproteins was discernible in the tomograms, suggesting random mixing.

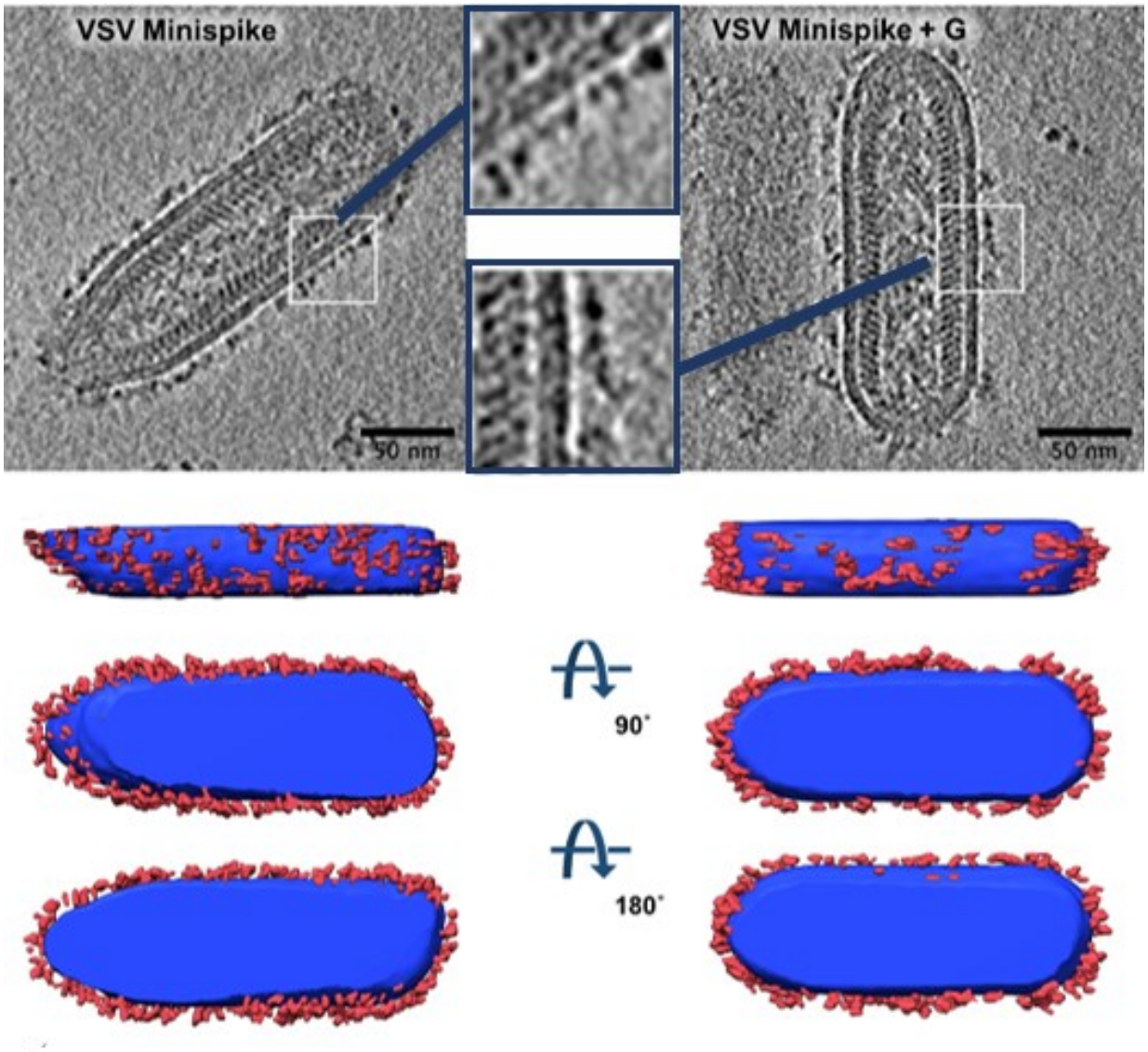

Figure 18: Cryo-electron tomogram of VSVΔG minispike supernatant particles. Left column: VLPs generated on non-G-complementing cells (VSV Minispike). The envelope of the particles is decorated with a layer of surface proteins of uniform size, corresponding to minispike. Right column: Particles produces in G-complementing cells (VSV Minispike + G) show a more varied surface protein layer, corresponding to a mix of VSV G and minispike.

As mentioned, VSV G is sufficient to drive budding of non-viral vesicular particles independent of other viral proteins. Accordingly, we observed non-viral, spherical vesicles with a homogenous, distinct surface protein layer clearly distinguishable from typical bullet-shaped rhabdovirus particles in virus preparations produced in the presence of VSV G. They likely represent 'Gesicles' or G-nanovesicles formed by the autonomous budding activity of the full length VSV G protein [25, 244]. We did not observe similar vesicular structures if RABV G or minispike were expressed on their own. These observations indicate that, as for the parental RABV G, the chimeric SARS-CoV-2/RABV minispike protein lacks the ability for efficient autonomous budding.

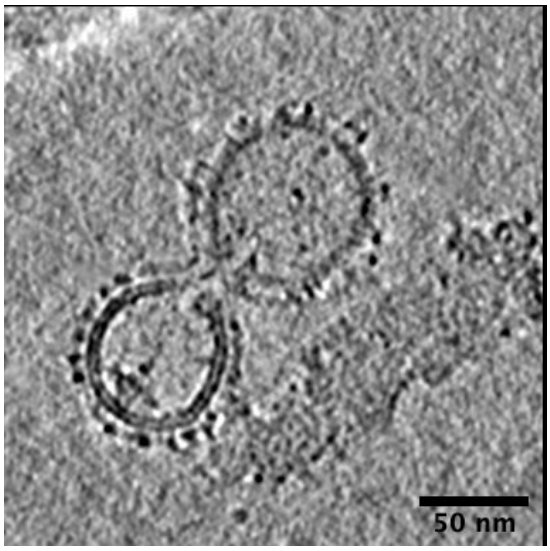

Figure 19: Balls among the bullets. Spherical vesicles, probably representing so-called G-nanovesicles or Gesicles, formed by the autonomous and self-sufficient budding of full-length VSV G.

Rhabdovirus-expressed minispike is recognized by COVID-19 patient sera

To corroborate that our rhabdovirus replicons express correctly folded, processed and cell surface targeted SARS-CoV-2-RBD antigens as observed previously for plasmid-expressed minispike protein, BHK-21 cells were infected with VSVΔG-minispike-eGFP (G) and, as a control, with a VSVΔG expressing only blue fluorescent protein (VSVΔG-tagBFP (G)). Infected cells were probed with a collection of sera from COVID-19 patients previously tested positive for anti-S IgG in a commercial ELISA. We used eGFP and tagBFP fluorescence as controls to identify virus-infected cells and distinguish between minispike-positive (VSVΔG-minispike-eGFP (G); green) and minispike-negative (VSVΔG-tagBFP (G)) infection. We then detected bound COVID-19 patient IgG with an AlexaFluor555-labelled anti-human IgG secondary antibody. As illustrated, S ELISA-positive sera brightly stained unfixed living cells infected with VSVΔG-minispike-eGFP, but not with VSVΔG-tagBFP. In contrast, no signal was observed for cells infected with either construct with COVID-19 ELISA-negative human control sera. To exclude that the staining is dependent on eGFP expression and to verify the finding with sera from diverse COVID-19 patients, we infected BHK-21 cells with VSVΔG-bimini, a virus construct expressing an additional minispike cistron instead of eGFP, and live stained with four different S-positive sera and a control serum donated by a SARS-CoV-2 naïve, healthy individual. Bound serum IgGs where stained with an AlexaFluor488-labelled anti-human IgG secondary antibody, cells were fixed, permeabilized and minispike expressing cells were identified with HCA05. As expected, only cells with detectable minispike expression exhibited binding by antibodies from S-positive sera, whereas the serum of the healthy donor did not show positive staining.

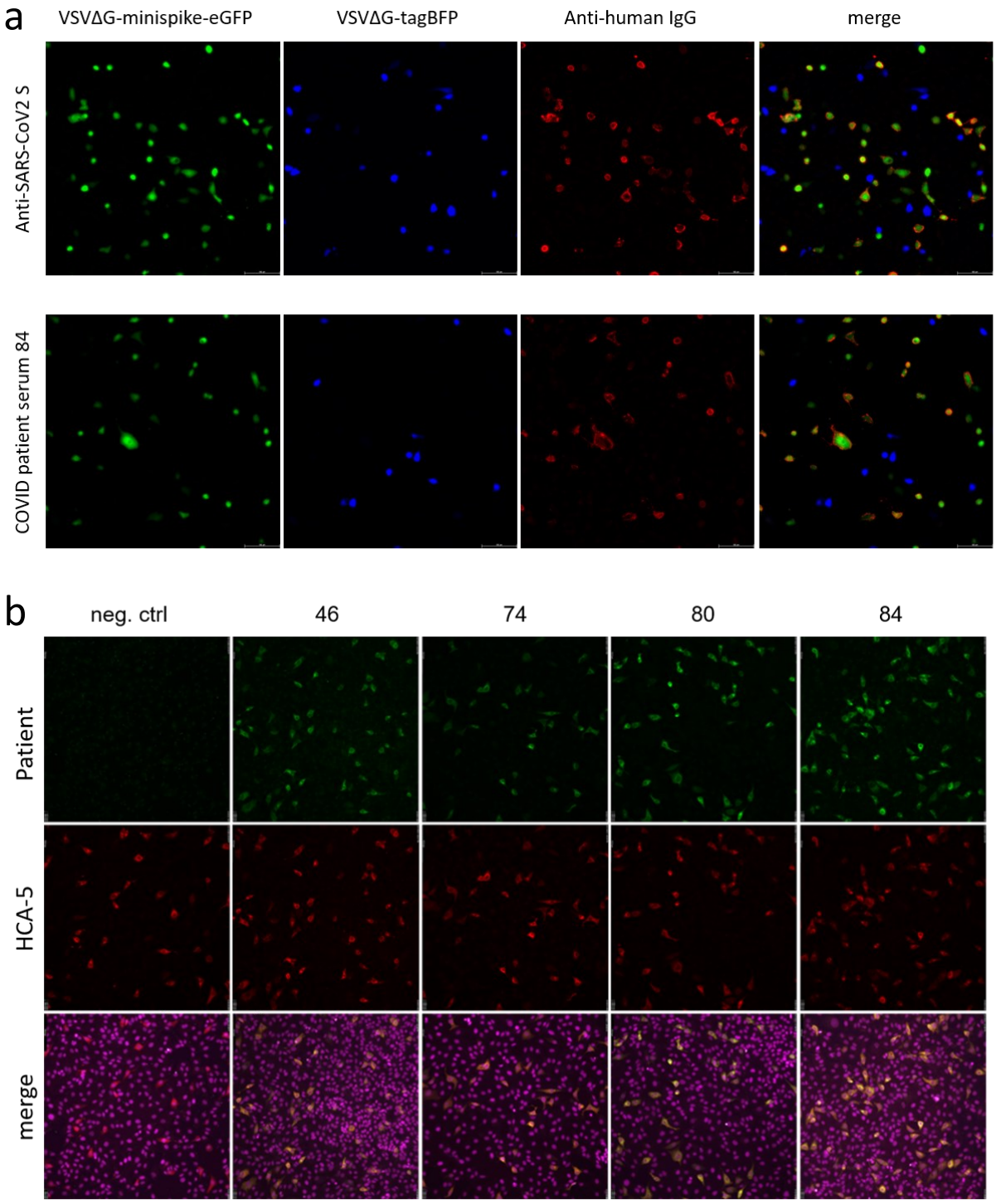

Figure 20: Minispike expressed from VSV is correctly processed and presented at the cell surface and specifically recognized by COVID-19 patients´ serum. a.) BHK-21 cell cultures were coinfected with VSVΔG-minispike-eGFP and VSVΔG tagBFP, incubated with S mAb CR3022 (anti-SARS-CoV-2-S, first row) or a S-positive COVID-19 patient serum (second row). VSVΔG-minispike-eGFP infected cells are depicted in green, VSVΔG tagBFP infected cells in blue and S-positive cells were detected with an AlexaFluor555-labelled anti-human IgG and depicted in red. Only green cells are co-stained with red, whereas blue cells are not, demonstrating a VSV-backbone independent, minispike-specific recognition by COVID-19 patient serum and α-S mAb CR3022. b.) BHK-21 cells were infected with VSVΔG-bimini (no eGFP expression), live stained with multiple S-positive COVID-19 patient sera ("46, "74", "80", "84"; columns 2-5) or an S-negative serum of a healthy donor ("neg. ctrl"; first row), fixed, permeabilized and probed with HCA05, recognizing the intracellular tail of the minispike construct. Cell nuclei were strained with DAPI and are depicted in magenta. Bound patient IgG was detected with an AlexaFluor488-labelled anti-human IgG secondary antibody (green) and HCA05 with an AlexaFluor555-labelled anti-rabbit IgG (red). Minispike protein is expressed and detected in all samples as demonstrated by HCA05 (red) staining. Serum antibodies from COVID-19 patients, but not COVID-19 naïve healthy donors are detecting the minispike-positive cells. 100x magnification.

Similarly, RABV replicon-expressed minispike was specifically stained at the cell surface. Interestingly, while the patient sera readily recognized the native minispike protein expressed by VSV and RABV replicons, they did not react effectively with reduced and SDS-denatured protein in Western blots. This indicates that the majority of the available human COVID-19 serum IgG antibodies directed against the RBD recognize native conformational RBD epitopes.

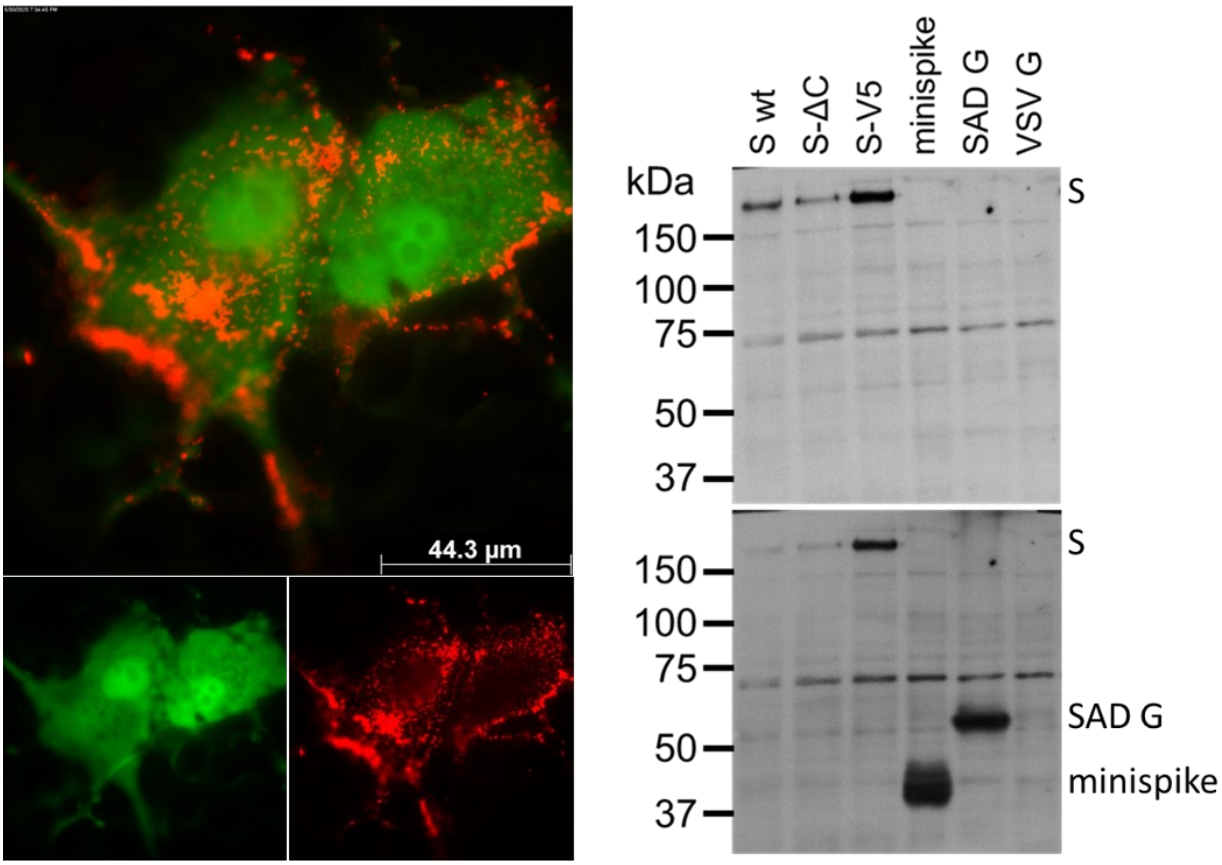

Figure 21: Minispike expressed from rhabdovirus-based replicons is recognized by COVID-19 patient sera in a native conformation, but not in a denatured state in Western blot. Left panel: Live cell staining of VeroE6 cells infected with RABV-ΔG-minispike-mNeonGreen (green) and stained with S-positive convalescent serum (red). 1000x magnification. Right panel: Top blot: Western blot of cells transfected with a full-length SARS-CoV-2 S construct (S wt), a S construct with a truncation of the 19 C-terminal residues (SΔC), a S construct with a C-terminal V5 tag (S-V5), minispike, SAD G or VSV G and detected with S-positive convalescent serum. Only the full-length S constructs show a specific staining; neither minispike nor SAD G or VSV G are recognized. Lower blot: the same membrane after incubation with HCA05, confirming the presence of minispike and SAD G (both of which contain the SAD G c-trail recognized by HCA05).

In summary, the results showed that the transmembrane minispike protein expressed from recombinant rhabdoviruses is well recognized by S targeting antibodies made in response to natural SARS-CoV-2 infection and which recognize conformational epitopes. This is strong evidence that the RBD of the chimeric minispike construct mimics the conformation of the natural SARS-CoV-2 S RBD. We reasoned that the minispike construct therefore represents a promising and innocuous COVID-19 vaccine candidate, especially when expressed by highly immunogenic but safe single-round or replication-controllable rhabdovirus replicons.

A single dose of VSVΔG-minispike-eGFP elicits SARS-CoV-2 neutralizing antibodies

To assess the suitability and the sufficiency of a single round VSVΔG-minispike replicon to elicit a specific and protective immune response against SARS-CoV-2, our collaborators at the Paul Ehrlich Institute (PEI) immunized BALB/c mice with VSVΔG-minispike-eGFP (G) by intramuscular (i.m.) administration of 1x 10^6 infectious units. As advised by the above results, virus stocks produced under limiting (6 h) VSV G complementation were used to limit the abundance of non-viral G vesicles. Four mice received a single immunization of 1x 10^6 IU, while 8 mice received an additional boost immunization with the same virus preparation and dose 28 days following prime vaccination. As controls, mice immunized the same way with VSVΔG-eGFP (G) (n=2 for each condition) or with PBS (n=1 for each condition) were used. The 4 mice receiving only prime vaccination were sacrificed at day 28, and 4 boosted mice each at day 35 (n=4) and day 56 (n=4), to collect serum.

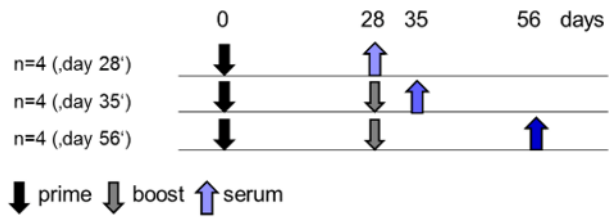

Figure 22: Vaccination regimen for the first mouse experiment. All mice were prime vaccinated at the same time. At day 28, the four mice in the single shot group were sacrificed and blood was drawn. The other eight mice received a boost vaccination corresponding to the prime vaccination. Four mice were sacrificed on day 35 and the remaining four on day 56.

Authentic SARS-CoV-2 virus neutralization assays were performed in a BSL3 laboratory at PEI with a SARS-CoV-2 virus isolate from Wetzlar, Germany. Notably, all 4 mice immunized only once with VSVΔG-minispike-eGFP developed detectable titers of SARS-CoV-2 neutralizing antibodies in the range of 1:20-1:40 dilutions. Boost vaccination further increased neutralizing titers to 1:160-1:640.

Establishment of a VSVeGFPΔG-based SARS-CoV-2-S dependent neutralization assay

To allow investigations of vaccine efficacy and functions of SARS-CoV-2 S proteins during virus entry on permissive cells, on a broader scope and under biosafety level 1/2 conditions, we established a VSVeGFP-ΔG-based virus neutralization assay that relies on transcomplemented SARS-CoV-2 S protein to facilitate entry and infection of susceptible cells (i.e., expressing ACE2). First, we cloned and rescued VSVeGFP-ΔG-Gaussia-Luciferase viruses, which allow to measure the extent of virus infection by counting GFP-positive cells as well as by measuring Luciferase activity in the supernatant. To this end, we PCR amplified the CDS of Gaussia Luciferase with a forward primer inserting a *MluI* restriction site flanking the N-terminus and a reverse primer inserting a *NotI* restriction site flanking the C-terminus.

The PCR product (insert) and a molecular clone of VSV with an eGFP CDS at the first position and a deletion of the G CDS (pVSV eGFP ΔG, kindly provided by Connie Cepko via addgene #31842)(vector) were digested with *MluI* and *NotI* and the insert ligated into the vector. While very intriguing in theory, the increased handling steps necessary, all of them potentially affected by variation and human error did not allow for a robust correlation of Gaussia Luciferase activity and eGFP positive cells. We therefore concentrated on automated counting of GFP-positive cells.

SARS-CoV-2, like most other coronaviruses, does not bud from the cell surface but from the endoplasmic reticulum (ER)-Golgi intermediate compartment (ERGIC). This has important ramifications for S localization. For efficient incorporation into virus particles, S must accumulate at the site of budding. However, proteins with an N-terminal signal peptide are primarily targeted to the secretory pathway, which also entails surface proteins inserted into the plasma membrane. S therefore must be redirected to the ERGIC; to this end, S contains a dibasic retrieval signal motif (KxHxx) in the cytoplasmic tail [245-247]. VSV on the other hand buds from the cell surface. To be efficiently incorporated into budding VSV particles, S therefore needs to be divested of the ERGIC localization signal. The S intracellular tail consists of the C-terminal 37 residues and is comprised of two distinct regions: a cysteine-rich part probably embedded into the cell membrane and a membrane-distal part that is sticking into the cytoplasm, with the retention signal located in the latter [245]. In our constructs we therefore first omitted the 19 C-terminal aa (ΔC19) to improve pseudotyping efficiency, a strategy already demonstrated to be effective for transcomplementation of VSV with the S of earlier coronaviruses [248]. In a bid to improve pseudotyping efficacy further, we removed five more residues for a total of 24 residues (ΔC24). All S constructs employed for pseudotyping had this identical ΔC24 cytoplasmic tail.

We then pseudotyped VSVeGFP-ΔG-Gaussia-Luciferase viruses with SARS-CoV-2 S constructs corresponding either to the original Wuhan strain or, later, one of the Variant-of-Concern (VOC) strains alpha, beta and delta or Variant-under-investigation (VUI) strain AV.1.

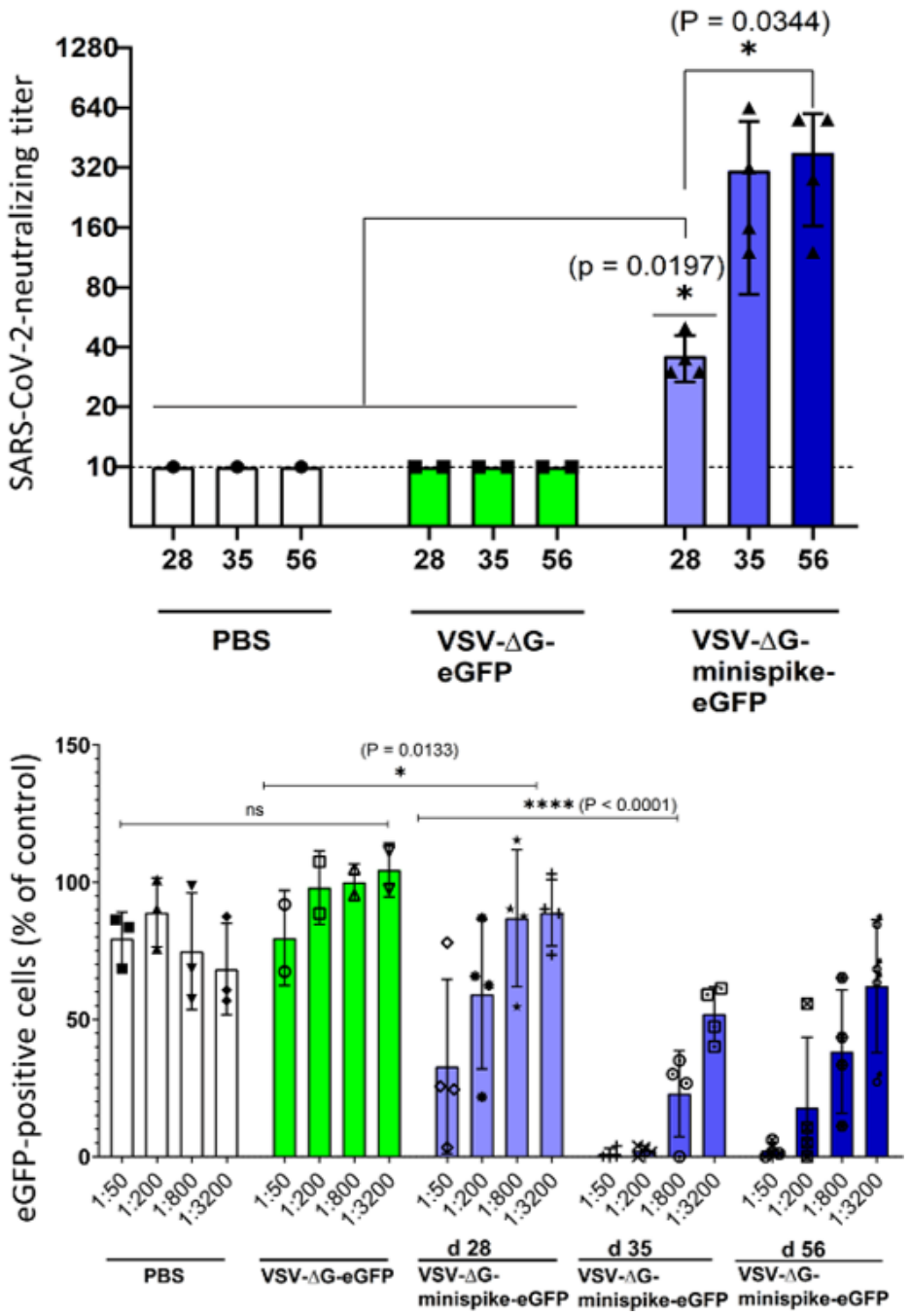

Figure 23: Vaccination of mice with VSV-ΔG-minispike-eGFP leads to the induction of S-specific neutralizing titers. Top: Virus neutralization assay with authentic SARS-CoV-2 (Wuhan strain, Wetzlar isolate). Sera from mice immunized with PBS (N=1), VSV-ΔG-eGFP (N=2) or VSV-ΔG-minispike-eGFP (single immunization, d28 (N=4); double immunization, d35 (N=4), double immunization, d56 (N=4) was tested for its ability to neutralize SARS-CoV-2. While sera from control mice vaccinated with either PBS (white bars) or VSV-ΔG-eGFP (green bars) fail to neutralize SARS-CoV-2, sera from mice vaccinated with VSV-ΔG-minispike-eGFP readily neutralize SARS-CoV-2 infection already after a single vaccination (28). Boost vaccination (35, 56) further increases neutralizing titers 6- to 8-fold. The neutralizing titer of sera from vaccinated and control mice as indicated is expressed as the reciprocal of the highest dilution at which no cytopathic effect was observed. Each point represents data from one animal at the indicated time points. The bars show the mean from each group and the error bars represent standard deviations. Bottom graph: Same sera as above show similar results in a VSV-eGFP-ΔG-GaussiaLuc (SARS-CoV-2 S Wuhan ΔC24) pseudovirus neutralization assay show similar results. The graph shows percentage of GFP-positive (infected) cells in relation to medium controls (set to 100 %) and in dependence of dilution. Data points represent the average of three technical replicates, bars indicate standard deviation, and statistical significance was determined by one-way ANOVA.

Pseudovirus neutralization assays with these constructs confirmed the induction of significant levels of S-neutralizing antibodies in mice receiving a single prime vaccination and further enhancement of the neutralization activity by boost immunization.

To directly compare the neutralizing activities of sera from vaccinated mice and from COVID-19 patients, VSV-eGFP-ΔG-GaussiaLuc (SARS-CoV-2 S ΔC24) neutralization assays were employed again. Four different sera from convalescents were utilized and showed a pronounced neutralizing capacity. Intriguingly, the group of mice immunized only once developed a serum neutralizing capacity reaching those of the group of COVID-19 patients, illustrating a powerful induction of humoral immunity by vaccination with the single round VSVΔG-minispike-eGFP replicon. Boost immunization further enhanced neutralizing titers to exceed those of patients. As expected, sera from control vaccinated mice exhibited no specific neutralization effect.

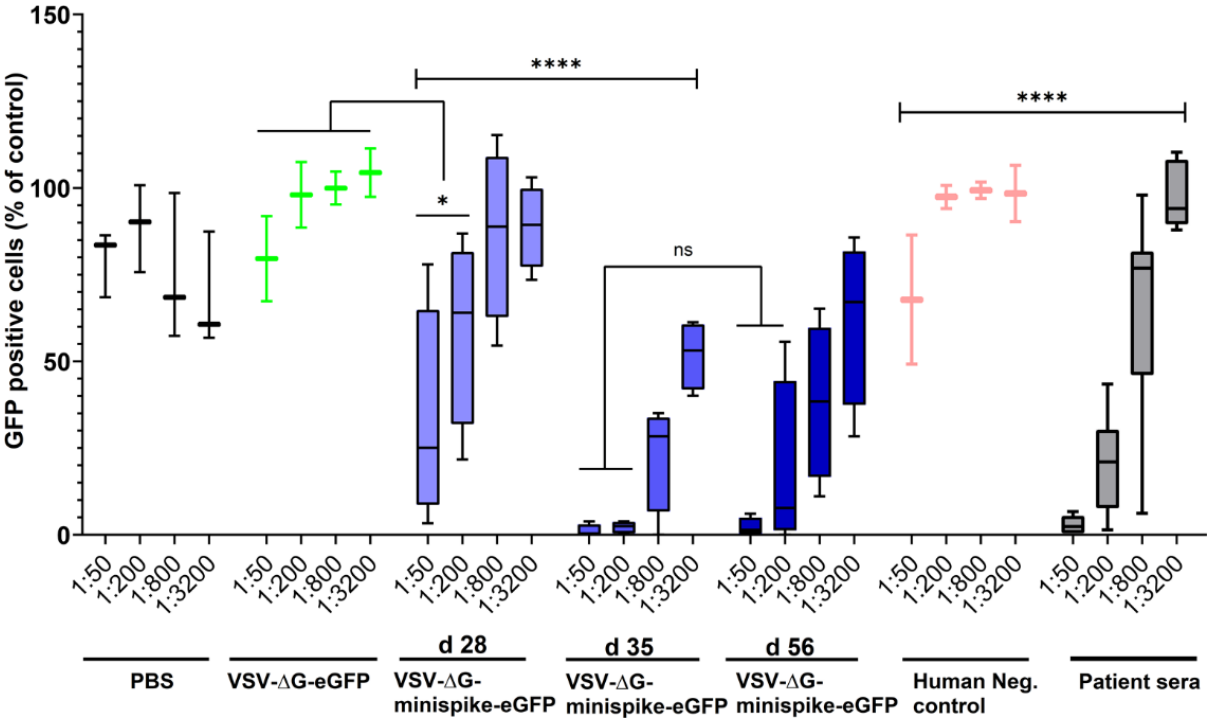

Figure 24: Prime vaccination of BALB/c mice with VSVΔG-minispike-eGFP induces a S specific neutralizing response almost on par with that of COVID-19 convalescents, boost vaccination further boosts neutralization capacity significantly. Sera from mice vaccinated once (mauve boxes) show a VSV-eGFP-ΔG-GaussiaLuc [SARS-CoV-2 Wuhan S] neutralization capacity comparable to that of the four tested convalescent sera (grey boxes). Sera from boost vaccinated animals (d35, d56, medium blue and dark blue boxes) increase neutralization titers to exceed those of convalescents. PBS: sera from mice vaccinated with PBS (control). VSVΔG-eGFP: sera from mice vaccinated with VSVΔG-eGFP (control). VSVΔG-minispike-eGFP d28: sera from mice vaccinated once with VSVΔG-minispike-eGFP. VSVΔG-minispike-eGFP d35: sera from mice vaccinated twice with VSVΔG-minispike-eGFP, sacrifice and blood draw on d35 post prime immunization. VSVΔG-minispike-eGFP d56: as previous group but sacrifice and blood draw on day 56. Human neg. control: control serum of a healthy donor. Patient sera: sera of S ELISA-positive convalescents.

K18-hACE2 mice are protected from SARS-CoV-2-induced respiratory disease after a single immunization

To assess the protective capacity of the VSV replicon vaccine *in vivo*, we used transgenic K18-hACE2 C57BL/6 mice, which express human ACE2 in relevant tissues under the human keratin 18 promoter. This mouse model was previously shown to be permissive for SARS-CoV-1 and SARS-CoV-2 and to develop respiratory disease resembling severe COVID-19 after infection [249, 250]. Five mice each were immunized by our collaborators at the Paul-Ehrlich-Institute, Langen, as before with VSVΔG-minispike-eGFP or VSVΔG-eGFP control and challenged intranasally with 1x 10^4 tissue culture infectious dose 50 % (TCID50) of SARS-CoV-2 Wetzlar, either 28 days after prime immunization or 28 days after a homologous boost immunization 28 days after the first immunization. Mice were monitored daily and assigned a clinical score assessed by body weight loss relative to weight at challenge infection, general appearance, and behavior. A score of 3 represents healthy animals, score 4–6 indicates mild disease, score 7–9 severe disease and mice with a score of 10–12 are considered moribund. Mice in the VSVΔG-eGFP control group developed respiratory disease beginning as early as day 5 after infection, which progressed over the following 3-4 days, and animals ultimately met euthanasia criteria due to deteriorating general condition and increasing clinical score 6-9 days after challenge infection. As the body weight loss of these animals was relatively minor with only approximately 10-15 % of their initial weight, they evidently experienced a largely respiratory syndrome.

In contrast, mice immunized with VSVΔG-minispike-eGFP experienced no clinical signs of disease, and all animals survived the challenge with little to no weight loss during the study and no increase in clinical score. This demonstrates the protective power of the VSVΔG-minispike-eGFP replicon vaccine since a single immunization was sufficient to prevent the development of lethal COVID-19-like respiratory disease. As all mice from the prime vaccination group were perfectly protected also from mild disease, no further *in-vivo* conclusions could be drawn regarding the utility and increase of protection offered by boost vaccination.

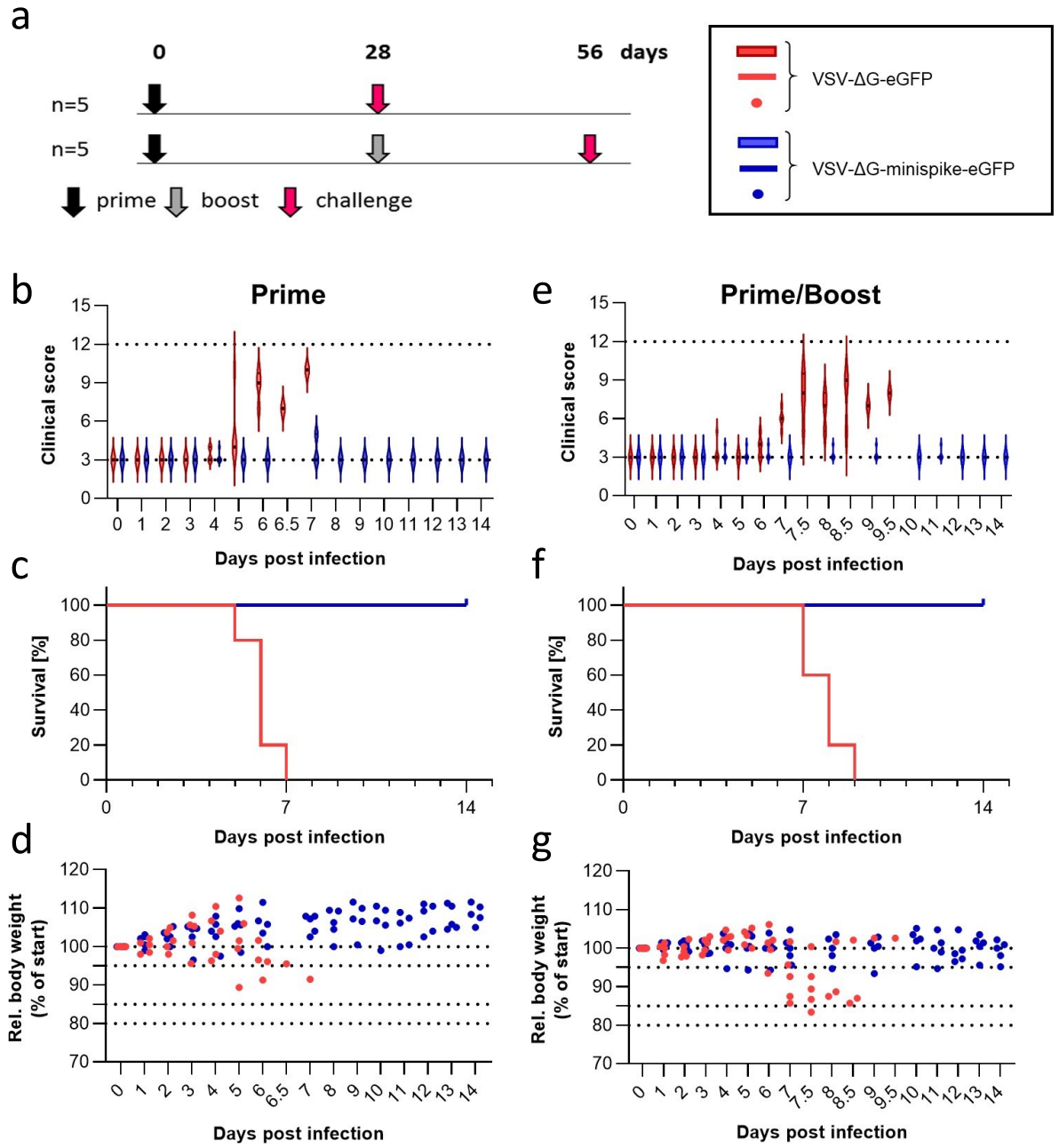

Figure 25: a: Immunization and challenge schematic. C57BL/6 K18-hACE2 mice (5 per group) were immunized (1x10^6 IU intramuscularly) once (prime, black arrow) or twice (boost, grey arrow) four weeks apart with either VSV-ΔG-minispike-eGFP (indicated in blue in panels b-g) or VSV-ΔG-eGFP (indicated in red in panels b-g) and challenged with 1x 10^4 TCID50 SARS-CoV-2 (Wetzlar isolate) administered intranasally four weeks after the last immunization. Mice were monitored daily for development of disease for 14 days. Left column (b-d): Evaluation of clinical disease of challenge after prime immunization. Right column (e-g): Evaluation of clinical disease of challenge after prime/boost immunization. b and e: Clinical score development assessed by body weight loss, general appearance, and behavior. 3: healthy; 4–6: mild disease; 7–9: severe disease; 10–12: moribund. (c and f) Survival plots. (d and g) Body weights of individual mice relative to the weight at challenge infection. Dotted lines indicate limits of clinical scores (>95 %: score = 1, 85–95 %: score = 2; 80–85 %: score = 3; <80 %: score = 4).

SARS-CoV-2 variants of concern

Soon after introduction of SARS-CoV-2 into the human population, the ancestral Wuhan strain (lineage A) has been almost completely superseded by the now prevalent B lineage of viruses, established by the S protein stabilizing D614G mutant. The B lineage comprises the VOCs alpha, beta and delta. The alpha variant (B.1.1.7, originally described in the United Kingdom) became the prevalent strain by beginning of 2021 and has in turn been displaced by delta (B.1617.2, originally described in samples from India) by the second half of 2021. Parallel to alpha, two other variants of concern with the N501Y substitution emerged in the end of 2020, beta (B.1351, first described in samples from South Africa) and gamma (P.1, first described in samples from Brazil). While the defining feature of alpha is a significantly increased transmissibility, beta and gamma show a marked escape from immune responses. The Delta strain was one of the driving forces behind the surge in infections in India at the beginning of 2021. Its defining feature is an even further increased infectivity combined with a complete escape from NTD-targeting nAbs and partial escape from RBD-targeting nAbs [166, 251]. It thereby combines two alarming traits; increased transmissibility and potent escape functions against NTD- and RBD- targeting nAbs. AV.1 is a variant that was first detected in the United Kingdom in March 2021 and combines several VOC/VUI-like mutations in the S protein, most notably N439K and E484K, both of which have been shown to contribute to immune escape. It had been originally designated variant under monitoring by the WHO but did not gain wider spread and has since been deescalated. Regarding minispike-elicited immunity it is of interest because it combines two RBD mutations conferring immune escape with N439K and E484K [252].

Mutations possibly directly affecting antibodies elicited by a minispike-based vaccine for the different strains are as follows: Alpha sports one mutated residue located in the RBD (N501Y), Delta two (L452R and T478K), AV.1 two (N439K, E484K) and beta/gamma three (K417N/T, E484K, N501Y). Mutations in the RBM are underlined. Due to the limited size and, as a result, reduced number of independent immunogenic epitopes of the minispike construct the diversity of the elicited antibody response is more focused compared to full-length S immunogens. It is therefore of utmost interest to see how robust minispike-induced immunity is against different VOC and other alarming emergent strains in comparison to naturally infected individuals and vaccinees.

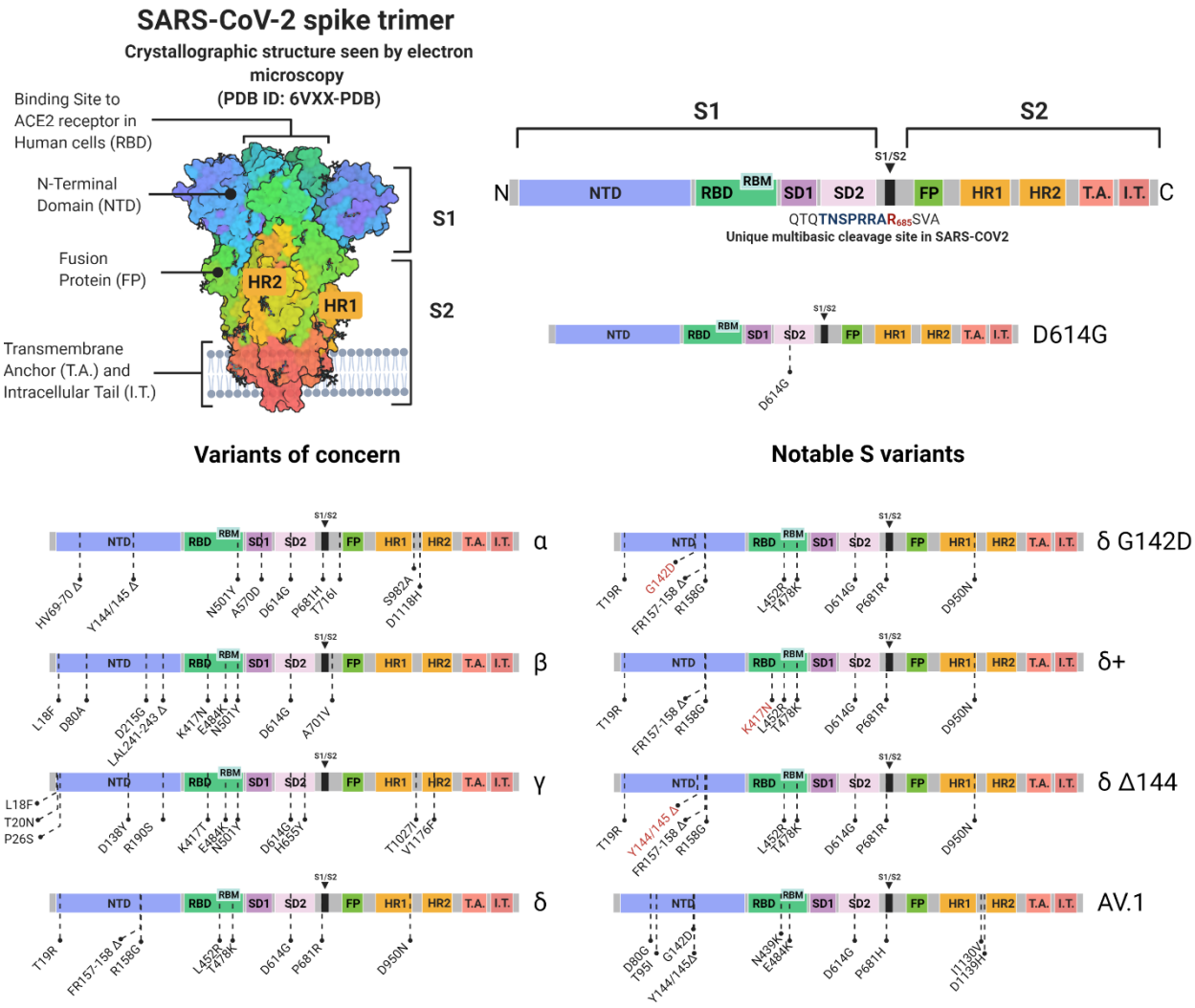

Figure 26: Overview of SARS-CoV-2 S domains, mutations present in the four variants of concern and other variants generated and utilized in this thesis. Immune escape mutations are located in either the NTD or the RBD. The stated mutations correspond to the constructs used in this thesis and represent the defining mutations of the different variants at time of cloning of the construct. (e.g., the G142D mutation in delta which became "canon" some time after most of the assays were performed). Due to the evolving nature of the pandemic and causative virus the variants are not necessarily identical to those circulating in the population.

To examine the neutralization efficacy of the Wuhan-minispike-elicited sera against relevant SARS-CoV-2 variants we generated expression plasmids of S proteins from all VOCs and other mutants of note. The constructs generated include the S of variants alpha, beta, gamma, delta as well as AV.1 and the delta variants delta plus (with an additional K417N mutation in the RBD) and delta Δ144 (corresponding to a delta variant detected in Vietnam that has a deletion of Y144/145 also found in alpha and which is thought to have an effect on the NTD "supersite"). We then pseudotyped VSV-eGFP-ΔG-GaussiaLuc with these S variants and proceeded as described above.

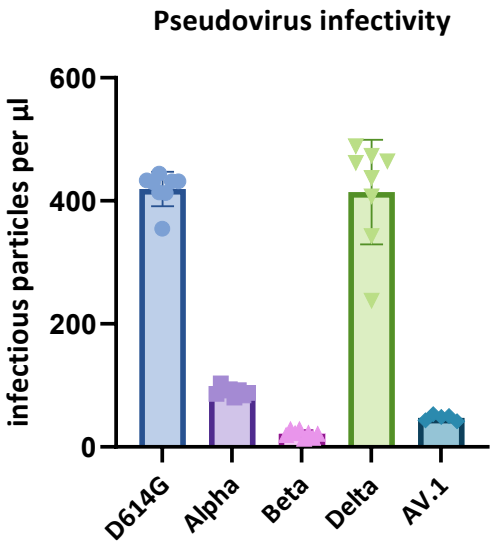

Figure 27: Pseudovirus infectivity for different S variants on VeroE6 cells. The parental D614G S and variants alpha, delta and AV.1 show similar infectious titers in the same order of magnitude, VSVeGFPΔG-GaussiaLuc pseudotyped with beta S consistently appeared to have a lower number of infectious particles. Mean of six (AV.1) or eight (D614G, alpha, beta, delta) independently infected wells with virus only control.

Interestingly, while virions pseudotyped with the B.1 D614G S, the Alpha S and the Delta S showed similar infectivity of ~100-400 IU/µl, pseudotyping with the S of the Beta strain consistently led to a lower number of infectious particles (~40 IU/µl).

Neutralization titers against VOCs

VSVeGFP-ΔG -GaussiaLuc pseudovirus neutralization assays

We limited our convalescent panel to one patient, namely the one with the highest S ELISA titers and the consistently highest neutralization capacity in the previous experiments. More precisely, the sample had the highest S ELISA titer (8,74) available at the time of sampling (17.04.2020) in the Virology Diagnostics department of the LMU Klinikum.

Similarly, the BNT162b2 vaccinee control consisted of one donor with the highest measured neutralization titers out of 12 samples of young, healthy donors tested against pseudoviruses transcomplemented with the D614G S.

For the minispike vaccination group, eight mice were immunized twice as described above and sacrificed seven or 28 days after the second vaccination. As we saw no significant difference between the two timepoints, we combined all mice into one group. Out of the eight mouse sera, we used the five with the highest neutralization activity against VSVeGFP-ΔG -GaussiaLuc (Spike Wuhan D614G) for the neutralization experiments against the variants.

Sera from minispike-immunized mice efficiently neutralized pseudoviruses carrying all VOC spikes and the AV.1 S. Against D614G and alpha, the neutralization potency is comparable to that of the BNT162b2 vaccinee and slightly higher than that of the convalescent. For beta, minispike-elicited sera are surpassing the neutralization capacity of the vaccinee and convalescent controls, although there are striking differences between the individual mice. We see the largest reduction in neutralization capacity against delta, with a reduction of the dilution at which a neutralization effect of 50 % is observed (inhibitory dilution 50 %, ID50) by 85 % or 6.4-fold.

Interestingly, for delta S transcomplemented pseudoviruses, the convalescent serum shows the smallest reduction in neutralization capacity, fitting with observations that convalescents are significantly better protected against reinfection with delta than vaccinees [253].

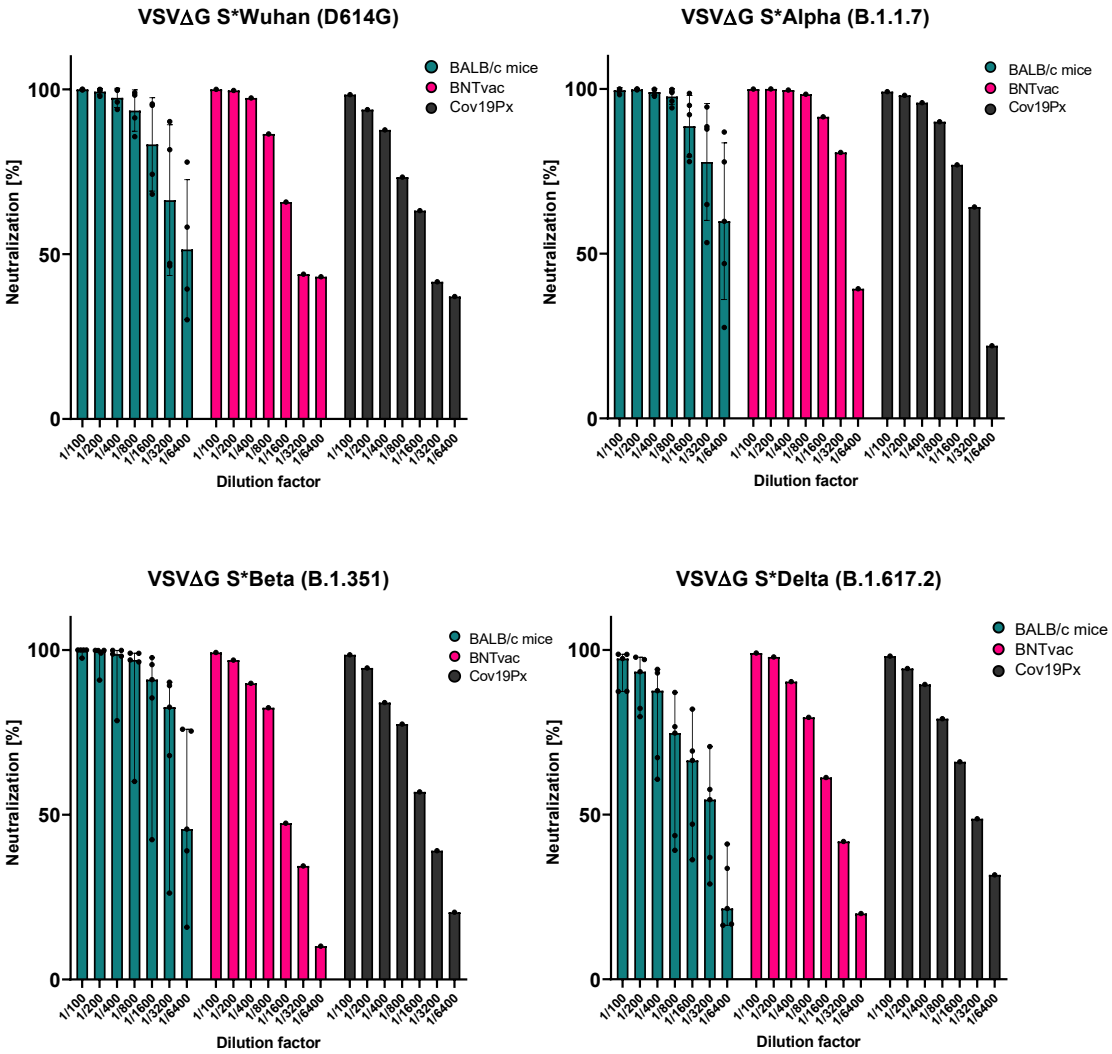

Figure 28: pseudovirus neutralization assays with sera of five VSVΔG-minispike-eGFP immunized BALB/c mice (green) compared to a BNTb162.2 vaccinee (BNTvac, magenta) and a COVID-19 convalescent (Cov19px, black). Plotted is the neutralization of S-mediated VSVeGFP-ΔG-GaussiaLuc infection compared to a non-neutralizing human serum vs. the serum dilution factor.

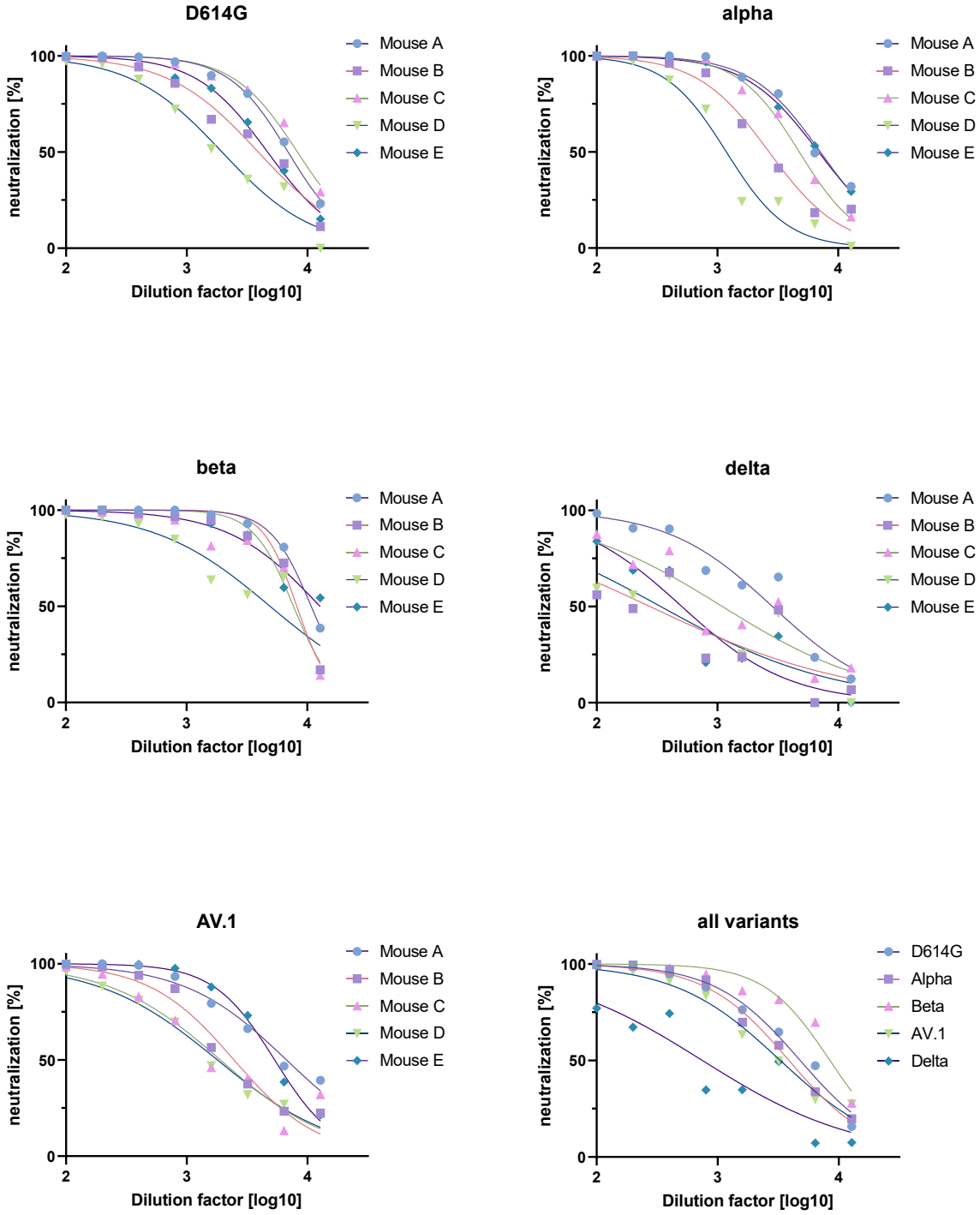

	D614G	Alpha (B.1.1.7)	Beta (B.1.351)	Delta (B.1.617.2)	AV.1
LogIC50	3,68	3,59	3,93	2,87	3,52
IC50	4805	3879	8458	747,4	3291
95% CI	3972 to 5845	3036 to 5015	7202 to 10149	477,3 to 1139	2620 to 4194
R squared (goodness of fit)	0,8631	0,8085	0,8218	0,6434	0,8447

Figure 29: First five graphs (D614G, alpha, beta, delta, AV.1): Representative individual mouse serum neutralization curves for the different variant S pseudoviruses. The symbols represent neutralization data points of sera from five individual mice (Mouse A-E). Bottom right graph (all variants): Combined data from the five mice for all variants. Of all tested S variants, neutralization of B.1.617.2 S (delta) pseudoviruses shows the shallowest Hill slope and the most problematic fit.

Authentic SARS-CoV-2 neutralization assays

To further validate the findings from the pseudovirus neutralization assay, sera from all eight VSVΔG-minispike-eGFP vaccinated mice were tested for their neutralization capacity against the authentic SARS-CoV-2 variants B.1.177, alpha (B.1.1.7), beta (B.1.351), gamma (P.1) and delta (B.1.617.2) by collaborators in a S3 laboratory at the Max von Pettenkofer-Institute in a S3 laboratory. The S protein of B.1.177 is identical with the original Wuhan S except for the D614G mutation; it therefore corresponds to the S Wuhan (D614G) utilized in the pseudovirus neutralization assays. The ID50 values were calculated normalized to 10^7 SARS-CoV-2 RNA copies. Encouragingly, the data fits very well with the data from the pseudovirus neutralization assays. Neutralization capacity compared to D614G is 77% for alpha, 44% for beta, 72% for gamma and 8% for delta. As seen before, the variant with the highest apparent escape is delta, with a 12-fold reduction in neutralization titer. Unlike published observations from vaccinees and convalescents, neutralization of beta by minispike-elicited sera is extremely robust with a reduction of only 56% compared to B.1.177 whereas alpha and gamma are neutralized with almost no loss in potency.

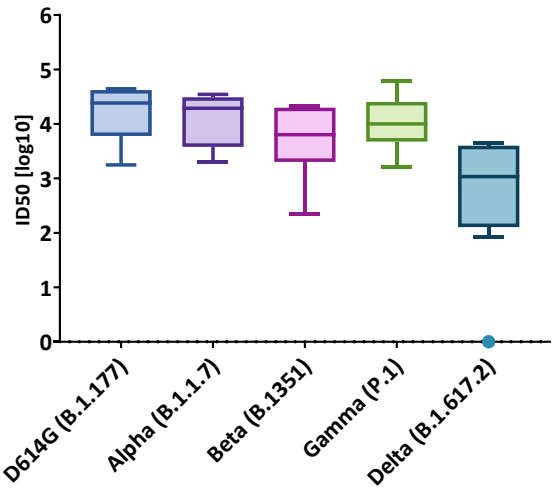

Figure 30: ID50 values of sera from VSVΔG-minispike-eGFP vaccinated mice against authentic SARS-CoV-2 virus variants B.1.177, alpha, beta, gamma and delta. Robust titers are achieved against all variants, with the largest reduction of neutralization potency seen against delta. One serum sample failed to neutralize beta completely. Box and whiskers were computed using the Tukey method of GraphPad Prism.

Looking at the mice individually reveals interesting patterns. Four mice (46.1, 46.2, 47.2, 48.2) show almost identical trends, with mostly constant ID50 values for B.1.177, alpha, beta and gamma and a significant drop in ID50 for delta. The second group of mice (49.1 and 46.2) show a slight decrease against all variants with again the largest reduction against delta. And finally, the third group of mice comprising 48.1 and 49.2 show the largest decline against beta and a smaller decrease against delta. Especially mouse 49.2 shows a trend that corresponds best with published vaccinee- and convalescent data [144, 185, 254].

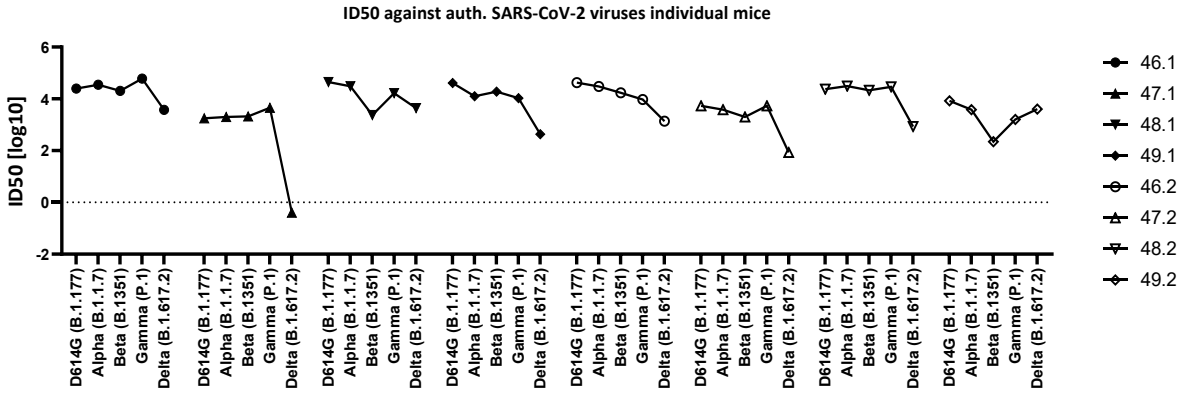

Figure 31: ID50 values for sera from eight VSVΔG-minispike-eGFP vaccinated mice (46.1-49.2) against authentic B.1.177 (first tick of each curve) and VOCs alpha (second tick), beta (third tick), gamma (fourth tick) and delta (last tick). The S protein of B.1.177 is identical with S Wuhan (D614G). Although the mice show individually distinct curves, sera from all mice show robust neutralization of all variants with the exception of mouse 47.1, which fails to neutralize delta. Only two mice (48.1 and 49.2), show a marked escape by the beta variant.

Comparison of serum neutralization titers of surrogate and authentic SARS-CoV-2 neutralization assays

To directly compare the results from pseudovirus and authentic virus neutralization assays, ID50 data from the three mouse sera not tested for all variants in the pseudovirus neutralization assay were omitted from the group and the IC50 values determined by authentic and pseudovirus neutralization of the remaining five sera juxtaposed. Both assays show a very similar pattern, arguing for the validity of results obtained from the pseudovirus neutralization assay.

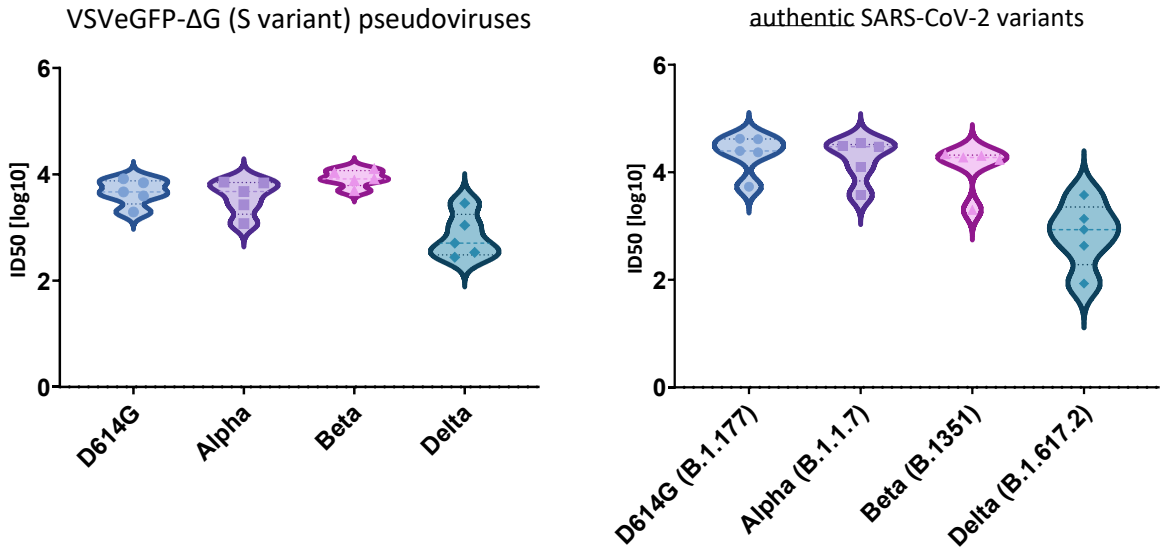

Figure 32: Side-by-side comparison of ID50 values of five minispike-vaccinated mouse sera obtained from VSVeGFP-ΔG-GaussiaLuc (S) (left) pseudovirus neutralization and authentic SARS-CoV-2 neutralization (right). Individual ID50 values are indicated by dots.

K18-hACE2 mice are protected from SARS-CoV-2-induced respiratory disease after a single immunization with the classic minispike, even against delta

In the beginning of 2021, B.1.351 or beta was the benchmark of a scary, immune-evasive mutant and the variant of greatest concern. Accordingly, we generated minispike constructs corresponding to the beta RBD and VSVΔG viruses expressing said constructs. Especially the E484K mutation was demonstrated repeatedly to facilitate a complete escape from multiple monoclonal antibodies and a significant escape from polyclonal vaccinee and convalescent sera [179, 182, 184, 255-267]. At the same time, the three B.1.617 variants started to emerge in India, all of them sharing the L452R mutation in the RBD already known from the epsilon variant. B.1.617.1 and B.1.617.3 combine this with an E484Q mutation, whereas B.1.617.2 or delta instead sports a T478K mutation. Due to public data from beta and gamma, we originally expected B.1.617.2 to be the most benign variant regarding immune escape due to the conservation of E484. Therefore, we focused on B.1.617.1/3 with the E484Q substitution. We generated VSVΔG-minispike(B.1.351)-eGFP, encoding a minispike with the RBD of B.1.351 and a bimodal VSVΔG-minispike(B.1.351)-eGFP-T2a-minispike(B.1.617.1/3) construct, whereby the first minispike has the K417N, E484K and N501Y mutations found in beta and a second minispike with L452R and E484Q mutations was fused via a T2a self-cleaving peptide to eGFP. Our collaborators at the Paul-Ehrlich-Institute, Langen, then proceeded to prime immunized five K18 hACE2 mice per group with VSVΔG-eGFP as vector control (control), the original VSVΔG-minispike-eGFP (Wuhan), the beta variant VSVΔG-minispike(B.1.351)-eGFP (beta), and the bimodal construct expressing both a beta- and a kappa-RBD minispike VSVΔG-minispike(B.1.351)-eGFP-T2a-minispike(B.1.617.1) (beta-kappa) as before and challenged them 28 days later with 1x 10^4 TCID50 of SARS-CoV-2 delta variant intranasally.

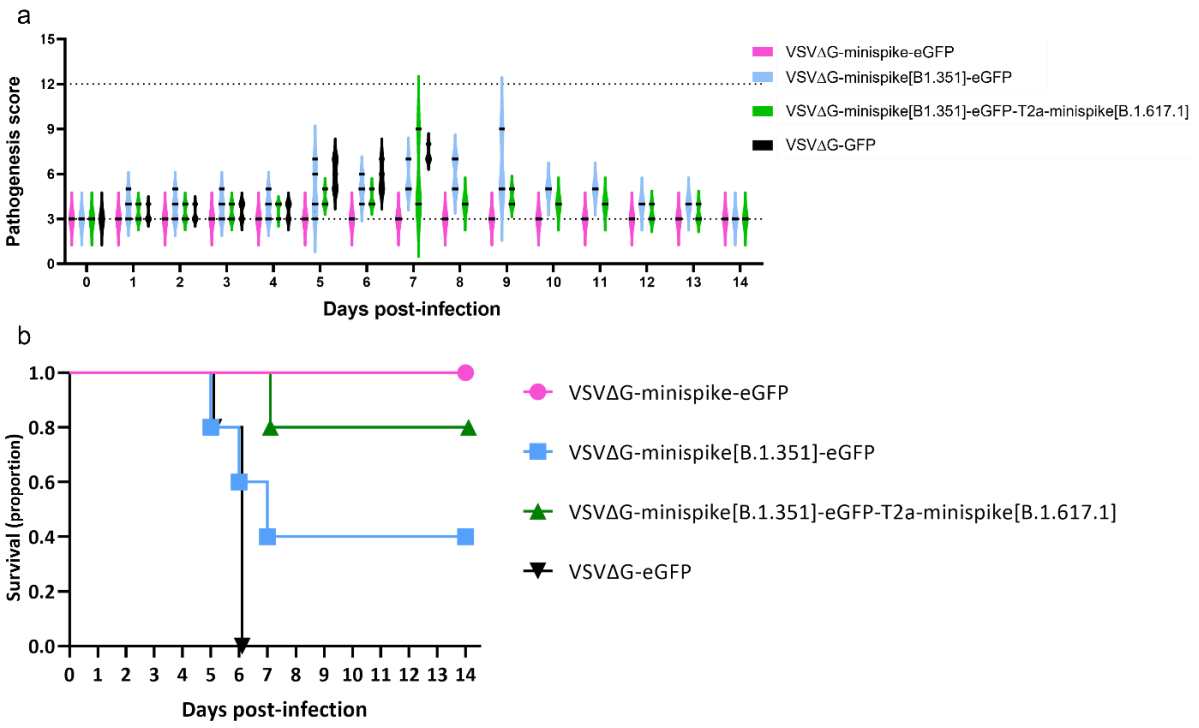

Figure 33: C57BL/6 K18 hACE2 mice (5 per group) were immunized (1x10^6 IU intramuscularly) once with either VSV-ΔG-minispike-eGFP (indicated in magenta), VSVΔG-minispike(B.1.351)-eGFP (indicated in blue), VSVΔG-minispike(B.1.351)-eGFP-T2a-minispike(B.1.617.1) (indicated in green) or VSV-ΔG-eGFP (indicated in black) and challenged with 1x 10^4 TCID50 SARS-CoV-2 ***delta*** *variant, administered intranasally four weeks after immunization. Mice were monitored daily for development of disease for 14 days. a: Evaluation of clinical disease of challenge with SARS-CoV-2 delta after prime immunization. Clinical score development assessed by body weight loss, general appearance, and behavior. 3: healthy; 4–6: mild disease; 7–9: severe disease; 10–12: moribund. b: Survival plots.*

Whereas mice in the Wuhan group were completely unaffected by the challenge with a survival rate of 100 % and constant pathogenesis score of 3 (corresponding to "healthy") thoughout the experiment, all mice from the control group developed severe clinical symptoms and succumbed to disease or reached humane endpoints by day six post challenge. The other two groups of vaccinated mice showed intermediate results, with two out of five mice from the beta group and four out of five mice in the beta-kappa group surviving. The beta-kappa- and especially the beta-minispike immunized mice developed severe clinical symptoms reflected by increasing pathogenesis scores from day five post challenge. These results so far are preliminary and need to be confirmed, however there are two major possible implications: A minispike construct based on the RBD of the beta variant is either a poor immunogen or induces a very narrow protection that is weakly transferred to virus challenge with other variants. This fits well with observations from other labs [268, 269] and in-depth characterizations of the E484K mutation [181]. The second, more positive implication is that a single vaccination with the original minispike perfectly protects K18-hACE mice against challenge not only with the parental Wuhan strain, but also with delta. This is especially intriguing as the 6- to 12-fold reduction in serum neutralizing titers seen in our neutralization assays apparently does not translate into breakthrough infections in our model system and with our parameters, as mice appeared protected from even of mild disease, indicated by an unchanging clinical score after virus challenge.

Discussion

Vaccines are used in healthy populations; therefore, the highest safety standards must be applied. Front-runner COVID-19 vaccines employ innocuous mRNA delivery for expression of the prefusion-stabilized form of the S antigen [270, 271] or replication incompetent adenoviruses [272]. Auspiciously, these combinations turned out to be safe, and proved to be invaluable in containing the pandemic. Other vaccines or proposed COVID-19 vaccine candidates employ unmodified S protein, existing in pre- and postfusion forms and/or are based on potentially perilous replication competent viruses.

Here, we used a structure-guided approach to generate a VSV replicon vaccine meeting the requirements in terms of both virus safety and antigen harmlessness, as well as in efficacy. Our results illustrate that a small antigen, the RBD of SARS-CoV-2, if expressed in the form of the present chimeric minispike protein from a safe, spreading-deficient single round biosafety level 1 rhabdovirus replicon is sufficient to elicit high levels of neutralizing antibodies. Most remarkably, a single immunization proved to protect SARS-CoV-2 permissive animals from lethal disease upon challenge with both the parental Wuhan strain of SARS-CoV-2 and the predominant VOC in 2021, delta. This finding is especially important because the delta variant showed the highest immune escape against minispike-elicited mouse sera of all tested SARS-CoV-2 variants, including beta. These results therefore suggest that a single vaccination with VSVΔG-minispike-eGFP is sufficient to protect mice against challenge with all variants tested in neutralization assays, including all current VOCs (α, β, γ and δ) as well as variants with other escape mutations like AV.1.

While SARS-CoV-1 and MERS-CoV S proteins encode a number of VNAb epitopes located outside of the RBD, the SARS-CoV-2 RBD accounts for almost all human antibodies with potent neutralization capacity [113, 273-276], with the only other domain prevalently targeted by VNAbs being an antigenic supersite on the NTD of S1 [191, 277]. A recent characterization of mAbs produced by memory B cells of a cohort of convalescent COVID-19 patients revealed seven distinct, commonly targeted epitope clusters on the S protein: three located on the RBD, two on the NTD, and finally two sites on the S2-domain. While all three epitopes on the RBD were potentially neutralizing, only one of the two NTD sites and none of the S2 sites gave rise to efficiently neutralizing antibodies [137]. The S2 sites are however the most conserved between coronavirus S proteins and allow for inter-clade cross-reactivity. Because of these numbers, choosing the RBD over the full-length spike retains three out of seven major immunodominant epitope clusters that comprise three out of four nAb-inducing targets while reducing size by 80 %.

These numbers are in the context of the RBD in its natural conformation, nested on top of the S trimers. To induce a tantamount landscape of epitopes without the framework provided by the full-length S, near-natural presentation of the antigen is key. In the meanwhile, data on various S protein constructs have become available [202, 278]. While soluble monomeric RBD protein was reported to suffer from limited immunogenicity, organizing two RBDs in a tandem repeat single chain construct enhanced immunogenicity [279]. Addition of a trimerization domain, leading to soluble RBD trimers, as applied for example in BNT162b1 mRNA clinical trials, showed very promising immunogenicity including stimulation of humoral and cellular responses [280-282]. In addition to arrangement as trimers, membrane anchoring seems to further improve reactogenicity of immunogens. Transmembrane anchored prefusion-stabilized full-length S protein was reported to elicit higher VNAb levels than corresponding secreted constructs [271, 283]. Reflecting previous observations that RABV and VSV G protein trimers are rather unstable [242, 284], we could not immediately demonstrate a trimeric form of the minispike in cell lysates. In the context of viral envelopes, however, in which the internal RNP and matrix protein layers determine organization [43, 48, 241, 285], trimeric G spikes form highly ordered paracrystalline arrays. It was previously suggested that the repetitive arrangement of G epitopes as observed in VSV is responsible for stimulating a very strong antibody response, by crosslinking of B cells via receptors, and possibly by contribution of T cell-independent activation mechanisms [286, 287]. VLPs in general are potent immunogens, and intact VLPs may be transported to local lymph nodes to promote immune responses [288]. We assume that the non-infectious minispike VLPs as described here are synergizing with cell membrane expressed antigen, although quantification of their exact contribution to the overall immune response will require further experimentation with purified VLPs.

Stoppable SMASh viruses

In addition to the single round VSVΔG vaccines, we precautionarily generated a series of full-length VSV constructs in which essential viral proteins are N-terminally tagged with the HCV-NS3/4A-protease derived SMASh-tag [86], which allowed for previr-dependent control of virus replication. Both N-terminal and C-terminal fusion to the protein of interest is conceivable, but due to the low fidelity of the RdRP and consequently high rates of mutation in VSV and similar RNA viruses [148], only N-terminal fusion can circumvent prompt viral escape by introduction of premature stop codons upstream of the SMASh-tag. In proof-of-principle experiments we showed that VSV with a SMASh-tagged P protein is viable, that addition of the inhibitor at time of infection completely blocks the establishment of infection whereas addition four hours post infection “freezes” the status quo, allowing for observable gene expression in the first round of infected cells but suppressing further

spread. We then cured a productively infected cell culture by cultivating the cells in the presence of an approved protease inhibitor. Due to a high stability of intracellular RNPs, complete curing required a prolonged period of time. We found that infection recommenced upon removal of the drug as late as nine days post commencement of treatment, but not any more after 16 days. As this allows to switch off (and turn on, within a certain time frame) virus replication and therefore gene and immunogen expression as well as virion and VLP release, VSV-based vectors equipped with the SMASh system are an intriguing alternative to single-round replicons. Especially in immunocompromised individuals, the elderly, the very young or unfortunate combinations the control over virus replication constitutes a fundamental safety feature which is sorely missing in replication-competent virus vectors used to date, potentially leading to harmful and unfortunate outcomes [82]. Furthermore, as-yet unpublished observations indicate that the VSV SMASh-system does not act as a binary system, i.e., has just two states, "ON" and "OFF". Rather, variation in drug concentration can modulate virus replication, enabling the fine-tuning of expression levels to best fit the middle ground between immunogenicity on the one side and tolerability and safety on the other. Whereas vaccination against SARS-CoV-2 appears to be relatively straightforward and efficient, with non-spreading subunit vaccines like our minispike approach described here able to induce a highly effective immune response, the potential of a controllable spreading-competent vector becomes more worthwhile when more challenging pathogens are concerned or in individuals that show a reduced and insufficient response to immunization with single-round viral vectors.

Spreading-deficient VSV: A tradeoff?

Although the spreading-deficient virus vector vaccine described here is highly safe and efficient, a replication- or rather spreading-competent vector might be preferable in terms of a simpler vaccine production process and appears potentially beneficial *in vivo* due to an escalated immune response caused by additional rounds of infection in immunized individuals. While the latter holds true in cell culture and similar artificial systems, it is not necessarily the case in complex organisms. VSV, aside from its use as vaccine vector, is an important vehicle for oncolytic virotherapy, mainly due to its interferon sensitivity and lytic growth kinetics when running free. Tumors often exhibit an immunosuppressive microenvironment which has the flip side of making them easy prey for viruses like VSV (for recent reviews see [289-291]). The initial replication of VSV is thought to be restricted to the tumor and the eventual lytic cell death is a powerful inducer of both innate and adaptive immunity that can lead to the formation anti-tumor immunological memory [292, 293]. Interestingly, it has been indicated that when in the context of an intact immune system, tumor regression is not associated with a replicative burst of the virus [294]. In a C57/Bl/6 mouse model with B16ova melanomas,

single-round VSVΔG was equally efficient as fully replication-competent VSV in causing tumor regression, which was mainly a function of viral gene expression and induction of a proinflammatory responses. Unlike observations from *in vitro* cell culture models were output virus increases exponentially, no replicative amplification was detected after intratumoral injection of full-length VSV *in vivo*. Instead, the titers consistently decreased and ten days post injection no infectious particles could be detected in the tumor. Additionally, while increased doses of input virus correlated with tumor lysis, they did not result in increased output titers. This further indicates that spread of full-length VSV is restricted almost immediately in mice with a functional immune system, which argues against an evident benefit conveyed by immunogen escalation through spreading-competent viruses. In other words, in immune-competent specimens full-length VSV does not spread from initially infected cells but does amplify in immune-suppressed mouse or man.

Previous studies on VSV-based SARS-CoV-1 vaccines come to a similar result. Even more pronounced than with SARS-CoV-2 S, the full-length S protein of SARS-CoV-1 does not readily rescue infectiousness of VSVΔG in cell culture and mice [295], possibly due to lower affinity for ACE2, absence of the polybasic cleavage site between S1 and S2 and inhibitory interactions of the S cytoplasmic tail with VSV assembly and budding [296-298]. Consequently, a VSV construct in which the VSV G gene is replaced with the SARS-CoV-1 S protein (VSVΔG-SARS-CoV-1 S; genome organization: 3´-N-P-M-S-L) is phenotypically a single round infectious particle when transcomplemented with VSV G. On the other hand, non-G-deleted VSV-SARS-CoV-1 S (3´-N-P-M-G-S-L-5´) still retains G expression and therefore can spread. Notably, sera from mice vaccinated with the single round ΔG constructs showed a two-fold increase in S neutralization capacity compared to sera from mice vaccinated with the G-encoding virus, an effect that is has also been described with other immunogens [299, 300]. One possible explanation is the attenuation of mRNA transcription by the VSV polymerase at each gene junction. Adding more transcription units upstream of the L gene leads to a decrease of L mRNA and protein levels, altered growth kinetics and ultimately attenuation. As VSV is a highly interferon sensitive virus and relies mainly on a fast, burst-type replication to outpace the host antiviral response, the positive aspect of adding the G gene, namely enabling spread and therefore amplification is offset by attenuation and might very well be a zero-sum game or a net loss. Another possibility is that the G protein, which is highly immunogenic in itself, diverts the immune system from the actual immunogen “cargo”.

Of further concern is the safety or rather residual pathogenicity of replication- and spreading-competent viruses like VSVΔG encoding a full length spike [76, 301, 302] or non-G-deleted VSV expressing S subunits, demonstrated rather impressively in a recent study by the death of two mice post vaccination with a spreading-competent VSV construct due to “unknown etiology” [233]. Regarding the use of full-length spike, the change in tropism is another potential hazard. The pantropic VSV G indiscriminately mediates entry and infection of virtually all cell types, including immune cells.

Infection of macrophages is a strong activator of the adaptive immune system and is discussed to be partially responsible for the relatively benign course of infection of VSV [303, 304].
S on the other hand uses ACE2 as cellular receptor. Apart from the altered and to date poorly defined tropism of SARS-CoV-2 S-expressing viruses, ACE2 is not or only minimally expressed in most immune cells [305, 306]. This altered tropism could conceivably impair recognition and immune response to infection, jeopardizing vaccine safety.
Even more critical, the mutational activity of VSV is at least an order of magnitude higher than that of SARS-CoV-2. Adding a functional SARS-CoV-2 S gene into VSVΔG therefore leads to a replication- and spreading-competent hybrid virus relying on S for entry which is extremely quick to adapt to immunological pressure. This has been exploited to "forward-screen" and predict possible escape mutations to monoclonal antibodies and polyclonal immune sera [185, 195, 307-309]. Taking into account the number and impact naturally occurring multiply mutated SARS-CoV-2 variants have (see virtually all variants of concern), the flip side of this is that it appears as an extremely poor idea to let loose full-length S encoding, replicating VSV on the general populace, including immune-compromised individuals possible unable to restrict and clear VSV infection promptly.

Envelope switching: Different glycoproteins for heterologous boost vaccinations

Drop of nAb levels below a functional "protective" threshold, either by natural decline of antibody titers over time or by escape from neutralization by mutated strains can lead to a surge of reinfections, especially if people consider themselves immune and don´t exercise due care in precautionary behaviors. As of fall 2021, an increasing number of breakthrough- and re-infections in fully vaccinated or convalescent individuals have been reported and correlated with lower nAb levels (mean serum neutralization titers in breakthrough cases were roughly three-fold lower than in controls) and increased time since vaccination [257, 310, 311]. Even consecutive breakthrough infections have been reported [312]. Virus variants that combine increased transmissibility with immune escape mutations like delta further aggravate the situation.
Accumulating real-world data from Israel already illustrates an alarming drop in vaccine effectiveness against infection: from 95 % in the timeframe from January 24 - April 3 (2021) to 64 % between June 6 - July 3 to just 39 % between June 20 – July 17. While the emergence of the delta variant might confound these findings, initial reports stated an 88 % efficacy of BNT162b2 against infection with that strain [313, 314]. This number had decreased to 39 % by mid of July. The vaccination campaign in Israel has been carried out swiftly in the beginning of 2021, with half of the population vaccinated twice by March 21, 2021 with BNT162b2 [315]. These observations indicate that protection after vaccination with the current vaccines might be limited to less than six months. An observational study from the

U.S. assessing the efficacy of vaccination with mRNA-1273 and BNT162b2 during January-July 2021 show agreeing data, with the overall protection provided by BNT162b2 vaccination of 76 % over the whole period sharply contrasted by a significant drop to 42 % for the last month of the study (July) [316]. The same trend was seen for Moderna´s mRNA-1273, although it generally offered better protection, most importantly at the endpoint, where a two-fold reduction in risk for breakthrough infection compared to BNTB162b2 was observed. Although the data is alarming, protection against hospitalization and severe COVID-19 with either vaccine remains at very high levels. Still, repeat boost vaccinations are indicated to stay on top of the pandemic and are already underway world-wide, with early results from a nation-wide prospective cohort study in Israel indicating that boost vaccination reduces the risk of SARS-CoV-2 infection by 11-fold in people aged over 60 [317].

As demonstrated, the VSVΔG replicon complemented with VSV G protein to mediate infection of muscle cells is highly effective in SARS-CoV-2 S RBD antigen expression after i.m. application, and intraperitoneal (i.p.) administration is thought to be similarly effective [295]. A boost immunization with the same virus led to strong increase in VNAb titers in vaccinated animals, arguing against an immediate sterilizing nAb response against VSV G, allowing both homologous and heterologous boost strategies. While results for RABVΔG-based minispike vaccines are not yet available, both VSV and RABV are amenable to envelope switching. Especially when considering prospective repeated booster shots to address emerging variants, the ability to use different envelope proteins allows to circumvent eventual problematic vector-specific immunity. The flip side of the highly immunogenic display of surface glycoproteins on virus particles is that successive immunizations with vectors decorated with the same glycoprotein invariably trigger increasing immune responses against both vector backbone and surface-displayed glycoprotein. This results in progressively reduced transduction efficiency. Data from clinical trials of the recently approved VSV based Ebola vaccine indicate that humoral immune responses directed against the vector backbone do not confer sterilizing immunity [318]. Instead, only antibodies directed against the surface glycoprotein are potentially neutralizing the virus particles.

As the Minispike platform functionally separates the immunogen payload (the SARS-CoV-2 minispike) from the infection-mediating surface glycoprotein (VSV G in this case) with the latter not being encoded in the vector but supplied in trans, straightforward heterologous boost regimens are possible by simply utilizing a different glycoprotein.

Due to the widespread use of VSV G for transcomplementation of lenti- or retroviral vectors, there have been efforts to find suitable alternatives that allow efficient transduction in hosts with pre-existing immunity against VSV G. Glycoproteins from the VSIV-related vesiculoviruses Piry and Chandipura virus have been proposed as compatible and similarly efficient alternatives to VSIV G. They are not seroprevalent in the population and confer a comparably broad tropism to VSIV G while being more resistant to neutralization [319]. Importantly, they are only weakly (Chandipura G) or not at all

(Piry G) recognized and cross-neutralized by nAbs directed against VSIV G. It would be therefore possible to increase boost vaccination efficacy, especially if multiple boost rounds are indicated to keep up with emerging VOCs, by using such a glycoprotein for transcomplementation. Optionally, RABVΔG or VSVΔG minispike vectors can also be (trans)complemented with the G protein of widely used RABV strains like SAD, which is in use for oral immunization of wildlife, offering the intriguing possibility of immunization *per os* and therefore increased compliance among needle-shy individuals.

Single vs multiple copies of the minispike gene

We generated and rescued VSVΔG minispike variants with one, two or three copies of the minispike gene (minispike, bimini, trimini). It could be expected that more genomic copies of a given gene in the vector result in more mRNA transcripts and, accordingly, more protein, tilting the ratio of VSV gene products/minispike towards the latter. Although no striking attenuation was apparent in terms of infectious titer, we also did not detect a marked increase in minispike protein after 24h of infection. This might be due to a similar effect as observed for G-encoding viruses, as each additional gene junction between transcription unit causes a drop of approximately 30 % in the abundance of downstream transcripts [7]. Consequently, the second copy of the minispike cistron is transcribed only at roughly 70 % of the level of the first copy, without considering that the transcription of the polymerase gene is also reduced. A recombinant VSV with two copies of an eGFP cistron at position 1 and 2 (VSV-12´GFP; 3´-eGFP-eGFP-N-P-M-G-L-5´) was described as highly attenuated, probably mainly due to a ten-fold reduction of L transcripts [320], resulting in a marked decrease of L protein and consequently viral replication. Although the virus had slower growth kinetics and formed smaller plaques in cell culture compared to the parental virus, it was effective at generating an immune response, demonstrated by the induction of high antibody titers against eGFP. The slower replication speed might also change the kinetics of VSV gene expression, delaying the timepoint of maximal minispike translation. While VSVΔG-minispike-eGFP has probably reached peak expression after 24h, bimini and trimini constructs might peak at later times after infection. Apart from all mechanistical explanations, another point to keep in mind is that western blots are poorly suited for quantification of small differences [321]. As we saw no striking differences in expression for constructs expressing one or two copies and similar titers, bivalent constructs appear feasible and excision of the eGFP gene would free another cargo slot for a third copy or increase the expression of a bi- or monovalent construct. Instead of increasing the expression level of an identical minispike version, however, one could make use of the ability to insert at least two different minispikes into the VSV backbone without handicapping virus titers to address SARS-CoV-2 antigenic drift by encoding for multiple minispike variants in the same vector.

Possible upsides of multivalent constructs

So far, the global SARS-CoV-2 infection landscape "post B.1" with its D614G mutation has been dominated by single variant strains. First alpha/B.1.1.7 and currently delta/B.1.617.2 are being responsible for most acute cases at a given time while most variant strains are relegated to regional impact. Mainly due to travel restriction imposed in the first year of the pandemic and extensive testing and isolation, local containment of variant strains has been by and large successful except for beta and delta, which are significantly more infectious than the ancestral strain. As restrictions are lifted and public immunity and, perhaps even more critical, perception of immunity and "pandemic fatigue" increase [322], vaccine efficacy against variants becomes increasingly crucial and broad protection against multiple strains can evolve into a determinative factor of how the pandemic will proceed.

All natural variants described to date are neutralized, albeit to varying extent, by vaccines based on the S protein of the original strain of SARS-CoV-2, with escape mechanisms predicted and quickly unraveled by an unprecedented focus of the entire scientific community. In respect to the RBD, the substitution of E484 to K, Q or A confers the largest immune escape from antibodies by reshuffling the antigenic footprint of a major epitope targeted by the predominant class of neutralizing antibodies in humans [184, 254]. Although minispike-elicited immune sera proved to be remarkably unaffected by E484K mutants, a construct encoding the "classic" RBD with E484 and one or more "Escape-RBDs", with mutations derived from artificial super-escape variants [195, 196], or a hypereffective ACE2-binding-enhanced RBD [323] is feasible and would be interesting to examine in regard to the potency and breadth of the neutralizing response. Emanating from our data, namely that the delta variant shows the most pronounced immune escape from Wuhan-minispike immunization, an additional minispike with the combination of L452R and T478K as present on delta appears especially advisable to address this vulnerability. Intriguingly, cross-clade immunization and/or prime/boost regimens with chimeric coronavirus Spike constructs have recently been demonstrated to induce a pan-sarbecovirus neutralizing antibody response [324-326]. This strategy could be easily adapted to the VSVΔG-minispike platform by including SARS-CoV-1- or MERS-based minispike constructs into the vector backbone. A trivalent minispike, possibly not as individual cistrons but linked by 2a-like peptides to avoid attenuation due to an excessive number of gene junctions would still be comparable in size to one copy of the full-length S. A further, more straightforward approach to address multiple variants, strains or viruses at once is to combine several monovalent constructs into one preparation, each encoding the RBD or major immunogen of a different virus. A similar strategy has been employed successfully in the context of VSV-based filovirus vaccination trials [327]. Such a composition could be easily updated and adapted to emerging virus strains and VOCs.

A single immunization with VSVΔG-minispike-eGFP protects mice against delta challenge

Even though sera from minispike-immunized mice reveal reduction of neutralizing activity against some variants, particularly in case of the delta variant of SARS-CoV-2, a single shot of the original minispike construct still protected k18-hACE mice from SARS-CoV-2 delta induced disease and death upon challenge. Considering the eight- to twelve-fold reduction in neutralizing activity against that variant, these findings argue for a protective effect of very low levels of NAbs or secondary mechanisms not immediately apparent from serum neutralizing activity in the context of our experimental model. Interestingly, while the original minispike construct provided perfect protection, neither immunization with a minispike construct based on the beta RBD nor with a bimodal construct expressing both the beta and the kappa minispike led to protection of all animals. With the big caveat that the data presented in this case is preliminary and requires confirmation and validation, the findings are nevertheless very interesting. While surprising at first sight, it can be speculated that the observation that the original minispike construct shows better protection against the delta variant than the other two constructs correspond to the findings of others and structural studies on the effect of substitutions in S [181, 268, 269]. E484 is located at the "tip" of the RBD, which can assume a "hook"-like, ordered state or a more flexible, disordered state. For the wild-type RBD, the probability for each state is roughly equal with 45% "hook"-like and 55% disordered. E484 is a crucial residue, as it stabilizes the "hook" by forming a hydrogen bond with residue F490. Substitution of E484 to K abolishes this intramolecular hydrogen bond and destabilizes the RBD tip, which is reflected by the fact that the beta RBD with N417, K484 and Y501 has a "hook" state probability of less than 20 % [181]. This higher probability for a disordered state almost certainly negatively impacts not only antibody binding but also immunogenicity of the epitope. In a study describing RBD subunit vaccines in form of circular RNAs, immunization with both Wuhan and beta RBD based constructs readily induced neutralizing antibodies against both strains. Remarkably, the Wuhan RBD led to substantially higher neutralization titers than immunization with a beta-derived RBD, even against the beta S [269]. Additionally, interim data from mRNA-1273 (Moderna) boost trials intriguingly show similar findings. Volunteers received a booster shot of either mRNA-1273 (encoding a modified ancestral Wuhan S), mRNA-1273.351 (encoding a modified beta S) or a 1:1 mix of both (mRNA-1273.211) six months after the first series of full vaccination with mRNA-1273. All three boost vaccination regimens led to a significant resurgence of serum neutralizing titers against ancestral and variant SARS-CoV-2 S transcomplemented pseudoviruses, but the group boosted with mRNA-1273.351 showed the lowest response [328]. This indicates that a possibly reduced immunogenicity of the beta S is not limited to RBD-based subunit vaccines, but also affects vaccination with full-length S. The assumption that the "culprit" responsible

for this phenomenon is the substitution of E484 is congruous with our results. The least effective construct, protecting only two out of five animals from critical disease or reaching humane endpoints, was expressing the beta-based minispike (with the mutations K417N, E484K and N501Y). The addition of the kappa minispike (with the mutations L452R and E484Q) led to protection of four out of five of animals, although the surviving animals still showed symptoms. The E484Q mutation from kappa is more conservative than E484K and probably still able to form stabilizing interactions with F490, possibly explaining the partial rescue. Finally, immunization with the Wuhan minispike not only protected all animals from death but additionally from any visible symptoms, arguing for the induction of a diverse and broadly protective immune response after a single shot. The exact contributions of each mutation to the observed phenotypes remain to be elucidated and challenge experiments with further variants, including beta, are pending. Based on the variant neutralization assays however, the expectation would be that minispike-elicited immune responses in mice vaccinated once are sufficient to protect against current SARS-CoV-2 variants and VOCs.

Induction of a differential antibody landscape by different vaccines and infection

The landscapes of antibodies elicited by natural SARS-CoV-2 infection or vaccination with different antigens like 2P- (substitution of residues K986 and V987 by two prolines, “2P”, and possibly abolishment of the polybasic furin cleavage site replacing residues 682-685 with Gly-Ser-Ala-Ser) [115]) or even further prefusion-stabilized S [329], non-stabilized, “authentic” S and subunit vaccines utilizing the RBD are fundamentally different [330].

In contrast to other betacoronaviruses, the entire spike is relatively impervious to nAbs with only two small regions of vulnerability that can lead to virus neutralization upon antibody binding: the RBD and an antigenic “supersite” cluster in the NTD [189, 190, 275, 277, 330]. Accordingly, immune pressure and forced evolution leads to escape variants that predominantly display changes in these sites to escape neutralization. A combination of both is observed in the most variants of concern.

Notably, the overall IgG repertoire directed against S in convalescent subjects is targeting mainly epitopes residing outside the RBD [330]. Additionally, it has been proposed that the RBD and especially the RBM deflect immune recognition in the context of full-length spike [200]. S-binding antibodies against non-neutralizing epitopes may still have beneficial effects by mediating phagocytosis and thus possibly mitigating pathological burden *in vivo* [331]. Conversely, they may be also detrimental, increasing the infectivity of SARS-CoV-2 and possibly enhancing severity of COVID-19 [332, 333]. Both in terms of immunogenicity and safety, additionally indicated by the potential association of circulating SARS-CoV-2 S1 subunits with enhanced blood clotting [334], the use of a small membrane-anchored antigen is therefore rational.

While natural immunity induced by infection with the ancestral SARS-CoV-2 strain, inactivated vaccines based thereon and vaccines based on non-stabilized S tend to protect poorly against variants like beta [259, 260, 335], mRNA vaccines encoding prefusion-stabilized S protein perform better [258, 265, 314, 336], although not all mRNA vaccines are created equal [337]. This indicates the induction of a robust, more broadly neutralizing IgG landscape. However, also mRNA vaccine induced sera show a profound reduction in neutralization capacity against some SARS-CoV-2 variants compared to the ancestral Wuhan strain. This is further exacerbated by the natural decline of post vaccination antibody titers over time [311, 338].

So far, SARS-CoV-2 has encountered a mainly naïve and unprotected population and accordingly, increased infectivity and transmission rather than immune evasion has been the most critical characteristic of highly successful strain, e.g., alpha and delta. Strains with a highly immune-evasive phenotype like beta, gamma or more recent strains such as A.VOI.V2, mu, or further evolved delta variants [166, 196, 339, 340] have so far played an underpart on the global scale. However, due to the success of both SARS-CoV-2 and the global vaccination effort, the dynamics might shift in favor of strains with pronounced escape from ancestral antibodies. Severe reductions in neutralizing titers are generally observed for multiple VOCs. In regard to immune evasion and escape from neutralization, the scientific consensus at the moment is that the most alarming variant to date is B.1351 or beta [341], although it appears that the recently described mu variant might give it a run for its money [339]. Compared to the original SARS-CoV-2 S, the beta S has mutations **D80A, D215G, L242_A243_L244del, K417N, E484K, N501Y**, D614G and A701V. The mutations and the deletion in the NTD (bold) lead to rearrangements of the "NTD supersite", the sole neutralizing NTD epitope [189, 190] and cause a near-complete escape from neutralizing antibodies targeting the ancestral NTD [256]. The beta S also contains the three RBD mutations K417N, E484K and N501Y, of which E484K and N501Y are situated in the RBM. Concerning RBD-targeting neutralizing antibodies, E484K is the main escape factor. The combination of K484 and the NTD supersite reorganization leads to complete escape from a disconcerting number of mAbs that show highly effective neutralization of the ancestral S. Polyclonal sera of COVID-19 survivors and vaccinees are also severely diminished in potency, with sera from convalescent patients show a decrease in nAb titers that range from 6-fold to 13-fold [261, 264, 267, 342-345], vaccinees show a 1.5 – 8 fold reduction [258, 262, 267, 346-351]. Large discrepancies in protectivity against beta are observed for the various vaccine candidates: The approved mRNA-based vaccines BNT162b2 and mRNA-1273 show a relatively modest decline in protection, at least at early timepoints after vaccination, while adenoviral vectors expressing unstabilized S almost completely failing to protect against this variant [260, 335, 352].

Antibodies targeting and binding to the RBD can be functionally divided into four basic classes, depending on the combination of two parameters: whether they compete with ACE2 binding and

which RBD state (up or down) is needed for epitope accessibility. Class-1 and -2 antibodies bind within the ACE2-binding motif, although at different, but partially overlapping sites. Class-1 Abs recognize a part of the RBM that is accessible only if the RBD is oriented in the "up" conformation whereas the epitope of class-2 Abs is accessible in both "open" and "closed" conformations. The epitope of class-3 antibodies is situated outside of the ACE2-binding face and accessible in both conformations. Finally, class-4 antibodies recognize a cryptic epitope outside of the RBM that is only accessible the open conformation [142, 230]. Another attempt to classify RBD-binding antibodies based on binding competition assays resulted in three separate groups (RBD-1, RBD-2, RBD-3) [137], with antibodies within one group competing for binding to the RBD within the group but not with other groups. The RBD-2 group hereby is roughly equivalent to class-1 and class-2 described previously [142]. The most impactful residues in regard to binding (and escape) for the four classes of nAbs are K417, N460 and F486 for class-1, F456, E484 and F490 for class-2, R346, K444 and G446 for class-3 and K378 and K417 for class-4 [144]. We included the AV.1 strain in our pseudovirus neutralization assays due to its combination of N439K and E484K mutations. N439K has been implied in immune escape [252] and shown to play a role in resistance to class-3 antibodies that do not directly interfere with ACE2 binding [353].

No S subunit vaccines are in clinical use so far; accordingly, there is only limited in-human real-world data available. The neutralization capacity of the plasma polyclonal antibody response of convalescents and vaccinees tends to be dominated by class-2 RBD-binding antibodies [144, 185, 254]. One reason for this observation is that this class of antibodies generally contains highly potent, near-germline neutralizers with low levels of somatic mutations [274]. Another explanation might be availability and exposure of the epitope irrespective of the orientation of the RBD. Unlike the epitope recognized by class-1 nAbs, which is accessible only in the RBD-up conformation, the class-2 epitope is always accessible; a detail that is further magnified by the finding that in the context of S trimers, the most frequent conformation is three-RBD-down or one-up-two-down. As potent neutralizers, class-2 mAbs exert a strong immunological pressure, driving mutational escape of the SARS-CoV-2 S. Unfortunately, class-2 mAbs are also very vulnerable to substitutions at key residues F456 and especially E484 which led to the convergent evolution of multiple strains carrying escape mutations at these positions. Consistent with these findings, RBD constructs comprising such mutations show reduced binding to polyclonal sera from COVID-19 patients which is also in line with the observation that strains like beta and gamma, which contain the E484K mutation, tend to be poorly neutralized by such sera. This might be different for sera from individuals vaccinated with S subunit vaccines like the minispike, where the RBD should be accessible from all angles by default. It remains to be seen how and if this translates into the differential induction of preferential antibody classes. From out data it

appears that the E484K mutation has a limited impact on the neutralization potency of our vaccinated mice sera.

Hardly surprising, neutralization assay methodology and results vary considerably between individuals, labs, and countries. Conversely, the serum neutralizing potency of convalescents should be relatively constant if averaged over a sufficiently large group of individuals. This so-called mean convalescent level could therefore be used as a standard to compare results from different labs. It has been proposed that a neutralization titer corresponding to 20 % of this mean convalescent level is sufficient to elicit a 50 % protection against detectable COVID-19 (e.g., the mean convalescent level in an assay has a ID50 (inhibitory dilution 50%) value of 1000. A serum with the ID50 of 200 should offer a 50 % protection against detectable COVID-19) [354]. In this thesis, our convalescent control sample had the highest S binding (ELISA titer 8.74) and neutralizing titer available at the time (June 2020) from the virology diagnostics department of the LMU Klinikum Munich and should therefore represent and probably overestimate the mean convalescent level. The ID50 value for the patient sample against VSVΔG pseudotyped with the parental S is 1:2601 (95 % confidence interval; 1:2234 to 1:3051) in our neutralization assays, which would position the protection cutoff at 1:520. The mean ID50-values of BALB/c mice twice-vaccinated with VSVΔG-minispike-eGFP are 1:4805, 1:3879, 1:8485, 1:747 and 1:3291 against B.1, alpha, beta, delta and AV.1, respectively. This puts them easily above the calculated protection cutoff and should translate into complete and durable protection, as demonstrated by the challenge experiments with delta.

Although the RBD has been proven to accommodate mutations, the types of exchanges tolerated are usually conservative and follow certain restraints as they must adhere to a structural interface that supports binding to ACE2 and thus enables attachment and cell entry. For this reason, viable point mutations in the RBD usually do not lead to complete abrogation of recognition, binding and neutralization by the RBD-targeting antibody aggregate. In contrast, the structural constraints on the NTD are likely lower than on the RBD. Combined with the fact that just singular neutralizing epitope has been described so far on the NTD, loss of protection by all NTD-targeting nAbs is a quick evolutionary step that is readily and recurrently occurring in persistently infected immunocompromised patients [186, 192, 355-359] and is a hallmark of most VOCs, including alpha, beta and delta [166, 193, 196, 256, 330]. It is still unclear if the rearranged NTD “supersite” in VOCs retains its immunogenicity and mechanistic vulnerability to neutralization and, if so, antibodies against one VOC NTD can cross-neutralize the other VOCs. Another peculiarity is of further concern: So far, detrimental, infection-enhancing antibodies do not appear to play a significant role *in vivo* in the presence of a neutralizing antibody response. However, their effect is amplified in S variants that show near-complete escape from ancestral Wuhan S induced immunity, as demonstrated for an artificial delta strain with four additional, common naturally occurring RBD mutations (K417N, N439K, E484K,

N501Y) [196]. While the epitopes of neutralizing antibodies are under immunological pressure and escape mutations under positive selection, the epitopes for non-neutralizing and possibly infection-enhancing antibodies are usually conserved between strains [193]. This further underlines the potential downside of unnecessarily large and complex immunogens. Hence, against current and constantly evolving VOCs, the benefit of the NTD neutralizing epitope is debatable and can even turn into a problem.

The RBD contains a diverse variety of neutralizing epitopes that can elicit a highly potent antibody response able to cross-neutralize all variants described to date [360]. As our and others´ data indicate [268, 269], vaccination with the RBD leads to a highly diverse aggregate of antibodies that in sum show a remarkable resistance to escape mutations and should therefore offer robust protection against circulating SARS-CoV-2 variants. Furthermore, as epitopes accessible only in the "up" conformation of the RBD appear to be readily displayed by the minispike as revealed by highly efficient positive staining with CR3022, it is plausible that vaccination with minispike leads to a more balanced nAb landscape compared to vaccination with the full-length S. Structural modeling studies on the binding of class-4 mAb CR3022 to S revealed that for the epitope to be accessible, at least two RBDs on the trimeric S protein must be in the "up" conformation and additionally slightly rotated [230]. The fact that most SARS-CoV-2 S trimers are primarily observed in either a 1-RBD up or 3-RBD-down structural state [121] might be part of the reason for the observed underrepresentation of class-4 mAbs in the plasma of convalescents and full-length S vaccinees and, as a possible consequence, the high conservation of the epitope throughout sarbecoviruses. Therefore, increased induction of class-4 antibodies could prove to be especially beneficial, as they have the potential to be potent pan-sarbecovirus neutralizers [361-364]. RBD based vaccines and especially surface-anchored, multimerized constructs like the present minispike might more readily display this vulnerable epitope and elicit an efficient and potentially broadly protective response [365]. This hypothesis is backed by the minor decrease in neutralization efficacy against SARS-CoV-2 variants beta and gamma by minispike-elicited sera.

A similar explanation might be behind another recently described highly conserved epitope located at the fusion peptide in the S2 subunit [139-141]. While the epitope has been described as vulnerable to neutralization for at least some coronaviruses and conserved throughout beta-coronaviruses, it is not readily accessible and apparently of limited immunogenicity. Additionally, the neutralizing antibodies targeting this epitope described so far have a relatively low neutralizing capacity compared to NTD- and RBD-targeting nAbs, therefore possibly not exerting enough pressure to drive escape mutations under natural circumstances [140]. The worth of this epitope, while intriguing due to its broad conservation, remains to be investigated. However, as it forms a stem helix, it seems to be inherently suited for insertion into the minispike construct between the SAD G derived stem and the globular SARS-CoV-2 RBD. We designed a minispike construct with the sequence in question of

different coronaviruses (SARS-CoV-2: D_{1146}SFKEELDKYFKN$_{1158}$, SARS-CoV-1: SFKEELDKYFKN, MERS: DFQDELDEFFKN, consensus: DFKEELDKYFKN) sequentially inserted in between the SARS-CoV-2 RBD and the RABV-derived stem and intracellular cytoplasmic tail. Further experiments will reveal if this new version of the minispike is able to induce functional antibodies against this epitope.

Aside from conformational B cell epitopes, The SARS-CoV-2 RBD and therefore the minispike contains several T cell epitopes. The RBD minispike as used in the VSVΔG minispike replicon comprises S residues 314–541 (QTSN…KCVNF), thus encompassing the known RBD B cell epitopes (residues 370-394, 450-469 and 480-499) and T cell epitopes (residues 375-394, 405-469, 495-521) including the immunodominant T cell nested epitope region of the S protein (residues 346-365) identified in convalescent patients [366-368]. These residues are highly conserved in SARS-CoV-2 variants alpha, beta, gamma, delta, and the closest relative of SARS-CoV-2 described so far, Bat-CoV-RaTG13. The RBD mutations found in the current VOCs are located at residues 417 (beta, gamma, delta plus), 452 (delta), 472 (delta), 484 (beta, gamma), 501 (alpha, beta, gamma) and therefore so far of limited impact on cellular immunity. The possibility of leveraging robust cross-reactive antibody responses and T helper cell functions against conserved sites of SARS-CoV-2 might be instrumental to complement neutralizing antibody responses to adaptive vaccines that incorporate escape mutations found in emerging SARS-CoV-2 variants. Furthermore, mounting evidence illustrates that infection offers a better and/or more durable protection than vaccination [369], possibly due to T cell immunity against epitopes present on other viral proteins than S. Due to the reduced size of minispike, additional, T-cell reactive viral proteins like N or an artificial peptide consisting of multiple described T cell epitopes [370] could be inserted into the VSVΔG minispike replicon.

Conclusion

Our data demonstrates that the antibody response induced by vaccination with a SARS-CoV-2 RBD presented at the cell surface and on virion particles in form of a “minispike” has a neutralizing capacity against the original Wuhan S at least comparable to that of sera from patients recovering from severe COVID-19 and BioNtech BNT162b2 vaccinees. The breadth of neutralization surpasses that of convalescents and at is at least equal to that of young and healthy BNTB162b2 vaccinees, offering protective titers against all tested variants. Therefore, from a point of view focused on the most efficient induction of a broadly neutralizing antibody response it appears worthwhile to forego the non-RBD epitopes present full-length S. Extensive characterization of natural human and animal mAbs revealed multiple, independent conformational epitopes in the RBD [113, 230, 273-275, 371, 372] as well as T cell epitopes [373]. The simultaneous targeting of distinct RBD antigenic sites is of relevance not only for the efficiency of a vaccine but also in the light of emergence and spread of SARS-CoV-2

variants resistant against individual mAbs [309, 372]. This qualifies VSVΔG minispike constructs as promising vaccine candidates meriting further investigation. While the chimeric minispike construct as described here appears to be immediately suitable in any genetic vaccine approach, including the auspicious mRNA platforms [279], its full potential is accomplished in the context of the highly flexible rhabdovirus vector system, which integrates antiviral innate and adaptive immune responses.

Appendix

Declarations

Part of the results presented in this thesis were obtained by collaborators. Those experiments are explicitly referenced in the text and consist of the following:

Cryo-EM experiments were done by Christiane Riedel, University of Veterinary Medicine Vienna, Vienna, Austria.

All mouse experiments and virus neutralization assays with authentic SARS-CoV-2, Wetzlar isolate, were performed by the group of Christian Pfaller and Bevan Sawatsky, Paul-Ehrlich-Institut, Langen, Hesse, Germany.

Virus neutralization assays with authentic SARS-CoV-2 strains B.1.177, B.1.1.7, B.1.351, P.1 and B.1.617.2 were performed by the group of Oliver Keppler, especially Paul-Robin Wratil-Song and most importantly Dr. Marcel Stern, at the Max von Pettenkofer-Institute, Munich, Germany.

Figures were created with BioRender.com and partially adapted from templates.

Parts of this thesis have been published initially as a preprint as:

Safe and effective two-in-one replicon-and-VLP minispike vaccine for COVID-19

Alexandru A. Hennrich, Dominic H. Banda, Martina Oberhuber, Anika Schopf, Verena Pfaffinger, Kevin Wittwer, Bevan Sawatsky, Christiane Riedel, Christian K. Pfaller, Karl-Klaus Conzelmann bioRxiv 2020.10.02.324046; doi: https://doi.org/10.1101/2020.10.02.324046

And after peer review as

Hennrich AA, Sawatsky B, Santos-Mandujano R, Banda DH, Oberhuber M, et al. (2021) Safe and effective two-in-one replicon-and-VLP minispike vaccine for COVID-19: Protection of mice after a single immunization. PLOS Pathogens 17(4): e1009064. https://doi.org/10.1371/journal.ppat.1009064

WHO	Pangolin	Mutations in the S protein relative to the ancestral Wuhan S
Alpha	B.1.1.7	H69-V70 del, Y144 del, N501Y, A570D, D614G, P681H, T716I, S982A, D1118H
Beta	B.1.351	D80A, D215G, L242_A243_L244 del, K417N, E484K, N501Y, D614G, A701V
Gamma	P.1	L18F, T20N, P26S, D138Y, R190S, K417T, E484K, N501Y, D614G, H655Y, T1027I
Delta	B.1.617.2	T19R, E156-F157 del, R158G, L452R, T478K, D614G, P681R, D950N
Epsilon	B.1.427/9	S13I, W152C, L452R, D614G
kappa	B.1.617.1	L452R, E484Q, D614G, P681R, Q1071H
mu	B.1.621	T95I, Y144S, Y145N, R346K, E484K, N501Y, D614G, P681H, D950N
AV.1		D80G, T95I, G142D, Y144 del, N439K, E484K, P681H, I1130V, D1139H
A.VOI.V2		D80Y, Y144 del, I210N, N211 del, D215G, R246M, L242_A243_L244 del, W258L, R346K, T478R, E484K, H655Y, P681H, Q957H

Table 1: Lineages of SARS-CoV-2 mentioned in this thesis with WHO denominator if applicable and mutation in the S protein relative to Wuhan S

Table 2: Abbreviations used in the thesis

Abbreviation	Description
%	per cent
α	Alpha, anti
Δ	delta-, deletion
2P	Two prolin stabilizing mutation; K986 and V987 in SARS-CoV-2 S
5´-ppp	5´-triphosphate
A	adenine
aa	amino acid
Amp	ampicllin
APS	ammonium persulfate
ATP	Adenosine triphosphate
bp	base pair
C	Cytosine
cDNA	complementary DNA
CNS	central nervous system

COVID-19	Coronavirus disease 2019
CPE	cytopathic effect
cRNA	Complementary RNA
C-tail	Cytoplasmic domain
CTD	C-terminal domain
C-terminal	carboxyterminal
d	day
Da	dalton
ddH_2O	bidestilled water
DMSO	Dimethyl sulfoxid
DNA	Deoxyribonucleic acid
dNTP	deoxyribonucleotide
dsRNA	double stranded RNA
EBOV	Ebola virus
eGFP	Enhanced green fluorescent protein
EM	electron microscopy
EnvA	Envelope protein A
EV	empty vector
FCS	fetal calf serum
ffu	focus forming unit
G	glycoprotein
G	Guanine
h	hour
HC	Heavy chain
ICTV	International Committee on Taxonomy of Viruses
IGS	intergenic sequence
ISG	interferon-stimulated genes
HA	Hemagglutinin-Tag (YPYDVPDYA)
HIV	Human immunodeficiency viurs
HRP	horseradish peroxidase
IF	immunofluorescence

k	kilo (1000)
L	Large protein
LC	Light chain
ID_{50}	Inhibitory dilution 50 %
Le	leader
LV	Lentiviral vector
M	Matrix protein
M	molar
MOI	multiplicity of infection
mRNA	messenger RNA
N	nucleoprotein
NGS	Next-generation sequencing
NNSV	non-segmented negative strand RNA viruse
nt	nucleotide
N-terminal	aminoterminal
NTD	N-terminal domain
P	Phosphoprotein
RNA	ribonucleic acid
RSV	Respiratory syncytial virus
SDS	Sodium dodecyl sulfate
T	thymidine
TCID50	Tissue culture infectious dose 50%
TM	Transmembrane domain
p.i.	post infection
PAGE	polyacrylamide gel electrophoresis
PBS	phosphate buffered saline
PCR	polymerase chain reaction
PEI	Paul Ehrlich Institut
PEI	polyethylenimine
PVDF	polyvinylidene fluoride
pH	Potential of hydrogen

RABV	Rabies virus
RABV G	Rabies virus glycoprotein
RABV L	Rabies virus large protein
RABV M	Rabies virus matrix protein
RABV N	Rabies virus nucleoprotein
RABV P	Rabies virus phosphoprotein
RFP	Red fluorescent protein
RIG-I	Retinoic acid inducible I
RNP	ribonucleoprotein
RT	room temperature
SAD	Street Alabama Dufferin
SeV	Sendai virus
SMASh	Small molecule assisted shutoff
SP	Signal peptide
ssRNA	single strand RNA
T7-Pol	T7 RNA polymerase
Tr	trailer
U	unit
VNAb	Virus-neutralizing antibody
VSV	Vesicular stomatitis virus
WB	Western blotting
wt	wildtype

Insert	Backbone	remark
Spike-HA	pCR3	Spike of orig. SARS-CoV-2 Wuhan strain, C-terminal HA tag
Spike-HA	pCAG	Spike of orig. SARS-CoV-2 Wuhan strain, C-terminal HA tag
Spike-HA [D614G]	pCR3	C-terminal HA tag, D614G mutation

Spike ΔC19	pCR3	C-terminal deletion of 19 residues
Spike ΔC24	pCR3	C-terminal deletion of 24 residues
Spike ΔC24 D614G	pCR3	Wuhan S with G614
Spike ΔC24 N501Y D614G ΔC24	pCR3	
Spike ΔC24 E484K D614G ΔC24	pCR3	
Spike ΔC24 K417N E484K N501Y D614G ΔC24	pCR3	Wuhan S + beta RBD
Spike ΔC24 K417T E484K N501Y D614G ΔC24	pCR3	Wuhan S + gamma RBD
Spike ΔC24 D614G A701V ΔC24	pCR3	For cloning of beta S
Spike ΔC24 L452R D614G ΔC24	pCR3	Wuhan S + Cal.20C RBD
Spike ΔC24 T478K D614G ΔC24	pCR3	
Spike ΔC24 L452R T478K D614G ΔC24	pCR3	Wuhan S + delta RBD
Spike ΔC24 L452R T478K E484Q D614G ΔC24	pCR3	Wuhan S + delta RBD + E484Q
Spike ΔC24 L452R E484Q D614G ΔC24	pCR3	Wuhan S + kappa RBD
Spike Alpha ΔC24	pCR3	Alpha S
Spike Alpha E484K ΔC24	pCR3	Alpha S with E484K
Spike Alpha K417T E484K ΔC24	pCR3	Alpha S with gamma-like RBD
Spike Beta ΔC24	pCR3	Beta S
Spike Gamma ΔC24	pCR3	Gamma S
Spike Delta ΔC24	pCR3	Delta S, G142
Spike Delta G142D ΔC24	pCR3	Delta S, G142D mutation
Spike Delta Δ144 ΔC24	pCR3	Delta S, G142, deletion Y144 (Vietnam)
Spike Delta K417N ΔC24	pCR3	“Delta plus” S, G142, K417N
Spike Delta Δ144 K417N ΔC24	pCR3	“Delta plus” S, G142, K417N, deletion Y144
Spike Delta G142D 4+ ΔC24	pCR3	“Delta 4+” [196] (K417N, N439K, E484K, N501Y), G142D
Spike D614G A701V P798H N801D ΔC24	pCR3	For cloning of PMS20-S[195]
Spike D614G 681R ΔC24	pCR3	For cloning of Delta S
Spike D614G 681R D950N ΔC24	pCR3	For cloning of Delta S

Minispike	pCR3	
Minispike	pIRESpuro	For the generation of a stable cell line
Minispike E484K	pCR3	
Minispike N501Y	pCR3	alpha
Minispike K417N	pCR3	
Minispike E484K N501Y	pCR3	
Minispike K417N E484K	pCR3	
Minispike K417N E484K N501Y	pCR3	beta
Minispike K417T E484K N501Y	pCR3	gamma
Minispike L452R	pCR3	Cal.20C
Minispike L452R T478K	pCR3	delta
Minispike L452R E484Q	pCR3	kappa
Minispike L452R E484K N501Y	pCR3	
TandeMinispike	pCR3	Minispike with 2 RBDs in tandem
Minispike 3D	pCR3	human collagen XVIII trimerization domain inserted after F249, between the SARS-CoV-2 RBD and the linker
TandeMinispike 3D	pCR3	Combination of the two above, insertion after F468
MinispikeΔtm-tail	pFuse	Truncated minispike without transmembrane anchor and c-tail; still contains RABV G derived stem
MinispikeΔstem-tm-tail	pFuse	Truncated minispike without transmembrane anchor and c-tail, effectively a secreted SARS-CoV-2 RBD
VSVΔG-minispike-eGFP	pVSVΔG	First of its name and so on
VSVΔG-bimini	pVSVΔG	Minispike minispike
VSVΔG-bimini-eGFP	pVSVΔG	Minispike minispike eGFP
VSVΔG-trimini	pVSVΔG	Minispike minispike minispike
VSVΔG-trimini-eGFP	pVSVΔG	Minispike minispike minispike eGFP
VSV-minispike-ΔG	pVSVΔG	Minispike at pos. 1
VSV-minispike-ΔG-eGFP	pVSVΔG	Minispike at pos. 1, eGFP at 5
VSV-minispike[beta]-ΔG-eGFP	pVSVΔG	Minispike of beta at pos. 1, eGFP at 5

VSV-minispike[beta]-ΔG-eGFP-T2a-minispike[kappa]	pVSVΔG	Minispike of beta at pos. 1, eGFP-T2a-minispike[kappa] at 5
VSV-tandeminispike-ΔG	pVSVΔG	Tandem-minispike at pos. 1
VSV-minispike-eGFP	pVSV	Retains G expression, spreading
VSV-bimini	pVSV	Minispike minispike, spreading
VSV-bimini-eGFP	pVSV	Minispike minispike eGFP, spreading
VSV-trimini	pVSV	Minispike minispike minispike, spreading
VSV-trimini-eGFP	pVSV	Minispike minispike minispike eGFP, spreading
VSVeGFP-ΔG-GaussiaLuc	pVSVΔG	eGFP at 1, Gaussia luciferase at 5
VSVeGFP-ΔG-FireflyLuc	pVSVΔG	eGFP at 1, Firefly luciferase at 5
VSVeGFP-ΔG-NanoLuc-PEST	pVSVΔG	eGFP at 1, destabilized NanoLuc at 5
VSVeGFP-ΔG-S[Wuhan ΔC24]	pVSVΔG	eGFP at 1, S of SARS-CoV-2 with ΔC24 at 5
VSVeGFP-ΔG-S[Delta ΔC24]	pVSVΔG	eGFP at 1, S of SARS-CoV-2 delta with ΔC24 at 5
VSV-SMASh-P-Minispike-eGFP	pVSV_SmP	Smash-tagged P protein, G expression

Table of figures and tables

References

1. Dietzgen R, Kuzmin I, editors. Rhabdoviruses : molecular taxonomy, evolution, genomics, ecology, host-vector interactions, cytopathology and control2012.
2. Leder RR, Maas J, Lane VM, Evermann JF. Epidemiologic investigation of vesicular stomatitis in a dairy and its economic impact. The Bovine Practitioner. 1983;1983(18):45-9. doi: 10.21423/bovine-vol1983no18p45-49.
3. Rozo-Lopez P, Drolet BS, Londono-Renteria B. Vesicular Stomatitis Virus Transmission: A Comparison of Incriminated Vectors. Insects. 2018;9(4):190. Epub 2018/12/14. doi: 10.3390/insects9040190. PubMed PMID: 30544935; PubMed Central PMCID: PMCPMC6315612.
4. Goodger WJ, Thurmond M, Nehay J, Mitchell J, Smith P. Economic impact of an epizootic of bovine vesicular stomatitis in California. J Am Vet Med Assoc. 1985;186(4):370-3. Epub 1985/02/15. PubMed PMID: 2982776.
5. Bridges VE, McCluskey BJ, Salman MD, Hurd HS, Dick J. Review of the 1995 vesicular stomatitis outbreak in the western United States. J Am Vet Med Assoc. 1997;211(5):556-60. Epub 1997/09/18. PubMed PMID: 9290819.
6. Jenni S, Bloyet LM, Diaz-Avalos R, Liang B, Whelan SPJ, Grigorieff N, et al. Structure of the Vesicular Stomatitis Virus L Protein in Complex with Its Phosphoprotein Cofactor. Cell Rep. 2020;30(1):53-60 e5. Epub 2020/01/09. doi: 10.1016/j.celrep.2019.12.024. PubMed PMID: 31914397; PubMed Central PMCID: PMCPMC7049099.
7. Iverson LE, Rose JK. Localized attenuation and discontinuous synthesis during vesicular stomatitis virus transcription. Cell. 1981;23(2):477-84. Epub 1981/02/01. doi: 10.1016/0092-8674(81)90143-4. PubMed PMID: 6258804.
8. Canter DM, Perrault J. Stabilization of vesicular stomatitis virus L polymerase protein by P protein binding: a small deletion in the C-terminal domain of L abrogates binding. Virology. 1996;219(2):376-86. Epub 1996/05/15. doi: 10.1006/viro.1996.0263. PubMed PMID: 8638403.
9. Yabukarski F, Leyrat C, Martinez N, Communie G, Ivanov I, Ribeiro EA, Jr., et al. Ensemble Structure of the Highly Flexible Complex Formed between Vesicular Stomatitis Virus Unassembled Nucleoprotein and its Phosphoprotein Chaperone. J Mol Biol. 2016;428(13):2671-94. Epub 2016/04/25. doi: 10.1016/j.jmb.2016.04.010. PubMed PMID: 27107640.
10. Masters PS, Banerjee AK. Complex formation with vesicular stomatitis virus phosphoprotein NS prevents binding of nucleocapsid protein N to nonspecific RNA. Journal of virology. 1988;62(8):2658-64. Epub 1988/08/01. doi: 10.1128/JVI.62.8.2658-2664.1988. PubMed PMID: 2839693; PubMed Central PMCID: PMCPMC253697.
11. Flood EA, Lyles DS. Assembly of nucleocapsids with cytosolic and membrane-derived matrix proteins of vesicular stomatitis virus. Virology. 1999;261(2):295-308. Epub 1999/09/25. doi: 10.1006/viro.1999.9856. PubMed PMID: 10497115.
12. Flood EA, McKenzie MO, Lyles DS. Role of M protein aggregation in defective assembly of temperature-sensitive M protein mutants of vesicular stomatitis virus. Virology. 2000;278(2):520-33. Epub 2000/12/19. doi: 10.1006/viro.2000.0675. PubMed PMID: 11118374.
13. Lenard J. Negative-strand virus M and retrovirus MA proteins: all in a family? Virology. 1996;216(2):289-98. Epub 1996/02/15. doi: 10.1006/viro.1996.0064. PubMed PMID: 8607258.
14. Harty RN, Brown ME, McGettigan JP, Wang G, Jayakar HR, Huibregtse JM, et al. Rhabdoviruses and the cellular ubiquitin-proteasome system: a budding interaction. Journal of virology. 2001;75(22):10623-9. Epub 2001/10/17. doi: 10.1128/JVI.75.22.10623-10629.2001. PubMed PMID: 11602704; PubMed Central PMCID: PMCPMC114644.
15. Harty RN, Paragas J, Sudol M, Palese P. A proline-rich motif within the matrix protein of vesicular stomatitis virus and rabies virus interacts with WW domains of cellular proteins: implications for viral budding. Journal of virology. 1999;73(4):2921-9. Epub 1999/03/12. doi: 10.1128/JVI.73.4.2921-2929.1999. PubMed PMID: 10074141; PubMed Central PMCID: PMCPMC104051.

16. Jayakar HR, Murti KG, Whitt MA. Mutations in the PPPY motif of vesicular stomatitis virus matrix protein reduce virus budding by inhibiting a late step in virion release. Journal of virology. 2000;74(21):9818-27. Epub 2000/10/12. doi: 10.1128/jvi.74.21.9818-9827.2000. PubMed PMID: 11024108; PubMed Central PMCID: PMCPMC102018.
17. Hoffmann M, Wu YJ, Gerber M, Berger-Rentsch M, Heimrich B, Schwemmle M, et al. Fusion-active glycoprotein G mediates the cytotoxicity of vesicular stomatitis virus M mutants lacking host shut-off activity. The Journal of general virology. 2010;91(Pt 11):2782-93. Epub 2010/07/16. doi: 10.1099/vir.0.023978-0. PubMed PMID: 20631091.
18. Kopecky SA, Willingham MC, Lyles DS. Matrix protein and another viral component contribute to induction of apoptosis in cells infected with vesicular stomatitis virus. Journal of virology. 2001;75(24):12169-81. Epub 2001/11/17. doi: 10.1128/JVI.75.24.12169-12181.2001. PubMed PMID: 11711608; PubMed Central PMCID: PMCPMC116113.
19. Lyles DS. Cytopathogenesis and inhibition of host gene expression by RNA viruses. Microbiol Mol Biol Rev. 2000;64(4):709-24. Epub 2000/12/06. doi: 10.1128/MMBR.64.4.709-724.2000. PubMed PMID: 11104816; PubMed Central PMCID: PMCPMC99011.
20. Publicover J, Ramsburg E, Robek M, Rose JK. Rapid pathogenesis induced by a vesicular stomatitis virus matrix protein mutant: viral pathogenesis is linked to induction of tumor necrosis factor alpha. Journal of virology. 2006;80(14):7028-36. Epub 2006/07/01. doi: 10.1128/JVI.00478-06. PubMed PMID: 16809308; PubMed Central PMCID: PMCPMC1489072.
21. Roche S, Albertini AA, Lepault J, Bressanelli S, Gaudin Y. Structures of vesicular stomatitis virus glycoprotein: membrane fusion revisited. Cell Mol Life Sci. 2008;65(11):1716-28. Epub 2008/03/18. doi: 10.1007/s00018-008-7534-3. PubMed PMID: 18345480.
22. Steven AC, Spear PG. Biochemistry. Viral glycoproteins and an evolutionary conundrum. Science (New York, NY). 2006;313(5784):177-8. Epub 2006/07/15. doi: 10.1126/science.1129761. PubMed PMID: 16840685.
23. Backovic M, Jardetzky TS. Class III viral membrane fusion proteins. Curr Opin Struct Biol. 2009;19(2):189-96. Epub 2009/04/10. doi: 10.1016/j.sbi.2009.02.012. PubMed PMID: 19356922; PubMed Central PMCID: PMCPMC3076093.
24. Finkelshtein D, Werman A, Novick D, Barak S, Rubinstein M. LDL receptor and its family members serve as the cellular receptors for vesicular stomatitis virus. Proceedings of the National Academy of Sciences of the United States of America. 2013;110(18):7306-11. Epub 2013/04/17. doi: 10.1073/pnas.1214441110. PubMed PMID: 23589850; PubMed Central PMCID: PMCPMC3645523.
25. Mangeot PE, Dollet S, Girard M, Ciancia C, Joly S, Peschanski M, et al. Protein transfer into human cells by VSV-G-induced nanovesicles. Mol Ther. 2011;19(9):1656-66. Epub 2011/07/14. doi: 10.1038/mt.2011.138. PubMed PMID: 21750535; PubMed Central PMCID: PMCPMC3182355.
26. Zuris JA, Thompson DB, Shu Y, Guilinger JP, Bessen JL, Hu JH, et al. Cationic lipid-mediated delivery of proteins enables efficient protein-based genome editing in vitro and in vivo. Nat Biotechnol. 2015;33(1):73-80. Epub 2014/10/31. doi: 10.1038/nbt.3081. PubMed PMID: 25357182; PubMed Central PMCID: PMCPMC4289409.
27. Mire CE, Whitt MA. The protease-sensitive loop of the vesicular stomatitis virus matrix protein is involved in virus assembly and protein translation. Virology. 2011;416(1-2):16-25. Epub 2011/05/21. doi: 10.1016/j.virol.2011.04.013. PubMed PMID: 21596416.
28. Connor JH, Lyles DS. Vesicular stomatitis virus infection alters the eIF4F translation initiation complex and causes dephosphorylation of the eIF4E binding protein 4E-BP1. Journal of virology. 2002;76(20):10177-87. Epub 2002/09/20. doi: 10.1128/jvi.76.20.10177-10187.2002. PubMed PMID: 12239292; PubMed Central PMCID: PMCPMC136556.
29. Whitlow ZW, Connor JH, Lyles DS. Preferential translation of vesicular stomatitis virus mRNAs is conferred by transcription from the viral genome. Journal of virology. 2006;80(23):11733-42. Epub 2006/09/29. doi: 10.1128/JVI.00971-06. PubMed PMID: 17005665; PubMed Central PMCID: PMCPMC1642595.

30. Whitlow ZW, Connor JH, Lyles DS. New mRNAs are preferentially translated during vesicular stomatitis virus infection. Journal of virology. 2008;82(5):2286-94. Epub 2007/12/21. doi: 10.1128/JVI.01761-07. PubMed PMID: 18094194; PubMed Central PMCID: PMCPMC2258916.
31. Morin B, Rahmeh AA, Whelan SP. Mechanism of RNA synthesis initiation by the vesicular stomatitis virus polymerase. EMBO J. 2012;31(5):1320-9. Epub 2012/01/17. doi: 10.1038/emboj.2011.483. PubMed PMID: 22246179; PubMed Central PMCID: PMCPMC3297992.
32. Swinteck BD, Lyles DS. Plasma membrane microdomains containing vesicular stomatitis virus M protein are separate from microdomains containing G protein and nucleocapsids. Journal of virology. 2008;82(11):5536-47. Epub 2008/03/28. doi: 10.1128/JVI.02407-07. PubMed PMID: 18367537; PubMed Central PMCID: PMCPMC2395217.
33. Ge P, Tsao J, Schein S, Green TJ, Luo M, Zhou ZH. Cryo-EM model of the bullet-shaped vesicular stomatitis virus. Science (New York, NY). 2010;327(5966):689-93. Epub 2010/02/06. doi: 10.1126/science.1181766. PubMed PMID: 20133572; PubMed Central PMCID: PMCPMC2892700.
34. Riedel C, Hennrich AA, Conzelmann KK. Components and Architecture of the Rhabdovirus Ribonucleoprotein Complex. Viruses. 2020;12(9):959. Epub 2020/09/03. doi: 10.3390/v12090959. PubMed PMID: 32872471; PubMed Central PMCID: PMCPMC7552012.
35. Cureton DK, Massol RH, Saffarian S, Kirchhausen TL, Whelan SP. Vesicular stomatitis virus enters cells through vesicles incompletely coated with clathrin that depend upon actin for internalization. PLoS Pathog. 2009;5(4):e1000394. Epub 2009/04/25. doi: 10.1371/journal.ppat.1000394. PubMed PMID: 19390604; PubMed Central PMCID: PMCPMC2667253.
36. Johannsdottir HK, Mancini R, Kartenbeck J, Amato L, Helenius A. Host cell factors and functions involved in vesicular stomatitis virus entry. Journal of virology. 2009;83(1):440-53. Epub 2008/10/31. doi: 10.1128/JVI.01864-08. PubMed PMID: 18971266; PubMed Central PMCID: PMCPMC2612308.
37. Mire CE, White JM, Whitt MA. A spatio-temporal analysis of matrix protein and nucleocapsid trafficking during vesicular stomatitis virus uncoating. PLoS Pathog. 2010;6(7):e1000994. Epub 2010/07/27. doi: 10.1371/journal.ppat.1000994. PubMed PMID: 20657818; PubMed Central PMCID: PMCPMC2904772.
38. Heinrich BS, Maliga Z, Stein DA, Hyman AA, Whelan SPJ. Phase Transitions Drive the Formation of Vesicular Stomatitis Virus Replication Compartments. mBio. 2018;9(5):e02290-17. Epub 2018/09/06. doi: 10.1128/mBio.02290-17. PubMed PMID: 30181255; PubMed Central PMCID: PMCPMC6123442.
39. Knipe DM, Baltimore D, Lodish HF. Separate pathways of maturation of the major structural proteins of vesicular stomatitis virus. Journal of virology. 1977;21(3):1128-39. Epub 1977/03/01. doi: 10.1128/JVI.21.3.1128-1139.1977. PubMed PMID: 191640; PubMed Central PMCID: PMCPMC515654.
40. Newcomb WW, Brown JC. Role of the vesicular stomatitis virus matrix protein in maintaining the viral nucleocapsid in the condensed form found in native virions. Journal of virology. 1981;39(1):295-9. Epub 1981/07/01. doi: 10.1128/JVI.39.1.295-299.1981. PubMed PMID: 6268817; PubMed Central PMCID: PMCPMC171289.
41. Zhu Y, Yongky A, Yin J. Growth of an RNA virus in single cells reveals a broad fitness distribution. Virology. 2009;385(1):39-46. Epub 2008/12/17. doi: 10.1016/j.virol.2008.10.031. PubMed PMID: 19070881; PubMed Central PMCID: PMCPMC2666790.
42. Timm A, Yin J. Kinetics of virus production from single cells. Virology. 2012;424(1):11-7. Epub 2012/01/10. doi: 10.1016/j.virol.2011.12.005. PubMed PMID: 22222212; PubMed Central PMCID: PMCPMC3268887.
43. Mebatsion T, Konig M, Conzelmann KK. Budding of rabies virus particles in the absence of the spike glycoprotein. Cell. 1996;84(6):941-51. Epub 1996/03/22. doi: 10.1016/s0092-8674(00)81072-7. PubMed PMID: 8601317.

44. Conzelmann K-K. ACTIVATION AND EVASION OF INNATE IMMUNE RESPONSE BY RHABDOVIRUSES. Biology and Pathogenesis of Rhabdo- and Filoviruses: WORLD SCIENTIFIC; 2014. p. 353-85.
45. Rieder M, Conzelmann KK. Rhabdovirus evasion of the interferon system. J Interferon Cytokine Res. 2009;29(9):499-509. Epub 2009/09/01. doi: 10.1089/jir.2009.0068. PubMed PMID: 19715459.
46. Faul EJ, Lyles DS, Schnell MJ. Interferon response and viral evasion by members of the family rhabdoviridae. Viruses. 2009;1(3):832-51. Epub 2009/12/01. doi: 10.3390/v1030832. PubMed PMID: 21994572; PubMed Central PMCID: PMCPMC3185512.
47. Garijo R, Cuevas JM, Briz A, Sanjuan R. Constrained evolvability of interferon suppression in an RNA virus. Scientific reports. 2016;6(1):24722. Epub 2016/04/22. doi: 10.1038/srep24722. PubMed PMID: 27098004; PubMed Central PMCID: PMCPMC4838867.
48. Mebatsion T, Weiland F, Conzelmann KK. Matrix protein of rabies virus is responsible for the assembly and budding of bullet-shaped particles and interacts with the transmembrane spike glycoprotein G. Journal of virology. 1999;73(1):242-50. Epub 1998/12/16. doi: 10.1128/JVI.73.1.242-250.1999. PubMed PMID: 9847327; PubMed Central PMCID: PMCPMC103828.
49. Stojdl DF, Lichty BD, tenOever BR, Paterson JM, Power AT, Knowles S, et al. VSV strains with defects in their ability to shutdown innate immunity are potent systemic anti-cancer agents. Cancer Cell. 2003;4(4):263-75. doi: Doi 10.1016/S1535-6108(03)00241-1. PubMed PMID: WOS:000186154200007.
50. Mebatsion T, Schnell MJ, Cox JH, Finke S, Conzelmann KK. Highly stable expression of a foreign gene from rabies virus vectors. Proceedings of the National Academy of Sciences of the United States of America. 1996;93(14):7310-4. Epub 1996/07/09. doi: 10.1073/pnas.93.14.7310. PubMed PMID: 8692989; PubMed Central PMCID: PMCPMC38980.
51. Wertz GW, Moudy R, Ball LA. Adding genes to the RNA genome of vesicular stomatitis virus: positional effects on stability of expression. Journal of virology. 2002;76(15):7642-50. Epub 2002/07/05. doi: 10.1128/jvi.76.15.7642-7650.2002. PubMed PMID: 12097578; PubMed Central PMCID: PMCPMC136382.
52. Lawson ND, Stillman EA, Whitt MA, Rose JK. Recombinant vesicular stomatitis viruses from DNA. Proceedings of the National Academy of Sciences of the United States of America. 1995;92(10):4477-81. Epub 1995/05/09. doi: 10.1073/pnas.92.10.4477. PubMed PMID: 7753828; PubMed Central PMCID: PMCPMC41967.
53. Whelan SP, Ball LA, Barr JN, Wertz GT. Efficient recovery of infectious vesicular stomatitis virus entirely from cDNA clones. Proceedings of the National Academy of Sciences of the United States of America. 1995;92(18):8388-92. Epub 1995/08/29. doi: 10.1073/pnas.92.18.8388. PubMed PMID: 7667300; PubMed Central PMCID: PMCPMC41162.
54. Schnell MJ, Buonocore L, Kretzschmar E, Johnson E, Rose JK. Foreign glycoproteins expressed from recombinant vesicular stomatitis viruses are incorporated efficiently into virus particles. Proceedings of the National Academy of Sciences of the United States of America. 1996;93(21):11359-65. Epub 1996/10/15. doi: 10.1073/pnas.93.21.11359. PubMed PMID: 8876140; PubMed Central PMCID: PMCPMC38062.
55. Liang B, Li Z, Jenni S, Rahmeh AA, Morin BM, Grant T, et al. Structure of the L Protein of Vesicular Stomatitis Virus from Electron Cryomicroscopy. Cell. 2015;162(2):314-27. Epub 2015/07/07. doi: 10.1016/j.cell.2015.06.018. PubMed PMID: 26144317; PubMed Central PMCID: PMCPMC4557768.
56. Rubin H. Genetic Control of Cellular Susceptibility to Pseudotypes of Rous Sarcoma Virus. Virology. 1965;26:270-6. Epub 1965/06/01. doi: 10.1016/0042-6822(65)90274-6. PubMed PMID: 14323995.
57. Takada A, Robison C, Goto H, Sanchez A, Murti KG, Whitt MA, et al. A system for functional analysis of Ebola virus glycoprotein. Proceedings of the National Academy of Sciences of the United States of America. 1997;94(26):14764-9. Epub 1998/02/07. doi: 10.1073/pnas.94.26.14764. PubMed PMID: 9405687; PubMed Central PMCID: PMCPMC25111.

58. Jae LT, Raaben M, Riemersma M, van Beusekom E, Blomen VA, Velds A, et al. Deciphering the glycosylome of dystroglycanopathies using haploid screens for lassa virus entry. Science (New York, NY). 2013;340(6131):479-83. Epub 2013/03/23. doi: 10.1126/science.1233675. PubMed PMID: 23519211; PubMed Central PMCID: PMCPMC3919138.
59. Jae LT, Raaben M, Herbert AS, Kuehne AI, Wirchnianski AS, Soh TK, et al. Virus entry. Lassa virus entry requires a trigger-induced receptor switch. Science (New York, NY). 2014;344(6191):1506-10. Epub 2014/06/28. doi: 10.1126/science.1252480. PubMed PMID: 24970085; PubMed Central PMCID: PMCPMC4239993.
60. Raaben M, Jae LT, Herbert AS, Kuehne AI, Stubbs SH, Chou YY, et al. NRP2 and CD63 Are Host Factors for Lujo Virus Cell Entry. Cell host & microbe. 2017;22(5):688-96 e5. Epub 2017/11/10. doi: 10.1016/j.chom.2017.10.002. PubMed PMID: 29120745; PubMed Central PMCID: PMCPMC5821226.
61. Kleinfelter LM, Jangra RK, Jae LT, Herbert AS, Mittler E, Stiles KM, et al. Haploid Genetic Screen Reveals a Profound and Direct Dependence on Cholesterol for Hantavirus Membrane Fusion. mBio. 2015;6(4):e00801. Epub 2015/07/02. doi: 10.1128/mBio.00801-15. PubMed PMID: 26126854; PubMed Central PMCID: PMCPMC4488941.
62. Zemp F, Rajwani J, Mahoney DJ. Rhabdoviruses as vaccine platforms for infectious disease and cancer. Biotechnology & genetic engineering reviews. 2018;34(1):122-38. Epub 2018/05/22. doi: 10.1080/02648725.2018.1474320. PubMed PMID: 29781359.
63. Maloy KJ, Burkhart C, Junt TM, Odermatt B, Oxenius A, Piali L, et al. CD4(+) T cell subsets during virus infection. Protective capacity depends on effector cytokine secretion and on migratory capability. The Journal of experimental medicine. 2000;191(12):2159-70. Epub 2000/06/22. doi: 10.1084/jem.191.12.2159. PubMed PMID: 10859340; PubMed Central PMCID: PMCPMC2193195.
64. Rose NF, Marx PA, Luckay A, Nixon DF, Moretto WJ, Donahoe SM, et al. An effective AIDS vaccine based on live attenuated vesicular stomatitis virus recombinants. Cell. 2001;106(5):539-49. Epub 2001/09/12. doi: 10.1016/s0092-8674(01)00482-2. PubMed PMID: 11551502.
65. Rose NF, Roberts A, Buonocore L, Rose JK. Glycoprotein exchange vectors based on vesicular stomatitis virus allow effective boosting and generation of neutralizing antibodies to a primary isolate of human immunodeficiency virus type 1. Journal of virology. 2000;74(23):10903-10. Epub 2000/11/09. doi: 10.1128/jvi.74.23.10903-10910.2000. PubMed PMID: 11069984; PubMed Central PMCID: PMCPMC113169.
66. Clarke DK, Hendry RM, Singh V, Rose JK, Seligman SJ, Klug B, et al. Live virus vaccines based on a vesicular stomatitis virus (VSV) backbone: Standardized template with key considerations for a risk/benefit assessment. Vaccine. 2016;34(51):6597-609. Epub 2016/07/11. doi: 10.1016/j.vaccine.2016.06.071. PubMed PMID: 27395563; PubMed Central PMCID: PMCPMC5220644.
67. Geisbert TW, Feldmann H. Recombinant vesicular stomatitis virus-based vaccines against Ebola and Marburg virus infections. J Infect Dis. 2011;204 Suppl 3(Suppl 3):S1075-81. Epub 2011/10/19. doi: 10.1093/infdis/jir349. PubMed PMID: 21987744; PubMed Central PMCID: PMCPMC3218670.
68. Fathi A, Dahlke C, Addo MM. Recombinant vesicular stomatitis virus vector vaccines for WHO blueprint priority pathogens. Hum Vaccin Immunother. 2019;15(10):2269-85. Epub 2019/08/02. doi: 10.1080/21645515.2019.1649532. PubMed PMID: 31368826; PubMed Central PMCID: PMCPMC6816421.
69. Jones SM, Feldmann H, Stroher U, Geisbert JB, Fernando L, Grolla A, et al. Live attenuated recombinant vaccine protects nonhuman primates against Ebola and Marburg viruses. Nat Med. 2005;11(7):786-90. Epub 2005/06/07. doi: 10.1038/nm1258. PubMed PMID: 15937495.
70. Geisbert TW, Jones S, Fritz EA, Shurtleff AC, Geisbert JB, Liebscher R, et al. Development of a new vaccine for the prevention of Lassa fever. PLoS Med. 2005;2(6):e183. Epub 2005/06/24. doi: 10.1371/journal.pmed.0020183. PubMed PMID: 15971954; PubMed Central PMCID: PMCPMC1160587.
71. Rodriguez SE, Cross RW, Fenton KA, Bente DA, Mire CE, Geisbert TW. Vesicular Stomatitis Virus-Based Vaccine Protects Mice against Crimean-Congo Hemorrhagic Fever. Scientific reports.

2019;9(1):7755. Epub 2019/05/28. doi: 10.1038/s41598-019-44210-6. PubMed PMID: 31123310; PubMed Central PMCID: PMCPMC6533279.
72. Lo MK, Bird BH, Chattopadhyay A, Drew CP, Martin BE, Coleman JD, et al. Single-dose replication-defective VSV-based Nipah virus vaccines provide protection from lethal challenge in Syrian hamsters. Antiviral Res. 2014;101:26-9. Epub 2013/11/05. doi: 10.1016/j.antiviral.2013.10.012. PubMed PMID: 24184127; PubMed Central PMCID: PMCPMC3874889.
73. Emanuel J, Callison J, Dowd KA, Pierson TC, Feldmann H, Marzi A. A VSV-based Zika virus vaccine protects mice from lethal challenge. Scientific reports. 2018;8(1):11043. Epub 2018/07/25. doi: 10.1038/s41598-018-29401-x. PubMed PMID: 30038228; PubMed Central PMCID: PMCPMC6056530.
74. Kapadia SU, Rose JK, Lamirande E, Vogel L, Subbarao K, Roberts A. Long-term protection from SARS coronavirus infection conferred by a single immunization with an attenuated VSV-based vaccine. Virology. 2005;340(2):174-82. Epub 2005/07/27. doi: 10.1016/j.virol.2005.06.016. PubMed PMID: 16043204; PubMed Central PMCID: PMCPMC7111745.
75. Liu R, Wang J, Shao Y, Wang X, Zhang H, Shuai L, et al. A recombinant VSV-vectored MERS-CoV vaccine induces neutralizing antibody and T cell responses in rhesus monkeys after single dose immunization. Antiviral Res. 2018;150:30-8. Epub 2017/12/17. doi: 10.1016/j.antiviral.2017.12.007. PubMed PMID: 29246504; PubMed Central PMCID: PMCPMC7113862.
76. Yahalom-Ronen Y, Tamir H, Melamed S, Politi B, Shifman O, Achdout H, et al. A single dose of recombinant VSV-G-spike vaccine provides protection against SARS-CoV-2 challenge. Nat Commun. 2020;11(1):6402. Epub 2020/12/18. doi: 10.1038/s41467-020-20228-7. PubMed PMID: 33328475; PubMed Central PMCID: PMCPMC7745033.
77. Furuyama W, Shifflett K, Pinski AN, Griffin AJ, Feldmann F, Okumura A, et al. Rapid protection from COVID-19 in nonhuman primates vaccinated intramuscularly but not intranasally with a single dose of a recombinant vaccine. bioRxiv. 2021. Epub 2021/01/28. doi: 10.1101/2021.01.19.426885. PubMed PMID: 33501447; PubMed Central PMCID: PMCPMC7836117.
78. Furuyama W, Reynolds P, Haddock E, Meade-White K, Quynh Le M, Kawaoka Y, et al. A single dose of a vesicular stomatitis virus-based influenza vaccine confers rapid protection against H5 viruses from different clades. NPJ Vaccines. 2020;5(1):4. Epub 2020/01/15. doi: 10.1038/s41541-019-0155-z. PubMed PMID: 31934358; PubMed Central PMCID: PMCPMC6954110.
79. Plummer FA, Jones SM. The story of Canada's Ebola vaccine. CMAJ. 2017;189(43):E1326-E7. Epub 2017/11/01. doi: 10.1503/cmaj.170704. PubMed PMID: 29084758; PubMed Central PMCID: PMCPMC5662448
80. Geisbert TW, Daddario-Dicaprio KM, Lewis MG, Geisbert JB, Grolla A, Leung A, et al. Vesicular stomatitis virus-based ebola vaccine is well-tolerated and protects immunocompromised nonhuman primates. PLoS Pathog. 2008;4(11):e1000225. Epub 2008/12/02. doi: 10.1371/journal.ppat.1000225. PubMed PMID: 19043556; PubMed Central PMCID: PMCPMC2582959.
81. Kennedy SB, Bolay F, Kieh M, Grandits G, Badio M, Ballou R, et al. Phase 2 Placebo-Controlled Trial of Two Vaccines to Prevent Ebola in Liberia. The New England journal of medicine. 2017;377(15):1438-47. Epub 2017/10/12. doi: 10.1056/NEJMoa1614067. PubMed PMID: 29020589; PubMed Central PMCID: PMCPMC5705229.
82. Stokke JL, Szymanski LJ, Bankamp B, Pratt F, Martines R, Dien-Bard J, et al. MMR Vaccine-Associated Disseminated Measles in an Immunocompromised Adolescent. The New England journal of medicine. 2021;385(13):1246-8. Epub 2021/09/23. doi: 10.1056/NEJMc2103772. PubMed PMID: 34551236.
83. Brunner K, Harder J, Halbach T, Willibald J, Spada F, Gnerlich F, et al. Cell-penetrating and neurotargeting dendritic siRNA nanostructures. Angewandte Chemie (International ed in English). 2015;54(6):1946-9. Epub 2014/12/19. doi: 10.1002/anie.201409803. PubMed PMID: 25522332.
84. Liang HR, Hu GQ, Li L, Gao YW, Yang ST, Xia XZ. Aptamers targeting rabies virus-infected cells inhibit street rabies virus in vivo. International immunopharmacology. 2014;21(2):432-8. Epub 2014/04/17. doi: 10.1016/j.intimp.2014.03.020. PubMed PMID: 24735817.

85. Yang YJ, Zhao PS, Zhang T, Wang HL, Liang HR, Zhao LL, et al. Small interfering RNAs targeting the rabies virus nucleoprotein gene. Virus Res. 2012;169(1):169-74. Epub 2012/08/14. doi: 10.1016/j.virusres.2012.07.024. PubMed PMID: 22884777.
86. Chung HK, Jacobs CL, Huo Y, Yang J, Krumm SA, Plemper RK, et al. Tunable and reversible drug control of protein production via a self-excising degron. Nat Chem Biol. 2015;11(9):713-20. Epub 2015/07/28. doi: 10.1038/nchembio.1869. PubMed PMID: 26214256; PubMed Central PMCID: PMCPMC4543534.
87. Fay EJ, Aron SL, Stone IA, Waring BM, Plemper RK, Langlois RA. Engineered Small-Molecule Control of Influenza A Virus Replication. J Virol. 2019;93(1). Epub 2018/10/05. doi: 10.1128/jvi.01677-18. PubMed PMID: 30282710; PubMed Central PMCID: PMCPMC6288343.
88. Heilmann E, Kimpel J, Hofer B, Rossler A, Blaas I, Egerer L, et al. Chemogenetic ON and OFF switches for RNA virus replication. Nat Commun. 2021;12(1):1362. Epub 2021/03/03. doi: 10.1038/s41467-021-21630-5. PubMed PMID: 33649317; PubMed Central PMCID: PMCPMC7921684.
89. Roth S, Fulcher LJ, Sapkota GP. Advances in targeted degradation of endogenous proteins. Cellular and molecular life sciences : CMLS. 2019;76(14):2761-77. Epub 2019/04/29. doi: 10.1007/s00018-019-03112-6. PubMed PMID: 31030225; PubMed Central PMCID: PMCPMC6588652.
90. Schapira M, Calabrese MF, Bullock AN, Crews CM. Targeted protein degradation: expanding the toolbox. Nature reviews Drug discovery. 2019;18(12):949-63. Epub 2019/11/02. doi: 10.1038/s41573-019-0047-y. PubMed PMID: 31666732.
91. Wu F, Zhao S, Yu B, Chen YM, Wang W, Song ZG, et al. A new coronavirus associated with human respiratory disease in China. Nature. 2020;579(7798):265-9. Epub 2020/02/06. doi: 10.1038/s41586-020-2008-3. PubMed PMID: 32015508; PubMed Central PMCID: PMCPMC7094943.
92. Zhou P, Yang XL, Wang XG, Hu B, Zhang L, Zhang W, et al. A pneumonia outbreak associated with a new coronavirus of probable bat origin. Nature. 2020;579(7798):270-3. Epub 2020/02/06. doi: 10.1038/s41586-020-2012-7. PubMed PMID: 32015507; PubMed Central PMCID: PMCPMC7095418.
93. Zhu N, Zhang D, Wang W, Li X, Yang B, Song J, et al. A Novel Coronavirus from Patients with Pneumonia in China, 2019. The New England journal of medicine. 2020;382(8):727-33. Epub 2020/01/25. doi: 10.1056/NEJMoa2001017. PubMed PMID: 31978945; PubMed Central PMCID: PMCPMC7092803.
94. Ksiazek TG, Erdman D, Goldsmith CS, Zaki SR, Peret T, Emery S, et al. A novel coronavirus associated with severe acute respiratory syndrome. The New England journal of medicine. 2003;348(20):1953-66. Epub 2003/04/12. doi: 10.1056/NEJMoa030781. PubMed PMID: 12690092.
95. Drosten C, Gunther S, Preiser W, van der Werf S, Brodt HR, Becker S, et al. Identification of a novel coronavirus in patients with severe acute respiratory syndrome. The New England journal of medicine. 2003;348(20):1967-76. Epub 2003/04/12. doi: 10.1056/NEJMoa030747. PubMed PMID: 12690091.
96. Lu R, Zhao X, Li J, Niu P, Yang B, Wu H, et al. Genomic characterisation and epidemiology of 2019 novel coronavirus: implications for virus origins and receptor binding. Lancet. 2020;395(10224):565-74. Epub 2020/02/03. doi: 10.1016/S0140-6736(20)30251-8. PubMed PMID: 32007145; PubMed Central PMCID: PMCPMC7159086.
97. Shrock E, Fujimura E, Kula T, Timms RT, Lee IH, Leng Y, et al. Viral epitope profiling of COVID-19 patients reveals cross-reactivity and correlates of severity. Science (New York, NY). 2020;370(6520):eabd4250. Epub 2020/10/01. doi: 10.1126/science.abd4250. PubMed PMID: 32994364; PubMed Central PMCID: PMCPMC7857405.
98. Bloom JD, Chan YA, Baric RS, Bjorkman PJ, Cobey S, Deverman BE, et al. Investigate the origins of COVID-19. Science (New York, NY). 2021;372(6543):694. Epub 2021/05/15. doi: 10.1126/science.abj0016. PubMed PMID: 33986172.
99. Burki T. The origin of SARS-CoV-2. Lancet Infect Dis. 2020;20(9):1018-9. Epub 2020/08/30. doi: 10.1016/S1473-3099(20)30641-1. PubMed PMID: 32860762; PubMed Central PMCID: PMCPMC7449661.

100. Rasmussen AL. On the origins of SARS-CoV-2. Nat Med. 2021;27(1):9. Epub 2021/01/15. doi: 10.1038/s41591-020-01205-5. PubMed PMID: 33442004.
101. Nie JB. In the Shadow of Biological Warfare: Conspiracy Theories on the Origins of COVID-19 and Enhancing Global Governance of Biosafety as a Matter of Urgency. J Bioeth Inq. 2020;17(4):567-74. Epub 2020/08/26. doi: 10.1007/s11673-020-10025-8. PubMed PMID: 32840850; PubMed Central PMCID: PMCPMC7445685.
102. Chan JF, Yuan S, Kok KH, To KK, Chu H, Yang J, et al. A familial cluster of pneumonia associated with the 2019 novel coronavirus indicating person-to-person transmission: a study of a family cluster. Lancet. 2020;395(10223):514-23. Epub 2020/01/28. doi: 10.1016/S0140-6736(20)30154-9. PubMed PMID: 31986261; PubMed Central PMCID: PMCPMC7159286.
103. Huang C, Wang Y, Li X, Ren L, Zhao J, Hu Y, et al. Clinical features of patients infected with 2019 novel coronavirus in Wuhan, China. Lancet. 2020;395(10223):497-506. Epub 2020/01/28. doi: 10.1016/S0140-6736(20)30183-5. PubMed PMID: 31986264; PubMed Central PMCID: PMCPMC7159299.
104. Rothe C, Schunk M, Sothmann P, Bretzel G, Froeschl G, Wallrauch C, et al. Transmission of 2019-nCoV Infection from an Asymptomatic Contact in Germany. The New England journal of medicine. 2020;382(10):970-1. Epub 2020/02/01. doi: 10.1056/NEJMc2001468. PubMed PMID: 32003551; PubMed Central PMCID: PMCPMC7120970.
105. Li W, Moore MJ, Vasilieva N, Sui J, Wong SK, Berne MA, et al. Angiotensin-converting enzyme 2 is a functional receptor for the SARS coronavirus. Nature. 2003;426(6965):450-4. Epub 2003/12/04. doi: 10.1038/nature02145. PubMed PMID: 14647384; PubMed Central PMCID: PMCPMC7095016.
106. Shang J, Ye G, Shi K, Wan Y, Luo C, Aihara H, et al. Structural basis of receptor recognition by SARS-CoV-2. Nature. 2020;581(7807):221-4. doi: 10.1038/s41586-020-2179-y.
107. Buchholz UJ, Bukreyev A, Yang L, Lamirande EW, Murphy BR, Subbarao K, et al. Contributions of the structural proteins of severe acute respiratory syndrome coronavirus to protective immunity. Proceedings of the National Academy of Sciences of the United States of America. 2004;101(26):9804-9. Epub 2004/06/24. doi: 10.1073/pnas.0403492101. PubMed PMID: 15210961; PubMed Central PMCID: PMCPMC470755.
108. Draft landscape of COVID-19 candidate vaccines 26 March 2021 [Internet]. 2021. Available from: https://www.who.int/publications/m/item/draft-landscape-of-covid-19-candidate-vaccines.
109. McMahan K, Yu J, Mercado NB, Loos C, Tostanoski LH, Chandrashekar A, et al. Correlates of protection against SARS-CoV-2 in rhesus macaques. Nature. 2021;590(7847):630-4. Epub 2020/12/05. doi: 10.1038/s41586-020-03041-6. PubMed PMID: 33276369; PubMed Central PMCID: PMCPMC7906955.
110. Wang Z, Schmidt F, Weisblum Y, Muecksch F, Barnes CO, Finkin S, et al. mRNA vaccine-elicited antibodies to SARS-CoV-2 and circulating variants. Nature. 2021;592(7855):616-22. Epub 2021/02/11. doi: 10.1038/s41586-021-03324-6. PubMed PMID: 33567448; PubMed Central PMCID: PMCPMC8503938.
111. Suthar MS, Zimmerman MG, Kauffman RC, Mantus G, Linderman SL, Hudson WH, et al. Rapid Generation of Neutralizing Antibody Responses in COVID-19 Patients. Cell reports Medicine. 2020;1(3):100040. Epub 2020/08/25. doi: 10.1016/j.xcrm.2020.100040. PubMed PMID: 32835303; PubMed Central PMCID: PMCPMC7276302.
112. Atyeo C, Slein MD, Fischinger S, Burke J, Schafer A, Leist SR, et al. Dissecting strategies to tune the therapeutic potential of SARS-CoV-2-specific monoclonal antibody CR3022. JCI insight. 2021;6(1). Epub 2021/01/12. doi: 10.1172/jci.insight.143129. PubMed PMID: 33427208; PubMed Central PMCID: PMCPMC7821590.
113. Zost SJ, Gilchuk P, Case JB, Binshtein E, Chen RE, Nkolola JP, et al. Potently neutralizing and protective human antibodies against SARS-CoV-2. Nature. 2020;584(7821):443-9. Epub 2020/07/16. doi: 10.1038/s41586-020-2548-6. PubMed PMID: 32668443; PubMed Central PMCID: PMCPMC7584396.

114. Krammer F. Correlates of protection from SARS-CoV-2 infection. Lancet. 2021;397(10283):1421-3. Epub 2021/04/13. doi: 10.1016/S0140-6736(21)00782-0. PubMed PMID: 33844964; PubMed Central PMCID: PMCPMC8040540.
115. Wrapp D, Wang N, Corbett KS, Goldsmith JA, Hsieh CL, Abiona O, et al. Cryo-EM structure of the 2019-nCoV spike in the prefusion conformation. Science (New York, NY). 2020;367(6483):1260-3. Epub 2020/02/23. doi: 10.1126/science.abb2507. PubMed PMID: 32075877; PubMed Central PMCID: PMCPMC7164637.
116. Ju B, Zhang Q, Ge J, Wang R, Sun J, Ge X, et al. Human neutralizing antibodies elicited by SARS-CoV-2 infection. Nature. 2020;584(7819):115-9. Epub 2020/05/27. doi: 10.1038/s41586-020-2380-z. PubMed PMID: 32454513.
117. Jiang S, Hillyer C, Du L. Neutralizing Antibodies against SARS-CoV-2 and Other Human Coronaviruses. Trends Immunol. 2020;41(5):355-9. Epub 2020/04/07. doi: 10.1016/j.it.2020.03.007. PubMed PMID: 32249063; PubMed Central PMCID: PMCPMC7129017.
118. Bestle D, Heindl MR, Limburg H, Van Lam van T, Pilgram O, Moulton H, et al. TMPRSS2 and furin are both essential for proteolytic activation of SARS-CoV-2 in human airway cells. Life science alliance. 2020;3(9). Epub 2020/07/25. doi: 10.26508/lsa.202000786. PubMed PMID: 32703818; PubMed Central PMCID: PMCPMC7383062.
119. Hoffmann M, Kleine-Weber H, Schroeder S, Kruger N, Herrler T, Erichsen S, et al. SARS-CoV-2 Cell Entry Depends on ACE2 and TMPRSS2 and Is Blocked by a Clinically Proven Protease Inhibitor. Cell. 2020;181(2):271-80 e8. Epub 2020/03/07. doi: 10.1016/j.cell.2020.02.052. PubMed PMID: 32142651; PubMed Central PMCID: PMCPMC7102627.
120. Hoffmann M, Kleine-Weber H, Pohlmann S. A Multibasic Cleavage Site in the Spike Protein of SARS-CoV-2 Is Essential for Infection of Human Lung Cells. Molecular cell. 2020;78(4):779-84 e5. Epub 2020/05/05. doi: 10.1016/j.molcel.2020.04.022. PubMed PMID: 32362314; PubMed Central PMCID: PMCPMC7194065.
121. Walls AC, Park YJ, Tortorici MA, Wall A, McGuire AT, Veesler D. Structure, Function, and Antigenicity of the SARS-CoV-2 Spike Glycoprotein. Cell. 2020;181(2):281-92 e6. Epub 2020/03/11. doi: 10.1016/j.cell.2020.02.058. PubMed PMID: 32155444; PubMed Central PMCID: PMCPMC7102599.
122. Lan J, Ge J, Yu J, Shan S, Zhou H, Fan S, et al. Structure of the SARS-CoV-2 spike receptor-binding domain bound to the ACE2 receptor. Nature. 2020;581(7807):215-20. Epub 2020/04/01. doi: 10.1038/s41586-020-2180-5. PubMed PMID: 32225176.
123. Cai Y, Zhang J, Xiao T, Peng H, Sterling SM, Walsh RM, Jr., et al. Distinct conformational states of SARS-CoV-2 spike protein. Science (New York, NY). 2020;369(6511):1586-92. Epub 2020/07/23. doi: 10.1126/science.abd4251. PubMed PMID: 32694201; PubMed Central PMCID: PMCPMC7464562.
124. Ke Z, Oton J, Qu K, Cortese M, Zila V, McKeane L, et al. Structures and distributions of SARS-CoV-2 spike proteins on intact virions. Nature. 2020;588(7838):498-502. Epub 2020/08/18. doi: 10.1038/s41586-020-2665-2. PubMed PMID: 32805734; PubMed Central PMCID: PMCPMC7116492.
125. Essalmani R, Jain J, Susan-Resiga D, Andréo U, Evagelidis A, Derbali RM, et al. Furin cleaves SARS-CoV-2 spike-glycoprotein at S1/S2 and S2' for viral fusion/entry: indirect role of TMPRSS2. bioRxiv. 2021:2020.12.18.423106. doi: 10.1101/2020.12.18.423106.
126. Bollavaram K, Leeman TH, Lee MW, Kulkarni A, Upshaw SG, Yang J, et al. Multiple sites on SARS-CoV-2 spike protein are susceptible to proteolysis by cathepsins B, K, L, S, and V. Protein Sci. 2021;30(6):1131-43. Epub 2021/04/01. doi: 10.1002/pro.4073. PubMed PMID: 33786919; PubMed Central PMCID: PMCPMC8138523.
127. Benton DJ, Wrobel AG, Xu P, Roustan C, Martin SR, Rosenthal PB, et al. Receptor binding and priming of the spike protein of SARS-CoV-2 for membrane fusion. Nature. 2020;588(7837):327-30. Epub 2020/09/18. doi: 10.1038/s41586-020-2772-0. PubMed PMID: 32942285; PubMed Central PMCID: PMCPMC7116727.
128. Tai W, He L, Zhang X, Pu J, Voronin D, Jiang S, et al. Characterization of the receptor-binding domain (RBD) of 2019 novel coronavirus: implication for development of RBD protein as a viral

attachment inhibitor and vaccine. Cellular & molecular immunology. 2020;17(6):613-20. Epub 2020/03/24. doi: 10.1038/s41423-020-0400-4. PubMed PMID: 32203189; PubMed Central PMCID: PMCPMC7091888.
129. Kim YI, Kim SG, Kim SM, Kim EH, Park SJ, Yu KM, et al. Infection and Rapid Transmission of SARS-CoV-2 in Ferrets. Cell host & microbe. 2020;27(5):704-9 e2. Epub 2020/04/08. doi: 10.1016/j.chom.2020.03.023. PubMed PMID: 32259477; PubMed Central PMCID: PMCPMC7144857.
130. Rockx B, Kuiken T, Herfst S, Bestebroer T, Lamers MM, Oude Munnink BB, et al. Comparative pathogenesis of COVID-19, MERS, and SARS in a nonhuman primate model. Science (New York, NY). 2020;368(6494):1012-5. Epub 2020/04/19. doi: 10.1126/science.abb7314. PubMed PMID: 32303590; PubMed Central PMCID: PMCPMC7164679.
131. Shi J, Wen Z, Zhong G, Yang H, Wang C, Huang B, et al. Susceptibility of ferrets, cats, dogs, and other domesticated animals to SARS-coronavirus 2. Science (New York, NY). 2020;368(6494):1016-20. Epub 2020/04/10. doi: 10.1126/science.abb7015. PubMed PMID: 32269068; PubMed Central PMCID: PMCPMC7164390.
132. Yan R, Zhang Y, Li Y, Xia L, Guo Y, Zhou Q. Structural basis for the recognition of SARS-CoV-2 by full-length human ACE2. Science (New York, NY). 2020;367(6485):1444-8. Epub 2020/03/07. doi: 10.1126/science.abb2762. PubMed PMID: 32132184; PubMed Central PMCID: PMCPMC7164635.
133. Du L, Zhao G, He Y, Guo Y, Zheng BJ, Jiang S, et al. Receptor-binding domain of SARS-CoV spike protein induces long-term protective immunity in an animal model. Vaccine. 2007;25(15):2832-8. Epub 2006/11/10. doi: 10.1016/j.vaccine.2006.10.031. PubMed PMID: 17092615; PubMed Central PMCID: PMCPMC7115660.
134. Kam YW, Kien F, Roberts A, Cheung YC, Lamirande EW, Vogel L, et al. Antibodies against trimeric S glycoprotein protect hamsters against SARS-CoV challenge despite their capacity to mediate FcgammaRII-dependent entry into B cells in vitro. Vaccine. 2007;25(4):729-40. Epub 2006/10/20. doi: 10.1016/j.vaccine.2006.08.011. PubMed PMID: 17049691; PubMed Central PMCID: PMCPMC7115629.
135. Adney DR, Wang L, van Doremalen N, Shi W, Zhang Y, Kong WP, et al. Efficacy of an Adjuvanted Middle East Respiratory Syndrome Coronavirus Spike Protein Vaccine in Dromedary Camels and Alpacas. Viruses. 2019;11(3). Epub 2019/03/06. doi: 10.3390/v11030212. PubMed PMID: 30832356; PubMed Central PMCID: PMCPMC6466352.
136. Li J, Ulitzky L, Silberstein E, Taylor DR, Viscidi R. Immunogenicity and protection efficacy of monomeric and trimeric recombinant SARS coronavirus spike protein subunit vaccine candidates. Viral Immunol. 2013;26(2):126-32. Epub 2013/04/12. doi: 10.1089/vim.2012.0076. PubMed PMID: 23573979; PubMed Central PMCID: PMCPMC3624630.
137. Tong P, Gautam A, Windsor I, Travers M, Chen Y, Garcia N, et al. Memory B cell repertoire for recognition of evolving SARS-CoV-2 spike. bioRxiv. 2021. Epub 2021/03/25. doi: 10.1101/2021.03.10.434840. PubMed PMID: 33758863; PubMed Central PMCID: PMCPMC7987022.
138. Ravichandran S, Coyle EM, Klenow L, Tang J, Grubbs G, Liu S, et al. Antibody signature induced by SARS-CoV-2 spike protein immunogens in rabbits. Sci Transl Med. 2020;12(550):eabc3539. Epub 2020/06/10. doi: 10.1126/scitranslmed.abc3539. PubMed PMID: 32513867; PubMed Central PMCID: PMCPMC7286538.
139. Hurlburt NK, Homad LJ, Sinha I, Jennewein MF, MacCamy AJ, Wan Y-H, et al. Structural definition of a pan-sarbecovirus neutralizing epitope on the spike S2 subunit. bioRxiv. 2021:2021.08.02.454829. doi: 10.1101/2021.08.02.454829.
140. Pinto D, Sauer MM, Czudnochowski N, Low JS, Tortorici MA, Housley MP, et al. Broad betacoronavirus neutralization by a stem helix-specific human antibody. Science (New York, NY). 2021;373(6559):1109-16. Epub 2021/08/05. doi: 10.1126/science.abj3321. PubMed PMID: 34344823.
141. Zhou P, Yuan M, Song G, Beutler N, Shaabani N, Huang D, et al. A protective broadly cross-reactive human antibody defines a conserved site of vulnerability on beta-coronavirus spikes. bioRxiv. 2021:2021.03.30.437769. Epub 2021/04/07. doi: 10.1101/2021.03.30.437769. PubMed PMID: 33821273; PubMed Central PMCID: PMCPMC8020973.

142. Barnes CO, Jette CA, Abernathy ME, Dam KA, Esswein SR, Gristick HB, et al. SARS-CoV-2 neutralizing antibody structures inform therapeutic strategies. Nature. 2020;588(7839):682-7. Epub 2020/10/13. doi: 10.1038/s41586-020-2852-1. PubMed PMID: 33045718; PubMed Central PMCID: PMCPMC8092461.
143. Yuan M, Huang D, Lee CD, Wu NC, Jackson AM, Zhu X, et al. Structural and functional ramifications of antigenic drift in recent SARS-CoV-2 variants. Science (New York, NY). 2021;373(6556):818-23. Epub 2021/05/22. doi: 10.1126/science.abh1139. PubMed PMID: 34016740; PubMed Central PMCID: PMCPMC8284396.
144. Greaney AJ, Starr TN, Barnes CO, Weisblum Y, Schmidt F, Caskey M, et al. Mapping mutations to the SARS-CoV-2 RBD that escape binding by different classes of antibodies. Nat Commun. 2021;12(1):4196. Epub 2021/07/09. doi: 10.1038/s41467-021-24435-8. PubMed PMID: 34234131; PubMed Central PMCID: PMCPMC8263750.
145. Yuan M, Liu H, Wu NC, Wilson IA. Recognition of the SARS-CoV-2 receptor binding domain by neutralizing antibodies. Biochem Biophys Res Commun. 2021;538:192-203. Epub 2020/10/19. doi: 10.1016/j.bbrc.2020.10.012. PubMed PMID: 33069360; PubMed Central PMCID: PMCPMC7547570.
146. Drake JW, Holland JJ. Mutation rates among RNA viruses. Proceedings of the National Academy of Sciences of the United States of America. 1999;96(24):13910-3. Epub 1999/11/26. doi: 10.1073/pnas.96.24.13910. PubMed PMID: 10570172; PubMed Central PMCID: PMCPMC24164.
147. Crotty S, Cameron CE, Andino R. RNA virus error catastrophe: direct molecular test by using ribavirin. Proceedings of the National Academy of Sciences of the United States of America. 2001;98(12):6895-900. Epub 2001/05/24. doi: 10.1073/pnas.111085598. PubMed PMID: 11371613; PubMed Central PMCID: PMCPMC34449.
148. Combe M, Sanjuan R. Variation in RNA virus mutation rates across host cells. PLoS Pathog. 2014;10(1):e1003855. Epub 2014/01/28. doi: 10.1371/journal.ppat.1003855. PubMed PMID: 24465205; PubMed Central PMCID: PMCPMC3900646.
149. Ogando NS, Ferron F, Decroly E, Canard B, Posthuma CC, Snijder EJ. The Curious Case of the Nidovirus Exoribonuclease: Its Role in RNA Synthesis and Replication Fidelity. Front Microbiol. 2019;10(1813):1813. Epub 2019/08/24. doi: 10.3389/fmicb.2019.01813. PubMed PMID: 31440227; PubMed Central PMCID: PMCPMC6693484.
150. Belshaw R, Pybus OG, Rambaut A. The evolution of genome compression and genomic novelty in RNA viruses. Genome Res. 2007;17(10):1496-504. Epub 2007/09/06. doi: 10.1101/gr.6305707. PubMed PMID: 17785537; PubMed Central PMCID: PMCPMC1987338.
151. Snijder EJ, Bredenbeek PJ, Dobbe JC, Thiel V, Ziebuhr J, Poon LL, et al. Unique and conserved features of genome and proteome of SARS-coronavirus, an early split-off from the coronavirus group 2 lineage. J Mol Biol. 2003;331(5):991-1004. Epub 2003/08/21. doi: 10.1016/s0022-2836(03)00865-9. PubMed PMID: 12927536; PubMed Central PMCID: PMCPMC7159028.
152. Minskaia E, Hertzig T, Gorbalenya AE, Campanacci V, Cambillau C, Canard B, et al. Discovery of an RNA virus 3'->5' exoribonuclease that is critically involved in coronavirus RNA synthesis. Proceedings of the National Academy of Sciences of the United States of America. 2006;103(13):5108-13. Epub 2006/03/22. doi: 10.1073/pnas.0508200103. PubMed PMID: 16549795; PubMed Central PMCID: PMCPMC1458802.
153. Cruz-Gonzalez A, Munoz-Velasco I, Cottom-Salas W, Becerra A, Campillo-Balderas JA, Hernandez-Morales R, et al. Structural analysis of viral ExoN domains reveals polyphyletic hijacking events. PLoS One. 2021;16(3):e0246981. Epub 2021/03/18. doi: 10.1371/journal.pone.0246981. PubMed PMID: 33730017; PubMed Central PMCID: PMCPMC7968707.
154. Eckerle LD, Becker MM, Halpin RA, Li K, Venter E, Lu X, et al. Infidelity of SARS-CoV Nsp14-exonuclease mutant virus replication is revealed by complete genome sequencing. PLoS Pathog. 2010;6(5):e1000896. Epub 2010/05/14. doi: 10.1371/journal.ppat.1000896. PubMed PMID: 20463816; PubMed Central PMCID: PMCPMC2865531.
155. Korber B, Fischer WM, Gnanakaran S, Yoon H, Theiler J, Abfalterer W, et al. Tracking Changes in SARS-CoV-2 Spike: Evidence that D614G Increases Infectivity of the COVID-19 Virus. Cell.

2020;182(4):812-27 e19. Epub 2020/07/23. doi: 10.1016/j.cell.2020.06.043. PubMed PMID: 32697968; PubMed Central PMCID: PMCPMC7332439.
156. Zhang J, Cai Y, Xiao T, Lu J, Peng H, Sterling SM, et al. Structural impact on SARS-CoV-2 spike protein by D614G substitution. Science (New York, NY). 2021;372(6541):525-30. Epub 2021/03/18. doi: 10.1126/science.abf2303. PubMed PMID: 33727252; PubMed Central PMCID: PMCPMC8139424.
157. Yurkovetskiy L, Wang X, Pascal KE, Tomkins-Tinch C, Nyalile TP, Wang Y, et al. Structural and Functional Analysis of the D614G SARS-CoV-2 Spike Protein Variant. Cell. 2020;183(3):739-51 e8. Epub 2020/09/30. doi: 10.1016/j.cell.2020.09.032. PubMed PMID: 32991842; PubMed Central PMCID: PMCPMC7492024.
158. Zhou B, Thao TTN, Hoffmann D, Taddeo A, Ebert N, Labroussaa F, et al. SARS-CoV-2 spike D614G change enhances replication and transmission. Nature. 2021;592(7852):122-7. Epub 2021/02/27. doi: 10.1038/s41586-021-03361-1. PubMed PMID: 33636719.
159. Weissman D, Alameh MG, de Silva T, Collini P, Hornsby H, Brown R, et al. D614G Spike Mutation Increases SARS CoV-2 Susceptibility to Neutralization. Cell host & microbe. 2021;29(1):23-31 e4. Epub 2020/12/12. doi: 10.1016/j.chom.2020.11.012. PubMed PMID: 33306985; PubMed Central PMCID: PMCPMC7707640.
160. Zhao WM, Song SH, Chen ML, Zou D, Ma LN, Ma YK, et al. The 2019 novel coronavirus resource. Yi Chuan. 2020;42(2):212-21. Epub 2020/02/28. doi: 10.16288/j.yczz.20-030. PubMed PMID: 32102777.
161. Song S, Ma L, Zou D, Tian D, Li C, Zhu J, et al. The Global Landscape of SARS-CoV-2 Genomes, Variants, and Haplotypes in 2019nCoVR. Genomics Proteomics Bioinformatics. 2020;18(6):749-59. Epub 2021/03/12. doi: 10.1016/j.gpb.2020.09.001. PubMed PMID: 33704069; PubMed Central PMCID: PMCPMC7836967.
162. Gong Z, Zhu JW, Li CP, Jiang S, Ma LN, Tang BX, et al. An online coronavirus analysis platform from the National Genomics Data Center. Zool Res. 2020;41(6):705-8. Epub 2020/10/13. doi: 10.24272/j.issn.2095-8137.2020.065. PubMed PMID: 33045776; PubMed Central PMCID: PMCPMC7671910.
163. Lubinski B, Tang T, Daniel S, Jaimes JA, Whittaker GR. Functional evaluation of proteolytic activation for the SARS-CoV-2 variant B.1.1.7: role of the P681H mutation. bioRxiv. 2021. Epub 2021/04/15. doi: 10.1101/2021.04.06.438731. PubMed PMID: 33851153; PubMed Central PMCID: PMCPMC8043443.
164. Liu Y, Liu J, Johnson BA, Xia H, Ku Z, Schindewolf C, et al. Delta spike P681R mutation enhances SARS-CoV-2 fitness over Alpha variant. bioRxiv. 2021:2021.08.12.456173. Epub 2021/09/01. doi: 10.1101/2021.08.12.456173. PubMed PMID: 34462752; PubMed Central PMCID: PMCPMC8404900.
165. Peacock TP, Sheppard CM, Brown JC, Goonawardane N, Zhou J, Whiteley M, et al. The SARS-CoV-2 variants associated with infections in India, B.1.617, show enhanced spike cleavage by furin. bioRxiv. 2021:2021.05.28.446163. doi: 10.1101/2021.05.28.446163.
166. McCallum M, Walls AC, Sprouse KR, Bowen JE, Rosen L, Dang HV, et al. Molecular basis of immune evasion by the delta and kappa SARS-CoV-2 variants. bioRxiv. 2021. Epub 2021/08/18. doi: 10.1101/2021.08.11.455956. PubMed PMID: 34401880; PubMed Central PMCID: PMCPMC8366796.
167. Bugembe DL, Phan MVT, Ssewanyana I, Semanda P, Nansumba H, Dhaala B, et al. Emergence and spread of a SARS-CoV-2 lineage A variant (A.23.1) with altered spike protein in Uganda. Nat Microbiol. 2021;6(8):1094-101. Epub 2021/06/25. doi: 10.1038/s41564-021-00933-9. PubMed PMID: 34163035; PubMed Central PMCID: PMCPMC8318884.
168. Butera Y, Mukantwari E, Artesi M, D'Arc Umuringa J, O'Toole ÁN, Hill V, et al. Genomic Sequencing of SARS-CoV-2 in Rwanda: evolution and regional dynamics. medRxiv. 2021:2021.04.02.21254839. doi: 10.1101/2021.04.02.21254839.
169. Fiorentini S, Messali S, Zani A, Caccuri F, Giovanetti M, Ciccozzi M, et al. First detection of SARS-CoV-2 spike protein N501 mutation in Italy in August, 2020. Lancet Infect Dis. 2021;21(6):e147. Epub 2021/01/16. doi: 10.1016/S1473-3099(21)00007-4. PubMed PMID: 33450180; PubMed Central PMCID: PMCPMC7836831.

170. Leung K, Shum MH, Leung GM, Lam TT, Wu JT. Early transmissibility assessment of the N501Y mutant strains of SARS-CoV-2 in the United Kingdom, October to November 2020. Euro Surveill. 2021;26(1):2002106. Epub 2021/01/09. doi: 10.2807/1560-7917.ES.2020.26.1.2002106. PubMed PMID: 33413740; PubMed Central PMCID: PMCPMC7791602.
171. Liu Y, Liu J, Plante KS, Plante JA, Xie X, Zhang X, et al. The N501Y spike substitution enhances SARS-CoV-2 transmission. bioRxiv. 2021. Epub 2021/03/25. doi: 10.1101/2021.03.08.434499. PubMed PMID: 33758836; PubMed Central PMCID: PMCPMC7986995.
172. Barton MI, MacGowan S, Kutuzov M, Dushek O, Barton GJ, van der Merwe PA. Effects of common mutations in the SARS-CoV-2 Spike RBD domain and its ligand the human ACE2 receptor on binding affinity and kinetics. bioRxiv. 2021:2021.05.18.444646. doi: 10.1101/2021.05.18.444646.
173. Motozono C, Toyoda M, Zahradnik J, Ikeda T, Saito A, Tan TS, et al. An emerging SARS-CoV-2 mutant evading cellular immunity and increasing viral infectivity. bioRxiv. 2021:2021.04.02.438288. doi: 10.1101/2021.04.02.438288.
174. Liu H, Zhang Q, Wei P, Chen Z, Aviszus K, Yang J, et al. The basis of a more contagious 501Y.V1 variant of SARS-COV-2. bioRxiv. 2021:2021.02.02.428884. Epub 2021/02/11. doi: 10.1101/2021.02.02.428884. PubMed PMID: 33564771; PubMed Central PMCID: PMCPMC7872372.
175. Tian F, Tong B, Sun L, Shi S, Zheng B, Wang Z, et al. Mutation N501Y in RBD of Spike Protein Strengthens the Interaction between COVID-19 and its Receptor ACE2. bioRxiv. 2021:2021.02.14.431117. doi: 10.1101/2021.02.14.431117.
176. Starr TN, Greaney AJ, Hilton SK, Ellis D, Crawford KHD, Dingens AS, et al. Deep Mutational Scanning of SARS-CoV-2 Receptor Binding Domain Reveals Constraints on Folding and ACE2 Binding. Cell. 2020;182(5):1295-310 e20. Epub 2020/08/26. doi: 10.1016/j.cell.2020.08.012. PubMed PMID: 32841599; PubMed Central PMCID: PMCPMC7418704.
177. Gámez G, Hermoso JA, Carrasco-López C, Gómez-Mejia A, Muskus CE, Hammerschmidt S. Atypical N-glycosylation of SARS-CoV-2 impairs the efficient binding of Spike-RBM to the human-host receptor hACE2. bioRxiv. 2021:2021.04.09.439154. doi: 10.1101/2021.04.09.439154.
178. Gu H, Chen Q, Yang G, He L, Fan H, Deng YQ, et al. Adaptation of SARS-CoV-2 in BALB/c mice for testing vaccine efficacy. Science (New York, NY). 2020;369(6511):1603-7. Epub 2020/08/01. doi: 10.1126/science.abc4730. PubMed PMID: 32732280; PubMed Central PMCID: PMCPMC7574913.
179. Xie X, Liu Y, Liu J, Zhang X, Zou J, Fontes-Garfias CR, et al. Neutralization of SARS-CoV-2 spike 69/70 deletion, E484K and N501Y variants by BNT162b2 vaccine-elicited sera. Nat Med. 2021;27(4):620-1. Epub 2021/02/10. doi: 10.1038/s41591-021-01270-4. PubMed PMID: 33558724.
180. Gupta N, Kaur H, Yadav P, Mukhopadhyay L, Sahay RR, Kumar A, et al. Clinical characterization and Genomic analysis of COVID-19 breakthrough infections during second wave in different states of India. medRxiv. 2021.
181. Gobeil SM, Janowska K, McDowell S, Mansouri K, Parks R, Stalls V, et al. Effect of natural mutations of SARS-CoV-2 on spike structure, conformation, and antigenicity. Science (New York, NY). 2021;373(6555):eabi6226. Epub 2021/06/26. doi: 10.1126/science.abi6226. PubMed PMID: 34168071; PubMed Central PMCID: PMCPMC8611377.
182. Wise J. Covid-19: The E484K mutation and the risks it poses. BMJ. 2021;372:n359. Epub 2021/02/07. doi: 10.1136/bmj.n359. PubMed PMID: 33547053.
183. Wibmer CK, Ayres F, Hermanus T, Madzivhandila M, Kgagudi P, Oosthuysen B, et al. SARS-CoV-2 501Y.V2 escapes neutralization by South African COVID-19 donor plasma. Nat Med. 2021;27(4):622-5. Epub 2021/03/04. doi: 10.1038/s41591-021-01285-x. PubMed PMID: 33654292.
184. Jangra S, Ye C, Rathnasinghe R, Stadlbauer D, Personalized Virology Initiative study g, Krammer F, et al. SARS-CoV-2 spike E484K mutation reduces antibody neutralisation. Lancet Microbe. 2021;2(7):e283-e4. Epub 2021/04/14. doi: 10.1016/S2666-5247(21)00068-9. PubMed PMID: 33846703; PubMed Central PMCID: PMCPMC8026167
185. Greaney AJ, Loes AN, Crawford KHD, Starr TN, Malone KD, Chu HY, et al. Comprehensive mapping of mutations in the SARS-CoV-2 receptor-binding domain that affect recognition by polyclonal human plasma antibodies. Cell host & microbe. 2021;29(3):463-76 e6. Epub 2021/02/17.

doi: 10.1016/j.chom.2021.02.003. PubMed PMID: 33592168; PubMed Central PMCID: PMCPMC7869748.
186. Andreano E, Piccini G, Licastro D, Casalino L, Johnson NV, Paciello I, et al. SARS-CoV-2 escape in vitro from a highly neutralizing COVID-19 convalescent plasma. bioRxiv. 2020:2020.12.28.424451. Epub 2021/01/06. doi: 10.1101/2020.12.28.424451. PubMed PMID: 33398278; PubMed Central PMCID: PMCPMC7781313.
187. Weisblum Y, Schmidt F, Zhang F, DaSilva J, Poston D, Lorenzi JCC, et al. Escape from neutralizing antibodies by SARS-CoV-2 spike protein variants. bioRxiv. 2020. Epub 2020/08/04. doi: 10.1101/2020.07.21.214759. PubMed PMID: 32743579; PubMed Central PMCID: PMCPMC7386497.
188. Liu Z, VanBlargan LA, Bloyet LM, Rothlauf PW, Chen RE, Stumpf S, et al. Landscape analysis of escape variants identifies SARS-CoV-2 spike mutations that attenuate monoclonal and serum antibody neutralization. bioRxiv. 2021:2020.11.06.372037. Epub 2021/01/15. doi: 10.1101/2020.11.06.372037. PubMed PMID: 33442690; PubMed Central PMCID: PMCPMC7805447.
189. Cerutti G, Guo Y, Zhou T, Gorman J, Lee M, Rapp M, et al. Potent SARS-CoV-2 neutralizing antibodies directed against spike N-terminal domain target a single supersite. Cell host & microbe. 2021;29(5):819-33 e7. Epub 2021/04/01. doi: 10.1016/j.chom.2021.03.005. PubMed PMID: 33789084; PubMed Central PMCID: PMCPMC7953435.
190. McCallum M, De Marco A, Lempp FA, Tortorici MA, Pinto D, Walls AC, et al. N-terminal domain antigenic mapping reveals a site of vulnerability for SARS-CoV-2. Cell. 2021;184(9):2332-47 e16. Epub 2021/03/25. doi: 10.1016/j.cell.2021.03.028. PubMed PMID: 33761326; PubMed Central PMCID: PMCPMC7962585.
191. Chi X, Yan R, Zhang J, Zhang G, Zhang Y, Hao M, et al. A neutralizing human antibody binds to the N-terminal domain of the Spike protein of SARS-CoV-2. Science (New York, NY). 2020;369(6504):650-5. Epub 2020/06/24. doi: 10.1126/science.abc6952. PubMed PMID: 32571838; PubMed Central PMCID: PMCPMC7319273.
192. McCarthy KR, Rennick LJ, Nambulli S, Robinson-McCarthy LR, Bain WG, Haidar G, et al. Recurrent deletions in the SARS-CoV-2 spike glycoprotein drive antibody escape. Science (New York, NY). 2021;371(6534):1139-42. Epub 2021/02/05. doi: 10.1126/science.abf6950. PubMed PMID: 33536258; PubMed Central PMCID: PMCPMC7971772.
193. Wilson P, Changrob S, Fu Y, Guthmiller J, Halfmann P, Li L, et al. Cross neutralization of emerging SARS-CoV-2 variants of concern by antibodies targeting distinct epitopes on spike. 2021.
194. Amanat F, Thapa M, Lei T, Ahmed SMS, Adelsberg DC, Carreno JM, et al. SARS-CoV-2 mRNA vaccination induces functionally diverse antibodies to NTD, RBD, and S2. Cell. 2021;184(15):3936-48 e10. Epub 2021/07/01. doi: 10.1016/j.cell.2021.06.005. PubMed PMID: 34192529; PubMed Central PMCID: PMCPMC8185186.
195. Schmidt F, Weisblum Y, Rutkowska M, Poston D, DaSilva J, Zhang F, et al. High genetic barrier to SARS-CoV-2 polyclonal neutralizing antibody escape. Nature. 2021. Epub 2021/09/21. doi: 10.1038/s41586-021-04005-0. PubMed PMID: 34544114.
196. Liu Y, Arase N, Kishikawa J-i, Hirose M, Li S, Tada A, et al. The SARS-CoV-2 Delta variant is poised to acquire complete resistance to wild-type spike vaccines. bioRxiv. 2021:2021.08.22.457114. doi: 10.1101/2021.08.22.457114.
197. Toniolo SP, Afkhami S, D'Agostino MR, Lichty BD, Cranston ED, Xing Z, et al. Spray dried VSV-vectored vaccine is thermally stable and immunologically active in vivo. Scientific reports. 2020;10(1):13349. Epub 2020/08/10. doi: 10.1038/s41598-020-70325-2. PubMed PMID: 32770018; PubMed Central PMCID: PMCPMC7414861.
198. Pollet J, Chen WH, Versteeg L, Keegan B, Zhan B, Wei J, et al. SARSCoV-2 RBD219-N1C1: A yeast-expressed SARS-CoV-2 recombinant receptor-binding domain candidate vaccine stimulates virus neutralizing antibodies and T-cell immunity in mice. Hum Vaccin Immunother. 2021;17(8):2356-66. Epub 2021/04/14. doi: 10.1080/21645515.2021.1901545. PubMed PMID: 33847226; PubMed Central PMCID: PMCPMC8054496.

199. Yang J, Wang W, Chen Z, Lu S, Yang F, Bi Z, et al. A vaccine targeting the RBD of the S protein of SARS-CoV-2 induces protective immunity. Nature. 2020;586(7830):572-7. Epub 2020/07/30. doi: 10.1038/s41586-020-2599-8. PubMed PMID: 32726802.
200. Hattori T, Koide A, Noval MG, Panchenko T, Romero LA, Teng KW, et al. The ACE2-binding Interface of SARS-CoV-2 Spike Inherently Deflects Immune Recognition. J Mol Biol. 2021;433(3):166748. Epub 2020/12/15. doi: 10.1016/j.jmb.2020.166748. PubMed PMID: 33310017; PubMed Central PMCID: PMCPMC7833242.
201. Dalvie NC, Rodriguez-Aponte SA, Hartwell BL, Tostanoski LH, Biedermann AM, Crowell LE, et al. Engineered SARS-CoV-2 receptor binding domain improves immunogenicity in mice and elicits protective immunity in hamsters. bioRxiv. 2021. Epub 2021/03/11. doi: 10.1101/2021.03.03.433558. PubMed PMID: 33688647; PubMed Central PMCID: PMCPMC7941618.
202. Tan HX, Juno JA, Lee WS, Barber-Axthelm I, Kelly HG, Wragg KM, et al. Immunogenicity of prime-boost protein subunit vaccine strategies against SARS-CoV-2 in mice and macaques. Nat Commun. 2021;12(1):1403. Epub 2021/03/05. doi: 10.1038/s41467-021-21665-8. PubMed PMID: 33658497; PubMed Central PMCID: PMCPMC7930087.
203. Vogel M, Bachmann MF. Immunogenicity and Immunodominance in Antibody Responses. In: Hangartner L, Burton DR, editors. Vaccination Strategies Against Highly Variable Pathogens. Cham: Springer International Publishing; 2020. p. 89-102.
204. Bachmann MF, Jennings GT. Vaccine delivery: a matter of size, geometry, kinetics and molecular patterns. Nature reviews Immunology. 2010;10(11):787-96. Epub 2010/10/16. doi: 10.1038/nri2868. PubMed PMID: 20948547.
205. Jennings GT, Bachmann MF. Designing recombinant vaccines with viral properties: a rational approach to more effective vaccines. Curr Mol Med. 2007;7(2):143-55. Epub 2007/03/10. doi: 10.2174/156652407780059140. PubMed PMID: 17346167.
206. Thyagarajan R, Arunkumar N, Song W. Polyvalent antigens stabilize B cell antigen receptor surface signaling microdomains. Journal of immunology (Baltimore, Md : 1950). 2003;170(12):6099-106. Epub 2003/06/10. doi: 10.4049/jimmunol.170.12.6099. PubMed PMID: 12794139.
207. Vogelstein B, Dintzis RZ, Dintzis HM. Specific cellular stimulation in the primary immune response: a quantized model. Proceedings of the National Academy of Sciences of the United States of America. 1982;79(2):395-9. Epub 1982/01/01. doi: 10.1073/pnas.79.2.395. PubMed PMID: 6952192; PubMed Central PMCID: PMCPMC345749.
208. Jegerlehner A, Storni T, Lipowsky G, Schmid M, Pumpens P, Bachmann MF. Regulation of IgG antibody responses by epitope density and CD21-mediated costimulation. European journal of immunology. 2002;32(11):3305-14. Epub 2003/01/31. doi: 10.1002/1521-4141(200211)32:11<3305::AID-IMMU3305>3.0.CO;2-J. PubMed PMID: 12555676.
209. Schnell MJ, Buonocore L, Boritz E, Ghosh HP, Chernish R, Rose JK. Requirement for a non-specific glycoprotein cytoplasmic domain sequence to drive efficient budding of vesicular stomatitis virus. EMBO J. 1998;17(5):1289-96. Epub 1998/04/18. doi: 10.1093/emboj/17.5.1289. PubMed PMID: 9482726; PubMed Central PMCID: PMCPMC1170477.
210. Smith ME, Koser M, Xiao S, Siler C, McGettigan JP, Calkins C, et al. Rabies virus glycoprotein as a carrier for anthrax protective antigen. Virology. 2006;353(2):344-56. Epub 2006/07/06. doi: 10.1016/j.virol.2006.05.010. PubMed PMID: 16820183; PubMed Central PMCID: PMCPMC1576297.
211. Klingen Y, Conzelmann KK, Finke S. Double-labeled rabies virus: live tracking of enveloped virus transport. Journal of virology. 2008;82(1):237-45. Epub 2007/10/12. doi: 10.1128/JVI.01342-07. PubMed PMID: 17928343; PubMed Central PMCID: PMCPMC2224359.
212. Knappskog S, Ravneberg H, Gjerdrum C, Trosse C, Stern B, Pryme IF. The level of synthesis and secretion of Gaussia princeps luciferase in transfected CHO cells is heavily dependent on the choice of signal peptide. J Biotechnol. 2007;128(4):705-15. Epub 2007/02/24. doi: 10.1016/j.jbiotec.2006.11.026. PubMed PMID: 17316861.
213. Kober L, Zehe C, Bode J. Optimized signal peptides for the development of high expressing CHO cell lines. Biotechnol Bioeng. 2013;110(4):1164-73. Epub 2012/11/06. doi: 10.1002/bit.24776. PubMed PMID: 23124363.

214. Zhang L, Leng Q, Mixson AJ. Alteration in the IL-2 signal peptide affects secretion of proteins in vitro and in vivo. J Gene Med. 2005;7(3):354-65. Epub 2004/12/25. doi: 10.1002/jgm.677. PubMed PMID: 15619290.
215. Hennrich AA, Sawatsky B, Santos-Mandujano R, Banda DH, Oberhuber M, Schopf A, et al. Safe and effective two-in-one replicon-and-VLP minispike vaccine for COVID-19: Protection of mice after a single immunization. PLoS Pathog. 2021;17(4):e1009064. Epub 2021/04/22. doi: 10.1371/journal.ppat.1009064. PubMed PMID: 33882114; PubMed Central PMCID: PMCPMC8092985 following competing interests: AAH and KKC are listed as inventors on a rhabdovirus minispike patent application.
216. Wood WN, Smith KD, Ream JA, Lewis LK. Enhancing yields of low and single copy number plasmid DNAs from Escherichia coli cells. J Microbiol Methods. 2017;133:46-51. Epub 2016/12/28. doi: 10.1016/j.mimet.2016.12.016. PubMed PMID: 28024984; PubMed Central PMCID: PMCPMC5286560.
217. Hanika A, Larisch B, Steinmann E, Schwegmann-Wessels C, Herrler G, Zimmer G. Use of influenza C virus glycoprotein HEF for generation of vesicular stomatitis virus pseudotypes. The Journal of general virology. 2005;86(Pt 5):1455-65. Epub 2005/04/16. doi: 10.1099/vir.0.80788-0. PubMed PMID: 15831958.
218. Buchholz UJ, Finke S, Conzelmann KK. Generation of bovine respiratory syncytial virus (BRSV) from cDNA: BRSV NS2 is not essential for virus replication in tissue culture, and the human RSV leader region acts as a functional BRSV genome promoter. Journal of virology. 1999;73(1):251-9. Epub 1998/12/16. PubMed PMID: 9847328; PubMed Central PMCID: PMCPMC103829.
219. Finke S, Mueller-Waldeck R, Conzelmann KK. Rabies virus matrix protein regulates the balance of virus transcription and replication. The Journal of general virology. 2003;84(Pt 6):1613-21. Epub 2003/05/29. doi: 10.1099/vir.0.19128-0. PubMed PMID: 12771432.
220. Ghanem A, Kern A, Conzelmann KK. Significantly improved rescue of rabies virus from cDNA plasmids. European Journal of Cell Biology. 2012;91(1):10-6. doi: 10.1016/j.ejcb.2011.01.008. PubMed PMID: WOS:000299358600003.
221. Garic D, Humbert L, Fils-Aime N, Korah J, Zarfabian Y, Lebrun JJ, et al. Development of buffers for fast semidry transfer of proteins. Anal Biochem. 2013;441(2):182-4. Epub 2013/07/23. doi: 10.1016/j.ab.2013.07.009. PubMed PMID: 23872007.
222. Laporte M, Raeymaekers V, Van Berwaer R, Vandeput J, Marchand-Casas I, Thibaut HJ, et al. The SARS-CoV-2 and other human coronavirus spike proteins are fine-tuned towards temperature and proteases of the human airways. PLoS Pathog. 2021;17(4):e1009500. Epub 2021/04/23. doi: 10.1371/journal.ppat.1009500. PubMed PMID: 33886690; PubMed Central PMCID: PMCPMC8061995.
223. Schindelin J, Arganda-Carreras I, Frise E, Kaynig V, Longair M, Pietzsch T, et al. Fiji: an open-source platform for biological-image analysis. Nat Methods. 2012;9(7):676-82. Epub 2012/06/30. doi: 10.1038/nmeth.2019. PubMed PMID: 22743772; PubMed Central PMCID: PMCPMC3855844.
224. Baek M, DiMaio F, Anishchenko I, Dauparas J, Ovchinnikov S, Lee GR, et al. Accurate prediction of protein structures and interactions using a three-track neural network. Science (New York, NY). 2021;373(6557):871-+. doi: 10.1126/science.abj8754. PubMed PMID: WOS:000686562400029.
225. Almagro Armenteros JJ, Tsirigos KD, Sonderby CK, Petersen TN, Winther O, Brunak S, et al. SignalP 5.0 improves signal peptide predictions using deep neural networks. Nat Biotechnol. 2019;37(4):420-3. Epub 2019/02/20. doi: 10.1038/s41587-019-0036-z. PubMed PMID: 30778233.
226. Almagro Armenteros JJ, Sonderby CK, Sonderby SK, Nielsen H, Winther O. DeepLoc: prediction of protein subcellular localization using deep learning. Bioinformatics. 2017;33(21):3387-95. Epub 2017/10/17. doi: 10.1093/bioinformatics/btx431. PubMed PMID: 29036616.
227. Klingen Y, Conzelmann KK, Finke S. Double-labeled rabies virus: live tracking of enveloped virus transport. JVirol. 2008;82(1):237-45.

228. Pinto D, Park YJ, Beltramello M, Walls AC, Tortorici MA, Bianchi S, et al. Cross-neutralization of SARS-CoV-2 by a human monoclonal SARS-CoV antibody. Nature. 2020;583(7815):290-5. Epub 2020/05/19. doi: 10.1038/s41586-020-2349-y. PubMed PMID: 32422645.
229. Mebatsion T, Finke S, Weiland F, Conzelmann KK. A CXCR4/CD4 pseudotype rhabdovirus that selectively infects HIV-1 envelope protein-expressing cells. Cell. 1997;90(5):841-7. doi: Doi 10.1016/S0092-8674(00)80349-9. PubMed PMID: WOS:A1997XV56300005.
230. Yuan M, Wu NC, Zhu X, Lee CD, So RTY, Lv H, et al. A highly conserved cryptic epitope in the receptor binding domains of SARS-CoV-2 and SARS-CoV. Science (New York, NY). 2020;368(6491):630-3. Epub 2020/04/05. doi: 10.1126/science.abb7269. PubMed PMID: 32245784; PubMed Central PMCID: PMCPMC7164391.
231. Conzelmann KK. Nonsegmented negative-strand RNA viruses: genetics and manipulation of viral genomes. Annu Rev Genet. 1998;32:123-62. Epub 1999/02/03. doi: 10.1146/annurev.genet.32.1.123. PubMed PMID: 9928477.
232. Flanagan EB, Ball LA, Wertz GW. Moving the glycoprotein gene of vesicular stomatitis virus to promoter-proximal positions accelerates and enhances the protective immune response. Journal of virology. 2000;74(17):7895-902. Epub 2000/08/10. doi: 10.1128/jvi.74.17.7895-7902.2000. PubMed PMID: 10933697; PubMed Central PMCID: PMCPMC112320.
233. Malherbe DC, Kurup D, Wirblich C, Ronk AJ, Mire C, Kuzmina N, et al. A single dose of replication-competent VSV-vectored vaccine expressing SARS-CoV-2 S1 protects against virus replication in a hamster model of severe COVID-19. NPJ Vaccines. 2021;6(1):91. Epub 2021/07/24. doi: 10.1038/s41541-021-00352-1. PubMed PMID: 34294728; PubMed Central PMCID: PMCPMC8298481.
234. Grakoui A, McCourt DW, Wychowski C, Feinstone SM, Rice CM. Characterization of the hepatitis C virus-encoded serine proteinase: determination of proteinase-dependent polyprotein cleavage sites. J Virol. 1993;67(5):2832-43. Epub 1993/05/01. doi: 10.1128/jvi.67.5.2832-2843.1993. PubMed PMID: 8386278; PubMed Central PMCID: PMCPMC237608.
235. Kolykhalov AA, Agapov EV, Rice CM. Specificity of the hepatitis C virus NS3 serine protease: effects of substitutions at the 3/4A, 4A/4B, 4B/5A, and 5A/5B cleavage sites on polyprotein processing. J Virol. 1994;68(11):7525-33. Epub 1994/11/01. doi: 10.1128/jvi.68.11.7525-7533.1994. PubMed PMID: 7933136; PubMed Central PMCID: PMCPMC237195.
236. Bartenschlager R, Ahlborn-Laake L, Yasargil K, Mous J, Jacobsen H. Substrate determinants for cleavage in cis and in trans by the hepatitis C virus NS3 proteinase. J Virol. 1995;69(1):198-205. Epub 1995/01/01. doi: 10.1128/jvi.69.1.198-205.1995. PubMed PMID: 7983710; PubMed Central PMCID: PMCPMC188564.
237. Ghanem A, Kern A, Conzelmann KK. Significantly improved rescue of rabies virus from cDNA plasmids. Eur J Cell Biol. 2012;91(1):10-6. Epub 2011/03/15. doi: 10.1016/j.ejcb.2011.01.008. PubMed PMID: 21397981.
238. Ghanem A, Conzelmann KK. G gene-deficient single-round rabies viruses for neuronal circuit analysis. Virus research. 2016;216:41-54. Epub 2015/06/13. doi: 10.1016/j.virusres.2015.05.023. PubMed PMID: 26065596.
239. Buchholz UJ, Finke S, Conzelmann KK. Generation of bovine respiratory syncytial virus (BRSV) from cDNA: BRSV NS2 is not essential for virus replication in tissue culture, and the human RSV leader region acts as a functional BRSV genome promoter. Journal of virology. 1999;73(1):251-9.
240. Gaudin Y, Ruigrok RW, Tuffereau C, Knossow M, Flamand A. Rabies virus glycoprotein is a trimer. Virology. 1992;187(2):627-32. Epub 1992/04/01. doi: 10.1016/0042-6822(92)90465-2. PubMed PMID: 1546457; PubMed Central PMCID: PMCPMC7131270.
241. Lyles DS, McKenzie M, Parce JW. Subunit interactions of vesicular stomatitis virus envelope glycoprotein stabilized by binding to viral matrix protein. Journal of virology. 1992;66(1):349-58. Epub 1992/01/01. doi: 10.1128/JVI.66.1.349-358.1992. PubMed PMID: 1309251; PubMed Central PMCID: PMCPMC238294.
242. Zagouras P, Rose JK. Dynamic equilibrium between vesicular stomatitis virus glycoprotein monomers and trimers in the Golgi and at the cell surface. Journal of virology. 1993;67(12):7533-8.

Epub 1993/12/01. doi: 10.1128/JVI.67.12.7533-7538.1993. PubMed PMID: 8230472; PubMed Central PMCID: PMCPMC238219.
243. Albertini AA, Merigoux C, Libersou S, Madiona K, Bressanelli S, Roche S, et al. Characterization of monomeric intermediates during VSV glycoprotein structural transition. PLoS Pathog. 2012;8(2):e1002556. Epub 2012/03/03. doi: 10.1371/journal.ppat.1002556. PubMed PMID: 22383886; PubMed Central PMCID: PMCPMC3285605.
244. Rolls MM, Webster P, Balba NH, Rose JK. Novel infectious particles generated by expression of the vesicular stomatitis virus glycoprotein from a self-replicating RNA. Cell. 1994;79(3):497-506. Epub 1994/11/04. doi: 10.1016/0092-8674(94)90258-5. PubMed PMID: 7954815.
245. Cattin-Ortola J, Welch LG, Maslen SL, Papa G, James LC, Munro S. Sequences in the cytoplasmic tail of SARS-CoV-2 Spike facilitate expression at the cell surface and syncytia formation. Nat Commun. 2021;12(1):5333. Epub 2021/09/11. doi: 10.1038/s41467-021-25589-1. PubMed PMID: 34504087; PubMed Central PMCID: PMCPMC8429659.
246. Ujike M, Huang C, Shirato K, Makino S, Taguchi F. The contribution of the cytoplasmic retrieval signal of severe acute respiratory syndrome coronavirus to intracellular accumulation of S proteins and incorporation of S protein into virus-like particles. The Journal of general virology. 2016;97(8):1853-64. Epub 2016/05/06. doi: 10.1099/jgv.0.000494. PubMed PMID: 27145752; PubMed Central PMCID: PMCPMC5764123.
247. Lontok E, Corse E, Machamer CE. Intracellular targeting signals contribute to localization of coronavirus spike proteins near the virus assembly site. Journal of virology. 2004;78(11):5913-22. Epub 2004/05/14. doi: 10.1128/JVI.78.11.5913-5922.2004. PubMed PMID: 15140989; PubMed Central PMCID: PMCPMC415842.
248. Schwegmann-Weßels C, Glende J, Ren X, Qu X, Deng H, Enjuanes L, et al. Comparison of vesicular stomatitis virus pseudotyped with the S proteins from a porcine and a human coronavirus. Journal of General Virology. 2009;90(7):1724-9. doi: https://doi.org/10.1099/vir.0.009704-0.
249. Yinda CK, Port JR, Bushmaker T, Offei Owusu I, Purushotham JN, Avanzato VA, et al. K18-hACE2 mice develop respiratory disease resembling severe COVID-19. PLoS Pathog. 2021;17(1):e1009195. Epub 2021/01/20. doi: 10.1371/journal.ppat.1009195. PubMed PMID: 33465158; PubMed Central PMCID: PMCPMC7875348.
250. Bao L, Deng W, Huang B, Gao H, Liu J, Ren L, et al. The pathogenicity of SARS-CoV-2 in hACE2 transgenic mice. Nature. 2020;583(7818):830-3. Epub 2020/05/08. doi: 10.1038/s41586-020-2312-y. PubMed PMID: 32380511.
251. Planas D, Veyer D, Baidaliuk A, Staropoli I, Guivel-Benhassine F, Rajah MM, et al. Reduced sensitivity of SARS-CoV-2 variant Delta to antibody neutralization. Nature. 2021;596(7871):276-80. Epub 2021/07/09. doi: 10.1038/s41586-021-03777-9. PubMed PMID: 34237773.
252. Thomson EC, Rosen LE, Shepherd JG, Spreafico R, da Silva Filipe A, Wojcechowskyj JA, et al. Circulating SARS-CoV-2 spike N439K variants maintain fitness while evading antibody-mediated immunity. Cell. 2021;184(5):1171-87 e20. Epub 2021/02/24. doi: 10.1016/j.cell.2021.01.037. PubMed PMID: 33621484; PubMed Central PMCID: PMCPMC7843029.
253. Gazit S, Shlezinger R, Perez G, Lotan R, Peretz A, Ben-Tov A, et al. Comparing SARS-CoV-2 natural immunity to vaccine-induced immunity: reinfections versus breakthrough infections. medRxiv. 2021:2021.08.24.21262415. doi: 10.1101/2021.08.24.21262415.
254. Greaney AJ, Starr TN, Barnes CO, Weisblum Y, Schmidt F, Caskey M, et al. Mutational escape from the polyclonal antibody response to SARS-CoV-2 infection is largely shaped by a single class of antibodies. bioRxiv. 2021. Epub 2021/03/25. doi: 10.1101/2021.03.17.435863. PubMed PMID: 33758856; PubMed Central PMCID: PMCPMC7987015
255. Jongeneelen M, Kaszas K, Veldman D, Huizingh J, van der Vlugt R, Schouten T, et al. Ad26.COV2.S elicited neutralizing activity against Delta and other SARS-CoV-2 variants of concern. bioRxiv. 2021:2021.07.01.450707. doi: 10.1101/2021.07.01.450707.
256. Wang P, Nair MS, Liu L, Iketani S, Luo Y, Guo Y, et al. Antibody resistance of SARS-CoV-2 variants B.1.351 and B.1.1.7. Nature. 2021;593(7857):130-5. Epub 2021/03/09. doi: 10.1038/s41586-021-03398-2. PubMed PMID: 33684923.

257. Staub T, Arendt V, Lasso de la Vega EC, Braquet P, Michaux C, Kohnen M, et al. Case series of four re-infections with a SARS-CoV-2 B.1.351 variant, Luxembourg, February 2021. Euro Surveill. 2021;26(18):2100423. Epub 2021/05/08. doi: 10.2807/1560-7917.ES.2021.26.18.2100423. PubMed PMID: 33960291; PubMed Central PMCID: PMCPMC8103728.
258. Abu-Raddad LJ, Chemaitelly H, Butt AA, National Study Group for C-V. Effectiveness of the BNT162b2 Covid-19 Vaccine against the B.1.1.7 and B.1.351 Variants. The New England journal of medicine. 2021;385(2):187-9. Epub 2021/05/06. doi: 10.1056/NEJMc2104974. PubMed PMID: 33951357; PubMed Central PMCID: PMCPMC8117967.
259. Shinde V, Bhikha S, Hoosain Z, Archary M, Bhorat Q, Fairlie L, et al. Efficacy of NVX-CoV2373 Covid-19 Vaccine against the B.1.351 Variant. The New England journal of medicine. 2021;384(20):1899-909. Epub 2021/05/06. doi: 10.1056/NEJMoa2103055. PubMed PMID: 33951374; PubMed Central PMCID: PMCPMC8091623.
260. Madhi SA, Baillie V, Cutland CL, Voysey M, Koen AL, Fairlie L, et al. Efficacy of the ChAdOx1 nCoV-19 Covid-19 Vaccine against the B.1.351 Variant. The New England journal of medicine. 2021;384(20):1885-98. Epub 2021/03/17. doi: 10.1056/NEJMoa2102214. PubMed PMID: 33725432; PubMed Central PMCID: PMCPMC7993410.
261. Zhou D, Dejnirattisai W, Supasa P, Liu C, Mentzer AJ, Ginn HM, et al. Evidence of escape of SARS-CoV-2 variant B.1.351 from natural and vaccine-induced sera. Cell. 2021;184(9):2348-61 e6. Epub 2021/03/18. doi: 10.1016/j.cell.2021.02.037. PubMed PMID: 33730597; PubMed Central PMCID: PMCPMC7901269.
262. Tada T, Dcosta BM, Samanovic-Golden M, Herati RS, Cornelius A, Mulligan MJ, et al. Neutralization of viruses with European, South African, and United States SARS-CoV-2 variant spike proteins by convalescent sera and BNT162b2 mRNA vaccine-elicited antibodies. bioRxiv. 2021:2021.02.05.430003. Epub 2021/02/11. doi: 10.1101/2021.02.05.430003. PubMed PMID: 33564768; PubMed Central PMCID: PMCPMC7872356.
263. Ikegame S, Siddiquey MNA, Hung CT, Haas G, Brambilla L, Oguntuyo KY, et al. Neutralizing activity of Sputnik V vaccine sera against SARS-CoV-2 variants. medRxiv. 2021:2021.03.31.21254660. Epub 2021/04/07. doi: 10.1101/2021.03.31.21254660. PubMed PMID: 33821288; PubMed Central PMCID: PMCPMC8020991 Icahn School of Medicine for some of the materials used in this work. J.P.K. is a consultant for BioNTech (advisory panel on coronavirus variants).
264. Hoffmann M, Arora P, Gross R, Seidel A, Hornich BF, Hahn AS, et al. SARS-CoV-2 variants B.1.351 and P.1 escape from neutralizing antibodies. Cell. 2021;184(9):2384-93 e12. Epub 2021/04/02. doi: 10.1016/j.cell.2021.03.036. PubMed PMID: 33794143; PubMed Central PMCID: PMCPMC7980144.
265. Planas D, Bruel T, Grzelak L, Guivel-Benhassine F, Staropoli I, Porrot F, et al. Sensitivity of infectious SARS-CoV-2 B.1.1.7 and B.1.351 variants to neutralizing antibodies. Nat Med. 2021;27(5):917-24. Epub 2021/03/28. doi: 10.1038/s41591-021-01318-5. PubMed PMID: 33772244.
266. Focosi D, Novazzi F, Genoni A, Dentali F, gasperina DD, Baj A, et al. Research Square. 2021. doi: 10.21203/rs.3.rs-524959/v1.
267. Alenquer M, Ferreira F, Lousa D, Valério M, Medina-Lopes M, Bergman M-L, et al. Amino acids 484 and 494 of SARS-CoV-2 spike are hotspots of immune evasion affecting antibody but not ACE2 binding. bioRxiv. 2021:2021.04.22.441007. doi: 10.1101/2021.04.22.441007.
268. Cao Y, Yisimayi A, Bai Y, Huang W, Li X, Zhang Z, et al. Humoral immune response to circulating SARS-CoV-2 variants elicited by inactivated and RBD-subunit vaccines. Cell Res. 2021;31(7):732-41. Epub 2021/05/23. doi: 10.1038/s41422-021-00514-9. PubMed PMID: 34021265; PubMed Central PMCID: PMCPMC8138844.
269. Qu L, Yi Z, Shen Y, Xu Y, Wu Z, Tang H, et al. Circular RNA Vaccines against SARS-CoV-2 and Emerging Variants. bioRxiv. 2021:2021.03.16.435594. doi: 10.1101/2021.03.16.435594.
270. Polack FP, Thomas SJ, Kitchin N, Absalon J, Gurtman A, Lockhart S, et al. Safety and Efficacy of the BNT162b2 mRNA Covid-19 Vaccine. The New England journal of medicine. 2020;383(27):2603-15. Epub 2020/12/11. doi: 10.1056/NEJMoa2034577. PubMed PMID: 33301246; PubMed Central PMCID: PMCPMC7745181.

271. Corbett KS, Edwards DK, Leist SR, Abiona OM, Boyoglu-Barnum S, Gillespie RA, et al. SARS-CoV-2 mRNA vaccine design enabled by prototype pathogen preparedness. Nature. 2020;586(7830):567-71. Epub 2020/08/07. doi: 10.1038/s41586-020-2622-0. PubMed PMID: 32756549; PubMed Central PMCID: PMCPMC7581537.
272. Sadoff J, Le Gars M, Shukarev G, Heerwegh D, Truyers C, de Groot AM, et al. Interim Results of a Phase 1-2a Trial of Ad26.COV2.S Covid-19 Vaccine. The New England journal of medicine. 2021;384(19):1824-35. Epub 2021/01/14. doi: 10.1056/NEJMoa2034201. PubMed PMID: 33440088; PubMed Central PMCID: PMCPMC7821985.
273. Cao Y, Su B, Guo X, Sun W, Deng Y, Bao L, et al. Potent Neutralizing Antibodies against SARS-CoV-2 Identified by High-Throughput Single-Cell Sequencing of Convalescent Patients' B Cells. Cell. 2020;182(1):73-84 e16. Epub 2020/05/20. doi: 10.1016/j.cell.2020.05.025. PubMed PMID: 32425270; PubMed Central PMCID: PMCPMC7231725.
274. Kreer C, Zehner M, Weber T, Ercanoglu MS, Gieselmann L, Rohde C, et al. Longitudinal Isolation of Potent Near-Germline SARS-CoV-2-Neutralizing Antibodies from COVID-19 Patients. Cell. 2020;182(4):843-54 e12. Epub 2020/07/17. doi: 10.1016/j.cell.2020.06.044. PubMed PMID: 32673567; PubMed Central PMCID: PMCPMC7355337.
275. Brouwer PJM, Caniels TG, van der Straten K, Snitselaar JL, Aldon Y, Bangaru S, et al. Potent neutralizing antibodies from COVID-19 patients define multiple targets of vulnerability. Science (New York, NY). 2020;369(6504):643-50. Epub 2020/06/17. doi: 10.1126/science.abc5902. PubMed PMID: 32540902; PubMed Central PMCID: PMCPMC7299281.
276. Dejnirattisai W, Zhou D, Ginn HM, Duyvesteyn HME, Supasa P, Case JB, et al. The antigenic anatomy of SARS-CoV-2 receptor binding domain. Cell. 2021;184(8):2183-200 e22. Epub 2021/03/24. doi: 10.1016/j.cell.2021.02.032. PubMed PMID: 33756110; PubMed Central PMCID: PMCPMC7891125.
277. Suryadevara N, Shrihari S, Gilchuk P, VanBlargan LA, Binshtein E, Zost SJ, et al. Neutralizing and protective human monoclonal antibodies recognizing the N-terminal domain of the SARS-CoV-2 spike protein. Cell. 2021;184(9):2316-31 e15. Epub 2021/03/28. doi: 10.1016/j.cell.2021.03.029. PubMed PMID: 33773105; PubMed Central PMCID: PMCPMC7962591.
278. Klasse PJ, Nixon DF, Moore JP. Immunogenicity of clinically relevant SARS-CoV-2 vaccines in nonhuman primates and humans. Sci Adv. 2021;7(12):eabe8065. Epub 2021/02/21. doi: 10.1126/sciadv.abe8065. PubMed PMID: 33608249; PubMed Central PMCID: PMCPMC7978427.
279. Dai L, Zheng T, Xu K, Han Y, Xu L, Huang E, et al. A Universal Design of Betacoronavirus Vaccines against COVID-19, MERS, and SARS. Cell. 2020;182(3):722-33 e11. Epub 2020/07/10. doi: 10.1016/j.cell.2020.06.035. PubMed PMID: 32645327; PubMed Central PMCID: PMCPMC7321023.
280. Mulligan MJ, Lyke KE, Kitchin N, Absalon J, Gurtman A, Lockhart S, et al. Phase I/II study of COVID-19 RNA vaccine BNT162b1 in adults. Nature. 2020;586(7830):589-93. Epub 2020/08/14. doi: 10.1038/s41586-020-2639-4. PubMed PMID: 32785213.
281. Sahin U, Muik A, Derhovanessian E, Vogler I, Kranz LM, Vormehr M, et al. COVID-19 vaccine BNT162b1 elicits human antibody and TH1 T cell responses. Nature. 2020;586(7830):594-9. Epub 2020/10/01. doi: 10.1038/s41586-020-2814-7. PubMed PMID: 32998157.
282. Li J, Hui A, Zhang X, Yang Y, Tang R, Ye H, et al. Safety and immunogenicity of the SARS-CoV-2 BNT162b1 mRNA vaccine in younger and older Chinese adults: a randomized, placebo-controlled, double-blind phase 1 study. Nat Med. 2021;27(6):1062-70. Epub 2021/04/24. doi: 10.1038/s41591-021-01330-9. PubMed PMID: 33888900.
283. Yang Y, Shi W, Abiona OM, Nazzari A, Olia AS, Ou L, et al. Newcastle Disease Virus-Like Particles Displaying Prefusion-Stabilized SARS-CoV-2 Spikes Elicit Potent Neutralizing Responses. Vaccines. 2021;9(2). Epub 2021/01/27. doi: 10.3390/vaccines9020073. PubMed PMID: 33494381; PubMed Central PMCID: PMCPMC7912142.
284. Sissoeff L, Mousli M, England P, Tuffereau C. Stable trimerization of recombinant rabies virus glycoprotein ectodomain is required for interaction with the p75NTR receptor. The Journal of general virology. 2005;86(Pt 9):2543-52. Epub 2005/08/16. doi: 10.1099/vir.0.81063-0. PubMed PMID: 16099913.

285. Riedel C, Vasishtan D, Prazak V, Ghanem A, Conzelmann KK, Rumenapf T. Cryo EM structure of the rabies virus ribonucleoprotein complex. Scientific reports. 2019;9(1):9639. Epub 2019/07/05. doi: 10.1038/s41598-019-46126-7. PubMed PMID: 31270364; PubMed Central PMCID: PMCPMC6610074.
286. Szomolanyi-Tsuda E, Welsh RM. T-cell-independent antiviral antibody responses. Current opinion in immunology. 1998;10(4):431-5. Epub 1998/09/02. doi: 10.1016/s0952-7915(98)80117-9. PubMed PMID: 9722919.
287. Bachmann MF, Hengartner H, Zinkernagel RM. T helper cell-independent neutralizing B cell response against vesicular stomatitis virus: role of antigen patterns in B cell induction? European journal of immunology. 1995;25(12):3445-51. Epub 1995/12/01. doi: 10.1002/eji.1830251236. PubMed PMID: 8566036.
288. Roldao A, Mellado MC, Castilho LR, Carrondo MJ, Alves PM. Virus-like particles in vaccine development. Expert review of vaccines. 2010;9(10):1149-76. Epub 2010/10/07. doi: 10.1586/erv.10.115. PubMed PMID: 20923267.
289. Hiam-Galvez KJ, Allen BM, Spitzer MH. Systemic immunity in cancer. Nat Rev Cancer. 2021;21(6):345-59. Epub 2021/04/11. doi: 10.1038/s41568-021-00347-z. PubMed PMID: 33837297; PubMed Central PMCID: PMCPMC8034277.
290. Harrington K, Freeman DJ, Kelly B, Harper J, Soria JC. Optimizing oncolytic virotherapy in cancer treatment. Nat Rev Drug Discov. 2019;18(9):689-706. Epub 2019/07/12. doi: 10.1038/s41573-019-0029-0. PubMed PMID: 31292532.
291. Gonzalez H, Hagerling C, Werb Z. Roles of the immune system in cancer: from tumor initiation to metastatic progression. Genes Dev. 2018;32(19-20):1267-84. Epub 2018/10/03. doi: 10.1101/gad.314617.118. PubMed PMID: 30275043; PubMed Central PMCID: PMCPMC6169832.
292. Kaufman HL, Kohlhapp FJ, Zloza A. Oncolytic viruses: a new class of immunotherapy drugs. Nat Rev Drug Discov. 2015;14(9):642-62. Epub 2015/09/02. doi: 10.1038/nrd4663. PubMed PMID: 26323545; PubMed Central PMCID: PMCPMC7097180.
293. Koks CA, Garg AD, Ehrhardt M, Riva M, Vandenberk L, Boon L, et al. Newcastle disease virotherapy induces long-term survival and tumor-specific immune memory in orthotopic glioma through the induction of immunogenic cell death. Int J Cancer. 2015;136(5):E313-25. Epub 2014/09/12. doi: 10.1002/ijc.29202. PubMed PMID: 25208916.
294. Galivo F, Diaz RM, Wongthida P, Thompson J, Kottke T, Barber G, et al. Single-cycle viral gene expression, rather than progressive replication and oncolysis, is required for VSV therapy of B16 melanoma. Gene Ther. 2010;17(2):158-70. Epub 2009/12/18. doi: 10.1038/gt.2009.161. PubMed PMID: 20016540; PubMed Central PMCID: PMCPMC3934361.
295. Kapadia SU, Simon ID, Rose JK. SARS vaccine based on a replication-defective recombinant vesicular stomatitis virus is more potent than one based on a replication-competent vector. Virology. 2008;376(1):165-72. Epub 2008/04/09. doi: 10.1016/j.virol.2008.03.002. PubMed PMID: 18396306; PubMed Central PMCID: PMCPMC7103385.
296. Fukushi S, Mizutani T, Saijo M, Matsuyama S, Miyajima N, Taguchi F, et al. Vesicular stomatitis virus pseudotyped with severe acute respiratory syndrome coronavirus spike protein. The Journal of general virology. 2005;86(Pt 8):2269-74. Epub 2005/07/22. doi: 10.1099/vir.0.80955-0. PubMed PMID: 16033974.
297. Fukushi S, Mizutani T, Saijo M, Matsuyama S, Taguchi F, Kurane I, et al. Pseudotyped vesicular stomatitis virus for functional analysis of SARS coronavirus spike protein. Adv Exp Med Biol. 2006;581:293-6. Epub 2006/10/14. doi: 10.1007/978-0-387-33012-9_50. PubMed PMID: 17037546; PubMed Central PMCID: PMCPMC7122926.
298. Giroglou T, Cinatl J, Jr., Rabenau H, Drosten C, Schwalbe H, Doerr HW, et al. Retroviral vectors pseudotyped with severe acute respiratory syndrome coronavirus S protein. Journal of virology. 2004;78(17):9007-15. Epub 2004/08/17. doi: 10.1128/jvi.78.17.9007-9015.2004. PubMed PMID: 15308697; PubMed Central PMCID: PMCPMC506966.
299. Publicover J, Ramsburg E, Rose JK. A single-cycle vaccine vector based on vesicular stomatitis virus can induce immune responses comparable to those generated by a replication-competent

vector. Journal of virology. 2005;79(21):13231-8. Epub 2005/10/18. doi: 10.1128/jvi.79.21.13231-13238.2005. PubMed PMID: 16227246; PubMed Central PMCID: PMCPMC1262593.
300. Majid AM, Ezelle H, Shah S, Barber GN. Evaluating replication-defective vesicular stomatitis virus as a vaccine vehicle. Journal of virology. 2006;80(14):6993-7008. doi: 10.1128/JVI.00365-06. PubMed PMID: 16809305.
301. Case JB, Rothlauf PW, Chen RE, Liu Z, Zhao H, Kim AS, et al. Neutralizing Antibody and Soluble ACE2 Inhibition of a Replication-Competent VSV-SARS-CoV-2 and a Clinical Isolate of SARS-CoV-2. Cell host & microbe. 2020;28(3):475-85 e5. Epub 2020/08/01. doi: 10.1016/j.chom.2020.06.021. PubMed PMID: 32735849; PubMed Central PMCID: PMCPMC7332453.
302. Dieterle ME, Haslwanter D, Bortz RH, 3rd, Wirchnianski AS, Lasso G, Vergnolle O, et al. A Replication-Competent Vesicular Stomatitis Virus for Studies of SARS-CoV-2 Spike-Mediated Cell Entry and Its Inhibition. Cell host & microbe. 2020;28(3):486-96 e6. Epub 2020/08/02. doi: 10.1016/j.chom.2020.06.020. PubMed PMID: 32738193; PubMed Central PMCID: PMCPMC7332447.
303. Honke N, Shaabani N, Cadeddu G, Sorg UR, Zhang DE, Trilling M, et al. Enforced viral replication activates adaptive immunity and is essential for the control of a cytopathic virus. Nature immunology. 2011;13(1):51-7. Epub 2011/11/22. doi: 10.1038/ni.2169. PubMed PMID: 22101728.
304. Shinde PV, Xu HC, Maney SK, Kloetgen A, Namineni S, Zhuang Y, et al. Tumor Necrosis Factor-Mediated Survival of CD169(+) Cells Promotes Immune Activation during Vesicular Stomatitis Virus Infection. Journal of virology. 2018;92(3). Epub 2017/11/17. doi: 10.1128/jvi.01637-17. PubMed PMID: 29142134; PubMed Central PMCID: PMCPMC5774891.
305. Uhlen M, Fagerberg L, Hallstrom BM, Lindskog C, Oksvold P, Mardinoglu A, et al. Proteomics. Tissue-based map of the human proteome. Science (New York, NY). 2015;347(6220):1260419. Epub 2015/01/24. doi: 10.1126/science.1260419. PubMed PMID: 25613900.
306. The Human Protein Atlas [Internet]. 2021 [cited 2021.10.12]. Available from: https://www.proteinatlas.org/ENSG00000130234-ACE2/tissue.
307. Case JB, Rothlauf PW, Chen RE, Liu Z, Zhao H, Kim AS, et al. Neutralizing Antibody and Soluble ACE2 Inhibition of a Replication-Competent VSV-SARS-CoV-2 and a Clinical Isolate of SARS-CoV-2. Cell host & microbe. 2020;28(3):475-85.e5. Epub 2020/08/01. doi: 10.1016/j.chom.2020.06.021. PubMed PMID: 32735849; PubMed Central PMCID: PMCPMC7332453.
308. Dieterle ME, Haslwanter D, Bortz RH, 3rd, Wirchnianski AS, Lasso G, Vergnolle O, et al. A Replication-Competent Vesicular Stomatitis Virus for Studies of SARS-CoV-2 Spike-Mediated Cell Entry and Its Inhibition. Cell host & microbe. 2020;28(3):486-96.e6. Epub 2020/08/02. doi: 10.1016/j.chom.2020.06.020. PubMed PMID: 32738193; PubMed Central PMCID: PMCPMC7332447.
309. Weisblum Y, Schmidt F, Zhang F, DaSilva J, Poston D, Lorenzi JC, et al. Escape from neutralizing antibodies by SARS-CoV-2 spike protein variants. eLife. 2020;9. Epub 2020/10/29. doi: 10.7554/eLife.61312. PubMed PMID: 33112236; PubMed Central PMCID: PMCPMC7723407.
310. Bergwerk M, Gonen T, Lustig Y, Amit S, Lipsitch M, Cohen C, et al. Covid-19 Breakthrough Infections in Vaccinated Health Care Workers. The New England journal of medicine. 2021;385(16):1474-84. Epub 2021/07/29. doi: 10.1056/NEJMoa2109072. PubMed PMID: 34320281; PubMed Central PMCID: PMCPMC8362591.
311. Mizrahi B, Lotan R, Kalkstein N, Peretz A, Perez G, Ben-Tov A, et al. Correlation of SARS-CoV-2-breakthrough infections to time-from-vaccine. Nature Communications. 2021;12(1):2021.07.29.21261317. doi: ARTN 6379

10.1038/s41467-021-26672-3. PubMed PMID: WOS:000714754400037.
312. Shastri J, Parikh S, Aggarwal V, Agrawal S, Chatterjee N, Shah R, et al. Severe SARS-CoV-2 Breakthrough Reinfection With Delta Variant After Recovery From Breakthrough Infection by Alpha Variant in a Fully Vaccinated Health Worker. Front Med (Lausanne). 2021;8(1379):737007. Epub 2021/09/08. doi: 10.3389/fmed.2021.737007. PubMed PMID: 34490316; PubMed Central PMCID: PMCPMC8418387.
313. Lopez Bernal J, Andrews N, Gower C, Gallagher E, Simmons R, Thelwall S, et al. Effectiveness of Covid-19 Vaccines against the B.1.617.2 (Delta) Variant. The New England journal of medicine.

2021;385(7):585-94. Epub 2021/07/22. doi: 10.1056/NEJMoa2108891. PubMed PMID: 34289274; PubMed Central PMCID: PMCPMC8314739.
314. Nasreen S, Chung H, He S, Brown KA, Gubbay JB, Buchan SA, et al. Effectiveness of COVID-19 vaccines against variants of concern in Ontario, Canada. medRxiv. 2021:2021.06.28.21259420. doi: 10.1101/2021.06.28.21259420.
315. "Coronavirus Pandemic (COVID-19)" [Internet]. https://ourworldindata.org/coronavirus. 2020 [cited 2020.08.02].
316. Puranik A, Lenehan PJ, Silvert E, Niesen MJM, Corchado-Garcia J, O'Horo JC, et al. Comparison of two highly-effective mRNA vaccines for COVID-19 during periods of Alpha and Delta variant prevalence. medRxiv. 2021:2021.08.06.21261707. Epub 2021/08/18. doi: 10.1101/2021.08.06.21261707. PubMed PMID: 34401884; PubMed Central PMCID: PMCPMC8366801
317. Bar-On YM, Goldberg Y, Mandel M, Bodenheimer O, Freedman L, Kalkstein N, et al. Protection of BNT162b2 Vaccine Booster against Covid-19 in Israel. The New England journal of medicine. 2021;385(15):1393-400. Epub 2021/09/16. doi: 10.1056/NEJMoa2114255. PubMed PMID: 34525275; PubMed Central PMCID: PMCPMC8461568.
318. Poetsch JH, Dahlke C, Zinser ME, Kasonta R, Lunemann S, Rechtien A, et al. Detectable Vesicular Stomatitis Virus (VSV)-Specific Humoral and Cellular Immune Responses Following VSV-Ebola Virus Vaccination in Humans. J Infect Dis. 2019;219(4):556-61. Epub 2018/11/20. doi: 10.1093/infdis/jiy565. PubMed PMID: 30452666; PubMed Central PMCID: PMCPMC6350948.
319. Hu S, Mohan Kumar D, Sax C, Schuler C, Akkina R. Pseudotyping of lentiviral vector with novel vesiculovirus envelope glycoproteins derived from Chandipura and Piry viruses. Virology. 2016;488:162-8. Epub 2015/12/10. doi: 10.1016/j.virol.2015.11.012. PubMed PMID: 26650691; PubMed Central PMCID: PMCPMC5898928.
320. van den Pol AN, Davis JN. Highly attenuated recombinant vesicular stomatitis virus VSV-12'GFP displays immunogenic and oncolytic activity. Journal of virology. 2013;87(2):1019-34. Epub 2012/11/09. doi: 10.1128/JVI.01106-12. PubMed PMID: 23135719; PubMed Central PMCID: PMCPMC3554062.
321. Taylor SC, Berkelman T, Yadav G, Hammond M. A defined methodology for reliable quantification of Western blot data. Mol Biotechnol. 2013;55(3):217-26. Epub 2013/05/28. doi: 10.1007/s12033-013-9672-6. PubMed PMID: 23709336; PubMed Central PMCID: PMCPMC3840294.
322. World Health Organization. Regional Office for E. Pandemic fatigue: reinvigorating the public to prevent COVID-19: policy framework for supporting pandemic prevention and management: revised version November 2020. Copenhagen: World Health Organization. Regional Office for Europe, 2020 2020. Report No.: Contract No.: WHO/EURO:2020-1573-41324-56242.
323. Zahradník J, Marciano S, Shemesh M, Zoler E, Chiaravalli J, Meyer B, et al. SARS-CoV-2 RBD in vitro evolution follows contagious mutation spread, yet generates an able infection inhibitor. bioRxiv. 2021:2021.01.06.425392. doi: 10.1101/2021.01.06.425392.
324. Cohen AA, Gnanapragasam PNP, Lee YE, Hoffman PR, Ou S, Kakutani LM, et al. Mosaic nanoparticles elicit cross-reactive immune responses to zoonotic coronaviruses in mice. Science (New York, NY). 2021;371(6530):735-41. Epub 2021/01/14. doi: 10.1126/science.abf6840. PubMed PMID: 33436524; PubMed Central PMCID: PMCPMC7928838.
325. Martinez DR, Schafer A, Leist SR, De la Cruz G, West A, Atochina-Vasserman EN, et al. Chimeric spike mRNA vaccines protect against Sarbecovirus challenge in mice. Science (New York, NY). 2021;373(6558):991-8. Epub 2021/07/03. doi: 10.1126/science.abi4506. PubMed PMID: 34214046.
326. Tan CW, Chia WN, Young BE, Zhu F, Lim BL, Sia WR, et al. Pan-Sarbecovirus Neutralizing Antibodies in BNT162b2-Immunized SARS-CoV-1 Survivors. The New England journal of medicine. 2021;385(15):1401-6. Epub 2021/08/19. doi: 10.1056/NEJMoa2108453. PubMed PMID: 34407341; PubMed Central PMCID: PMCPMC8422514.
327. Matassov D, Mire CE, Latham T, Geisbert JB, Xu R, Ota-Setlik A, et al. Single-Dose Trivalent VesiculoVax Vaccine Protects Macaques from Lethal Ebolavirus and Marburgvirus Challenge. Journal

of virology. 2018;92(3):JVI.01190-17. Epub 2017/11/17. doi: 10.1128/JVI.01190-17. PubMed PMID: 29142131; PubMed Central PMCID: PMCPMC5774882.
328. Choi A, Koch M, Wu K, Chu L, Ma L, Hill A, et al. Safety and immunogenicity of SARS-CoV-2 variant mRNA vaccine boosters in healthy adults: an interim analysis. Nat Med. 2021;27(11):2025-31. Epub 2021/09/17. doi: 10.1038/s41591-021-01527-y. PubMed PMID: 34526698; PubMed Central PMCID: PMCPMC8604720.
329. Hsieh CL, Goldsmith JA, Schaub JM, DiVenere AM, Kuo HC, Javanmardi K, et al. Structure-based design of prefusion-stabilized SARS-CoV-2 spikes. Science (New York, NY). 2020;369(6510):1501-5. Epub 2020/07/25. doi: 10.1126/science.abd0826. PubMed PMID: 32703906; PubMed Central PMCID: PMCPMC7402631.
330. Voss WN, Hou YJ, Johnson NV, Delidakis G, Kim JE, Javanmardi K, et al. Prevalent, protective, and convergent IgG recognition of SARS-CoV-2 non-RBD spike epitopes. Science (New York, NY). 2021;372(6546):1108-12. Epub 2021/05/06. doi: 10.1126/science.abg5268. PubMed PMID: 33947773; PubMed Central PMCID: PMCPMC8224265.
331. Shiakolas AR, Kramer KJ, Wrapp D, Richardson SI, Schafer A, Wall S, et al. Cross-reactive coronavirus antibodies with diverse epitope specificities and Fc effector functions. Cell reports Medicine. 2021;2(6):100313. Epub 2021/06/01. doi: 10.1016/j.xcrm.2021.100313. PubMed PMID: 34056628; PubMed Central PMCID: PMCPMC8139315.
332. Liu Y, Soh WT, Kishikawa JI, Hirose M, Nakayama EE, Li S, et al. An infectivity-enhancing site on the SARS-CoV-2 spike protein targeted by antibodies. Cell. 2021;184(13):3452-66 e18. Epub 2021/06/18. doi: 10.1016/j.cell.2021.05.032. PubMed PMID: 34139176; PubMed Central PMCID: PMCPMC8142859.
333. Li D, Edwards RJ, Manne K, Martinez DR, Schafer A, Alam SM, et al. In vitro and in vivo functions of SARS-CoV-2 infection-enhancing and neutralizing antibodies. Cell. 2021;184(16):4203-19 e32. Epub 2021/07/10. doi: 10.1016/j.cell.2021.06.021. PubMed PMID: 34242577; PubMed Central PMCID: PMCPMC8232969.
334. Grobbelaar LM, Venter C, Vlok M, Ngoepe M, Laubscher GJ, Lourens PJ, et al. SARS-CoV-2 spike protein S1 induces fibrin(ogen) resistant to fibrinolysis: implications for microclot formation in COVID-19. Biosci Rep. 2021;41(8). Epub 2021/07/31. doi: 10.1042/BSR20210611. PubMed PMID: 34328172; PubMed Central PMCID: PMCPMC8380922.
335. Ikegame S, Siddiquey MNA, Hung CT, Haas G, Brambilla L, Oguntuyo KY, et al. Neutralizing activity of Sputnik V vaccine sera against SARS-CoV-2 variants. Nat Commun. 2021;12(1):4598. Epub 2021/07/28. doi: 10.1038/s41467-021-24909-9. PubMed PMID: 34312390; PubMed Central PMCID: PMCPMC8313705.
336. Kustin T, Harel N, Finkel U, Perchik S, Harari S, Tahor M, et al. Evidence for increased breakthrough rates of SARS-CoV-2 variants of concern in BNT162b2-mRNA-vaccinated individuals. Nat Med. 2021;27(8):1379-84. Epub 2021/06/16. doi: 10.1038/s41591-021-01413-7. PubMed PMID: 34127854; PubMed Central PMCID: PMCPMC8363499.
337. Cohen J. What went wrong with CureVac's mRNA vaccine? Science (New York, NY). 2021;372(6549):1381-. doi: 10.1126/science.372.6549.1381.
338. Shrotri M, Navaratnam AMD, Nguyen V, Byrne T, Geismar C, Fragaszy E, et al. Spike-antibody waning after second dose of BNT162b2 or ChAdOx1. Lancet. 2021;398(10298):385-7. Epub 2021/07/19. doi: 10.1016/S0140-6736(21)01642-1. PubMed PMID: 34274038; PubMed Central PMCID: PMCPMC8285117
339. Uriu K, Kimura I, Shirakawa K, Takaori-Kondo A, Nakada T-a, Kaneda A, et al. Ineffective neutralization of the SARS-CoV-2 Mu variant by convalescent and vaccine sera. bioRxiv. 2021:2021.09.06.459005. doi: 10.1101/2021.09.06.459005.
340. Choi A, Koch M, Wu K, Dixon G, Oestreicher J, Legault H, et al. Serum Neutralizing Activity of mRNA-1273 against SARS-CoV-2 Variants. bioRxiv. 2021:2021.06.28.449914. doi: 10.1101/2021.06.28.449914.

341. Acosta PL, Caballero MT, Polack FP. Brief History and Characterization of Enhanced Respiratory Syncytial Virus Disease. Clin Vaccine Immunol. 2015;23(3):189-95. Epub 2015/12/18. doi: 10.1128/CVI.00609-15. PubMed PMID: 26677198; PubMed Central PMCID: PMCPMC4783420.
342. Hoffmann M, Hofmann-Winkler H, Kruger N, Kempf A, Nehlmeier I, Graichen L, et al. SARS-CoV-2 variant B.1.617 is resistant to bamlanivimab and evades antibodies induced by infection and vaccination. Cell Reports. 2021;36(3):2021.05.04.442663. doi: ARTN 109415

10.1016/j.celrep.2021.109415. PubMed PMID: WOS:000675844000014.
343. Kuzmina A, Khalaila Y, Voloshin O, Keren-Naus A, Boehm-Cohen L, Raviv Y, et al. SARS-CoV-2 spike variants exhibit differential infectivity and neutralization resistance to convalescent or post-vaccination sera. Cell host & microbe. 2021;29(4):522-8.e2. doi: https://doi.org/10.1016/j.chom.2021.03.008.
344. Stamatatos L, Czartoski J, Wan YH, Homad LJ, Rubin V, Glantz H, et al. mRNA vaccination boosts cross-variant neutralizing antibodies elicited by SARS-CoV-2 infection. Science (New York, NY). 2021;372(6549):1413-8. Epub 2021/03/27. doi: 10.1126/science.abg9175. PubMed PMID: 33766944; PubMed Central PMCID: PMCPMC8139425.
345. Wang Z, Muecksch F, Schaefer-Babajew D, Finkin S, Viant C, Gaebler C, et al. Naturally enhanced neutralizing breadth against SARS-CoV-2 one year after infection. Nature. 2021;595(7867):426-31. Epub 2021/06/15. doi: 10.1038/s41586-021-03696-9. PubMed PMID: 34126625; PubMed Central PMCID: PMCPMC8277577.
346. Garcia-Beltran WF, Lam EC, St Denis K, Nitido AD, Garcia ZH, Hauser BM, et al. Multiple SARS-CoV-2 variants escape neutralization by vaccine-induced humoral immunity. Cell. 2021;184(9):2372-83 e9. Epub 2021/03/21. doi: 10.1016/j.cell.2021.03.013. PubMed PMID: 33743213; PubMed Central PMCID: PMCPMC7953441.
347. Huang B, Dai L, Wang H, Hu Z, Yang X, Tan W, et al. Neutralization of SARS-CoV-2 VOC 501Y.V2 by human antisera elicited by both inactivated BBIBP-CorV and recombinant dimeric RBD ZF2001 vaccines. bioRxiv. 2021:2021.02.01.429069. doi: 10.1101/2021.02.01.429069.
348. Lustig Y, Nemet I, Kliker L, Zuckerman N, Yishai R, Alroy-Preis S, et al. Neutralizing Response against Variants after SARS-CoV-2 Infection and One Dose of BNT162b2. The New England journal of medicine. 2021;384(25):2453-4. Epub 2021/04/08. doi: 10.1056/NEJMc2104036. PubMed PMID: 33826815; PubMed Central PMCID: PMCPMC8063887.
349. Solforosi L, Kuipers H, Jongeneelen M, Rosendahl Huber SK, van der Lubbe JEM, Dekking L, et al. Immunogenicity and efficacy of one and two doses of Ad26.COV2.S COVID vaccine in adult and aged NHP. The Journal of experimental medicine. 2021;218(7). Epub 2021/04/29. doi: 10.1084/jem.20202756. PubMed PMID: 33909009; PubMed Central PMCID: PMCPMC8085771
350. Wang GL, Wang ZY, Duan LJ, Meng QC, Jiang MD, Cao J, et al. Susceptibility of Circulating SARS-CoV-2 Variants to Neutralization. The New England journal of medicine. 2021;384(24):2354-6. Epub 2021/04/07. doi: 10.1056/NEJMc2103022. PubMed PMID: 33822491; PubMed Central PMCID: PMCPMC8063885.
351. Zhou H, Dcosta BM, Samanovic MI, Mulligan MJ, Landau NR, Tada T. B.1.526 SARS-CoV-2 variants identified in New York City are neutralized by vaccine-elicited and therapeutic monoclonal antibodies. bioRxiv. 2021:2021.03.24.436620. Epub 2021/04/02. doi: 10.1101/2021.03.24.436620. PubMed PMID: 33791698; PubMed Central PMCID: PMCPMC8010725.
352. Cohen J. 'Landmark' African vaccine trial faces impasse. Science (New York, NY). 2021;372(6547):1135-6. Epub 2021/06/12. doi: 10.1126/science.372.6547.1135. PubMed PMID: 34112671.
353. Gaebler C, Wang Z, Lorenzi JCC, Muecksch F, Finkin S, Tokuyama M, et al. Evolution of antibody immunity to SARS-CoV-2. Nature. 2021;591(7851):639-44. doi: 10.1038/s41586-021-03207-w.
354. Khoury DS, Cromer D, Reynaldi A, Schlub TE, Wheatley AK, Juno JA, et al. Neutralizing antibody levels are highly predictive of immune protection from symptomatic SARS-CoV-2 infection. Nat Med. 2021;27(7):1205-11. Epub 2021/05/19. doi: 10.1038/s41591-021-01377-8. PubMed PMID: 34002089.

355. Khatamzas E, Rehn A, Muenchhoff M, Hellmuth J, Gaitzsch E, Weiglein T, et al. Emergence of multiple SARS-CoV-2 mutations in an immunocompromised host. medRxiv. 2021:2021.01.10.20248871. doi: 10.1101/2021.01.10.20248871.
356. Clark SA, Clark LE, Pan J, Coscia A, McKay LGA, Shankar S, et al. SARS-CoV-2 evolution in an immunocompromised host reveals shared neutralization escape mechanisms. Cell. 2021;184(10):2605-17 e18. Epub 2021/04/09. doi: 10.1016/j.cell.2021.03.027. PubMed PMID: 33831372; PubMed Central PMCID: PMCPMC7962548.
357. Chen L, Zody MC, Di Germanio C, Martinelli R, Mediavilla JR, Cunningham MH, et al. Emergence of Multiple SARS-CoV-2 Antibody Escape Variants in an Immunocompromised Host Undergoing Convalescent Plasma Treatment. mSphere. 2021;6(4):e0048021. Epub 2021/08/26. doi: 10.1128/mSphere.00480-21. PubMed PMID: 34431691; PubMed Central PMCID: PMCPMC8386433.
358. Choi B, Choudhary MC, Regan J, Sparks JA, Padera RF, Qiu X, et al. Persistence and Evolution of SARS-CoV-2 in an Immunocompromised Host. The New England journal of medicine. 2020;383(23):2291-3. Epub 2020/11/12. doi: 10.1056/NEJMc2031364. PubMed PMID: 33176080; PubMed Central PMCID: PMCPMC7673303.
359. Avanzato VA, Matson MJ, Seifert SN, Pryce R, Williamson BN, Anzick SL, et al. Case Study: Prolonged Infectious SARS-CoV-2 Shedding from an Asymptomatic Immunocompromised Individual with Cancer. Cell. 2020;183(7):1901-12 e9. Epub 2020/11/30. doi: 10.1016/j.cell.2020.10.049. PubMed PMID: 33248470; PubMed Central PMCID: PMCPMC7640888.
360. Wang L, Zhou T, Zhang Y, Yang ES, Schramm CA, Shi W, et al. Ultrapotent antibodies against diverse and highly transmissible SARS-CoV-2 variants. Science (New York, NY). 2021;373(6556). Epub 2021/07/03. doi: 10.1126/science.abh1766. PubMed PMID: 34210892.
361. Wu NC, Yuan M, Bangaru S, Huang D, Zhu X, Lee CD, et al. A natural mutation between SARS-CoV-2 and SARS-CoV determines neutralization by a cross-reactive antibody. PLoS Pathog. 2020;16(12):e1009089. Epub 2020/12/05. doi: 10.1371/journal.ppat.1009089. PubMed PMID: 33275640; PubMed Central PMCID: PMCPMC7744049.
362. Gupta A, Gonzalez-Rojas Y, Juarez E, Crespo Casal M, Moya J, Falci DR, et al. Early Treatment for Covid-19 with SARS-CoV-2 Neutralizing Antibody Sotrovimab. The New England journal of medicine. 2021;385(21):1941-50. Epub 2021/10/28. doi: 10.1056/NEJMoa2107934. PubMed PMID: 34706189.
363. Cathcart AL, Havenar-Daughton C, Lempp FA, Ma D, Schmid M, Agostini ML, et al. The dual function monoclonal antibodies VIR-7831 and VIR-7832 demonstrate potent in vitro and in vivo activity against SARS-CoV-2. bioRxiv. 2021.
364. Jette CA, Cohen AA, Gnanapragasam PNP, Muecksch F, Lee YE, Huey-Tubman KE, et al. Broad cross-reactivity across sarbecoviruses exhibited by a subset of COVID-19 donor-derived neutralizing antibodies. Cell Rep. 2021;36(13):109760. Epub 2021/09/18. doi: 10.1016/j.celrep.2021.109760. PubMed PMID: 34534459; PubMed Central PMCID: PMCPMC8423902.
365. Huo J, Zhao Y, Ren J, Zhou D, Duyvesteyn HME, Ginn HM, et al. Neutralization of SARS-CoV-2 by Destruction of the Prefusion Spike. Cell host & microbe. 2020;28(3):445-54.e6. Epub 2020/06/26. doi: 10.1016/j.chom.2020.06.010. PubMed PMID: 32585135; PubMed Central PMCID: PMCPMC7303615.
366. Zhang BZ, Hu YF, Chen LL, Yau T, Tong YG, Hu JC, et al. Mining of epitopes on spike protein of SARS-CoV-2 from COVID-19 patients. Cell Res. 2020;30(8):702-4. Epub 2020/07/03. doi: 10.1038/s41422-020-0366-x. PubMed PMID: 32612199; PubMed Central PMCID: PMCPMC7327194.
367. Piccoli L, Park YJ, Tortorici MA, Czudnochowski N, Walls AC, Beltramello M, et al. Mapping Neutralizing and Immunodominant Sites on the SARS-CoV-2 Spike Receptor-Binding Domain by Structure-Guided High-Resolution Serology. Cell. 2020;183(4):1024-42 e21. Epub 2020/09/30. doi: 10.1016/j.cell.2020.09.037. PubMed PMID: 32991844; PubMed Central PMCID: PMCPMC7494283.
368. Low JS, Vaqueirinho D, Mele F, Foglierini M, Jerak J, Perotti M, et al. Clonal analysis of immunodominance and cross-reactivity of the CD4 T cell response to SARS-CoV-2. Science (New York, NY). 2021;372(6548):1336-41. Epub 2021/05/20. doi: 10.1126/science.abg8985. PubMed PMID: 34006597; PubMed Central PMCID: PMCPMC8168615.

369. Science Brief: SARS-CoV-2 Infection-induced and Vaccine-induced Immunity https://www.cdc.gov/coronavirus/2019-ncov/science/science-briefs/vaccine-induced-immunity.html#print: CDC – National Center for Health Statistics; 2021 [cited 2021 12.12.2021]. Available from: https://www.cdc.gov/coronavirus/2019-ncov/science/science-briefs/vaccine-induced-immunity.html#print.
370. Heitmann JS, Bilich T, Tandler C, Nelde A, Maringer Y, Marconato M, et al. A COVID-19 peptide vaccine for the induction of SARS-CoV-2 T cell immunity. Nature. 2021. Epub 2021/11/24. doi: 10.1038/s41586-021-04232-5. PubMed PMID: 34814158.
371. Wrapp D, De Vlieger D, Corbett KS, Torres GM, Wang N, Van Breedam W, et al. Structural Basis for Potent Neutralization of Betacoronaviruses by Single-Domain Camelid Antibodies. Cell. 2020;181(5):1004-15 e15. Epub 2020/05/07. doi: 10.1016/j.cell.2020.04.031. PubMed PMID: 32375025; PubMed Central PMCID: PMCPMC7199733.
372. Baum A, Fulton BO, Wloga E, Copin R, Pascal KE, Russo V, et al. Antibody cocktail to SARS-CoV-2 spike protein prevents rapid mutational escape seen with individual antibodies. Science (New York, NY). 2020;369(6506):1014-8. Epub 2020/06/17. doi: 10.1126/science.abd0831. PubMed PMID: 32540904; PubMed Central PMCID: PMCPMC7299283.
373. Meyers LM, Gutierrez AH, Boyle CM, Terry F, McGonnigal BG, Salazar A, et al. Highly conserved, non-human-like, and cross-reactive SARS-CoV-2 T cell epitopes for COVID-19 vaccine design and validation. NPJ Vaccines. 2021;6(1):71. Epub 2021/05/15. doi: 10.1038/s41541-021-00331-6. PubMed PMID: 33986292; PubMed Central PMCID: PMCPMC8119491.